Distribution Agreement

In presenting this thesis or dissertation as a partial fulfillment of the requirements for an advanced degree from Emory University, I hereby grant to Emory University and its agents the non-exclusive license to archive, make accessible, and display my thesis or dissertation in whole or in part in all forms of media, now or hereafter known, including display on the world wide web. I understand that I may select some access restrictions as part of the online submission of this thesis or dissertation. I retain all ownership rights to the copyright of the thesis or dissertation. I also retain the right to use in future works (such as articles or books) all or part of this thesis or dissertation.

Signature:

_____ _____

Kendra Quicke Date

Molecular Mechanisms Governing Host Responses
and Cellular Tropism During Flavivirus Infection

By

Kendra M. Quicke
Doctor of Philosophy

Graduate Division of Biological and Biomedical Science
Microbiology and Molecular Genetics

_____
Mehul S. Suthar
Advisor

_____
Arash Grakoui
Committee Member

_____
Bali Pulendran
Committee Member

_____
Paul Rota
Committee Member

_____
David Weiss
Committee Member

Accepted:

_____
Lisa A. Tedesco, Ph.D.
Dean of the James T. Laney School of Graduate Studies

_____
Date

Molecular Mechanisms Governing Host Responses and Cellular Tropism During Flavivirus Infection

By

Kendra M. Quicke
B.S., University of Arizona, 2011

Advisor: Mehul S. Suthar, Ph.D.

An abstract of
A dissertation submitted to the Faculty of the
James T. Laney School of Graduate Studies of Emory University
in partial fulfillment of the requirements for the degree of
Doctor of Philosophy
in Graduate Division of Biological and Biomedical Science,
Microbiology and Molecular Genetics
2018

Abstract

Molecular Mechanisms Governing Host Responses
and Cellular Tropism During Flavivirus Infection
By Kendra M. Quicke

The RIG-I-like receptors (RLRs) are crucial to initiating innate immune responses to multiple flaviviruses. LGP2, a non-signaling member of this family, is a central regulator of the RIG-I and MDA5 pathways. However, the molecular mechanism underlying the regulatory function of LGP2 is still unclear. Additionally, very little is currently known about the specific role of RLRs in responding to Zika virus (ZIKV), a re-emerging flavivirus. ZIKV has exhibited several characteristics that are not observed with other flaviviruses, and as such it should not be assumed that the same host factors will efficiently control infection with this virus. Antiviral responses also vary based on cell type. As ZIKV appears to have a broad tropism, including innate immune cells, neuroprogenitor cells, and placental cells, it is important to evaluate the responses induced in each of these tissues. The work presented within this dissertation provides insight into the molecular mechanisms of RLR signaling regulation, antiviral responses to ZIKV infection, and ZIKV cellular tropism. Specifically, we demonstrate a heretofore undescribed mechanism of LGP2 negative regulation, wherein LGP2 inhibits early RIG-I activation by preventing K63-ubiquitination of the RIG-I CARDs through an interaction with the E3 ligase TRIM25. We also explore the susceptibility and immune responses to ZIKV infection within human primary dendritic cells (DCs), placental macrophages (Hofbauer cells [HCs]), and cytotrophoblasts (CTBs). DCs and HCs, and CTBs to a lesser extent, were found to support productive ZIKV infection. ZIKV induced antiviral gene expression in these cells, but this did not always correspond to increased protein production, particularly in the case of type I interferons (IFNs). Furthermore, ZIKV was found to potently inhibit type I IFN signaling by inhibiting activation of the transcription factors STAT1/2. In addition, the presence of cross-reactive flavivirus antibodies may further impact the immune responses and tropism of ZIKV. DENV-induced monoclonal antibodies cross-reacted with ZIKV and resulted in attenuated antiviral responses in HCs and enhanced infection of HCs and human placental explant tissues, suggesting a mechanism for the vertical transmission of ZIKV. These findings may have translational consequences on the development of new vaccines and antiviral therapies.

Molecular Mechanisms Governing Host Responses and Cellular Tropism During Flavivirus Infection

By

Kendra M. Quicke
B.S., University of Arizona, 2011

Advisor: Mehul S. Suthar, Ph.D.

A dissertation submitted to the Faculty of the
James T. Laney School of Graduate Studies of Emory University
in partial fulfillment of the requirements for the degree of
Doctor of Philosophy
in Graduate Division of Biological and Biomedical Science,
Microbiology and Molecular Genetics
2018

Acknowledgements

Mehul, for supporting my work and re-stoking my enthusiasm for projects when I lost it, and for trusting me with a legacy project and the initiation of your research laboratory.

Suthar lab members, past and present, for creating a supportive and enjoyable work environment, and for the comradery over the years.

Friends, present and otherwise, for helping maintain my mental health, and for helping me build a life, not just a career.

Mom and Dad, for instilling me with a love of science, for always encouraging me to follow my dreams, and for all the life lessons along the way.

Lex, for never giving up on me, for loving me despite my faults, and for helping me find the greatest adventure.

Table of Contents

List of Figures and Tables

Chapter 1

Chapter 2

Chapter 3

Chapter 4

Chapter 5

Chapter 6

Chapter 7

Chapter 1: Introduction

*Contains content originally published as a review in the *European Journal of Immunology*: Quicke KM, Diamond MS, Suthar MS. Negative regulators of the RIG-I-like receptor signaling pathway. *European journal of immunology*. 2017;47(4):615-628.

It has been modified in part for this dissertation.

Introduction to RIG-I-like receptors

Recognition of viral pathogen-associated molecular patterns (PAMPs) is one of the first lines of defense during virus infection. Binding of viral PAMPs by pattern recognition receptors (PRRs) triggers the production of type I interferons (IFNs), and pro-inflammatory cytokines and chemokines. This response subsequently primes activation of innate immune cells (dendritic cells (DCs), macrophages, monocytes, innate lymphoid cells, and γ/δ T cells) and adaptive immune responses (T and B cells). Each aspect of the immune response is regulated by stimulatory and inhibitory signals that modulate the strength and nature of the response. Positive regulators enhance the antiviral immune response to control and clear viral infection. Conversely, negative regulators dampen inflammatory responses to prevent immune-mediated tissue damage and spontaneous autoimmunity (Hugot et al., 2001; Ogura et al., 2001; Oldstone and Rosen, 2014; Rice et al., 2013; Sun et al., 2012).

The retinoic acid-inducible gene I (RIG-I)-like receptors (RLRs), are a family of three RNA helicase PRRs that are essential for mediating intracellular antiviral responses. The RLRs are expressed within the cytoplasm of nearly every mammalian cell. RIG-I and melanoma differentiation-associated gene 5 (MDA5), are important initiators of the innate immune response to RNA virus infection (Loo and Gale, 2011). The third member, Laboratory of Genetics and Physiology 2 (LGP2), regulates the signaling potential of RIG-I and MDA5 (Rothenfusser et al., 2005; Yoneyama et al., 2005).

Structure of the RLRs

RIG-I was first discovered in 1997 by Sun and colleagues at Shanghai Second Medical University within actively differentiating promyelocytic leukemia cells. The RIG-I gene was induced by retinoic acid and was found to share homology with other human DExH

RNA helicases (Imaizumi et al., 2002). Additionally, it was determined that the RIG-I protein contained an RNA binding and an ATP hydrolysis motif (Imaizumi et al., 2002). Later work identified RIG-I as an essential innate immune signaling protein in response to transfected dsRNA and viral infection (Yoneyama et al., 2004). The caspase activation and recruitment domains (CARDs) of RIG-I were found to be necessary for downstream signaling activation. Specifically, the isolated CARDs (N-RIG) activated the transcription factors IRF-3 and NF-κB, resulting in IFN-β production. Intact helicase activity was also required for signaling by full-length RIG-I, as a mutation in the ATP-binding site resulted in a dominant negative form of RIG-I. Additionally, RIG-I was found to bind the dsRNA ligand poly(I:C) (Yoneyama et al., 2004).

MDA5 was identified in 2002 by Kang and colleagues at Columbia University in a screen to define genes involved in the terminal differentiation of human melanoma cells. The gene produced a 3.4kb cDNA and a 1025 amino acid protein. The MDA5 protein contained a DExH box RNA helicase domain and an N-terminal caspase activation and recruitment domain (CARD). Additionally, MDA5 was found to exhibit ATPase activity, but only in the presence of double-stranded RNA (dsRNA). The authors determined that MDA5 localized to the cytoplasm of HEK293 cells, and expression was detected in almost all organs tested. MDA5 was also later found to play an important role in activating innate immune responses to viral infection (Andrejeva et al., 2004; Yoneyama et al., 2005). Similar to RIG-I, the MDA5 CARDs were required for induction of downstream signaling and activated IRF-3 and NF-κB promoter activities. A functional helicase domain was found to be necessary for full signaling potential, and MDA5 also bound dsRNA substrates (Yoneyama et al., 2005).

As mentioned, RIG-I and MDA5 both contain two N-terminal CARDs that act as signaling domains, a central DExD/H RNA helicase domain that facilitates ATP hydrolysis and RNA binding, and a C-terminal domain (CTD) that aids in RNA ligand

recognition and binding specificity (reviewed in detail in (Bruns and Horvath, 2012)). RIG-I and MDA5 share 35% overall amino acid identity (reviewed in (Bruns and Horvath, 2012)). Specifically, their CARDs share 23-24% amino acid identity, their helicase domains share 35-37% identity, and their CTDs share 30% identity (Bruns and Horvath, 2012; Yoneyama et al., 2005). The CARDs contain protein-protein interaction domains that allow for the construction of signaling complexes (Bouchier-Hayes and Martin, 2002). The helicase domains of all three RLRs contain six highly conserved sequence motifs (I-VI) (Bamming and Horvath, 2009; Cordin et al., 2006). Motifs I and II are known as the Walker A and Walker B motif, respectively, and are important for binding ATP and for ATP hydrolysis. Motif III plays a role in mediating interactions between the two ends of the helicase domain. Motifs IV and V are involved in RNA binding. Motif V has also been found to bind nucleotides, along with motif VI (Bamming and Horvath, 2009). The CTDs of RIG-I and MDA5 are important for binding specific RNA substrates (Cui et al., 2008; Takahasi et al., 2009; Takahasi et al., 2008). RIG-I has been found to preferentially bind short (<2kb) double-stranded RNA (dsRNA) and single-stranded RNA (ssRNA) with 5'-triphosphate modifications, and dsRNA with blunt ends (Hornung et al., 2006; Kato et al., 2008; Kato et al., 2006; Lu et al., 2010; Pichlmair et al., 2006; Takahasi et al., 2008). MDA5 preferentially binds longer (>2kb) dsRNA with blunt ends (Kato et al., 2008; Kato et al., 2006; Li et al., 2009a). RIG-I was also found to recognize certain RNA sequences, including the polyU/UC tract of the 3' untranslated region (UTR) of the hepatitis C virus (HCV) genome, and 5'ppp was required for recognition of this sequence by RIG-I (Saito et al., 2008). Additionally, this RNA ligand was found to specifically activate RIG-I and not MDA5.

LGP2 was discovered in 2001 by Cui and colleagues in the Laboratory of Genetics and Physiology at the NIH in Bethesda, Maryland in an effort to identify regions of the *Stat3/5* locus of murine chromosome 11 that play a role in mammary gland

development and tumor formation (Cui et al., 2001). The *Lgp2* gene was found downstream of the *Stat5b* gene, and produced a 2.4kb mRNA. The mouse *Lgp2* cDNA showed 80% similarity to the corresponding human cDNA. At the protein level, the authors determined that mouse and human LGP2 shared 94% similarity and 79% identity. They also identified a DExD/H box domain, containing ATP binding and ATPase motifs as well as an unwinding motif, and a helicase carboxy-terminal domain, containing an RNA binding motif. LGP2 expression was detected in a broad range of mouse tissues, including heart, lung, liver, spleen, mammary gland, and mammary gland tumors. When over-expressed in HeLa cells, it was found that LGP2 localizes to the cytoplasm, and is not secreted (Cui et al., 2001).

While LGP2 lacks the CARDs required for signaling, it shares homology with RIG-I and MDA5 within its DExD/H helicase domain and CTD (Murali et al., 2008; Takahasi et al., 2009; Yoneyama et al., 2005). Specifically, the LGP2 helicase domain shares 34% amino acid identity with RIG-I and 43% identity with MDA5. The LGP2 CTD shares 29% amino acid identity with RIG-I and 33% identity with MDA5 (reviewed in (Bruns and Horvath, 2012)). Similar to the other RLRs, the DExD/H helicase domain of LGP2 is capable of ATP hydrolysis and RNA binding (Bamming and Horvath, 2009; Bruns et al., 2013; Cui et al., 2001), whereas the CTD confers specificity to RNA ligand recognition and binding (Cui et al., 2008; Pippig et al., 2009). LGP2 can bind a range of RNA ligands, including short dsRNAs (<2kb) and 5′-triphosphate ssRNAs, which serve as RIG-I ligands (Kato et al., 2008; Saito et al., 2008; Takahasi et al., 2009; Takahasi et al., 2008), and long dsRNAs (>2kb), which serve as MDA5 ligands (Bruns et al., 2013; Kato et al., 2008; Li et al., 2009b).

Function of RIG-I and MDA5

RIG-I and MDA5 are normally maintained in an inactive state. This is, in part, due to an auto-regulatory function of the CTD, also called the regulatory domain (RD), which, in the case of RIG-I, interacts with the CARDs to prevent unwarranted interaction with downstream factors (Saito et al., 2007; Yoneyama et al., 2004). Phosphorylation of the CARDs, by PKCα/βII for RIG-I, also helps maintain an inactive state by blocking the CARD activation site (Gack et al., 2010; Maharaj et al., 2012). Following binding to non-self RNAs, however, the interaction between the regulatory domain and the CARDs is disrupted and the RLRs undergo post-translational modification to reach an activated state. It is thought that Riplet, an E3 ubiquitin ligase, adds K63-linked polyubiquitin to the CTD of RIG-I at K788, and that this polyubiquitination disrupts the RIG-I self CTD-CARD interaction (Oshiumi et al., 2013). PP1α/γ dephosphorylates the CARDs of both RIG-I and MDA5 (Wies et al., 2013), which, on RIG-I, opens up the binding site for the E3 ubiquitin ligase TRIM25. TRIM25 binds RIG-I via its C-terminal SPRY domain and promotes K63-polyubiquitionation of the second CARD of RIG-I at K172, which appears to be necessary for CARD-CARD interactions with MAVS (Gack et al., 2007). For MDA5, TRIM65 binds via its SPRY domain and K63-polyubiquitinates the helicase domain of MDA5 at position K743 (Lang et al., 2017).

Upon activation, the RLRs translocate to mitochondria and mitochondrial-associated membranes where they interact with the essential adaptor protein mitochondrial antiviral signaling (MAVS; also known as IPS-1, VISA, Cardif) (Horner et al., 2011; Liu et al., 2012) via binding of the RLR CARDs with a CARD region on MAVS. MAVS must also be post-translationally modified to attain an activated state - it is phosphorylated by TBK1 (Liu et al., 2015). Binding of RIG-I or MDA5 to MAVS triggers the formation of a signaling synapse that recruits adaptor proteins (TRAF3, TRAF6), kinases (TBK1, IKKε), and transcription factors (IRF-3, NF-κB) (Horner et al., 2011; Liu

et al., 2012) resulting in the formation of the canonical IFN-β enhanceosome complex that promotes IFN-β transcription. Subsequent type I IFN signaling through the JAK-STAT pathway rapidly induces expression of hundreds of IFN-stimulated genes (ISGs), which restrict virus infection and replication through direct effector functions (reviewed in (Schoggins and Rice, 2011)).

The differences in RNA ligand binding specificity allow RIG-I and MDA5 to recognize different virus families with varying viral RNA genome characteristics. For instance, RIG-I is known to recognize viral RNA from Paramyxoviridae (e.g. Sendai virus [SeV], measles virus, Newcastle disease virus [NDV]), Rhabdoviridae (e.g. vesicular stomatitis virus [VSV]), Orthomyxoviridae (e.g. influenza), and Flaviviridae (e.g. hepatitis C virus [HCV]) among others, while MDA5 has been shown to recognize viral RNA from Picornaviridae (e.g. encephalomyocarditis virus [EMCV], Mengo virus) (Reviewed in (Loo and Gale, 2011)). Both RIG-I and MDA5 play a role in recognizing and responding to viral RNA from other members of the Flaviviridae family (e.g. dengue virus [DENV], West Nile virus [WNV], Japanese encephalitis virus [JEV]) and Reoviridae (e.g. reovirus) (Reviewed in (Loo and Gale, 2011)).

Additional studies have suggested that the RLRs recognize infection by viruses with DNA genomes as well. For example, Samanta and colleagues demonstrate RIG-I signaling in response to small, untranslated dsRNAs produced by Epstein-Barr virus (EBV; Herpesviridae; dsDNA genome) during latent infection, and these dsRNAs pull down with RIG-I, indicating binding by RIG-I (Samanta et al., 2006). RIG-I was also shown to play a key role in inducing IFN-β- and TNF-driven antiviral responses to Myxoma virus (Poxviridae; dsRNA genome) (Wang et al., 2008). Similarly, MDA5 was pulled down with dsRNA intermediates of vaccinia virus (Poxviridae; dsRNA genome) and was required for antiviral responses to vaccinia virus and modified vaccinia virus Ankara (Delaloye et al., 2009; Pichlmair et al., 2009). Other groups have suggested that,

instead of recognizing RNA replication intermediates of DNA viruses directly, RIG-I recognizes 5'-triphosphorylated dsRNAs (5'-ppp dsRNA) produced by DNA-dependent RNA polymerase III (Pol-III) from the viral DNA genomes (Ablasser et al., 2009; Chiu et al., 2009). Pol-III produces 5'-ppp dsRNAs from the extracellular DNA ligand poly(dA-dT), as well as from herpes simplex virus 1 (HSV-1) and EBV. 5'-ppp dsRNA acts as a RIG-I agonist and results in RIG-I-mediated antiviral signaling (Ablasser et al., 2009; Chiu et al., 2009).

Furthermore, this may hold true for the DNA genomes of intracellular bacteria as RLRs have been implicated in initiating immune responses to *Legionella pneumophila* and *Listeria monocytogenes* (Chiu et al., 2009; Pollpeter et al., 2011). Bone marrow-derived macrophages (BMDMs) from $MAVS^{-/-}$ mice had strikingly reduced IFN-β transcription during infection with *L. pneumophila* compared to wild type (WT) BMDMs, suggesting that the RLRs are involved in the innate immune response to this bacterial pathogen. Additionally, treatment of Raw264.7 macrophages with a Pol-III inhibitor reduced *L. pneumophila*-induced IFN-β transcript levels and led to increased bacterial replication indicating that Pol-III is required for RLR-mediated control of *L. pneumophila* infection (Chiu et al., 2009). Upon infection with *L. monocytogenes*, $LGP2^{-/-}$ mouse embryonic fibroblasts (MEFs) induced significantly less IFN-β and CXCL10 compared to WT MEFs. Transcript levels of IL-6 and CCL5 were also depressed in $LGP2^{-/-}$ MEFs at later time points post-infection (Pollpeter et al., 2011). These findings suggest that here too the RLRs play a role in the response to the DNA PAMPs of bacterial pathogens.

Function of LGP2

RLR signaling is tightly regulated to achieve an orchestrated response aimed at maximizing antiviral immunity and minimizing immune- or nonimmune-mediated collateral damage. To achieve an appropriately balanced response, downregulation of

antiviral signaling is equally important to its activation. LGP2, the third member of the RLR family, is a known regulator of both RIG-I and MDA5.

LGP2 was initially believed to negatively regulate RIG-I and MDA5 (Rothenfusser et al., 2005; Yoneyama et al., 2005). However, these studies were performed prior to the discovery that RIG-I and MDA5 recognize and respond to different viruses (reviewed in (Loo and Gale, 2011)). The results from these initial studies showed that LGP2 can inhibit SeV- and NDV-induced IFN-β promoter activity. Both SeV and NDV are now known to be recognized preferentially by RIG-I; so while these early studies suggest that LGP2 negatively regulates RIG-I-mediated signaling, the same may not be true for MDA5-dependent signaling. Indeed in a later study, Venkataraman and colleagues describe disparate phenotypes during infection with different viruses (Venkataraman et al., 2007). In MEFs infected with VSV, a RIG-I-targeted virus, type I IFN mRNA and protein levels were elevated in LGP2$^{-/-}$ cells compared to WT controls, suggesting a negative regulatory role for LGP2 during RIG-I signaling. Additionally, VSV-infected LGP2$^{-/-}$ mice exhibited enhanced survival and lower viral titers in the brain compared to WT mice. In contrast, macrophages and DCs infected with EMCV, an MDA5-targeted virus, showed reduced IFN-β production in the absence of LGP2. LGP2$^{-/-}$ mice infected with EMCV exhibited reduced survival compared to WT controls, suggesting a positive regulatory role for LGP2 during MDA5 signaling (Venkataraman et al., 2007).

It was subsequent demonstrated that LGP2 potentiates MDA5 signaling by binding MDA5-targeted RNA ligands. LGP2 ATP hydrolysis enhances the affinity of LGP2 for dsRNA substrates and diversifies the range of dsRNA structures that LGP2 can recognize and bind (Bruns et al., 2013). This ATP hydrolysis activity of LGP2 increases the rate at which MDA5 binds RNA ligands (Bruns et al., 2014), and stabilizes MDA5 affinity for stimulatory RNA which subsequently enhances innate antiviral signaling (Bruns et al., 2014; Bruns et al., 2013; Childs et al., 2013). However, the

precise link between ATP hydrolysis-enhanced LGP2 RNA binding, and the following LGP2-mediated upregulation of MDA5 RNA binding has yet to be elucidated. In this context, the ability of LGP2 to modulate MDA5 function appears to depend on intracellular expression levels - in human embryonic kidney 293T (HEK293T) cells stimulated with either poly(I:C) or EMCV, low levels of LGP2 potentiate MDA5 activation whereas high levels of LGP2 inhibit MDA5 activation (Bruns et al., 2014; Bruns et al., 2013). However, these findings have only been demonstrated through ectopic expression of LGP2 and have not been corroborated with endogenous LGP2 during virus infection.

The role of LGP2 in regulating RIG-I-mediated signaling is less well understood, and there are studies supporting both positive and negative regulatory functions. One study found that, in the absence of LGP2, IFN-β production by bone marrow-derived dendritic cells (BM-DCs) was diminished upon infection with MDA5-targeted viruses (i.e. EMCV and Mengo virus), RIG-I-targeted viruses (i.e. SeV and VSV), and viruses targeted by both MDA5 and RIG-I (i.e. JEV and reovirus), suggesting a positive regulatory role for LGP2 in both MDA5 and RIG-I signaling (Satoh et al., 2010). However, the RIG-I virus phenotype was not investigated further, and it should be noted that the LGP2$^{-/-}$ mice generated for these studies incurred some seemingly genetics-related health issues. In another study, Suthar and colleagues observed that upon infection with pathogenic WNV, LGP2$^{-/-}$ MEFs, as well as DCs and macrophages, all exhibited decreased IFN-β protein production compared to WT controls (Suthar et al., 2012b). Complementarily, higher virus replication was seen in LGP2$^{-/-}$ DCs and macrophages compared to WT cells. LGP2$^{-/-}$ mice exhibited increased mortality over WT mice upon WNV infection and higher viral loads were found in the brains of mice lacking LGP2, similarly suggesting a positive regulatory role for LGP2. However, the authors concede that the effects of LGP2 appear to be limited in this context as peripheral innate

immune responses were comparable between LGP2$^{-/-}$ and WT mice. It should also be noted that both RIG-I and MDA5 are important for the antiviral response to WNV (Fredericksen et al., 2008), which may confound conclusions from this study about the role of LGP2 in regulating RIG-I-specific signaling.

Another study suggests that LGP2 is required for adequate responses to DNA PAMPs (Pollpeter et al., 2011). LGP2$^{-/-}$ MEFs and BMDMs transfected with poly(dA-dT), a dsDNA ligand, or infected with *Listeria monocytogenes*, an intracellular bacterial pathogen, exhibited reduced IFN-β and pro-inflammatory cytokine transcription, and decreased IFN-β protein secretion. *In vivo*, LGP2$^{-/-}$ mice (Venkataraman et al., 2007) showed increased colonization of the liver and spleen by *L. monocytogenes* compared to WT controls (Pollpeter et al., 2011). Antiviral responses to modified vaccinia virus Ankara (MVA), a poxvirus with a dsDNA genome, were also suppressed in LGP2$^{-/-}$ MEFs (Pollpeter et al., 2011). In this case, it should be noted that MVA has been shown to be preferentially recognized by MDA5 (Delaloye et al., 2009) and as LGP2 is a positive regulator of MDA5 signaling activity it is not surprising that antiviral responses would be depressed in the absence of LGP2. As the non-coding RNAs generated by Pol-III are generally between 100-1500 nucleotides in length (Lesniewska and Boguta, 2017; Olivas et al., 1997), placing them within the size range preferentially recognized by RIG-I (<2kb), this may support the direct recognition of longer RNA replication intermediates by MDA5, which would make LGP2 a necessary part of the innate immune response to dsDNA-containing pathogens.

In other cases, LGP2 appeared to have little to no effect on the innate response to virus infection. While Suthar and colleagues demonstrated that WNV infection of LGP2$^{-/-}$ MEFs, DCs and macrophages resulted in a slight decrease of IFN-β production compared to WT cells, there was no difference in downstream ISG induction (Suthar et al., 2012b). Satoh and colleagues also showed a negligible difference in IFN-β

production by Lgp2$^{-/-}$ BM-DCs following influenza virus (PR8 ΔNS1) infection (Satoh et al., 2010), another RIG-I-targeted virus. However, another group observed that infection of Lgp2$^{-/-}$ MEFs with a human seasonal H3N2 influenza virus resulted in enhanced IFN-β transcription compared to WT MEFs (Malur et al., 2012), suggesting negative regulation by LGP2. Complementary to this finding, Si-Tahar and colleagues demonstrated a decrease in type I IFN and pro-inflammatory mediators during infection with H3N2 in mice overexpressing human LGP2 (Si-Tahar et al., 2014). Additionally, infection with seasonal H1N1 viruses that activate IRF3, but not those that avoid activation of IRF3, also resulted in increased IFN-β transcription (Malur et al., 2012). H1N1 viruses that do not activate IRF3 showed no difference in induction of IFN-β mRNA in WT and Lgp2$^{-/-}$ MEFs.

Several other studies support LGP2 as a negative regulator of RIG-I signaling. Three distinct mechanisms have been proposed for how LGP2 inhibits RIG-I signaling: (i) LGP2 binds to and sequesters RIG-I ligands. In this model, LGP2 would compete for RIG-I stimulatory RNAs, leading to reduced RIG-I activation (Rothenfusser et al., 2005; Yoneyama et al., 2005). While plausible, recent evidence suggests that LGP2 inhibits RIG-I signaling independently of its ability to bind RNA, as mutations within LGP2 that ablate RNA binding and ATP hydrolysis were shown to have no effect on its capacity to inhibit RIG-I in human 2fTGH cells infected with SeV (Bamming and Horvath, 2009). (ii) The CTD of LGP2 blocks RIG-I activation. In this model, it is believed that the CTD of LGP2 interacts with the helicase domain of RIG-I to inhibit downstream signaling (Saito et al., 2007). This hypothesis is based on amino acid sequence homology between the LGP2 and RIG-I CTDs, as the CTD of RIG-I has an auto-regulatory function through its interaction with the N-terminal CARDs. In support of this idea, the LGP2 CTD associates with RIG-I in Huh7 cells (human hepatocyte-derived cellular carcinoma line). Nonetheless, other studies have shown that the helicase domain of LGP2 also may be

necessary for its full regulatory activity (Pippig et al., 2009), and that LGP2 may not even interact directly with RIG-I (Rothenfusser et al., 2005). (iii) LGP2 binds to an activation region within MAVS. Komuro and colleagues found that, in HEK293T cells, LGP2 competes for binding to MAVS with IKKε, a key kinase for activating NF-κB (Komuro and Horvath, 2006). However, subsequent studies have questioned this model as IKKε may not directly bind MAVS, but rather associate indirectly through NEMO or TANK (Guo and Cheng, 2007; Zhao et al., 2007). Furthermore, LGP2 is now known to differentially regulate RIG-I and MDA5 (Venkataraman et al., 2007), and inhibiting signaling at the level of MAVS might be expected to have a similar effect on both RIG-I- and MDA5-mediated signaling. Thus, despite significant effort from multiple groups, the molecular mechanism underlying the negative regulation of RIG-I by LGP2 remains uncertain.

The variable phenotypes surrounding LGP2 function may be complicated by the fact that LGP2 has been implicated in several non-canonical pathways, including $CD8^+$ T cell fitness, cancer cell survival, and regulation of RNA interference (RNAi) (Komuro et al., 2016; Suthar et al., 2012b; van der Veen et al., 2018; Widau et al., 2014). Suthar and colleagues found that LGP2 was required for $CD8^+$ T cell survival and fitness during WNV infection of mice (Suthar et al., 2012b). Antigen-specific $CD8^+$ T cells from $LGP2^{-/-}$ mice infected with either WNV or lymphocytic choriomeningitis virus (LCMV)-Armstrong showed a decrease in numbers due to elevated frequency of apoptosis compared to cells from WT controls. $LGP2^{-/-}$ $CD8^+$ T cells from the spleens of infected mice also exhibited reduced secretion of IFN-γ and TNF-α. It was determined that LGP2 increases antigen-specific CD8+ T cell sensitivity to the CD95-mediated apoptosis pathway (Suthar et al., 2012b).

LGP2 has also been implicated in the survival of several cancer cell lines, including colorectal adenocarcinoma (WiDr cell line), head and neck squamous cell carcinoma (Scc61 cell line), and glioblastoma (D54 cell line) (Widau et al., 2014). siRNA

depletion of LGP2 in these cells reduced survival upon treatment with ionizing radiation (IR), whereas over-expression of LGP2 increased cancer cell survival of IR. IR treatment induces IFN-β gene expression and IFN-β protein was found to be cytotoxic to cancer cells. Mechanistically, LGP2 appears to negatively regulate IR-induced IFN-β production, thus increasing cell survival (Widau et al., 2014).

Recently, a role for LGP2 was discovered in the inhibition of the RNAi response within mammalian cells (Komuro et al., 2016; van der Veen et al., 2018). LGP2 was found to interact with several components of the RNAi machinery, including the TAR-RNA binding protein (TRBP) (Komuro et al., 2016) and the endoribonuclease Dicer (van der Veen et al., 2018). During virus infection, Dicer is responsible for cleaving viral dsRNA into small interfering RNAs (siRNAs). These siRNAs become part of the RNA-induced silencing complex (RISC) and target RISC cleavage activity to their complementary viral RNAs. However, in the presence of LGP2, Dicer activity was inhibited both *in vitro* and within MEF cells and production of siRNA was reduced (van der Veen et al., 2018).

Introduction to Zika virus

Zika virus (ZIKV) is a member of the *Flaviviridae* family, flavivirus genus, along with WNV, DENV, JEV, and yellow fever virus (YFV), among others. The viral genome is positive-sense, single-stranded RNA (ssRNA; 11kb) that, upon infection, is translated into a single polyprotein. The polyprotein is cleaved by both virus- and host-derived proteases into three structural proteins – capsid (C), membrane (M), and envelope (E) – which comprise the outer structure of the virus particle, and seven non-structural (NS) proteins – NS1, NS2a, NS2b, NS3, NS4a, NS4b, and NS5 – which function in viral replication, assembly and antagonism of host immune responses. ZIKV is most commonly spread by the bite of infected mosquitoes, with *Aedes* spp. considered to be

the primary vectors (Haddow et al., 1964; Marchette et al., 1969; Weaver et al., 2016). ZIKV is thought to circulate in a sylvatic cycle between mosquitoes and non-human primates, but can also circulate in an urban cycle between mosquitoes and humans. Unlike other flaviviruses, there have also been reported instances of ZIKV sexual transmission and vertical transmission from mother to child in utero (Besnard et al., 2014; Brasil et al., 2016a; Foy et al., 2011; McCarthy, 2016; Musso et al., 2015b; Noronha et al., 2016). In adults, the majority of ZIKV infections (~80%) are asymptomatic. In symptomatic cases, illness is normally mild and is characterized by fever, headache, joint and muscle pain, conjunctivitis, and rash, which normally resolve within seven days (Lazear and Diamond, 2016). However, in some cases, ZIKV can result in more severe neurological sequelae (Brasil et al., 2016c). ZIKV has also been implicated as a causative agent of infant microcephaly and may be responsible for neurodevelopmental issues in children who were infected in utero (Delaney et al., 2018; Rasmussen et al., 2016; van der Linden et al., 2016).

ZIKV was originally isolated from a rhesus macaque in the Ziika forest of Uganda in 1947 (Dick et al., 1952). The first confirmed human case of ZIKV was described in 1954 in Nigeria (Macnamara, 1954), but human outbreaks of ZIKV were relatively small and infrequent until 2007. In the spring of 2007 a large outbreak occurred in the Federated States of Micronesia on the island of Yap (Duffy et al., 2009). Then in 2013, another large outbreak occurred in French Polynesia, which correlated with an increase in cases of Guillain-Barre syndrome (Cao-Lormeau et al., 2016; Oehler et al., 2014), an autoimmune disorder wherein the immune system damages peripheral nerves, resulting in widespread muscle weakness. ZIKV emerged in Brazil in 2015 (Campos et al., 2015; Zanluca et al., 2015) and rapidly spread to multiple other countries in South and Central America and the Caribbean (Musso and Gubler, 2016). It was during this epidemic that the association between ZIKV and microcephaly in newborns was described and

confirmed. ZIKV RNA was detected in the amniotic fluid of three women whose fetuses developed microcephaly (Calvet et al., 2016; Sarno et al., 2016). Brain tissue from fetuses and newborns with microcephaly born to mothers who reported ZIKV infection during pregnancy were also positive for ZIKV RNA (Driggers et al., 2016; Martines et al., 2016; Mlakar et al., 2016; Noronha et al., 2016; Sarno et al., 2016). In one case, viral particles were detected and infectious virus was isolated from fetal brain tissue (Driggers et al., 2016). Studies examining cohorts of pregnant women during this outbreak observed that a significantly higher number of ZIKV-infected mothers delivered infants with microcephaly or other brain abnormalities compared to non-ZIKV-infected mothers, indicating trans-placental transmission of ZIKV from mother to fetus (Brasil et al., 2016a; Hoen et al., 2018; Honein et al., 2017; Noronha et al., 2016).

Excluding the observed eccentricities of ZIKV sexual and vertical transmission, much about the virus infection cycle within the host has been presumed based on what is known about the tropism and virus-host interactions of other, related flaviviruses. However, considering ZIKV has already displayed several apparently unique characteristics, it is important to evaluate ZIKV-specific cellular targets of infection, host immune responses, and mechanisms of antiviral antagonism. It is also important to define the mechanisms of ZIKV trans-placental transmission, as ZIKV infection of the developing fetus is responsible for the most concerning outcomes of ZIKV infection.

Flavivirus innate immunology

Flaviviruses are known to initially target tissue-resident DCs and macrophages, such as Langerhans cells and dermal DCs within the skin (Suthar et al., 2013b). DCs and macrophages are essential innate immune cells that orchestrate the primary innate immune response, and prime the secondary adaptive immune response (T and B cells). These cells traffic to the draining lymph nodes, allowing the virus to infect more DCs,

and from there travel to the spleen. Flaviviruses typically proliferate to high levels in splenocytes, resulting in viremia. Once the virus has entered the blood stream it can travel to and infect additional tissues, depending on the cell/tissue tropism of the virus. Several flaviviruses, such as WNV and JEV are neurotropic, and can infect the cells comprising the central nervous system (CNS).

It seems likely that ZIKV also targets DCs and macrophages for initial infection upon transmission to a human host. Hamel and colleagues demonstrated infection of primary human immature DCs with a low-passage ZIKV strain from French Polynesia (PF-25013-18), and another group demonstrated ZIKV (PRVABC59) infection of human monocyte-derived macrophages (Hamel et al., 2015; Van der Hoek et al., 2017). Additionally, both African (MR766) and Asian (PRVABC59) lineage viruses productively infected the THP-1 monocytic cell line (Hou et al., 2017). However, overall there is a dearth of data regarding the infection of innate immune cells, such as DCs and macrophages, and the cellular subtypes that are permissive to ZIKV.

Similar to other flaviviruses, ZIKV replication was detected in lymph nodes and spleens of rhesus macaques infected with ZIKV GZ01/2016 strain, and in spleens of owl monkeys infected with ZIKV Mex_1_44 strain (Li et al., 2016b; Vanchiere et al., 2018). ZIKV RNA has also been detected in the spleens of mice lacking the IFN-α/β receptor (Dowall et al., 2016; Lazear et al., 2016; Rossi et al., 2016). ZIKV is also able to productively infect in vitro-differentiated human neural progenitor cells (hNPCs), though further differentiated immature neurons were less susceptible to infection (Garcez et al., 2016; Tang et al., 2016). Three-dimensional neurospheres, representing the early stages of neurogenesis, and brain organoids, representing the environment of first-trimester fetal brain development, differentiated from NPCs were also infected by ZIKV (MR766) (Garcez et al., 2016). Additionally, in three cases of pregnant women with ZIKV infection, glial cells in brain tissues from three newborns who died shortly after birth were

positive for ZIKV E protein by immunohistochemistry (IHC) staining and ZIKV RNA by RT-PCR (Noronha et al., 2016). ZIKV may also infect cells within the placenta. ZIKV RNA and viral protein were detected in placental tissues from infected mothers, specifically within placental macrophages (Martines et al., 2016; Noronha et al., 2016). Additionally, human trophoblast-derived cell lines have been shown to be susceptible to ZIKV (MR766 and FSS13025 strains) infection (Bayer et al., 2016). Several other studies have demonstrated ZIKV infection of other tissues as well, including the eyes, vagina and testes (reviewed in (Miner and Diamond, 2017)).

Several studies suggest that viral entry is mediated by AXL, DC-SIGN, or Tyro3. Expressing these surface proteins on non-permissive HEK293T cells allowed ZIKV infection (Hamel et al., 2015; Liu et al., 2016). Conversely, in A549 cells and human umbilical vein endothelial cells (HUVECs), knockdown of endogenous AXL or blocking the receptor with an anti-AXL antibody inhibited ZIKV infection of these cells. It was also observed that levels of AXL expression on the surface of several endothelial cell lines positively correlated with levels of ZIKV infection (Liu et al., 2016). However, genetic ablation of AXL in neural progenitor cells (NPCs) had no effect on levels of ZIKV infection or cell viability (Wells et al., 2016). Similarly, $AXL^{-/-}$ cerebral organoids experienced similar levels of growth restriction upon ZIKV infection as WT organoids, indicating that AXL is not an important viral entry factor on these cells. The authors instead suggest a role for Tyro3, as this receptor is also highly expressed on NPCs, though DC-SIGN and TIM-1 are not. These discrepancies highlight the importance of defining the cellular tropism of ZIKV, as the shared and unique characteristics of different cells types will help define the mechanisms of ZIKV infection. There is a need for additional studies to evaluate the ZIKV infection of innate immune cells, particularly DC and macrophage subtypes, as these are likely key targets of ZIKV infection. The

cellular receptors that aid ZIKV binding and entry of DCs and macrophages are also still unknown, but their discovery may help clarify the host cell markers utilized by ZIKV.

Once inside a cell, flaviviruses replicate within the cytosol where the viral RNA is recognized by cytosolic PRRs such as the RLRs. As described in detail above, RLR signaling results in the production of type I IFN. Secreted type I IFN can bind the IFN-α/β receptor 1 (IFNAR1) on the surface of adjacent cells and initiate downstream signaling though the JAK/STAT pathway. Janus kinase 1 (JAK1) and tyrosine kinase 2 (TYK2) associate with the intracellular domain of IFNAR1. Upon binding of IFN-α/β, JAK1 and TYK2 are phosphorylated, and in turn phosphorylate signal transducer and activator of transcription 1 and 2 (STAT1 and STAT2), which form a heterodimer and interact with interferon regulatory factor 9 (IRF9). The transcription complex translocates to the nucleus and induces expression of hundreds of ISGs and other antiviral effector genes, which help control infection and prevent viral spread (Suthar et al., 2013b).

Few studies have explored the innate immune responses to ZIKV in detail. In humans it appears that ZIKV infection can induce a pro-inflammatory response characterized by elevated protein levels of multiple cytokines and chemokines, including IL-6, IL-1β, IP-10 (CXCL10), RANTES (CCL5), MIP-1α, MIP-1β, and IFN-γ (Tappe et al., 2016). However, this is a limited analysis of six patients and the cell populations responsible for these responses are still poorly defined. In vitro studies using human primary cells and transformed cell lines have determined that ZIKV infection results in increased transcription of type I, II, and III IFN and other antiviral effector genes in a cell type-specific manner. Some cells exhibit potent innate immune responses to ZIKV while others generate only poor antiviral responses. Hamel and colleagues described the induction of mRNA expression for PRRs (*Tlr3*, *Ifih1* [MDA5], *Ddx58* [RIG-I]), transcription factors (*Irf7*), type I IFNs (*Ifnα*, *Ifnβ*), pro-inflammatory cytokines (*Il6*, *Cxcl10*, *Ccl5*), and ISGs (*Isg15*, *Oas2*, *Mx1*) in ZIKV-infected primary human skin fibroblasts (Hamel et al.,

2015), but protein production/secretion was not quantified. TLR3, MDA5, and RIG-I were shown to be important for limiting viral infection by siRNA knockdown in human foreskin fibroblast (HFF1) cells, and pre-treatment of primary skin fibroblasts with type I (IFN-α, IFN-β) or type II (IFN-γ) IFN reduced ZIKV replication in a dose-dependent manner. In contrast, subsequent work in JEG-3 cells (human trophoblast choriocarcinoma cell line) found that IFN-γ treatment enhanced ZIKV (PRVABC59) replication (Chaudhary et al., 2017). Infection of A549 cells (human lung carcinoma epithelial cell line) with ZIKV (PF-25013-18) resulted in elevated *Ifnβ* transcripts, as well as transcription factors (*Irf3*, *Irf7*), pro-inflammatory cytokines (*Il6*, *Il1β*, *Mcp1*), and ISGs (*Ifit1*, *Ifit2*) (Frumence et al., 2016). IFN-β and IL-6 secretion into the supernatant was also higher in ZIKV-infected cells. Additionally, pre-treatment of A549 cells with IFN-β reduced levels of ZIKV infection. Another study observed that Huh7 (human liver epithelial cell line), HTR8/SVNeo (extravillious trophoblast cell line), and JEG-3 cells have attenuated IFN-β and ISG (*Isg15*, *Oas1*, *Mx1*, *Ifitm1*) mRNA expression upon infection with ZIKV (MR766) (Van der Hoek et al., 2017). Monocyte-derived macrophages had moderate increases in IFN-β and ISG transcription.

In neuronal and placental cells, antiviral responses again vary based on cell type. Several studies describe delayed or attenuated signaling activation in neuronal cells. For example, mouse neural progenitor cells (mNPCs) exhibited delayed transcription of *Ifnβ*, *Ifit1*, *MxA*, and *viperin* during infection with ZIKV MR766 or PRVABC59 (Van der Hoek et al., 2017). Another group failed to detect a cytokine response in human fetal neural progenitor cells (hNPCs) at either the mRNA or protein level upon infection with ZIKV PRVABC59 (Hanners et al., 2016). Notably, one study observed ZIKV infection of in vitro-derived cranial neural crest cells (CNCCs) which, while producing an underwhelming IFN response (low IFN-α, β, γ), elicited secretion of several pro-inflammatory cytokines that had detrimental effects on the morphology and survival of

NPCs (Bayless et al., 2016). Bayer and colleagues found that primary human trophoblast (PHT) cells, which form the outer layers of the placenta, constitutively secrete IFN-λ1 and that the supernatant can protect human brain microvascular endothelial cells (HBMECs) from infection with both African (MR766) and Asian (FSS13025) lineage ZIKV strains (Bayer et al., 2016). PHT supernatants can also induce ISG production in other cell types, including 2fTGH (human fibrosarcoma cell line) and THP-1 cells. PHTs naturally differentiate into fused syncytiotrophoblasts, and this differentiation and fusion was found to be necessary for the production of IFN-λ1. It is thought that the constitutive secretion of IFN-λ1 is one of the primary reasons syncytiotrophoblasts are highly resistant to infection by ZIKV and other viruses (Bayer et al., 2016; Delorme-Axford et al., 2013).

Savidis and colleagues found a specific role for interferon-inducible transmembrane protein 1 and 3 (IFITM1 and IFITM3) in restricting ZIKV replication (Savidis et al., 2016). IFITM3 or IFITM1 overexpression in HeLa cells (human cervical carcinoma cell line) decreased ZIKV (MR766) infection, whereas shRNA knockdown of IFITM3 increased ZIKV infection. Mechanistically, IFITM3 appears to block ZIKV entry into HeLa cells. Viperin (RSAD2) has also been implicated in the inhibition of ZIKV replication. Huh7 cells overexpressing viperin were able to prevent replication of ZIKV MR766, as cells positive for both viperin expression and ZIKV antigen did not co-localize by immunofluorescence microscopy assay (IFA) (Van der Hoek et al., 2017). Additionally, viperin$^{-/-}$ MEFs exhibited higher levels of infection and a significant increase in ZIKV NS4b protein expression. A later study found that viperin interacts with the ZIKV NS3 protein in HEK293T cells when NS3 is exogenously expressed (Panayiotou et al., 2018). Mechanistically, viperin reduces the stability of NS3 by mediating its degradation by the proteasome.

Additional support for the importance of IFN signaling in controlling ZIKV infection comes from models in which IFN signaling is genetically ablated. Indeed, immunocompetent mice exhibit no symptoms of disease (Dowall et al., 2016; Lazear et al., 2016; Rossi et al., 2016). Only those deficient in IFN signaling, such as IFNAR$^{-/-}$ or IRF3$^{-/-}$ IRF5$^{-/-}$ IRF7$^{-/-}$ triple knockout (TKO) mice (Lazear et al., 2016), or A129 mice which lack type I IFN receptors (Dowall et al., 2016; Rossi et al., 2016), develop disease symptoms and enhanced mortality. AG129 mice, which lack receptors for both type I and type II IFN, were also highly susceptible to ZIKV (Dakar-41519 or H/PF/2013) infection and exhibited high mortality (Aliota et al., 2016; Lazear et al., 2016). Treatment of WT mice with an IFNAR1 blocking antibody prior to ZIKV (H/PF/2013) infection resulted in higher viral loads in the serum, but no weight loss or mortality (Lazear et al., 2016). Notably, mice lacking only a single antiviral signaling component (e.g. MAVS$^{-/-}$, IRF3$^{-/-}$, IFITM3$^{-/-}$) were phenotypically the same as WT mice upon infection with ZIKV Dakar strains (41519, 41667, 41671), with no morbidity or mortality.

Naturally, flaviviruses have developed a multitude of mechanisms for evading and antagonizing the innate immune response (Miorin et al., 2017). ZIKV also appears to have multiple mechanisms for inhibiting both IFN production and downstream IFN signaling. ZIKV (PLCa1 strain) infection of A549 cells led to inhibition of poly(I:C)-stimulated IFN-β promoter activity and *Ifnβ* gene expression (Kumar et al., 2016). This inhibition was attributed to ZIKV NS1, NS4a and NS5. IFIT1 promoter activity and *Ifit1* gene expression were also inhibited by ZIKV infection. ZIKV reduced induction of *Ifit1* transcription by type I (IFN-α) and type III (IFN-λ) IFNs, but was unable to inhibit induction by type II IFN (IFN-γ). It was discovered that overexpressed ZIKV NS5 interacts with the host STAT2 protein and mediates STAT2 degradation by the proteasome (Grant et al., 2016; Kumar et al., 2016). STAT2 protein expression was similarly reduced upon infection of Vero cells with ZIKV. No interaction was detected

between ZIKV NS5 and STAT1 in these studies and STAT1 protein levels were unaffected. Notably, ZIKV NS5 also failed to interact with murine STAT2, and STAT2 protein expression was unaffected in ZIKV-infected MEFs. Wu and colleagues described roles for ZIKV NS1, NS4b, and NS2b3 as well (Wu et al., 2017). Overexpression of NS1 or NS4b alone in HEK293T cells inhibited IFN-β promoter activity induced by poly(I:C) or SeV infection, and *Ifnβ* gene expression was reduced. NS1 and NS4b were found to interact with TBK1 and prevent TBK1 phosphorylation and oligomerization. However, infection with intact ZIKV was not used to confirm these observations. It was also shown that ZIKV infection of A549 cells resulted in reduced phosphorylation of JAK1 and STAT1, and that overall protein levels of JAK1 were reduced, though there was no effect on STAT1 protein. This was attributed to ZIKV NS2B3 which binds to JAK1 when overexpressed in HEK293T cells and promotes JAK1 proteasomal degradation.

Much has been learned about ZIKV virology, pathogenesis and immunology since 2015. However, there are still many gaps in our knowledge. More studies are needed to determine the range of cell types and tissues susceptible to ZIKV infection and to evaluate innate immune responses within these cells. Ideally, the focus should be on those tissues that are known to harbor virus during a natural infection. There is also a need to further define the host restriction factors responsible for directly controlling ZIKV infection and replication within the cell, and the viral factors that oppose these host defenses. Studies performed in primary cells or in vivo in animal models will be particularly valuable and protein overexpression studies should be validated by virus infection where possible.

Potential impact of cross-reactive flavivirus antibodies

Another important facet of flavivirus immunity is the humoral response. Most flavivirus infections induce potent antibody responses that provide long lasting immunity to

subsequent infection with the same virus. One notable exception is DENV. DENV exists in nature as four distinct serotypes (DENV1, 2, 3, and 4), which display different viral antigens. Thus, infection with one serotype does not necessarily confer complete humoral immunity to infection with a second serotype (Katzelnick et al., 2017; Sangkawibha et al., 1984). In fact, it has been hypothesized that pre-existing immunity to one DENV serotype may actually increase the risk of developing dengue shock syndrome (DSS) or dengue hemorrhagic fever (DHF) (Katzelnick et al., 2017; Kliks et al., 1989; Sangkawibha et al., 1984). In this scenario, the secondary DENV infection is similar enough to the initial DENV infection that it induces a memory response, resulting in a skewed production of antibodies specific to the initial virus. While these antibodies can recognize and bind the second DENV serotype, they are either non-neutralizing or the neutralizing antibodies are not present at concentrations needed to potently neutralize the second DENV serotype (Katzelnick et al., 2017). When DENV is bound by these cross-reactive, non-/sub-neutralizing antibodies, these immune complexes can be taken up, through a process termed opsonization, by Fc receptor (FcR)-expressing cells, which are typically found on antigen presenting cells such as DCs and macrophages. This allows the virus to gain entry to the cells and initiate replication (Culshaw et al., 2017). This phenomenon is known as antibody-dependent enhancement of infection (ADE) and is thought to occur through two non-exclusive, broadly defined mechanisms. The first, extrinsic ADE, is an antibody-mediated increase in the number of virus particles that bind and/or enter the cell, enhancing infection on a per cell basis as well as increasing the overall number of infected cells. The second, intrinsic ADE, is a suppression of antiviral signaling facilitated by the antibody binding to the FcRs and inducing signaling pathways that temper antiviral responses within the cell (Flipse et al., 2016; Taylor et al., 2015).

While ADE has been studied in the context the four distinct DENV serotypes, the impact of pre-existing flavivirus immunity on the susceptibility, disease severity and tissue tropism of infection with a subsequent, different flavivirus has not been widely explored. Unlike DENV, the ZIKV strains all appear to belong to a single serotype (Dowd et al., 2016). Serum or plasma from eight confirmed ZIKV-infected patients was able to neutralize both African (MR766) and Asian (H/PF/2013 and Paraiba/2015) strains of ZIKV to similar levels. Similarly, serum from IRF3$^{-/-}$ mice infected with either ZIKV MR766 or ZIKV H/PF/2013 was able to equivalently neutralize reporter virus particles (RVPs) of both MR766 and H/PF/2013. These observations indicate that humoral responses to ZIKV are broadly neutralizing against subsequent ZIKV infections. However, the geographical overlap (Bhatt et al., 2013) and the close phylogenetic similarity between DENV and ZIKV (Lanciotti et al., 2008; Musso and Gubler, 2016) has raised the question of cross-reactive antibodies and whether these would be protective or harmful. Indeed, the E proteins of these viruses, generally considered to contain the immunodominant epitopes for many flaviviruses (Beltramello et al., 2010; Deng et al., 2011; Oliphant et al., 2005; Sultana et al., 2009; Xu et al., 2012), share just over 50% homology (Sirohi et al., 2016). Yet very few studies have evaluated the potential for DENV antibodies that may cross-react with ZIKV and the impact this may have on ZIKV infection.

Dowd and colleagues describe a limited study using reporter virus particles (RVPs) that incorporate the structural proteins from DENV (DENV2 16681) and WNV (NY99) (Dowd et al., 2016). ZIKV immune serum from two human patients was able to neutralize both DENV and WNV RVPs, though less efficiently than ZIKV (H/PF/2013) RVPs. It should also be noted that the ZIKV immune sera were able to more efficiently neutralize DENV RVPs compared to WNV RVPs. This suggests the presence of cross-reactive antibodies that can recognize both ZIKV and DENV structural proteins. Another

group demonstrated that a mouse monoclonal antibody (2A10G6), previously shown to bind and neutralize DENV1-4, WNV, and YFV, binds the ZIKV E protein with high affinity and neutralizes ZIKV (SZ01 strain) (Dai et al., 2016). This antibody was also able to completely protect A129 mice from fatal ZIKV infection. Similarly, two human monoclonal antibodies (EDE1 C8 and EDE1 C10), previously shown to cross-neutralize DENV1-4, were capable of neutralizing ZIKV H/PF/2013 and PRVABC59 strains in U937 cells (Swanstrom et al., 2016). The EDE1 C10 was further found to protect AG129 mice during ZIKV (H/PF/2013) infection. When convalescent-phase DENV-immune sera were tested for ZIKV neutralization, only three out of 17 samples were able to do so. Notably, one of the other monoclonal antibodies tested (EDE2 B7) was able to bind ZIKV H/PF/2013, but not neutralize the virus. However, it was not evaluated whether this antibody or the non-neutralizing sera could conversely enhance ZIKV infection.

In addition to DENV, it may be worthwhile to evaluate the potential effects of cross-reactive antibodies from other flaviviruses such as YFV and WNV, which are also closely related to ZIKV. The ZIKV virion surface has been shown to be similar to that of WNV (Mukhopadhyay et al., 2003), which could generate cross-reactive antibodies that recognize structural epitopes. Non-neutralizing, cross-reactive antibodies may be of particular importance in the context of infection during pregnancy. One of the many roles of the placenta is the transfer of IgG antibodies from the mother to the developing fetus to provide transient, passive immunity. This transfer is mediated by neonatal FcR (FcRn)-expressing cells at the maternal-fetal interface (Simister and Story, 1997).

Biology of the placenta

The placenta is responsible for efficient gas, nutrient, and waste exchange during pregnancy. It also acts as the sole physical and immunological barrier between the maternal blood supply and the fetal compartment. During the first seven days of

pregnancy, a layer of syncytiotrophoblast cells (STBs) forms around the embryo, creating a protective shield that interfaces with the intervillous space. The intervillous space contains a clear fluid for the first few weeks, and contains maternal blood for the duration of pregnancy. The fetal-derived trophoblast progenitor cells that generate the first layer of STBs subsequently form structures called chorionic villi. These consist of a single outer layer of terminally differentiated, fused STBs, and several inner layers of proliferative cytotrophoblasts (CTBs) which help replenish the STB layer. STBs are known to be extremely resistant to infection (Delorme-Axford et al., 2013). Surrounded by the trophoblast layers is the villous stroma, which contains fibroblasts, vascular endothelial cells surrounding the fetal capillaries, and resident macrophages (Hofbauer cells, HCs). There are two types of chorionic villi – floating and anchoring. Floating villi protrude into the intervillous space and are continuously bathed in maternal blood, exposing them to any pathogens that may be present in the maternal circulation. Anchoring villi are formed by CTBs known as extravillous trophoblasts that invade the maternal decidua (maternal-derived placental tissue) and anchor the fetal-derived villi to the uterine wall, putting them in contact with maternal immune cells (reviewed in (Arora et al., 2017; Coyne and Lazear, 2016)). As the fetal-derived cells are semi-allogeneic, the placenta is kept in an immune tolerant state so that the maternal immune system does not attack the developing fetus. This is thought to be achieved by the strict regulation of cytokine and chemokine expression by maternal and fetal cells, which limits both inflammatory responses and maternal lymphocyte access to the placenta (Arora et al., 2017).

While the placenta is largely successful in protecting the developing fetus from infection, some pathogens have found a way to circumvent this barrier, resulting in vertical transmission from mother to fetus. These are known as the TORCH pathogens (*Toxoplasma gondii*, other [e.g. *Listeria monocytogenes*, varicella zoster virus, HIV],

rubella virus, cytomegalovirus, and herpes simplex virus) and are known to cause congenital abnormalities and disease (reviewed in (Coyne and Lazear, 2016)). There are several possible mechanisms by which pathogens could cross the placenta and gain access to the fetal compartment: 1) Ascending infection from the vagina, wherein pathogens infect the epithelial cells of the vagina and spread from cell to cell into the uterus and placental tissues; 2) Physical or immune-mediated damage to the chorionic villi resulting in disruption of the STB layer and exposure of more permissive cells; 3) Infection of maternal endothelial cells within the decidua and subsequent cell to cell spread to the invading fetal extravillous trophoblasts; 4) Infection of maternal immune cells that are then trafficked across the placenta; and 5) Passive transfer across the villi by a transcellular process such as antibody-mediated transcytosis (Coyne and Lazear, 2016).

Some studies have attempted to model ZIKV vertical transmission in mice. One found ZIKV RNA in the placentas of 5/9 mice infected with ZIKV SZ01 (Wu et al., 2016). However, these mice were infected by the intraperitoneal route, which does not recapitulate the normal route of infection for ZIKV. Miner and colleagues demonstrated ZIKV (H/PF/2013) infection of placenta and fetuses in $IFNAR^{-/-}$ mice and WT mice treated with an anti-IFNAR blocking antibody prior to infection (Miner et al., 2016). ZIKV RNA and virions were detected in both maternal and fetal placental tissues, specifically CTBs, suggesting trans-placental transmission. Additionally, both maternal and fetal placental tissues showed signs of damage – apoptotic trophoblasts and reduced microvasculature. However, it should be noted that WT mice exhibited little to no infection of the placenta or fetuses. Yockey and colleagues performed intravaginal infections of ZIKV (FSS13025) and found ZIKV RNA in placentas and fetuses of $IRF3^{-/-}$ $IRF7^{-/-}$ double knockout (DKO) mice and $IFNAR^{-/-}$ mice (Yockey et al., 2016). Again however, no virus was detected in the placentas or fetuses of WT mice, though virus

replication was observed in the vaginal tract. The architecture of the mouse placenta is also quite different from that of the human placenta. Mouse placenta are labyrinthine, to accommodate multiple fetuses at once, and have two layers of STBs and another layer of CTBs that all contact the maternal blood. This, combined with the necessity for the absence of type I IFN signaling, suggests that mice may not be the most reliable model for examining trans-placental transmission of ZIKV.

Maternal IgG antibodies are regularly passed through the placenta during the second and third trimesters to provide passive immunity to the developing fetus. This process of transcytosis is mediated by neonatal Fc receptors (FcRn) on the surface of STBs. Antibodies are bound by the FcRn and enter STBs through endocytosis. They are then released into the villous stroma where they interact with HCs and are likely transported to the fetal capillaries (Simister and Story, 1997; Simister et al., 1996a). As alluded to above, this natural biological process is of particular interest as a potential mechanism of ZIKV vertical transmission. Zika virus has shown the hallmarks of a TORCH pathogen, successfully crossing the placental barrier to infect the developing fetus and causing microcephaly, other fetal developmental defects and even fetal demise (Brasil et al., 2016a; Sarno et al., 2016; Ventura et al., 2016). The recent ZIKV epidemics that have been associated with unusually high occurrence of microcephaly overlap geographically with DENV endemic regions (Bhatt et al., 2013). The high degree of similarity between DENV and ZIKV (~60% amino acid identity) increases the likelihood of cross-reactive antibodies (Sirohi et al., 2016; Ye et al., 2016). Thus, DENV antibodies may bind ZIKV and be transcytosed across the placenta, where ZIKV could then enter the fetal circulation and infect fetal tissues, including neuroprogenitor cells.

RLRs and ZIKV infection

While the RLRs are known to initiate innate immune responses to many flaviviruses (Loo and Gale, 2011), their specific role during ZIKV infection is still obscure. However, considering the efficient attenuation of type I IFN signaling by ZIKV (Grant et al., 2016; Kumar et al., 2016), it seems likely that an IFN-independent antiviral response, potentially mediated by RLR signaling, would be crucial to controlling infection. As such, the regulation of this pathway would be equally important to prevent adverse immune-mediated sequelae. The work presented here provides insight into the molecular mechanisms of RLR signaling regulation, antiviral responses to ZIKV infection, and ZIKV cellular tropism. Specifically, we demonstrate a novel mechanism of LGP2 negative regulation, wherein LGP2 inhibits early RIG-I activation by preventing K63-ubiquitination of the RIG-I N-terminal CARDs through an interaction with the E3 ligase TRIM25. We also evaluate the susceptibility and immune responses to ZIKV infection within human primary monocyte-derived dendritic cells (moDCs), placental macrophages (HCs), and cytotrophoblasts. DCs and HCs, and to a lesser extent CTBs, were found to support productive ZIKV infection. ZIKV induced antiviral gene expression in these cells, but this did not always correspond to increased protein production, particularly in the case of type I IFNs. Indeed, ZIKV was found to potently inhibit type I IFN signaling by inhibiting activation of the transcription factors STAT1/2. In addition, the presence of pre-existing, cross-reactive flavivirus antibodies may further impact the immune responses and tropism of ZIKV. DENV-induced monoclonal antibodies cross-reacted with ZIKV and resulted in attenuated antiviral responses in HCs and enhanced infection of HCs and human placental explant tissues, suggesting a mechanism for the vertical transmission of ZIKV.

Chapter 2: The RNA Helicase LGP2 Negatively Regulates RIG-I Signaling by Preventing TRIM25-mediated CARD Ubiquitination

Kendra M. Quicke[1,2], Kristin Y. Kim[1,2], Curt M. Horvath[3], Mehul S. Suthar[1,2]

[1]Department of Pediatrics, Division of Infectious Diseases, Emory University School of Medicine, Atlanta, GA, USA.

[2]Emory Vaccine Center, Yerkes National Primate Research Center, Atlanta, GA, USA.

[3]Department of Molecular Biosciences, Northwestern University, Evanston, IL 60208, USA.

*Manuscript in preparation.

Introduction

Pattern recognition receptor (PRR) signaling is essential for regulating immune responses to virus infection. The RIG-I-like receptors (RLRs) are a family of cytosolic RNA helicases that, upon recognition of pathogen associated molecular patterns (PAMPs) such as non-self RNAs, trigger a robust antiviral defense response characterized by the production of type I IFN, pro-inflammatory cytokines, and expression of hundreds of antiviral effector genes. The RLRs are comprised of three structurally related proteins: LGP2, RIG-I and MDA5. All three RLRs contain a DExD/H box helicase domain with ATP hydrolysis and RNA binding activities (Bamming and Horvath, 2009; Bruns et al., 2013) and a C-terminal domain (CTD) that aids in RNA substrate recognition and prevents signaling activation (Cui et al., 2008; Saito et al., 2007; Takahasi et al., 2009). RIG-I and MDA5 bind distinct RNA ligands, allowing for recognition of different viruses (Loo and Gale, 2011). Upon binding RNA, RIG-I and MDA5 undergo several post-translational modifications to reach an activated state, including de-phosphorylation by PP1 (Wies et al., 2013), and K63-ubiquitination by TRIM25 in the case of RIG-I (Gack et al., 2007). Once activated, RIG-I and MDA5 translocate to mitochondrial membranes where they interact with mitochondrial antiviral signaling (MAVS), the central RLR signaling adaptor protein, via two N-terminal caspase activation and recruitment domains (CARDs) to initiate downstream signaling.

LGP2 lacks N-terminal CARDs, which are important for mediating signaling activation, but has been identified as both a positive and a negative regulator of RIG-I signaling during virus infection (Rothenfusser et al., 2005; Satoh et al., 2010; Venkataraman et al., 2007). One study found that IFN-β and pro-inflammatory cytokine protein levels were depressed in $Dhx58^{-/-}$ BM-DCs upon infection with a diverse panel of viruses, and that this positive regulation is dependent on the ATP hydrolysis function of LGP2 (Satoh et al., 2010). Others however, have demonstrated a negative regulatory

function of LGP2 in cells infected with HCV or SeV, or treated with poly(I:C) (Saito et al., 2007; Venkataraman et al., 2007; Yoneyama et al., 2005). These conflicting results may arise from the use of Dhx58$^{-/-}$ mice of mixed genetic background, as individual genetics and passenger mutations found within mixed background mice impact immune responses (Querec et al., 2009; Thio, 2008; Vanden Berghe et al., 2015), or the use of non-specific agonists for RIG-I, which decrease the specificity of observed phenotypes. Alternatively, these results could be indicative of a more complex set of roles for LGP2.

Indeed, functions for LGP2 have been described in several non-canonical cellular processes. LGP2 was found to play a role in the inhibition of Dicer-mediated RNA interference (RNAi), a process in which small interfering RNAs (siRNAs) bind and target viral RNA for degradation. Dicer is an endoribonuclease known to generate siRNAs by cleaving viral dsRNA. The CTD of LGP2 interacts with Dicer and prevents Dicer cleavage of dsRNA (Komuro et al., 2016; van der Veen et al., 2018). Additionally, LGP2 has been found to promote CD8+ T cell survival and fitness during virus infection and inhibit apoptosis of cancer cells subjected to ionizing radiation (Suthar et al., 2012b; Widau et al., 2014).

Here, we examine the effects of LGP2 on RIG-I-specific signaling and myeloid cell responses and reveal how LGP2 inhibits RIG-I signaling. We first probed RIG-I signaling in WT and Dhx58$^{-/-}$ BM-DCs using a highly specific and well-characterized RIG-I agonist derived from the 3' untranslated region (UTR) of the HCV genome (PAMP RNA) and compared transcriptional profiles at early times following RIG-I signaling activation (Saito et al., 2008; Schnell et al., 2012). As early as one hour post-treatment, Dhx58$^{-/-}$ BM-DCs displayed a marked increase in the kinetics and magnitude of type I IFN genes as well as a broader antiviral response, characterized by genes encoding pro-inflammatory cytokines, chemokines and ISGs. Using reporter-based assays, we found that LGP2 inhibited RIG-I-mediated IFN-β, interferon regulatory factor 3 (IRF-3) and

nuclear factor-κB (NF-κB) promoter activities, indicating that LGP2 functions upstream of the RLR adaptor protein MAVS. Further, we found that the RNA binding and ATP hydrolysis functions of LGP2 as well as the CTD fragment of LGP2 were dispensable for negatively regulating RIG-I signaling. Full-length LGP2 potently inhibited constitutively active RIG-I, suggesting that LGP2 functions at a point between RIG-I and MAVS on the signaling pathway. Using mass spectrometry, we discovered that LGP2 interacted with TRIM25, an E3 ubiquitin ligase that post-translationally modifies RIG-I into a signaling 'active' form by K63-ubiquitinating the RIG-I CARDs, and this interaction was confirmed at the endogenous level. Finally, we found that LGP2 inhibits TRIM25-mediated K63-ubiquitination of full-length and constitutively active RIG-I. These results demonstrate that LGP2 negatively regulates RIG-I activation by blocking RIG-I ubiquitination and this is critical for dampening RIG-I signaling and antiviral gene expression.

The RLR signaling pathway is essential for promoting antiviral immune responses during virus infection. As such, it is crucial to understand how the RLR pathway is regulated to successfully combat infection, yet prevent cytokine-mediated tissue damage (Clyde et al., 2006; Oldstone and Rosen, 2014; Sun et al., 2012). Understanding the role of LGP2 in attenuating RIG-I signaling will strengthen the platform for studying viral interactions with this pathway.

Methods

Cells. HEK293 cells were maintained in 1x Dulbecco's Modification of Eagle's Medium (DMEM; Corning Cellgro) containing 10% FBS, 25mM HEPES Buffer (Corning Cellgro), 2mM L-glutamine (Corning Cellgro), 1mM sodium pyruvate (Corning Cellgro), 1x Non-essential Amino Acids (Corning Cellgro), and 1x antibiotics (penicillin, streptomycin, amphotericin B; Corning Cellgro). DCs were derived from C57BL6J WT and Dhx58$^{-/-}$ mouse bone marrow cells cultured in 1x RPMI (Corning Cellgro) containing 10% FBS,

2mM L-glutamine, 1mM sodium pyruvate, 1x Non-essential Amino Acids, 1x antibiotics, and 20ng/ml GM-CSF cytokine. Media was changed on days 3 and 6 and cells were harvested on day 8 post-bone marrow extraction.

Plasmids. Plasmids used in these experiments include Flag-RIG-I (pEF-Bos), HA-RIG-I (pEF-Tak), Flag-N-RIG (pEF-Bos), Flag-LGP2 (p3xFLAG-CMV10), Flag-LGP2 MI-MVI (p3xFLAG-CMV10), Flag-LGP2 1-546, 1-350, 1-176 (p3xFLAG-CMV10), Flag-LGP2 1-159, 1-121, 122-678, 160-678, 177-678, CTD (547-678) (p3xFLAG-CMV10), Myc-LGP2, HA-TRIM25 (pCAGGS), HA-ubiquitin (Ub; pRK5), HA-K63-Ub (pRK5), HA-K48-Ub (pRK5), p125-luc, pRL-CMV, pEF-Bos empty vector, pEF-Tak empty vector. LGP2 deletion mutants were generated from the p3xFLAG-CMV10 construct containing full-length WT LGP2. WT LGP2 construct was amplified via PCR with primers specific to the region of interest. Vector and PCR fragments were digested and gel purified. Desired fragments were extracted from gel via the 5 Prime Agarose GelExtract Mini Kit and PCR fragments ligated into linearized p3xFLAG-CMV10 vector.

Reagents and Antibodies. Mirus TransIT-293, Mirus TransIT-mRNA, MG132 (Fisher), DMSO (Fisher), N-ethylmaleimide (Sigma), Dual-Luciferase Reporter Assay System (Promega), SuperSignal West Femto Maximum Sensitivity Substrate (ThermoScientific), Anti-FLAG M2 Magnetic Beads (Sigma), Dynabeads Protein G magnetic beads (Novex), Mouse Cytokine Magnetic 20-Plex Panel (Invitrogen), ProcartaPlex Mouse IFN alpha/IFN beta Panel (Affymetrix eBioscience), Ms anti-Flag 1:1000 (Sigma), Rb anti-GAPDH 1:2500 (Cell Signaling), Rb anti-RIG-I 1:1000 (Gale Lab), Rb anti-LGP2 1:100 (IBL), Rb anti-MDA5 1:1000 (IBL), Ms anti-TRIM25 1:2000 (BD Bioscience), Rb anti-HA Tag 1:1000 (Cell Signaling), Rb anti-Myc 1:5000 (Novus), Ms anti-β-actin 1:1000 (Cell Signaling).

RNA-Seq Analysis. WT and Dhx58$^{-/-}$ DCs were CD11c+-purified using EasySep Mouse CD11c Positive Selection Kit II (Stemcell) per the manufacturer's protocol, and transfected with 20ng PAMP RNA, or left untreated. Cells were plated in triplicate for each condition/time point. PAMP RNA-treated cells and time-matched mock-treated cells were collected at 1, 3, and 6h post-agonist transfection in Buffer RLT (QIAGEN). Total RNA was isolated (QIAGEN RNeasy Plus Mini Kit) according to the manufacturer's protocol. RNA quality was assessed using an Agilent 2000 Bioanalyzer capillary electrophoresis and all RNA integrity (RIN) scores were greater than 8. mRNA sequencing libraries were prepared, and the quality of the libraries was verified using DNA-1000 Kits (Agilent Bioanalyzer) and quantified using the Qubit 2.0 Fluorometer (LifeTechnologies). Libraries were clustered and sequenced on an Illumina HiSeq 2500 System (100bp single end reads). Sequencing reads were mapped to the mouse reference genome mm10. Reads were normalized and differential expression analysis performed using DESeq2 (Love et al., 2014). The raw data of all RNA sequencing will be deposited into the Gene Expression Omnibus (GEO) repository and the accession number will be available following acceptance of this manuscript.

Cytokine secretion. Cell supernatants from WT and Dhx58$^{-/-}$ DCs used in RNA-Seq were analyzed for cytokines using multiplex bead assays - Mouse Cytokine Magnetic 20-Plex Panel (Invitrogen) and ProcartaPlex Mouse IFN alpha/IFN beta Panel (Affymetrix eBioscience) - according to the manufacturers' protocols.

Flow cytometry. WT and Dhx58$^{-/-}$ DCs were transfected with 20ng PAMP RNA or left untreated. Cells were plated in quadruplicate for each condition/time point. PAMP RNA-treated cells and time-matched mock-treated cells were collected at 24h post-agonist

transfection. Cells were blocked with Anti-mouse CD16/CD32 Fc block (TONBO Biosciences) and stained for surface markers CD11c-PE/Cy7 (TONBO Biosciences), CD80-FITC (TONBO Biosciences), CD86-PE (TONBO Biosciences), MHC I-Alexa647 (TONBO Biosciences). Viability was determined by staining with Ghost Dye 780 (TONBO Biosciences). Cells were run on BD LSR II.

Generation of knockdown HEK293 cells. HEK293T cells were transfected with LGP2- or RIG-I-targeting shRNAs, along with the lentiviral packaging plasmids pMG2 and pSPAX. 48h post-transfection cell supernatant was harvested for lentivirus containing LGP2 or RIG-I shRNA. Polybrene (8ug/ml) and cell supernatant containing lentivirus was added to HEK293 cells. Cells were transduced by centrifugation at 800 RPM for 30 min at RT. Transduction was confirmed by expression of GFP fluorescence in HEK293 cells.

Signaling Assays. RIG-I-dependent signaling was determined via luciferase assay, using reagents from Promega's Dual-Luciferase Reporter Assay System. 1x105 HEK293 cells were transfected with 50ng p125-luc containing the luciferase gene under the control of the IFN-β promoter region, 20ng pRL-CMV containing the renilla gene under the control of the CMV promoter, and 100ng other indicated plasmid DNA, using 1x Opti-MEM reduced serum media (LifeTechnologies) and Mirus TransIT-293 transfection reagent, for 24 hours. Cells were subsequently transfected with 100ng/ul PAMP RNA for six hours using 1x Opti-MEM and Mirus TransIT-mRNA transfection reagent. Lysates were collected in 1x Passive Lysis Buffer and results were read on a SynergyH1 Hybrid Reader (BioTek). Luciferase measurements were normalized to Renilla expression, which serves as a transfection control. Firefly luciferase values were divided by Renilla values to produce a normalized value (relative luciferase units; RLU). Technical triplicates were tested for each sample under each condition.

Immunoprecipitation and Immunoblotting. 1-1.5x106 HEK293 cells were transfected with 500ng indicated plasmid DNA using 1x Opti-MEM reduced serum media (LifeTechnologies) and Mirus TransIT-293 transfection reagent. 24h post-transfection, cells were transfected with 100ng/ul PAMP RNA using 1x Opti-MEM and Mirus TransIT-mRNA transfection reagent. Lysates were collected in modified RIPA buffer (10mM Tris, 150mM NaCl, 1% NA-deoxycholate, 1% Triton X-100) containing protease and phosphatase inhibitors, and deubiquitinase inhibitor, N-Ethylmaleimide (Sigma), for ubiquitination assays. In co-expression assays, IP was performed with either anti-Flag (Sigma) or anti-HA (Pierce) magnetic beads. In endogenous assays, IP was performed with magnetic Protein G Dynabeads (LifeTechnologies) conjugated to the appropriate antibody. Proteins were eluted in 2x loading buffer (0.25M Tris, 40% glycerol, 20% β-ME, 9.2% SDS, 0.04% Bromophenol Blue). IP supernatants and whole cell lysate controls were run on polyacrylamide gel via SDS-PAGE and transferred to nitrocellulose membrane for immunoblotting. Blocking was performed in 5% milk in 0.1% PBST. Primary antibodies were prepared in 0.1% PBST containing 10% FBS. Secondary antibodies were prepared in 0.1% PBST containing 1% FBS. Blots were developed using ThermoScientific SuperSignal West Femto Maximum Sensitivity Substrate and a BioRad ChemiDocXRS+.

RNA Immunoprecipitation. HEK293 cells were transfected with 1ug/ul unlabeled or biotin-labeled PAMP RNA using 1x Opti-MEM and Mirus TransIT-mRNA transfection reagent. Lysates were collected three hours later in RIPA buffer containing RNase, protease, and phosphatase inhibitors (Cell Signaling). IP was performed with streptavidin-conjugated magnetic beads (Pierce). Proteins were eluted in 2x loading

buffer. IP supernatants and whole cell lysate controls were run on polyacrylamide gel via SDS-PAGE and transferred to nitrocellulose membrane for immunoblotting.

Statistical analysis. mRNA-sequencing samples were submitted in triplicate for each condition tested, with triplicate time-matched, mock-treated controls. Differentially expressed genes were identified through DESeq2 analysis and thresholds were set at fold change >2 and $p<0.01$. Supernatants used for protein secretion analysis were collected from the same cells used for mRNA-seq. Samples were run in biological triplicates and analyzed by 2-way ANOVA followed by Sidak's test for multiple comparisons, $p<0.05$. Flow cytometry samples were run in biological quadruplicates and analyzed by 2-way ANOVA followed by Sidak's test for multiple comparisons, $p<0.05$. Flow cytometry data is representative of at least three separate experiments. Luciferase assays were run in biological triplicates for each condition tested. Relative luciferase units (RLU) were calculated by normalizing luciferase expression readings to Renilla transfection control expression within the same sample. Data was analyzed by 1-way ANOVA followed by either Tukey's or Dunnett's test for multiple comparisons, $p<0.05$. All luciferase assay and immunoblot data is representative of at least three separate experiments. Statistical analysis was performed using GraphPad Prism, version 6 software.

Results

LGP2 negative regulates RIG-I-mediated innate immune responses in BM-DCs

The mechanism underlying LGP2-mediated regulation of RIG-I signaling is not well defined. To understand the impact of LGP2 on RIG-I antiviral signaling, we probed RIG-I signaling using a previously characterized RIG-I agonist (Saito et al., 2008), derived from the 3' UTR of HCV (PAMP RNA) and performed transcriptomic analysis. Specifically, we

transfected WT and Dhx58$^{-/-}$ CD11c+ BM-DCs with PAMP RNA and harvested mock and treated cells at 1, 3 and 6 hours post-treatment followed by mRNA sequencing (**Figure 1A**). We compared gene expression changes between treated and time-matched mock controls and determined differential gene expression by 2-fold change and $p<0.01$. Through this analysis, we observed that the genetic ablation of LGP2 led to enhanced and broader transcriptional responses following PAMP RNA treatment. We found that at one hour post-treatment Dhx58$^{-/-}$ cells exhibited 44 differentially expressed genes (DEGs; WT=0, Shared=30), at three hours post-treatment Dhx58$^{-/-}$ cells exhibited 1374 DEGs (WT=102, Shared=950), and at six hours post-treatment Dhx58$^{-/-}$ cells exhibited 2763 DEGs (WT=136, Shared=2024; **Figure 1B**). Furthermore, many of the shared genes at 1, 3, and 6 hours post-treatment were induced to a greater extent in Dhx58$^{-/-}$ cells compared to WT cells (**Figure 1C**, orange circles).

We next focused on the transcriptional differences at one hour post-treatment (**Figure 1D**). Using hierarchical clustering, we defined four gene clusters that were differentially enhanced in WT and Dhx58$^{-/-}$ BM-DCs: 1) Genes only expressed in Dhx58$^{-/-}$ cells (purple), which include antiviral effectors (Gbp5), chemokines (Ccl2, Ccl3, Cxcl1), and a transcription factor (Jun); 2) Genes expressed to similar levels in both WT and Dhx58$^{-/-}$ cells (grey), which include antiviral effectors (Mx2, Oasl1), a cytokine (Tnfsf15), a transcription factor (Fos, otherwise known as AP-1), and a cell cycle-related gene (Ccno); 3) Shared genes induced to a higher level in Dhx58$^{-/-}$ cells (blue), which include type I IFNs (Ifna1, Ifna2, Ifna5), antiviral effectors (Isg15, Ifit2, Rsas2) and pro-inflammatory cytokines/chemokines (Tnf, Cxcl2); and 4) Shared genes highly expressed in WT cells but exceeded in Dhx58$^{-/-}$ cells (pink), which include type I IFNs (Ifnb1, Ifna4), antiviral effectors (Ifit1, Ifit3) and pro-inflammatory cytokines/chemokines (Il6, Cxcl10, Ccl4). A select set of genes known to promote an antiviral state, including type I IFNs (Ifnb1, Ifna2, Ifna4), pro-inflammatory cytokines (Il6) and ISGs (Ifit1, Ifit2, Ifit3, Isg15),

were significantly increased in Dhx58$^{-/-}$ BM-DCs compared to WT cells at the one hour time point (**Figure 1E**).

We next evaluated whether the differences in gene induction at one hour post-treatment were attributable to differences in basal expression of RIG-I. We found that Ddx58 (RIG-I) transcripts were expressed at similar levels in WT and Dhx58$^{-/-}$ BM-DCs, confirming previous findings at the protein level in these cells by our group (22). While other antiviral effector genes were robustly elevated above mock at one hour post-treatment (**Figure 1E**), RIG-I transcripts were not significantly induced in WT or Dhx58$^{-/-}$ cells (**Figure 1F**). We also evaluated the kinetics of Dhx58 (LGP2) expression in WT BM-DCs and found that LGP2 mRNA was present under mock conditions (normalized read counts=103.6) and that LGP2 expression was induced between 1 and 3 hours post-treatment (**Figure 1G**). Combined, these findings indicate that LGP2 is important for negatively regulating early events within the RIG-I signaling cascade.

Next, we evaluated the impact of LGP2 on cytokine production and costimulatory molecule expression following RIG-I signaling activation. We performed multiplex bead assays to determine the secretion of type I IFN and pro-inflammatory cytokines by WT and Dhx58$^{-/-}$ BM-DCs in matching samples used in the mRNA-sequencing analysis. Protein secretion of IFN-β, IFN-α (**Figure 2A**) and pro-inflammatory cytokines, including IL-6, TNF-α and IP-10 (**Figure 2B**), was elevated in Dhx58$^{-/-}$ BM-DCs compared to WT cells. Additionally, we observed that protein expression of the costimulatory markers CD86 and CD80 was higher on the surface of Dhx58$^{-/-}$ BM-DCs compared to WT cells (**Figure 2C**), suggesting more pronounced activation of BM-DCs in the absence of LGP2. Taken together, these results illustrate that LGP2 functions as a negative regulator in the early stages of RIG-I-mediated antiviral immune signaling in BM-DCs.

LGP2 is a negative regulator of RIG-I signaling in human cells

To dissect the mechanism by which LGP2 negatively regulates RIG-I signaling, we performed reporter-based assays in cultured human cells (HEK293 cells). To ensure LGP2 functions in a similar manner in this model, we assessed IFN-β promoter-driven luciferase production with increasing amounts of over-expressed LGP2. We found that PAMP RNA-induced IFN-β promoter activity was inhibited in a dose-dependent manner by LGP2 (**Figure 3A**), with inhibition observed with as little as 800pg of over-expressed LGP2 plasmid and maximum inhibitory effect with 100ng of LGP2 plasmid. Additionally, we observed that IFN-β promoter activity was significantly increased in LGP2 shRNA knockdown cells as compared to scrambled control shRNA cells (**Figure 3B**). Combined, these results confirm our findings in BM-DCs and demonstrate that LGP2 is a negative regulator of RIG-I signaling following PAMP RNA treatment.

Following activation, RIG-I interacts with the central adaptor protein MAVS which leads to the activation of latent transcription factors, namely IRF-3 and NF-κB. The minimal IFN-β promoter contains binding sites for both IRF-3 (PRD I and PRD III) and NF-κB (PRD II) (Lenardo et al., 1989; Schafer et al., 1998; Visvanathan and Goodbourn, 1989). Thus, we evaluated the specific activities of these promoter sites to determine whether LGP2 attenuates RIG-I signaling downstream of MAVS by inhibiting activation of IRF-3 or NF-κB transcription factors. To this end, we utilized luciferase constructs driven by either IRF-3 or NF-κB alone. We observed a dose-dependent inhibition of both IRF-3- and NF-κB-specific promoter activities with increasing amounts of over-expressed LGP2 (**Figure 4A and 4B**). These findings strongly suggest that LGP2 inhibits RIG-I signaling upstream of IRF-3 and NF-κB activation.

The CTD of LGP2 is dispensable for inhibition of RIG-I signaling

We next attempted to define the motifs within LGP2 that are responsible for inhibiting RIG-I signaling. To this end, we generated a panel of LGP2 deletion mutants (**Figure**

3C). The helicase domain of LGP2 contains six defined motifs responsible for RNA binding and ATP hydrolysis (Bamming and Horvath, 2009; Bruns et al., 2013) (**Figure 3C** (I-VI) **and 5A**). Additionally, previous studies have implicated the CTD of LGP2 as a regulatory domain that inhibits RIG-I through interaction with the RIG-I helicase domain (Saito et al., 2007). When transfected into HEK293 cells, LGP2 1-121 and the LGP2 CTD (amino acids 547-678) failed to inhibit IFN-β promoter activity, whereas LGP2 1-159, 1-176, 1-546, 122-678, 160-678 and 177-678 reduced IFN-β promoter activity compared to empty vector control (LGP2 -, PAMP RNA +; **Figure 3D**). These results indicate that the first 121 amino acids within the N-terminus and the CTD of LGP2 are not sufficient for the negative regulation of RIG-I. However, it appears that multiple regions within the helicase domain are involved in the inhibition of RIG-I signaling.

RNA binding and ATP hydrolysis are dispensable for negative regulation

Previous studies have proposed that LGP2 binds and sequesters RNA ligands to prevent RIG-I activation (Rothenfusser et al., 2005; Yoneyama et al., 2005). Additionally, LGP2 hydrolyzes ATP to increase its affinity for particular RNA substrates, allowing it to enhance MDA5 signaling (Bruns et al., 2013). To determine whether these functions play a role in the negative regulation of RIG-I, we evaluated a panel of six LGP2 constructs, each with mutations within one of the motif domains that result in the loss of motif function (MI-MVI, **Figure 5A**) (Bamming and Horvath, 2009). We found that all six mutants retained the ability to inhibit IFN-β promoter activity when introduced into HEK293 cells (**Figure 5B**). In particular, the MIII mutant, which lacks both RNA binding and ATP hydrolysis activities (Bamming and Horvath, 2009; Bruns et al., 2013) was able to inhibit IFN-β promoter activity almost as effectively as WT LGP2, indicating that neither RNA binding nor ATP hydrolysis is required for inhibition of RIG-I signaling. To further confirm our findings, we immunoprecipitated (IP) biotin-labeled PAMP RNA from

transfected cells and found that RIG-I, but not LGP2, recognized and bound the PAMP RNA (**Figure 5C**), indicating that LGP2 is not negatively regulating RIG-I signaling by sequestering the PAMP RNA ligand. We next evaluated the effects of LGP2 on a constitutively active RIG-I mutant (N-RIG), which consists of only the two N-terminal CARDs and lacks the RNA binding helicase domain. We found that full-length LGP2 (FL) and LGP2 lacking the CTD (aa 1-546), but not the CTD fragment (aa 547-678), were able to attenuate N-RIG-induced IFN-β promoter activity (**Figure 5D**), indicating that RIG-I binding to RNA is also dispensable for LGP2 inhibition of RIG-I activity. Combined, these findings indicate that LGP2 negatively regulates RIG-I signaling independent of the ability of LGP2 to bind or sequester RIG-I ligands but is instead influencing the N-terminal signaling domains.

LGP2 associates with TRIM25

Our data strongly suggest that LGP2 functions after RIG-I binds RNA but before MAVS activation of downstream transcription factors. To more precisely determine the step within the RIG-I signaling pathway that LGP2 is inhibiting, we performed mass spectrometry analysis on immunoprecipitated Flag-LGP2. Through this analysis, we identified tripartite motif-containing protein 25 (TRIM25), an E3 ubiquitin ligase responsible for the K63-ubiquitination of the RIG-I N-terminus (Gack et al., 2007). We confirmed this interaction by over-expressing LGP2 in HEK293 cells and found that LGP2 associates with endogenous TRIM25 (**Figure 6A**). Treatment with PAMP RNA did not appear to influence the interaction between TRIM25 and LGP2, intimating that LGP2 and TRIM25 interact at homeostasis. Furthermore, we immunoprecipitated endogenous TRIM25 and confirmed an association with endogenous LGP2 in cells either untreated or treated with PAMP RNA (**Figure 6B**). We also observed that the helicase domain of LGP2 (aa 1-546) associated with TRIM25, but that the CTD of LGP2, which did not

inhibit RIG-I signaling, did not interact (**Figure 6C**). Lastly, we found that LGP2 efficiently inhibits TRIM25-enhanced N-RIG-mediated IFN-β promoter activity in a dose-dependent manner (**Figure 6D**).

Previous studies have established that following RIG-I binding to non-self RNA, TRIM25 interacts with RIG-I (Gack et al., 2007). Given that LGP2 also interacts with TRIM25, we next investigated whether LGP2 interacts with RIG-I. Previous studies have demonstrated that LGP2 and RIG-I associate when both proteins are ectopically expressed (Komuro and Horvath, 2006; Saito et al., 2007), a finding which we were able to independently confirm (**Figure 7A**). We also found that over-expressed LGP2 interacted with endogenous RIG-I, in the presence or absence of stimulatory PAMP RNA (**Figure 7B**). However, we were unable to demonstrate an interaction between endogenous LGP2 and endogenous RIG-I, in contrast to our finding with endogenous LGP2 and TRIM25 (**Figure 7C and Figure 6B**). This may indicate that LGP2 interacts with RIG-I under conditions when both proteins are expressed at high levels, such as late times during signaling activation, or that the interaction between LGP2 and RIG-I is an artifact of over-expression. Nonetheless, our findings demonstrate that full-length LGP2 associates with TRIM25 and that the CTD of LGP2 is dispensable for mediating this interaction.

LGP2 suppresses K63-ubiquitination of RIG-I

The observed association of LGP2 and TRIM25, led us to evaluate the effects of LGP2 on RIG-I ubiquitination. Upon binding non-self RNA, RIG-I undergoes K63-ubiquitination on its N-terminus to reach a fully active state (Gack et al., 2007). To determine the impact of LGP2 on the ubiquitination state of RIG-I, we co-expressed RIG-I, LGP2, and ubiquitin within HEK293 cells. We observed decreased total ubiquitination of RIG-I in these cells compared to cells transfected with RIG-I and a vector control (**Figure 8A**). To

determine whether this decrease was due to increased degradation of RIG-I, we performed this experiment in the presence of MG132, a proteasomal inhibitor. We found that co-expression of LGP2 with RIG-I resulted in a noticeable reduction of ubiquitinated RIG-I even in cells treated with MG132 (**Figure 8A**). Lastly, we observed that RIG-I ubiquitination was increased in LGP2 shRNA knockdown cells compared to control shRNA-expressing cells (**Figure 8B**). Combined, these findings strongly suggest that LGP2 is negatively regulating the activation of RIG-I rather than destabilizing RIG-I protein expression in HEK293 cells.

While RIG-I is initially K63-ubiquitinated during its activation, it is subsequently marked for proteasomal degradation by RNF125-mediated K48-ubiquitination (Arimoto et al., 2007). To determine the specific ubiquitination step being affected by LGP2, we utilized ubiquitin mutants which either specifically form K63-linked chains or K48-linked chains on proteins. We observed diminished K63-specific and K48-specific ubiquitination of RIG-I in the presence of LGP2 (**Figure 8C and 8D**). This suggests that LGP2 is likely inhibiting K63-ubiquitination of RIG-I, as inhibition of RIG-I activation would result in less RIG-I protein production and therefore a decreased need for subsequent K48-ubiquitin-mediated degradation of RIG-I. Additionally, ubiquitination of N-RIG was reduced in the presence of LGP2 (**Figure 8E**), supporting a role for LGP2 in negatively regulating RIG-I-specific signaling by preventing the K63-ubiquitinaiton of the RIG-I N-terminal CARD through an association with the E3 ubiquitin ligase TRIM25. Inhibiting this post-translational modification prevents RIG-I activation and dampens subsequent innate immune responses during virus infection (**Figure 9**).

Discussion

In this study, we have elucidated an as yet undescribed role for LGP2 in negatively regulating RIG-I antiviral signaling and BM-DC activation. First, we used primary cells

from WT and Dhx58$^{-/-}$ mice and compared the transcriptional responses following RIG-I activation. We found that as early as one hour post-treatment, Dhx58$^{-/-}$ BM-DCs displayed a more robust antiviral response than WT BM-DCs that was characterized by enhanced expression of type I IFNs, pro-inflammatory cytokines and antiviral effector genes. This was not due to differences in basal expression of RIG-I between WT and Dhx58$^{-/-}$ BM-DCs. Furthermore, LGP2 is basally expressed in WT BM-DCs and is transcriptionally induced between 1-3 hours post-treatment, which is subsequent to the induction of type I IFN gene expression (**Figure 1E**), indicating that LGP2 functions at early times following RIG-I signaling activation rather than at later time points as suggested by previous studies (Rothenfusser et al., 2005). We confirmed that increased type I IFN mRNA expression corresponded to a greater amount of type I IFN protein secretion and subsequently led to enhanced co-stimulatory molecule expression on cells lacking LGP2. Second, we modeled LGP2 function in cultured human cells and confirmed that LGP2 is a negative regulator of RIG-I signaling at a point between RIG-I and MAVS in the signaling cascade. Third, we performed structure function studies and found that the LGP2 CTD was insufficient and dispensable for inhibiting RIG-I signaling. Furthermore, we determined that the RNA binding and ATP hydrolysis functions of the LGP2 helicase domain were similarly dispensable for reducing RIG-I activity. Finally, we discovered that LGP2 interacted with the E3 ligase TRIM25 and that LGP2 inhibited TRIM25-mediated K63-ubiquitination of RIG-I. These findings reveal that LGP2 functions at early times to inhibit RIG-I signaling and elucidate the mechanistic underpinnings for how LGP2 negatively impacts RIG-I activation.

Previous studies suggest that LGP2 may compete for and sequester RIG-I ligands to inhibit RIG-I signaling (Rothenfusser et al., 2005; Yoneyama et al., 2005). However, our in vitro studies demonstrated that neither LGP2 binding to RNA nor RIG-I binding to RNA was required for LGP2 inhibition of RIG-I signaling. Furthermore, other

studies propose that the CTD of LGP2 (aa 476-678) directly binds RIG-I and inhibits signaling activation (Saito et al., 2007). It has been shown that the CTD of RIG-I performs an auto-regulatory role, and that the CTD of LGP2 shares homology with the RIG-I CTD (Saito et al., 2007). However, in our studies, we found that the LGP2 CTD (aa 547-678) was insufficient and dispensable for inhibiting RIG-I. It should be noted that our LGP2 CTD deletion mutant is 71 amino acids shorter than the CTD fragment used in previous studies (Saito et al., 2007). These additional amino acids include a portion of motif VI within the LGP2 helicase domain (Cui et al., 2008; Li et al., 2009b; Pippig et al., 2009; Takahasi et al., 2009). Thus, it is still plausible that the previously described version of the LGP2 CTD may interact with TRIM25 and inhibit RIG-I ubiquitination.

Our LGP2 deletion mutants containing parts of the helicase domain, with the exception of LGP2 1-121, retained the ability to attenuate RIG-I signaling. However, it is worth noting that no single deletion mutant was as effective as full-length LGP2. This likely indicates the importance of a complete, intact tertiary structure and requires further investigation. One report has evaluated the structure of LGP2 in the context of RNA binding (Murali et al., 2008), but little is known about how this structure influences protein-protein interactions or regulation of RIG-I ubiquitination. It is plausible that the LGP2 helicase domain forms long-distance interactions within LGP2 and that this allows for more efficient binding to TRIM25 and inhibition of RIG-I signaling activation. It is also plausible that LGP2 requires post-translational modifications to interact with TRIM25. Given that post-translational modifications are responsible for both induction and repression of RIG-I and MDA5 activity, it would be informative to determine whether there are similar post-translational modifications, including phosphorylation, ubiquitination or sumoylation, that regulate the activity of LGP2.

Indeed, post-translational modifications to LGP2 could be a contributing factor to its inhibitory mechanism if LGP2 is itself a target of TRIM25-mediated ubiquitination. It is

possible that LGP2 competes with RIG-I for binding and/or ubiquitination by TRIM25. However, considering that the TRIM25 binding site on RIG-I is located within the CARDs (Gack et al., 2007), it seems unlikely that LGP2, which lacks CARDs, would be bound by the same region of TRIM25. Alternatively, if LGP2 is binding to a different region of TRIM25, it may be directly disrupting the E3 ligase function of TRIM25. For instance, if LGP2 binds the N-terminal RING domain of TRIM25, which is responsible for binding E2 ubiquitin-conjugating enzymes (Napolitano et al., 2011), it could prevent this necessary step for TRIM25-mediated ubiquitination of target proteins. MAVS is another ubiquitination target of TRIM25. In this case, TRIM25 K48-ubiquitinates the MAVS CARD, targeting it for proteasomal degradation, which is reported to potentiate IRF-3 signaling (Castanier et al., 2012). Disruption of MAVS ubiquitination was shown to hinder IRF-3, but not NF-κB signaling. In our studies, we observe inhibition of both IRF-3- and NF-κB-specific signaling in the presence of LGP2, however, the effect on IRF-3 signaling is more dramatic. Thus, it seems plausible that LGP2 is also affecting other substrates of TRIM25-mediated ubiquitination, including MAVS.

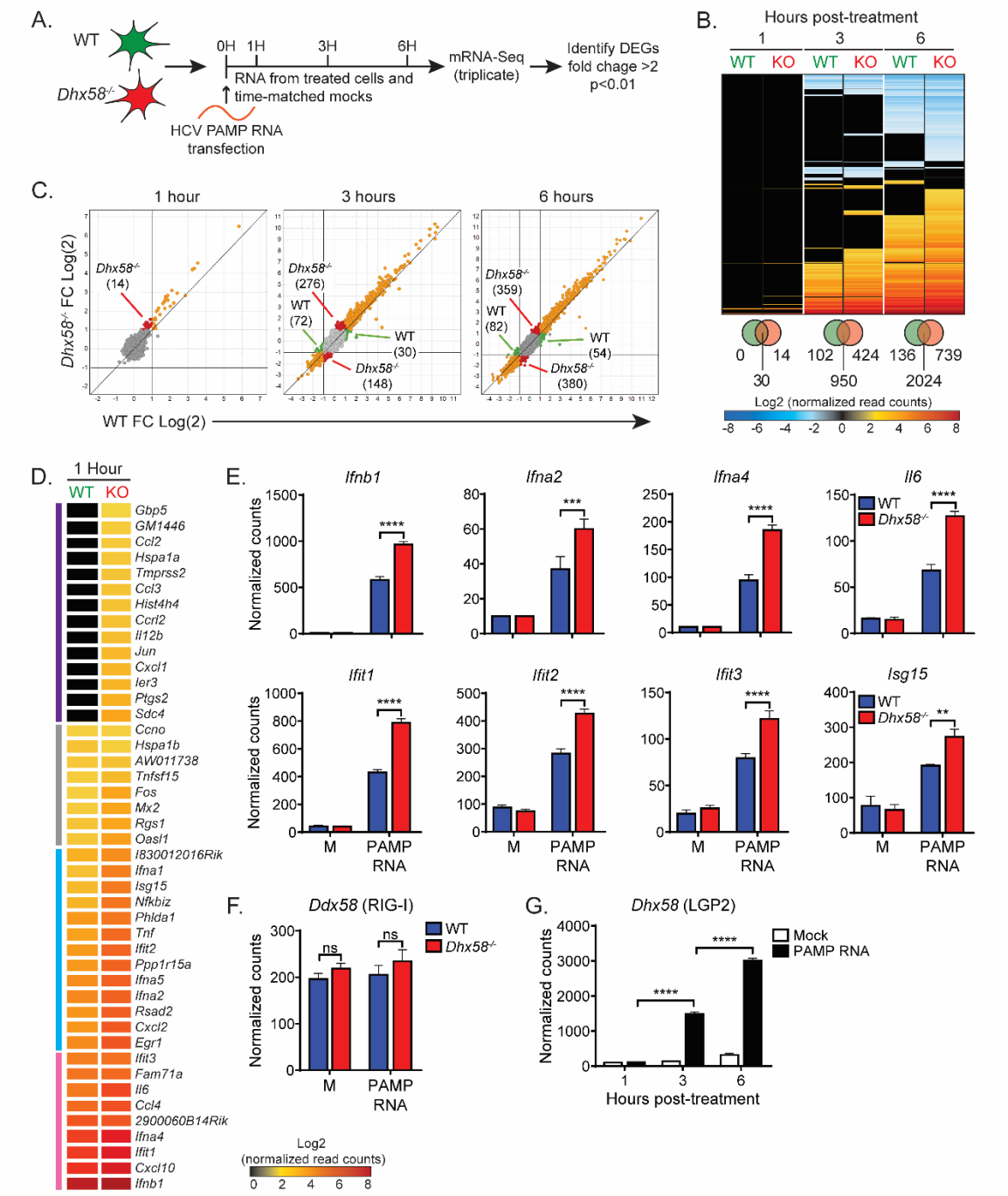

Figure 2-1: LGP2 negatively regulates RIG-I-mediated antiviral transcriptional responses in BM-DCs.

(**A**) WT and *Dhx58*$^{-/-}$ BM-DCs were treated with PAMP RNA and collected in triplicate with time-matched, mock-treated cells and submitted for mRNA-sequencing. Transcripts with a fold change >2, p<0.01 were identified for further analysis. (**B**) Heat map of genes

differentially regulated in WT and *Dhx58*$^{-/-}$ (KO) BM-CDs post-treatment. Venn diagrams illustrate numbers of differentially expressed and shared genes. (**C**) Differentially expressed and shared genes in WT and *Dhx58*$^{-/-}$ BM-DCs plotted to illustrate ratio of expression (*Dhx58*$^{-/-}$/WT). Genes expressed in both WT and *Dhx58*$^{-/-}$ cells (orange); genes expressed only in *Dhx58*$^{-/-}$ cells (red); genes expressed only in WT cells (green). (**D**) Heat map of genes induced in WT and *Dhx58*$^{-/-}$ (KO) BM-CDs at 1 hour post-treatment, with gene clusters indicated by vertical colored bars. Purple, genes induced only in *Dhx58*$^{-/-}$ BM-DCs; grey, shared genes expressed at similar levels in WT and *Dhx58*$^{-/-}$ cells; blue, shared genes with higher induction in *Dhx58*$^{-/-}$ cells; pink, shared genes highly expressed in WT BM-DCs but even more highly expressed in *Dhx58*$^{-/-}$ cells. (**E**) Individual analysis of select of transcripts at 1 hour post-treatment with PAMP RNA or mock-treated (M). Data shown are average normalized transcript counts of biological triplicates ±SD of WT (blue) and *Dhx58*$^{-/-}$ (red) analyzed by Sidak's test, $p<0.01$. (**F**) *Ddx58* (RIG-I) transcripts at 1 hour post-treatment with PAMP RNA or mock-treated (M). Data shown are average normalized transcript counts of biological triplicates ±SD of WT (blue) and *Dhx58*$^{-/-}$ (red) analyzed by Sidak's test, $p<0.01$. (**G**) Analysis of *Dhx58* (LGP2) gene expression in WT BM-DCs treated with PAMP RNA (black), or mock-treated (white). Data shown are average normalized transcript counts of biological triplicates ±SD analyzed by Tukey's test, $p<0.01$.

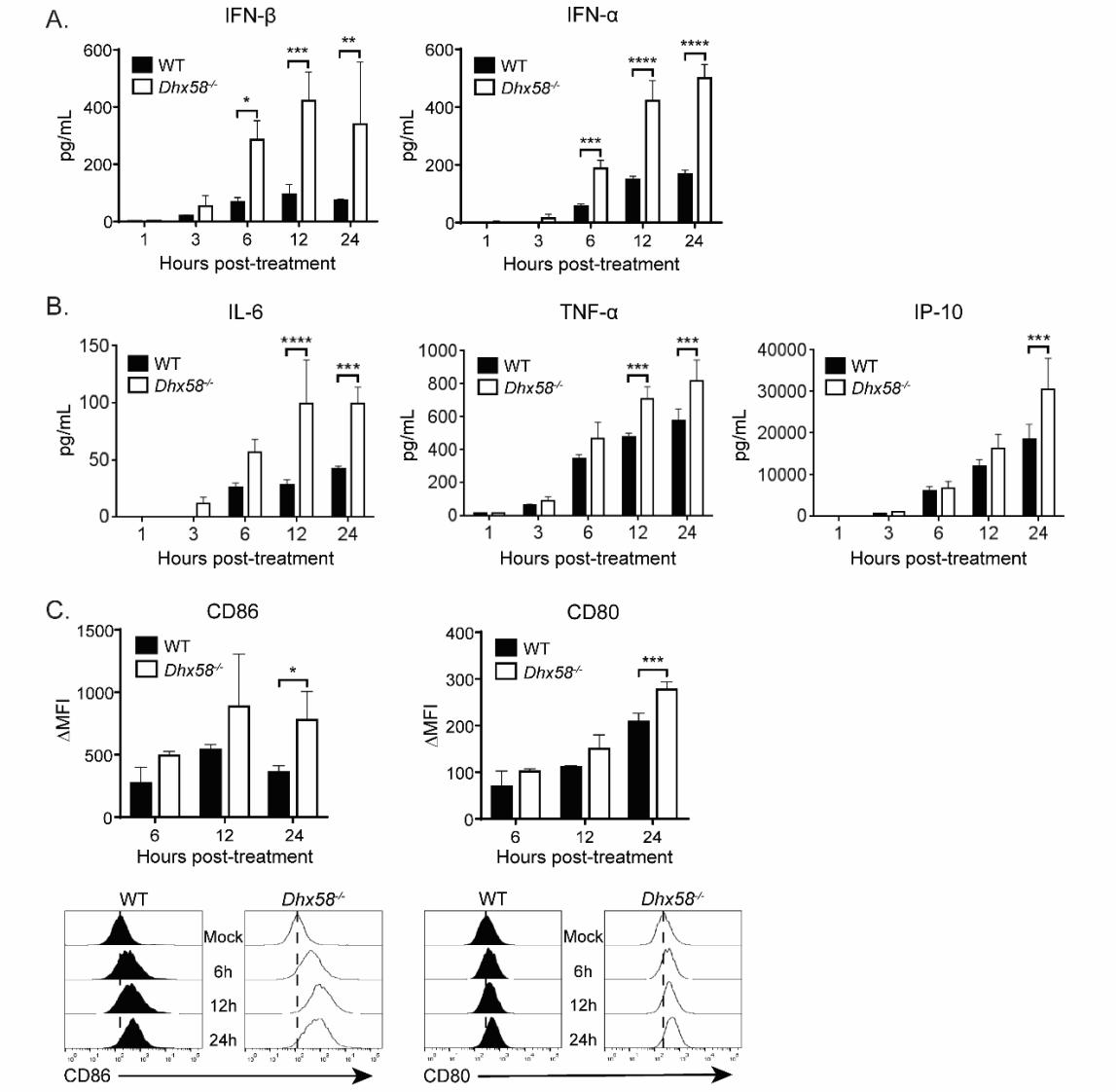

Figure 2-2: LGP2 negatively regulates downstream antiviral immune responses.

Protein secretion (pg/ml) of (**A**) type I IFNs and (**B**) pro-inflammatory cytokines/chemokines in the supernatant of PAMP RNA-treated WT (black) and *Dhx58*$^{-/-}$ (white) BM-DCs. Data shown are biological triplicates ±SD analyzed by Sidak's test, $p<0.05$. (**C**) Surface expression of co-stimulatory markers CD86 and CD80 in PAMP RNA-treated WT (black) and *Dhx58*$^{-/-}$ (white) BM-DCs. Data is shown as average ΔMFI (mean fluorescence intensity) of biological quadruplicates ±SD. Data were analyzed by Sidak's test, $p<0.05$. Representative histograms are shown below.

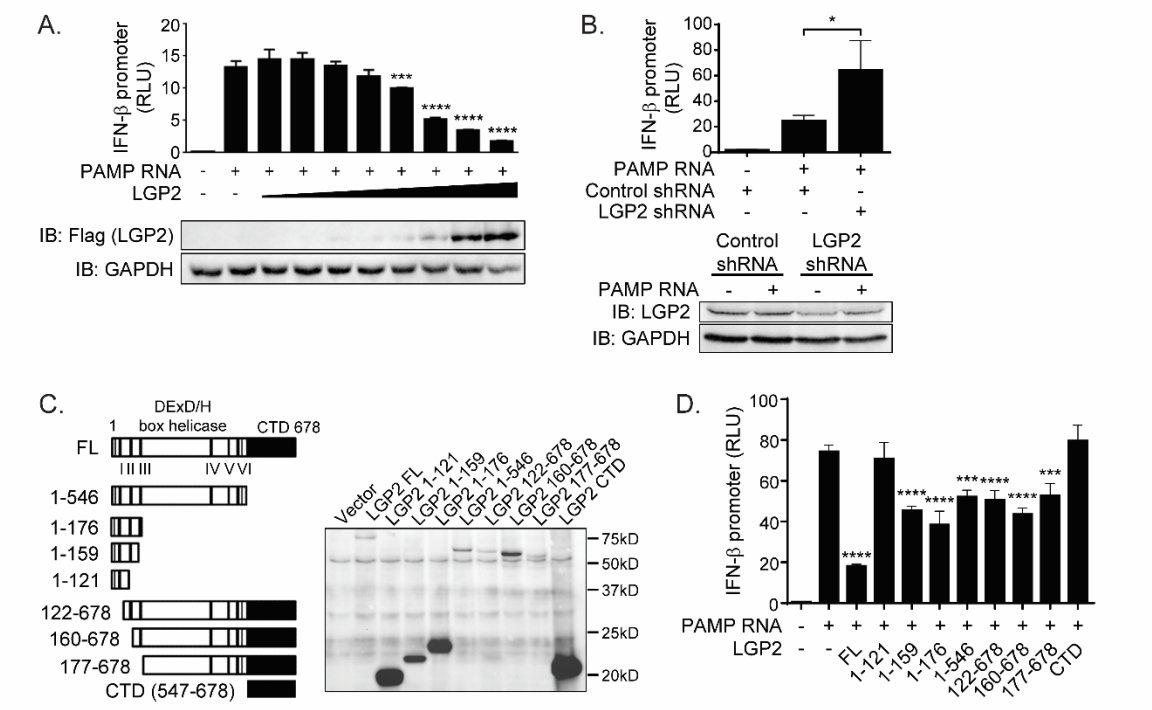

Figure 2-3: LGP2 is a negative regulator of RIG-I signaling in human cells and the CTD is not required for this function.

(**A**) HEK293 cells were transfected with LGP2 plasmid at increasing doses (1.28pg, 6.4pg, 32pg, 160pg, 800pg, 4ng, 20ng and 100ng) and treated with 100ng/ul PAMP RNA. Data shown are average relative luciferase units (RLU) of biological triplicates ±SD analyzed by Dunnett's test with comparisons made to PAMP RNA-treated vector control (LGP2 -), $p<0.05$. Immunoblotting (IB) performed with remaining lysate shown below to illustrate LGP2 expression. (**B**) LGP2 shRNA knockdown and scrambled control shRNA HEK293 cells were transfected with 100ng/ul PAMP RNA. Data shown are average relative luciferase units (RLU) of biological triplicates ±SD analyzed by Tukey's test, $p<0.05$. IB performed with remaining lysate shown below to illustrate LGP2 knockdown. (**C**) Flag-tagged LGP2 deletion mutants with lengths indicated by number of amino acids. Defined motifs of the DExD/H box helicase domain are labeled I-VI. FL, full length.

CTD, C-terminal domain. IB illustrates deletion mutant expression in HEK293 cells. (**D**) HEK293 cells were transfected with full-length LGP2 (FL) or LGP2 deletion mutants and treated with 100ng/ul PAMP RNA. Data shown are average relative luciferase units (RLU) of biological triplicates ±SD analyzed by Dunnett's test with comparisons made to PAMP RNA-treated vector control (LGP2 -), $p<0.05$.

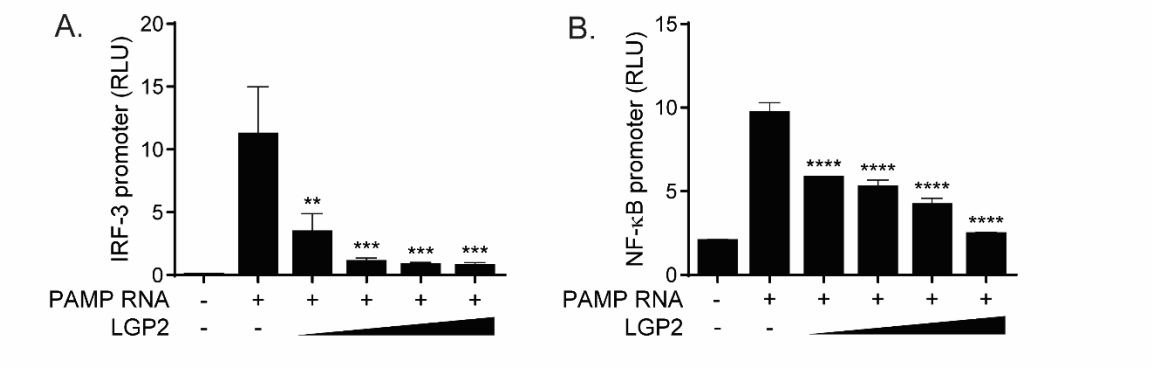

Figure 2-4: LGP2 negatively regulates both IRF-3 and NF-κB promoter activities.

HEK293 cells were transfected with 50ng either IRF-3 promoter luciferase (**A**) or NF-κB promoter luciferase (**B**), 20ng CMV promoter Renilla, and increasing doses of LGP2 plasmid (10, 50, 100 and 200ng) and treated with 100ng/ul PAMP RNA. Data shown are average relative luciferase units (RLU) of biological triplicates ±SD analyzed by Dunnett's test with comparisons made to PAMP RNA-treated vector control (LGP2 -), $p<0.05$.

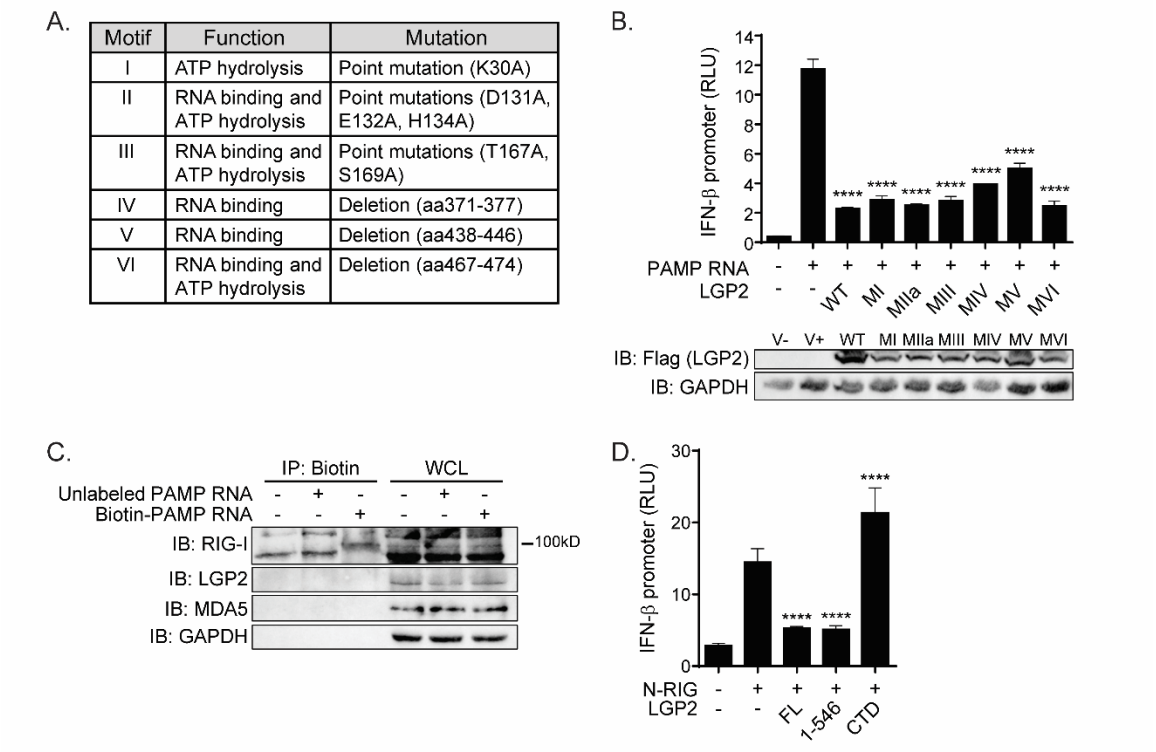

Motif	Function	Mutation
I	ATP hydrolysis	Point mutation (K30A)
II	RNA binding and ATP hydrolysis	Point mutations (D131A, E132A, H134A)
III	RNA binding and ATP hydrolysis	Point mutations (T167A, S169A)
IV	RNA binding	Deletion (aa371-377)
V	RNA binding	Deletion (aa438-446)
VI	RNA binding and ATP hydrolysis	Deletion (aa467-474)

Figure 2-5: RNA binding and ATP hydrolysis are dispensable for negative regulation.

(**A**) LGP2 helicase domain motifs, their associated functions, and the mutations made to generate functionally deficient motifs. (**B**) HEK293 cells were transfected with LGP2 motif mutants (MI-MVI) and treated with 100ng/ul PAMP RNA. Data shown are average relative luciferase units (RLU) of biological triplicates ±SD analyzed by Dunnett's test with comparisons made to PAMP RNA-treated vector control (LGP2 -), $p<0.05$. IB performed with remaining lysate shown below to illustrate LGP2 motif mutant expression (V, empty vector plasmid control; (-), mock treated; (+), PAMP RNA-treated). (**C**) HEK293 cells were transfected with 1ug/ul either unlabeled, or biotin-labeled PAMP RNA. Immunoprecipitation (IP) was performed with streptavidin beads that bind the biotin-labeled RNA. IB was performed for indicated proteins. WCL, whole cell lysate (input control). (**D**) HEK293 cells were transfected with N-RIG (10ng), and either full-length LGP2 (FL), LGP2 1-546 or LGP2 CTD for 24h. Data shown are average relative

luciferase units (RLU) of biological triplicates ±SD analyzed by Dunnett's test with comparisons made to N-RIG + vector control (LGP2 -), $p<0.05$.

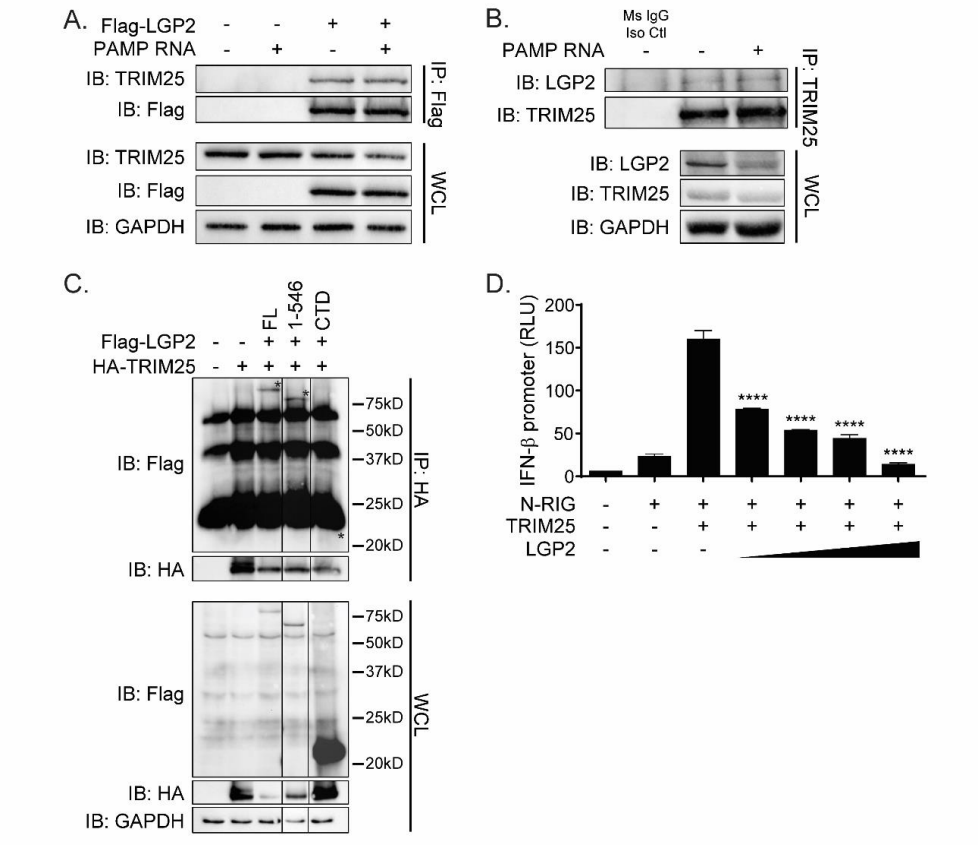

Figure 2-6: LGP2 associates with TRIM25.

(**A**) HEK293 cells were transfected with Flag-LGP2 or empty vector control (-) and treated with 100ng/ul PAMP RNA. IP was performed for Flag-LGP2. IB was performed for indicated proteins. WCL, whole cell lysate (input control). (**B**) HEK293 cells were transfected with 100ng/ul PAMP RNA. IP was performed for endogenous TRIM25 using Protein G beads conjugated to anti-TRIM25 antibody or a mouse IgG isotype control antibody. IB was performed for indicated proteins. (**C**) HEK293 cells were transfected with HA-TRIM25, and either full-length Flag-LGP2 (FL), Flag-LGP2 1-546 or Flag-LGP2 CTD fragment and treated with 100ng/ul PAMP RNA. IP was performed for HA-TRIM25.

IB was performed for indicated proteins. Non-contiguous panels are from the same blot. (**D**) HEK293 cells were transfected with N-RIG (10ng), TRIM25 and increasing doses of LGP2 (10, 50, 100 and 200ng) for 24h. Data shown are average relative luciferase units (RLU) of biological triplicates ±SD analyzed by Dunnett's test with comparisons made to N-RIG+TRIM25+vector control (LGP2 -), $p<0.05$.

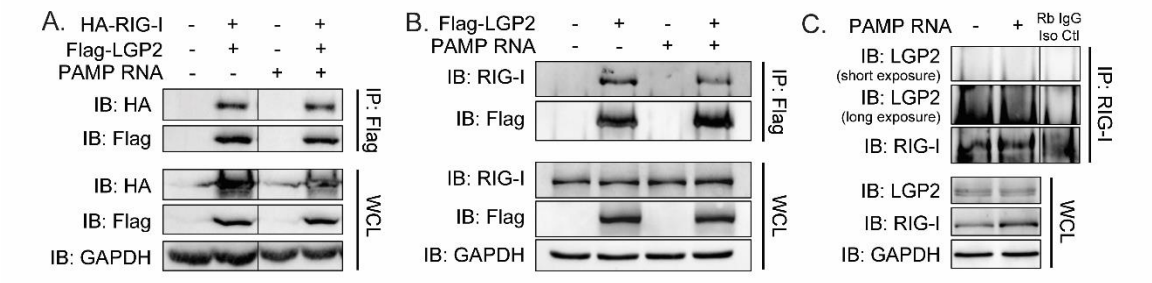

Figure 2-7: LGP2 interacts with RIG-I when co-expressed, but not at the endogenous level.

(**A**) HEK293 cells were transfected with HA-RIG-I and Flag-LGP2 and treated with 100ng/ul PAMP RNA. IP was performed for Flag-LGP2. IB was performed for indicated proteins. Non-contiguous panels are from the same blot. WCL, whole cell lysate (input control). (**B**) HEK293 cells were transfected with Flag-LGP2 and treated with 100ng/ul PAMP RNA. IP was performed for Flag-LGP2. IB was performed for indicated proteins. (**C**) HEK293 cells were transfected with 100ng/ul PAMP RNA. IP was performed for endogenous RIG-I using Protein G beads conjugated to an anti-RIG-I antibody or rabbit IgG isotype control antibody. IB was performed for indicated proteins. Non-contiguous panels are from the same blot.

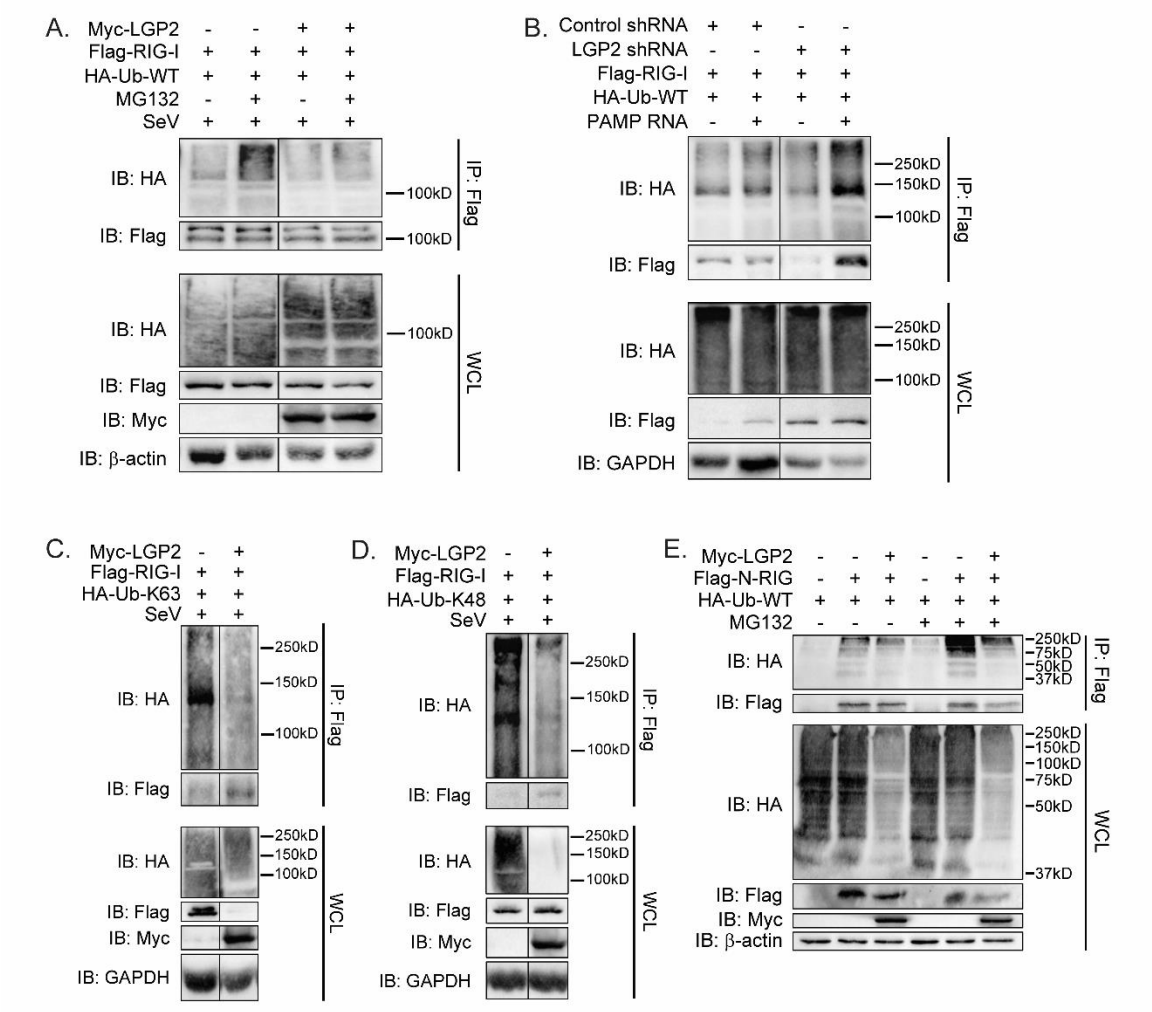

Figure 2-8: LGP2 inhibits K63-ubiquitination of RIG-I.

(**A**) HEK293 cells were transfected with Myc-LGP2, Flag-RIG-I and HA-ubiquitin (Ub-WT). Cells were treated with MG132 or DMSO control and infected with SeV for 8h. IP was performed for Flag-RIG-I. IB was performed for indicated proteins. Non-contiguous panels are from the same blot. WCL, whole cell lysate (input control). (**B**) LGP2 shRNA knockdown and scrambled control shRNA HEK293 cells were transfected with Flag-RIG-I and HA-ubiquitin (Ub-WT). Cells were transfected with 100ng/ul PAMP RNA. IB was performed for indicated proteins. Non-contiguous panels are from the same blot. (**C, D**) HEK293 cells were transfected with Myc-LGP2, Flag-RIG-I and either HA-Ub-K63 (C) or HA-Ub-K48 (D). Cells were infected with SeV for 8h. IB was performed for indicated

proteins. Non-contiguous panels are from the same blot. (**E**) HEK293 cells were transfected with Myc-LGP2, Flag-N-RIG and HA-ubiquitin (Ub-WT). Cells were then treated with MG132 or DMSO control. IP was performed for Flag-N-RIG. IB was performed for indicated proteins.

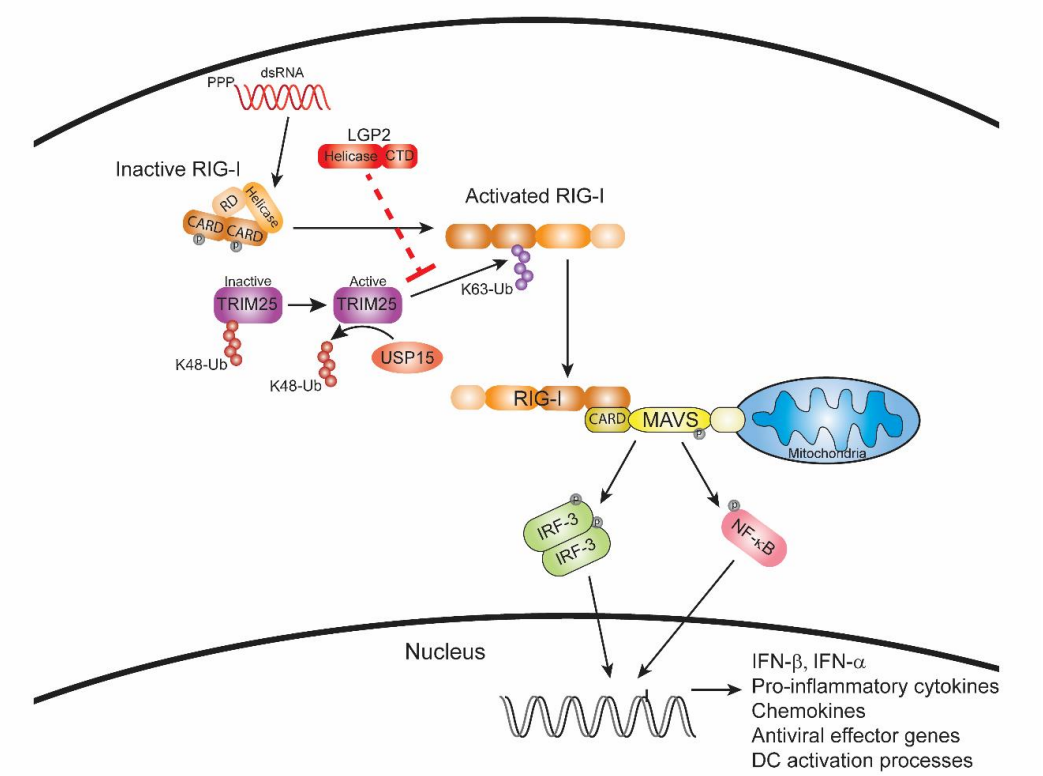

Figure 2-9: Molecular mechanism of LGP2 negative regulation of RIG-I signaling. Upon binding non-self RNA, RIG-I undergoes conformational changes and post-translational modifications to reach a signaling active state that can interact with MAVS to initiate downstream antiviral signaling. LGP2 negatively regulates RIG-I signaling by inhibiting the TRIM25-mediated K63-ubiquitination step of RIG-I activation.

Chapter 3: Zika Virus Antagonizes Type I Interferon Responses During Infection of Human Dendritic Cells

James R. Bowen[1,2,¶], Kendra M. Quicke[1,2,¶], Mohan S. Maddur [2,3], T. Justin O'Neal[1,2], Circe E. McDonald[1,2], Nadia B. Fedorova[4], Vinita Puri[4], Reed S. Shabman[4], Bali Pulendran[2,3], Mehul S. Suthar[1,2]

[1]Department of Pediatrics, Division of Infectious Diseases, Emory University School of Medicine, Atlanta, GA 30322, USA.

[2]Emory Vaccine Center, Yerkes National Primate Research Center, Atlanta, GA 30329, USA.

[3]Department of Pathology and Laboratory Medicine, Emory University School of Medicine, Atlanta, GA 30329, USA

[4]J. Craig Venter Institute, 9714 Medical Center Drive, Suite 1214, Rockville, MD

[¶]These authors contributed equally to this work.

*Originally published in *PLoS Pathogens*: Bowen JR, Quicke KM, Maddur MS, O'Neal JT, McDonald CE, Fedorova NB, Puri V, Shabman RS, Pulendran B, Suthar MS. Zika Virus Antagonizes Type I Interferon Responses during Infection of Human Dendritic Cells. *PLoS Pathogens*. 2017 Feb 2;13(2):e1006164.

Introduction

ZIKV is an emerging mosquito-borne flavivirus that is causally linked to severe neonatal birth defects upon congenital infection, including microcephaly and spontaneous abortion (Brasil et al., 2016b; Cugola et al., 2016; Driggers et al., 2016; Miner et al., 2016; Mlakar et al., 2016), and is associated with Guillain-Barre syndrome (Oehler et al., 2014) and severe thrombocytopenia (Sharp et al., 2016) in adults. Phylogenetic analysis has identified three ZIKV lineages, the East African, West African and Asian genotypes, and suggests initial emergence from East Africa and subsequent spread to other regions (Lanciotti et al., 2016). For decades, ZIKV remained in Africa and Asia where it sparked local epidemics characterized by mild, self-limiting disease in humans. In recent years, Asian lineage viruses have emerged as a global public health threat with widespread epidemics in Micronesia (2007), the Pacific Islands (2013-2014), and the ongoing outbreak in the Americas (2015-2016), where over 35 countries have reported local transmission (Petersen et al., 2016b). In December of 2015, local transmission of ZIKV was first confirmed in Puerto Rico, where an ongoing and widespread outbreak has caused over 29,345 confirmed cases as of October 20th, 2016 (Adams et al., 2016; Lozier et al., 2016). Of most concern, local mosquito-borne transmission of ZIKV has been reported in both Texas and Florida and has resulted in a sporadic, yet troubling increase in the number of confirmed cases (Likos et al., 2016). Recent human cases and studies in mice have highlighted the role of sexual transmission in spreading ZIKV (D'Ortenzio et al., 2016; Davidson et al., 2016; Govero et al., 2016; Yockey et al., 2016), and concerns of transmission through blood transfusions (Motta et al., 2016) has led to the Federal Drug Administration to advise screening of all blood and blood products for ZIKV. This growing public health crisis underpins the need to better understand viral replication dynamics and the induction of protective immune responses during ZIKV infection.

Dendritic cells (DCs) are critical immune sentinel cells, bridging pathogen detection to activation of innate and adaptive antiviral immunity. Recent studies have found that multiple subsets of murine DCs in the skin and draining lymph nodes (Schmid and Harris, 2014), as well as human Langerhans cells, dermal DCs, and moDCs are important cells of DENV replication (Cerny et al., 2014). Furthermore, a selective loss of type I IFN signaling in DCs ablates host restriction of WNV, resulting in lethality in a murine infection model (Pinto et al., 2014). Moreover, tick-borne encephalitis virus interferes with DC maturation through degradation of IRF-1 (Robertson et al., 2014), while JEV impairs CD8 T cell immunity through depletion of cross-presenting CD8α+ DCs and impaired up-regulation of MHC class II and the T cell co-stimulatory molecule CD40 (Aleyas et al., 2010). Despite these studies with closely related flaviviruses, the interplay between ZIKV and DCs remains poorly defined.

The RIG-I-like receptor (RLR) and type I IFN signaling axis is essential for inducing an antiviral response during flavivirus infection (Suthar et al., 2013a). The RLRs, which include RIG-I, MDA5, and LGP2, are a family of innate viral RNA sensors that reside in the cytoplasm of nearly every cell of the host (Loo and Gale, 2011). RIG-I and MDA5, signaling through the central adaptor protein mitochondrial antiviral signaling (MAVS), act in concert to restrict flavivirus replication by triggering the production of type I IFN, antiviral effector genes, and pro-inflammatory cytokines (Errett et al., 2013; Lazear et al., 2011; Pinto et al., 2014; Suthar et al., 2013a; Suthar et al., 2010). Recent work has shown evolutionarily distinct ZIKV strains antagonize innate immunity by targeting STAT2 for degradation, an essential signal transducer downstream of the type I IFN receptor (Grant et al., 2016). However, the contributions of the RLR signaling pathway to restrict ZIKV replication remain unknown.

In this study, we demonstrate that human moDCs are permissive to productive infection by a contemporary Puerto Rican ZIKV. We observed variation in virus

replication between individuals, despite similar levels of viral binding to cells. Historic ZIKV isolates from Africa and Asia also infected human DCs, wherein African lineage viruses replicated more rapidly and reached a higher infection magnitude, while also uniquely induced cell death. During infection with either contemporary or historic ZIKV strains, we observed minimal up-regulation of DC activation markers and pro-inflammatory cytokine secretion. ZIKV infection of human DCs led to significant induction of *IFNB1* at the transcript level, however, we observed impaired translation of type I IFN proteins despite induced protein expression of the RLRs (RIG-I, MDA5, and LGP2), STAT proteins (STAT1 and 2), and antiviral effectors (IFIT1, IFIT3, and viperin). Treatment with a highly specific RIG-I agonist, but not type I IFN, strongly restricted ZIKV replication in human DCs. The impaired ability of type I IFN to block infection reflected viral antagonism of type I IFN-mediated phosphorylation of STAT1 and STAT2. Altogether, we show that human DCs have limited immunogenicity following ZIKV infection, in part due to viral antagonism of type I IFN responses.

Methods

Ethics statement. Human peripheral blood mononuclear cells (PBMCs) were obtained from healthy donors in accordance with the Emory University Institutional review board according to IRB protocol IRB00045821.

Virus stocks. Zika virus strains PRVABC59 (PR-2015), P6-740 (P6-1966), MR-766 (MR-1947), and DakAr 41524 (Dak-1984) were obtained from the Centers for Disease Control and Prevention. All strains were passaged once in Vero cells cultured in MEM (Life Technologies Gibco) supplemented with 10% FBS (Optima, Atlanta Biologics) to generate working viral stocks. WNV-TX was generated from a previously described

infectious clone and passaged once in Vero cells (Suthar et al., 2012a). Viral stocks were titrated by plaque assay on Vero cells and stored at -80°C in MEM with 20% FBS.

Viral stock sequencing and genome annotation. The following Zika virus isolates in this study were subjected to whole genome sequencing using previously described methods (Moser et al., 2016). Briefly, total viral RNA was subjected to next generation sequencing library construction with random hexamer-based priming methods. Libraries were sequenced on the Illumina MiSeq platform and genome assembly was performed with CLC Bio (clc_ref_assemble_long v. 3.22.55705). Viral genome annotation was performed with VIGOR (Wang et al., 2012). The Genbank accession numbers are: KX601166.1 (Zika virus strain ZIKV/Aedes africanus/SEN/DakAr41524/1984); KX601167.1 (Zika virus strain ZIKV/Aedes sp./MYS/P6-740/1966); KX601168.1 (Zika virus strain ZIKV/Homo Sapiens/PRI/PRVABC59/2015); KX601169.1 (Zika virus strain ZIKV/Macaca mulatta/UGA/MR-766/1947).

Cells. Vero and A549 cells were obtained from ATCC and maintained in complete DMEM (DMEM medium [Corning] supplemented with 10% fetal bovine serum [Optima, Atlanta Biologics], 2mM L-Glutamine [Corning], 1mM HEPES [Corning], 1mM sodium pyruvate [Corning], 1x MEM Non-essential Amino Acids [Corning], and 1x Antibiotics/Antimycotics [Corning]). moDCs, monocytes, mDCs and pDCs were maintained in complete RPMI (RPMI 1640 medium [Corning] supplemented with 10% fetal bovine serum [Optima, Atlanta Biologics], 2mM L-Glutamine [Corning], 1mM Sodium Pyruvate [Corning], 1x MEM Non-essential Amino Acids [Corning], and 1x Antibiotics/Antimycotics [Corning]).

Primary cell isolation. PBMCs were isolated from freshly obtained healthy donor peripheral blood using lymphocyte separation media (MP Biomedicals or StemCell Technologies) per manufacturer's instructions. CD14+ monocytes were magnetically purified by positive selection using the EasySep Human CD14 Positive Selection Kit (Stem Cell Technologies) per manufacturer's instructions. CD14+ monocytes were re-suspended in complete RPMI medium with 100ng/mL each of recombinant human IL-4 and GM-CSF (PeproTech) at a cell density of 2e6 cells/mL. Spent media and non-adherent cells were removed 24 hours later and replaced with fresh media and cytokines. Suspension cells were harvested 5-6 days later for use in experiments. moDCs were consistently CD14-, CD11c+, HLA-DR+, DC-SIGN+, and CD1a+ by flow cytometry. To obtain mDCs and pDCs, monocytes were removed by positive selection using CD14 microbeads (Miltenyi Biotech, Germany) and the CD14- fraction was enriched for DCs using a human Pan-DC Enrichment Kit (Miltenyi Biotech, Germany). Enriched cells were surface stained to identify mDCs and pDCs for FACS sorting. Within the lineage-negative HLA-DR+ population, CD1c+ mDC1 and CD141+ mDC2 were collected together as CD11c+ mDCs, and CD123+ cells were collected as pDCs. Purity of microbead-sorted monocytes and FACS-sorted DC populations was >95%. Monocytes, mDCs and pDCs were maintained in complete RPMI medium. mDCs were cultured in the presence of human GM-CSF (2 ng/ml). pDCs were cultured in the presence of human IL-3 (10ng/ml).

Cell culture infections. moDCs were harvested after 5-6 days of differentiation and re-suspended in complete RPMI (without GM-CSF or IL-4) at 1e5 cells per well of a 96-well v-bottom plate for infections. moDCs, monocytes, mDCs, and pDCs were infected with the indicated ZIKV strain or WNV-TX at MOIs of 1 or 10 (based on Vero cell titer) for 1hr

at 37°C. After 1hr, virus inoculum was washed off and cells were re-suspended in 200µL fresh media and incubated at 37°C for 3-72hr.

Viral binding assay. moDCs were infected with ZIKV at MOI of 1 for 1hr on ice and washed 4x with cold PBS (Fig S1C). To remove bound virus, cells were then incubated with trypsin for 60 minutes on ice and washed 4x with cold PBS. Bound virus was quantitated by qRT-PCR for ZIKV RNA.

Agonist stimulation of moDCs. After 5-6 days of differentiation, moDCs were harvested and plated at 1e5 cells per well of a 96-well v-bottom plate in complete RPMI medium (without GM-CSF or IL-4) and stimulated with innate immune agonists. To stimulate RIG-I signaling, 10ng of a highly specific RIG-I agonist derived from the 3'-UTR of hepatitis C virus (Saito et al., 2008) was transfected per 1e5 cells using an mRNA transfection kit (Mirus). To stimulate type I IFN signaling, 1e5 cells were cultured in 200µL complete RPMI media in the presence of 100 IU/mL of human recombinant IFN-β (PBL Assay Science). To inhibit endogenous type I IFN signaling, 1e5 cells were cultured in 200µL complete RPMI media in the presence of 1.25µg/mL anti-human Interferon-α/β Receptor Chain 2 (clone MMHAR-2, EMD Millipore) blocking monoclonal antibody.

Focus forming assay. Supernatants collected from moDCs were diluted in DMEM supplemented with 1% FBS and used to infect Vero cells for 1hr at 37°C. Cells and inoculum were overlaid with methylcellulose (OptiMEM [Corning], 1% Antibiotic/Antimycotic [Corning], 2% FBS, and 2% methylcellulose [Sigma Aldrich]) and incubated for 72hr at 37°C. Cells were washed with PBS to remove methylcellulose and fixed with a 1:1 methanol:acetone mixture for 30min. Cells were blocked with 5% milk in

PBS at RT for 20min. Cells were incubated with primary antibody (mouse 4G2 monoclonal antibody) at 1µg/mL in 5% milk in PBS for 2hr at RT. Cells were incubated with secondary antibody (HRP-conjugated goat anti-mouse IgG) diluted 1:3000 in 5% milk in PBS for 1hr at RT. Foci were developed with TrueBlue Peroxidase Substrate (KPL). Plates were read on a CTL-ImmunoSpot S6 Micro Analyzer.

Quantitative reverse transcription-PCR (qRT-PCR). Total RNA was purified from 1e5 moDCs using the Quick-RNA MiniPrep kit (Zymo Research) per the manufacturer's instructions. Purified RNA was reverse transcribed using the High Capacity cDNA Reverse Transcription Kit (Applied Biosystems) using random hexamers. For quantitation of viral RNA and host gene expression, qRT-PCR was performed as described in Chapter 4 Methods.

Sequence Alignment. All pairwise alignments between ZIKV PR-2015, P6-1966, MR-1947, and Dak-1984 were performed using MegAlign and the Jotun Hein method. For calculations of nucleotide sequence similarity indices, the Martinez/Needleman-Wunsch method was used, and the parameters included a minimum match of 9, gap penalty of 1.1, and gap length penalty of 0.33.

Flow cytometry and Imagestream analysis. The following mouse anti-human antibodies were purchased from BioLegend or Becton Dickinson: CD11c (B-Ly6), HLA-DR (G46-6), CD1a (HI149), CD209 (9E9A8), CD14 (M5E2), CD80 (2D10), CD86 (IT2.2), and CD40 (5C3). Unconjugated monoclonal 4G2 antibody was kindly provided by Jens Wrammert and conjugated to APC (Novus Lightning-Link). Following 10min of Fc receptor blockade on ice (Human TruStain FcX, BioLegend), 1e5 cells were sequentially stained for surface markers and viability (Ghost Dye Red 780, Tonbo Biosciences) for

20min on ice. For intracellular staining of ZIKV E protein, cells were fixed and permeabilized (Foxp3/Transcription Factor Staining Buffer Kit, Tonbo Biosciences), blocked for 10 minutes (Human TruStain FcX and 10% normal mouse serum), and stained with 4G2-APC for 20min at room temperature. Multi-color flow cytometry acquisition was performed on a BD LSR II data was analyzed using FlowJo version 10. ImageStream data acquisition was performed on an ImageStream X Mark II and data was analyzed using Amnis IDEAS software. Monocytes, mDCs and pDCs were stained for viability using Zombie Aqua Fixable Viability Kit in protein-free buffer. Cells for surface staining were suspended in 10% FCS/PBS and incubated with antibodies for 20min at 4°C. Cells were washed, fixed with BD Fix buffer, and acquired on a BD LSR II with all analysis performed using FlowJo version 10.

Multiplex bead array. Cytokine analysis was performed on supernatants obtained from 1e5 moDCs following the indicated treatment conditions using a human magnetic 25-plex panel (ThermoScientific) and a custom magnetic 3-plex panel with human IFNβ, IFNα, and IFNλ1 (eBioscience) per the manufacturer's instructions, and read on a Luminex 100 Analyzer (Luminex). For cytokine analysis within cell lysates, 1e5 moDCs were collected in modified radioimmunoprecipitation assay buffer and diluted 1:10 prior to Luminex analysis. Culture supernatants from monocytes, mDCs or pDCs were analyzed for cytokine and chemokines using Cytokine Bead Array (CBA) kits (BD Biosciences, San Diego, US) as per the manufacturer's instructions. Cytokines analyzed included: GM-CSF, TNF-α, IL-4, IL-6, MIP-1α, IL-8, IL-15, IL-2R, IP-10, MIP-1β, Eotaxin, RANTES, MIG, IL-1RA, IL-12 (p40/p70) IL-13, IFN-γ, MCP-1, IL-7, IL-17, IL-10, IL-5, IL-2, IL-1β, IFNα, IFNβ, and IFNλ1.

Western blot analysis. STAT1 and STAT2 signaling was studied in A549 cells as previously described (Suthar et al., 2012a). Briefly, A549 cells were infected with the indicated ZIKV strain at an MOI of 0.1 and 1 (based on Vero cell titration). At 48hpi, cells were pulse treated with 1000 IU/mL of recombinant human IFNβ (PBL Assay Science) for 30 minutes and whole-cell lysates were collected in modified radioimmunoprecipitation assay buffer (10 mM Tris [pH 7.5], 150 mM NaCl, 1% sodium deoxycholate, and 1% Triton X-100 supplemented with Halt Protease Inhibitor Cocktail [ThermoFisher] and phosphatase inhibitor cocktail II [Calbiochem]). Western blot analysis was performed to detect STAT1 phosphotyrosine residue 701 (Cell Signaling), total STAT1 (Cell Signaling), STAT2 phosphotyrosine residue 689 (Upstate, EMD Millipore), total STAT2 (Cell Signaling), and glyceraldehyde 3-phosphate dehydrogenase (GAPDH; Cell Signaling). Protein expression levels were quantified using Image Lab software. For analysis of antiviral effector proteins within human moDCs, 4e5 cells were used per condition and protein lysates were collected as described for A549 cells. The following antibodies were obtained from Cell Signaling: RIG-I, MDA5, LGP2, STAT1, STAT2, IFIT1, viperin, and GAPDH. The IFIT3 antibody was kindly provided by Dr. G. Sen.

Results

Contemporary Puerto Rican ZIKV isolate productively infects human DCs

To understand viral replication in human DCs, we generated moDCs from healthy donors and challenged with PRVABC59, a low passage and sequence-verified ZIKV strain isolated in December of 2015 from the serum of a patient infected while traveling in Puerto Rico (hereafter referred to as “PR-2015”). Genome sequencing and phylogenetic analysis have revealed PR-2015 is closely related to clinical isolates responsible for the 2015-2016 outbreak in Brazil (Faria et al., 2016; Lanciotti et al.,

2016). To comprehensively profile PR-2015 replication kinetics in human moDCs, we performed parallel analyses of viral RNA synthesis and release of infectious virus. Viral replication began between 12 and 24 hours post infection (hpi), as evidenced by notable increases in viral RNA synthesis that plateaued between 48 and 72hpi (**Figure 1A**). No viral RNA was detected in mock-infected cells. The kinetics of viral RNA synthesis corresponded to increased release of infectious virus between 12 and 24hpi with continued log phase growth through 48hpi (**Figure 1B**). Together, our findings show that human moDCs support productive ZIKV replication with a contemporary Puerto Rican strain.

Cellular level analysis of Puerto Rican ZIKV replication in human DCs

We next determined how PR-2015 infection at the single cell level impacts viral growth kinetics in the bulk cell population. Infected moDCs were labeled for expression of ZIKV antigen using the pan-flavivirus 4G2 antibody, which recognizes an epitope in the structural envelope protein (E), and percent infection was assessed by flow cytometry. Infected cells were first detected in low numbers at 12hpi (Mock, 0.2 – 0.9%; PR-2015, 0.2 – 3.2%), and increased in percentage and staining intensity over the next 36 hours (**Figure 1C**). When we infected moDCs with ultraviolet (UV)-inactivated virus, we observed no E protein staining above uninfected cells, confirming detection of newly synthesized viral protein (**Figure 2A**). To confirm antibody staining, we performed ImageStream analysis of PR-2015-infected moDCs. ZIKV E protein was detected within the cytoplasm and did not co-localize with the cell surface marker CD11c (**Figure 1D**). This staining pattern is consistent with our recent observations of in placental macrophages, where viral protein localized to perinuclear regions within the cytoplasm (see Chapter 4), and with previously observed flavivirus ER-associated assembly sites

(Welsch et al., 2009). As expected, increases in the percentage of infected cells corresponded to the kinetics of viral RNA synthesis and infectious virus release.

Variability in Puerto Rican ZIKV infection occurs after viral binding

Notably, moDCs generated from four of the nine donors used in this analysis released lower amounts of infectious virus, and in some cases, synthesized lower amounts of viral RNA (**Figure 1A and 1B**). When we directly compared infectious virus release and viral E protein staining, the same 4 donors with the lowest infectious virus release at 48 and 72hpi ("low infection") also had lower percentages of E protein positive cells at 48hpi (0.4 – 3.1%) as compared to the other 5 "high infection" donors (9.8 – 18.9%) (**Figure 2B**). One explanation for variability in viral replication may be differences in viral binding to host receptors on moDCs generated from different donors. To test this, we developed a qRT-PCR-based viral binding assay (**Figure 2C**) (Liu et al., 2016; Nybakken et al., 2005). To verify we were measuring bound virus, we compared viral RNA levels with and without washing, as well as after trypsin treatment, which will likely cleave cellular receptors and remove bound virus from the cell surface. Washing cells significantly reduced the amount of virus detected and trypsin treatment further diminished viral RNA levels, confirming our ability to measure cell-bound virus (**Figure 1E**). In contrast to the differences observed in viral RNA synthesis, viral E protein staining, and infectious virus release, there was minimal difference in the amount of bound virus between different donors. This suggests that the variability in ZIKV infection between donors occurs after viral binding.

Differential infection of human DCs by evolutionarily distinct ZIKV strains

We next infected moDCs with sequence-verified ZIKV isolates spanning the evolution of the virus since its discovery, including ancestral isolates from East Africa (MR-766, "MR-

1947"), West Africa (DakAr 41524, "Dak-1984"), and Asia (P6-740, "P6-1966") (Haddow et al., 2012; Lanciotti et al., 2016). The MR-1947 strain was isolated in 1947 from an infected sentinel *Rhesus macaque,* monkey number 766, in the Ziika forest of Uganda. The Dak-1984 strain was later isolated from an infected *Aedes africanus* mosquito in Senegal in 1984. The P6-1966 strain was isolated in 1966 from an infected *Aedes aegypti* mosquito in Malaysia, and represents the oldest known ancestor of the Asian lineage since divergence from the African lineages. The laboratory passage history of each viral isolate varies, including multiple passages in suckling mouse brains in the case of MR-1947 and P6-1966, which must also be taken into consideration (**Table 1**). We independently sequenced each of the four ZIKV strains and performed nucleotide sequence alignments (see **Table 1** for genome accessions), finding P6-1966 shares 95.5% of its coding region with PR-2015, while MR-1947 and Dak-1984 only share 88.6% with PR-2015 (**Table 1**). This corresponds to 1.1%, 3.2%, and 3.0% differences in amino acids between PR-2015 and P6-1966, MR-1947, and Dak-194, respectively. Of note, MR-1947 diverged from PR-2015 more notably in the structural (4.4%) than non-structural proteins (2.9%).

Using the same moDCs generated from six of the previous donors (**Figure 1**), we directly compared infection kinetics of the ancestral strains with that of PR-2015. The infections were performed in parallel with PR-2015 to allow for direct cross-comparison of viral growth between the different viral strains (**Figure 4A**). MR-1947 exhibited rapid replication kinetics with increased infectious virus release and viral RNA synthesis occurring between 12 and 24hpi (**Figure 3A and 4B**). The percentage of infected cells peaked at 24hpi (**Figure 3C**). We next compared MR-1947 replication with Dak-1984, which is closely related to MR-1947 but has undergone less laboratory passaging. Despite reaching a similar infection magnitude, Dak-1984 exhibited slower growth kinetics as compared to MR-1947, with percent infection and release of infectious virus

peaking between 48 and 72hpi. The P6-1966 strain replicated with similar kinetics and magnitude to PR-2015 through 48hpi, although we did observe subtle differences in virus infection. In particular, P6-1966 replicated to modestly higher levels at 24hpi than PR-2015. Despite this, P6-1966 replication plateaued more rapidly than PR-2015 and failed to reach a comparable magnitude of infection. These subtle differences may reflect genetic changes between ancestral Asian lineage strains and current circulating strains (**Table 1**). Of note, P6-1966 was found to produce smaller viral plaques and foci (**Figure 4C**) on Vero cells as compared to the other three strains. Given recent studies linking ZIKV to cell death of neural progenitor cells, we evaluated cell viability during ZIKV infection of human moDCs (Dang et al., 2016; Garcez et al., 2016; Li et al., 2016a). While MR-1947 and Dak-1984 induced significant decreases in cell viability by 72hpi, neither of the Asian lineage strains resulted in loss of viability as compared to time-matched, uninfected cells (**Figure 3E**). Together, our data suggest that evolutionarily distinct ZIKV strains exhibit varying replicative and cell death capacities during infection of human moDCs.

Differential susceptibility of human DCs to ancestral and circulating ZIKV strains

Given our finding that moDCs generated from different donors have differential susceptibilities to PR-2015 infection (**Figure 1**), we next compared replication between the four ZIKV strains on a donor-by-donor basis. The MR-1947 strain replicated well within all donors, showing the least amount of variation in viral replication (**Figure 2B, 3B, and 3D**). The Dak-1984 strain also replicated well in most donors, albeit to modestly diminished peak levels in donors with lower PR-2015 replication. In contrast, P6-1966 replicated similarly to PR-2015 for any given donor, likely representing their shared ancestry. Together, these data suggest both viral factors, as found between different

strains, as well as non-viral factors, as found between different donors, influence ZIKV replication in human DCs.

ZIKV infection minimally activates human DCs

A critical function of DCs is the programming of virus-specific T cell responses that are required for clearance of virally infected cells. Engagement of virus-associated molecular patterns increases the surface expression of co-stimulatory and MHC molecules on activated DCs, potently enhancing their ability to prime virus-specific T cell responses (Pulendran, 2015). To determine the ability of ZIKV infection to activate DCs, we measured cell surface expression of co-stimulatory (CD80, CD86, and CD40) and MHC class II molecules at 48hpi with all four ZIKV strains. We labeled cells with 4G2 antibody and divided infected samples based on viral E protein staining (E protein-, bystander cells; E protein+, infected cells). Following infection with PR-2015, we observed significant but modest activation in E protein+ cells only, while infection of moDCs with P6-1966 or Dak-1984 induced minimal activation (**Figure 5A**). In comparison, MR-1947 induced modest activation, but primarily within the E protein- cell population. This is in contrast to the strong activation induced by RIG-I agonist treatment of moDCs (**Figure 6A**). Next, we confirmed our findings in more physiologically relevant human antigen presenting cell subsets. Similar to moDCs, *ex vivo* infection of primary monocytes, myeloid DCs, and plasmacytoid DCs from the blood of healthy donors with PR-2015 failed to induce up-regulation of co-stimulatory or MHC molecules (**Figure 6B-D**).

We next asked whether the donor variability in viral replication with PR-2015 (**Figure 1**) corresponded to differences in DC activation during infection. We grouped samples into “low” or “high” infection donors on the basis of viral E protein staining (**Figure 2B**). We found no differences in the up-regulation of CD80 and CD86 when we stratified by viral replication (**Figure 5B**). In contrast, both CD40 and MHC class II

showed greater up-regulation during infection of moDCs from donors with higher viral replication. This suggests that the induction of DC activation is influenced by the magnitude of viral replication. Altogether, these data show that ZIKV induces minimal DC activation and consequently, infected DCs may be compromised in their ability to prime antiviral T cell responses.

ZIKV does not induce pro-inflammatory cytokine secretion by human DCs

In addition to providing T cell co-stimulation, DCs promote innate and adaptive immunity through the secretion of pro-inflammatory mediators. We next assessed inflammatory cytokine and chemokine release following PR-2015 infection of moDCs. Consistent with minimal increases in surface expression of co-stimulatory molecules, ZIKV PR-2015 infection failed to induce the secretion of most pro-inflammatory cytokines assayed, despite the ability of RIG-I agonist to induce their secretion (**Figure 7A**). The ancestral strains also failed to induce substantial cytokine release during infection of human moDCs. Of exception, P6-1966 induced significant IL-6 secretion, and along with MR-1947 and Dak-1984, triggered modest yet significant IP-10 secretion. Finally, to confirm these findings in more physiologically relevant myeloid cell subsets, we stimulated primary monocytes (**Figure 7B**), myeloid DCs (**Figure 7C**), and plasmacytoid DCs (**Figure 7D**) with PR-2015 to assess cytokine and chemokine secretion. Despite the ability of LPS (monocytes and myeloid DCs) or R848 (plasmacytoid DCs) to induce cytokine production, infection with ZIKV did not promote notable pro-inflammatory cytokine secretion. Together, our data suggests that human antigen-presenting cells exposed to ZIKV are compromised in their ability to promote inflammatory responses.

Human DCs infected with ZIKV secrete minimal type I and III IFNs

During viral infection, early innate immune signaling triggers the production of type I and III IFNs and antiviral effector molecules that block viral replication (Schoggins and Rice, 2011). In particular, RLR and type I IFN signaling are essential for host restriction of flavivirus replication and ultimate control of infection (Olagnier et al., 2014; Pinto et al., 2014; Suthar et al., 2013a). Specific to ZIKV, mice with intact type I IFN responses support only limited and low level viral replication, while genetic ablation or antibody blockade of type I IFN signaling shifts the balance towards sustained, high level ZIKV replication and pathology, including neuroinvasive disease (Aliota et al., 2016; Lazear et al., 2016; Rossi et al., 2016). Moreover, mice deficient in their ability to produce type I IFN are similarly compromised in their ability to restrict viral replication (Lazear et al., 2016; Yockey et al., 2016).

To determine the potential of human DCs to trigger antiviral IFN responses during ZIKV infection, we measured the secretion of type I IFNs into the supernatant by infected populations of moDCs at 48hpi. Surprisingly, all four ZIKV strains failed to induce detectable IFNβ secretion and induced only minimal secretion of IFNα (**Figure 8A**). Given this intriguing finding and the recently appreciated role of type III IFNs in antiviral immunity, we next measured the secretion of IFNλ1 (Lazear et al., 2015a). Similar to type I IFNs, ZIKV infection induced minimal secretion of type III IFN protein (**Figure 8B**). Notably, treatment of the same donor cells with RIG-I agonist induced significant secretion of all three molecules, confirming these cells are capable of producing type I and type III IFNs. Similarly, pDCs produced low amounts of IFNα following ZIKV infection (data not shown).

Next, as a complementary measurement of type I IFN secretion, we infected moDCs with ZIKV in the presence of an anti-IFNAR2 blocking antibody. Blockade of type I IFN signaling enhanced ZIKV infection modestly across all four ZIKV strains, resulting in only a 2-3 fold increase in the percentage of virally infected cells (**Figure 8C**). Despite

this increase in the percentage of infected cells, we observed minimal differences in the release of infectious virus in the presence of anti-IFNAR2 blocking antibody. Combined, these findings suggest that moDCs secrete protective type I IFN during ZIKV infection, but at near undetectable levels.

ZIKV infection of human DCs induces type I IFN transcription, but not translation

Given that multiple pathogenic human viruses have evolved mechanisms to interfere with type I IFN transcription (Anglero-Rodriguez et al., 2014; Horner et al., 2012; Mibayashi et al., 2007; Prins et al., 2009), we next assessed the levels of *IFNB1* transcripts in ZIKV-infected moDCs. Despite near undetectable protein secretion, all four ZIKV strains induced notable *IFNB1* gene transcription at 48hpi, with MR-1947 showing the highest induction (**Figure 8D**). When we assessed *IFNB1* gene induction over an infection time-course, up-regulation of transcription occurred as early as 12hpi and remained at or near peak levels through 72hpi (**Figure 9A**). We also observed induction of *IFNA* transcription, but with delayed kinetics and magnitude as compared to *IFNB1*. *IFNA* transcription was up-regulated at 24hpi during infection with MR-1947, and at 48hpi during infection with the other three strains. These findings are consistent with our recent studies performed in placental macrophages, which showed minimal type I IFN protein secretion, but strong induction at the transcript level (see Chapter 4).

Given that RIG-I agonist induced IFNβ secretion, we directly compared *IFNB1* transcript levels in matched moDCs treated with RIG-I agonist or infected with ZIKV PR-2015. RIG-I agonist treatment induced modestly higher, but overall similar levels of *IFNB1* transcription as compared to ZIKV PR-2015 infection (**Figure 8E**). Next, to determine if there was impairment in type I IFN protein translation or secretion, we measured type I IFN protein in the supernatant and whole cell lysate from matched samples following RIG-I agonist treatment or infection with ZIKV PR-2015. We

hypothesized that if ZIKV blocked protein secretion, but not translation, we would find an accumulation of type I IFN protein in the whole cell lysate. However, we did not detect IFNβ or IFNα protein in either the supernatants or whole cell lysates above mock levels at either low or high MOI infection with ZIKV (**Figure 8F**). In contrast, both IFNβ and IFNα were observed in the supernatants and whole cell lysates following RIG-I agonist treatment. To determine if ZIKV could actively block type I IFN translation, we treated ZIKV PR-2015-infected moDCs with RIG-I agonist at 48hpi and measured IFNβ protein production. ZIKV infection resulted in an average 2-fold decrease in the induction of IFNβ protein translation as compared to RIG-I agonist alone (**Figure 8G**). Altogether, our data suggests that ZIKV antagonizes type I IFN translation during infection of human DCs.

Of relevance to our findings, protein kinase R (PKR) is important for maintaining mRNA stability of type I IFN transcripts during infection with certain RNA viruses (Schulz et al., 2010). In these studies, EMCV infected cells were found to strongly induce *Ifnb1* gene expression, but in the absence of PKR these transcripts lacked poly(A) tails, leading to diminished transcript stability and minimal protein translation. To determine if a similar phenomenon occurs during ZIKV infection of human DCs, we compared *IFNB1* transcript levels after performing cDNA synthesis with random hexamers, which will prime all RNA species, or Oligo(dT), which will only prime polyadenylated transcripts. We found no differences in *IFNB1* transcript levels between the two methods, suggesting ZIKV does not influence *IFNB1* transcript stability as a mechanism to inhibit protein translation (**Figure 9B**).

ZIKV infection induces an antiviral state within human DCs

Given the minimal secretion of type I and type III IFNs, we evaluated gene expression of the RLRs and host antiviral effectors. We observed up-regulation of RIG-I (*DDX58*),

MDA5 (*IFIH1*), and LGP2 (*DHX58*) in response to PR-2015 and P6-1966 at 24hpi, consistent with increases in virus load (**Figure 10A**). RLR expression continued to increase through 72hpi. While RLR expression was higher at 24hpi in moDCs infected with P6-1966 as compared to PR-2015, expression peaked at similar levels at 48 and 72hpi, potentially reflecting the slightly enhanced replication kinetics of P6-1966. In contrast to the Asian lineages, MR-1947 exhibited strong RLR up-regulation by 12hpi with peak expression between 24 and 48hpi. Moreover, the magnitude of RLR transcription during peak responses was notably higher for MR-1947 infection. The kinetics of RLR expression during infection with Dak-1984 were more similar to the Asian lineage strains than MR-1947, first increasing at 24hpi. Interestingly, despite reaching a similar overall magnitude of infection as MR-1947, Dak-1984 induced lower RLR transcription at all time-points.

We next evaluated expression of the IFIT gene family members, *OAS1*, and viperin (*RSAD2*), antiviral effectors with known activity against flaviviruses (Schoggins et al., 2011). In moDCs infected with PR-2015, we observed up-regulation of *IFIT1*, *IFIT2* and *IFIT3* beginning at 12hpi, with peak expression between 48 and 72hpi (**Figure 10B**). P6-1966 infection resulted in slightly delayed IFIT gene induction as compared to PR-2015. Despite this delay, P6-1966 induced stronger IFIT gene expression by 24hpi. We observed similar findings with *RSAD2* expression, with PR-1966 infection inducing lower transcript levels at 12hpi, but increased responses at 24hpi as compared to PR-2015. We found *OAS1* transcripts were up-regulated at 24hpi by both PR-2015 and P6-1966, although to higher levels during P6-1966 infection. MR-1947 infection exhibited enhanced kinetics and magnitude of antiviral effector gene transcription, with *IFIT* family members and *RSAD2* being induced as early as 12hpi. While *OAS1* was up-regulated with similar kinetics to the Asian lineage strains, the magnitude was also notably higher

during MR-1947 infection. In general, Dak-1984 was transcriptionally most similar to the Asian lineage viruses, despite higher levels of viral replication during Dak-1984 infection.

Given observed differences in PR-2015 replication between donors, we compared gene expression between donors with “low” or “high” infection (**Figure 1 and 2B**). For all RNA samples, we labeled infected cells in parallel for viral E protein, allowing us to stratify our RNA data by the percentage of viral E protein+ cells. Donors with low infection had overall lower expression of RLR, type I IFN, and antiviral effector genes as compared to donors with high infection (**Figure 11**). Furthermore, there were no differences in the expression of any of the measured host genes at 3hpi between “low” and “high” infection donors, a time that likely represents basal level expression. Overall, these data show that ZIKV infection is capable of initiating antiviral responses in moDCs, with expression of certain antiviral effector genes being induced rapidly after infection, prior to log phase viral growth.

We next questioned whether the observed up-regulation of antiviral effector genes led to corresponding increases at the protein level, in light of our findings with type I IFN. As expected, overnight stimulation with RIG-I agonist induced up-regulation of the RLRs (RIG-I, MDA5, and LGP2), STAT proteins (STAT1 and STAT2), and multiple proteins directly involved in restriction of viral replication (IFIT1, IFIT3, and viperin) (**Figure 10C**). Notably, we observed no induction of IFIT1, IFIT3, or viperin in untreated cells. In contrast to impaired translation of type I IFN proteins, infection of moDCs for 48hrs with ZIKV PR-2015 or MR-1947 strongly up-regulated production of the RLRs, STAT proteins, and viral restriction factors to similar levels observed following RIG-I agonist treatment. We observed MOI-dependent increases in many cases (STAT1, IFIT1, IFIT3, viperin) following infection with PR-2015 at MOIs of 1 and 10. Similar to what was observed at the transcript level, MR-1947 induced higher levels of antiviral proteins as compared to PR-2015 when comparing infections at MOI of 1. This

is likely explained by the greater magnitude of infection seen with MR-1947. Together, these findings suggest that ZIKV selectively inhibits in type I IFN protein translation, while translation of other antiviral host proteins remains intact.

ZIKV replication is blocked by RIG-I, but not type I IFN signaling

Given our findings that ZIKV infection of moDCs induced an antiviral state, and the importance of RLR and type I IFN signaling in restriction of flavivirus replication (Errett et al., 2013; Pinto et al., 2014; Suthar et al., 2013a; Suthar et al., 2010), we next determined the ability of innate immune signaling pathways to restrict ZIKV replication within human DCs. At 1hpi, we treated infected moDCs with innate immune agonists and assessed viral replication at 48hpi (**Figure 12A**). To trigger RLR signaling, moDCs were transfected with a highly specific RIG-I agonist, derived from the 3' UTR of hepatitis C virus (Saito et al., 2008; Schnell et al., 2012). To trigger type I IFN signaling, we treated moDCs with 100 IU/mL of recombinant human IFNβ. RIG-I agonist treatment potently blocked ZIKV replication, significantly lowering infectious virus release to levels at or near the assay limit of detection (**Figure 12B**). Notably, the levels of infectious virus remaining after RIG-I agonist treatment were similar to levels found at 3 and 12hpi (**Figure 3A**), prior to the log phase viral growth, and may represent residual input virus rather than replicating virus. Importantly, RIG-I agonist treatment restricted replication of all four ZIKV strains. In contrast, type I IFN treatment resulted in only modest, and non-significant decreases in viral replication. Altogether, RLR signaling, but not type I IFN signaling, potently blocks replication of four evolutionarily distinct ZIKV strains.

ZIKV antagonizes type I IFN signaling by targeting STAT1 and STAT2 phosphorylation

Secreted type I IFN binds to the type I IFN receptor (IFNAR), a heterodimeric complex found on the cell surface of almost all nucleated cells, triggering activation of the receptor associated kinases JAK1 and TYK2 (Schoggins and Rice, 2011). JAK1 and TYK2 phosphorylate and activate the latent transcription factors STAT1 and STAT2, which translocate to the nucleus and associate with IRF-9 to trigger antiviral gene transcription. Most flaviviruses known to infect humans have evolved mechanisms to inhibit type I IFN responses through antagonism of JAK/STAT signaling (Best et al., 2005; Keller et al., 2006; Laurent-Rolle et al., 2010; Laurent-Rolle et al., 2014). Given our finding that type I IFN treatment was not effective at blocking ZIKV replication in moDCs, we evaluated the ability of ZIKV to antagonize STAT1 and STAT2. For these studies, we utilized human A549 cells, which have been previously shown to be permissive to ZIKV infection (Frumence et al., 2016) and have been employed to study antiviral innate immune signaling (Goulet et al., 2013; Keller et al., 2006; Suthar et al., 2012a). We pulse treated uninfected or ZIKV-infected cells (48hpi, MOIs 0.1 and 1) for 30 minutes with IFNβ (1000 IU/mL) and evaluated phosphorylation of STAT1 (Y701) and STAT2 (Y689) by western blot. Cells infected with any of the four ZIKV strains did not show enhanced STAT1 or STAT2 phosphorylation above untreated ZIKV-infected cells (**Figures 13A and 13B, top panels**). Infection alone increased the total levels of STAT1 and STAT2 protein, although notably less so at an MOI of 1 as compared to MOI 0.1. Given the different levels of total STAT proteins between conditions, we calculated the ratio of phosphorylated:total protein to allow for a better comparison of the phosphorylation status (**Figures 13A and 13B, bottom panels**). Indeed, even in instances where ZIKV infection increased total STAT protein levels, the majority remained in an unphosphorylated state. Interestingly, while ZIKV infection alone did induce low levels of STAT1 and STAT2 phosphorylation, in most conditions, there was a notable decrease in phosphorylation at MOIs of 1 as compared to MOIs of 0.1, a finding

most profound with the African lineage viruses. We next determined the percentage of ZIKV infected cells at MOIs of 0.1 and 1 using flow cytometry. The percentage of infected cells ranged from 32.7 – 74% at an MOI of 0.1 and increased to 60.1 – 87.8% at an MOI of 1 across infection with the four strains (**Figure 14**). Of note, we observed higher CPE and cell death at MOIs of 1 as compared to MOI of 0.1 when preparing cells for staining. Given the presence of uninfected cells, even at MOIs of 1, it remains possible that the STAT1 and STAT2 phosphorylation observed during infection is likely from uninfected cells. Nevertheless, this confirms that the majority of cells were ZIKV-infected at the time of pulse treatment with IFNβ and inhibition of type I IFN signaling can be attributed to ZIKV infection.

We next determined whether ZIKV infection antagonizes type I IFN signaling within human DCs. ZIKV PR-2015-infected moDCs (48hpi, MOI 10) were left untreated or pulse treated with IFNβ for 30 minutes and evaluated for STAT1 and STAT2 phosphorylation. Infection with ZIKV PR-2015 in the absence of IFNβ treatment induced minimal STAT1 phosphorylation and low levels of STAT2 phosphorylation, despite notable up-regulation of STAT1 and STAT2 total proteins (**Figure 13C, left panel**). Treatment of ZIKV-infected cells with IFNβ increased phosphorylation of STAT2, and to a lesser extent STAT1, but to notably lower levels than treatment of uninfected cells when compared to total STAT1 and STAT2 protein levels (**Figure 13C, right panel**). Combined, this shows that similar to A549 cells, ZIKV antagonizes the phosphorylation of STAT1 and STAT2.

Discussion

In our study, we show a contemporary Puerto Rican ZIKV strain, PR-2015, productively infects human moDCs with notable donor variation in viral replication, despite no differences in viral binding. Ancestral ZIKV strains of the African (MR-1947 and Dak-

1984) and Asian (P6-1966) lineages also infected human moDCs. Each strain exhibited unique viral growth curves, with cell death only observed during infection with African lineage strains. We observed minimal up-regulation of co-stimulatory and MHC molecules, inflammatory cytokine secretion, as well as antagonism of type I IFN translation during ZIKV infection, despite notable transcriptional up-regulation of *IFNB1*. Despite this, ZIKV infection induced an antiviral state as noted by strong up-regulation of the RLRs (RIG-I, MDA5, and LGP2), STAT proteins (STAT1 and 2), and antiviral effectors (IFIT1, IFIT3, and viperin). Finally, RIG-I agonist treatment potently restricted ZIKV replication, while type I IFN was significantly less effective due to ZIKV antagonism of STAT1 and STAT2 phosphorylation.

Despite their evolutionary distance (Lanciotti et al., 2016), minimal attention has been given to studying infection differences between African and contemporary Asian lineage strains. In general, MR-1947 and Dak-1984 replicated with more rapid kinetics and to a higher magnitude than the Asian lineage viruses. The African lineage viruses were also unique in their ability to induce cell death during infection, potentially attributed to their replication characteristics. This raises the possibility that Asian lineage viruses may have adapted to be less cytopathic in DCs, potentially resulting from, or contributing to lower viral replication rates. Alternatively, this phenotype may be partly attributed to the extensive passage history and cell culture adaption of MR-1947, a process known to impact ZIKV and WNV glycosylation patterns (Chambers et al., 1998; Haddow et al., 2012), *in vitro* replication of multiple RNA viruses (Chambers et al., 1998; Klimstra et al., 1998), and *in vivo* pathogenesis of hepatitis C virus (Kaul et al., 2007). In support of this, MR-1947, which has undergone a multitude of passages in suckling mouse brains (**Table 1**), replicated with more rapid kinetics than Dak-1984, which has been minimally passaged. Despite differences in kinetics, both viruses reach similar peak infection magnitudes and induced cell death at 72hpi, suggesting cell culture adaption alone does

not explain their unique features. Future studies comparing low passaged African and Asian lineage viruses or infectious clone derived viruses (Shan et al., 2016) are needed to further study differences between these viral genotypes.

While a previous study identified as high as 60% viral E protein-positive cells at 24hr following infection of human moDCs with a French Polynesian strain of ZIKV, we did not observe infection rates this high in our study (Hamel et al., 2015). This may be explained by differences in ZIKV strains, donor-to-donor variation, or technical differences in virus stock propagation or cell infections. Furthermore, our study did not rely solely on 4G2 staining, which cross-reacts with DENV and other flaviviruses, but also included sequence-specific detection of ZIKV RNA to verify infection.

We observed striking variability in viral replication between moDCs generated from different healthy donors. In fact, we found a subset of donors with moDCs that were less susceptible to infection with PR-2015. Although differences in receptor expression or affinity for viral proteins between donors could explain this variability, we found minimal differences in the amount of virus bound to moDCs from different donors. Instead, variability occurred after viral binding, with striking differences in the kinetics and magnitude of viral RNA synthesis, viral E protein staining, and infectious virus release between donors. One plausible explanation for infection differences is that moDCs from less susceptible donors are capable of mounting more rapid and stronger antiviral responses. However, induction of antiviral effector genes was found to be less pronounced in donors with lower viral replication. Moreover, differences in ZIKV replication did not correspond to differential DC activation or pro-inflammatory cytokine release. Of note, susceptibility to PR-2015 replication corresponded to P6-1966, where moDCs with lower PR-2015 infection rates also had lower P6-1966 replication. This raises the possibility that moDCs from some donors are better at controlling ZIKV infection. However, MR-1947 was found to replicate to high levels in moDCs from all

donors, even those with low PR-2015 replication. Although this may be related to the aforementioned cell culture adaptation of MR-1947, it is possible that differential host adaption of Asian lineage strains during their evolution has resulted in differences in infection rates. Altogether, complex host factors, such as genetics, metabolism, ER stress, or redox state might explain differential susceptibility to ZIKV infection. Indeed, the collaborative cross, a mouse model of genetic diversity, has recently revealed the importance of host genetics in influencing susceptibility to WNV infection (Graham et al., 2015). Similar donor variability in viral replication has also been observed during HIV infection of human monocyte derived macrophages (Bol et al., 2009). Although some donor variability in HIV infection was found to correspond with the presence of the CCR5 Δ32 mutation, most of the variability remained unexplained. Influenza A infection of primary human bronchial epithelial cells has also been found to vary notably between donors (Travanty et al., 2015). Interestingly, cells isolated from obese donors were more susceptible to viral infection, highlighting how complex, non-genetic factors can also influence susceptibility to viral infection at the cellular level. It is interesting to speculate that differential susceptibility of DCs to ZIKV may correspond to pathogenesis during human infection, where 80% of infected individuals are asymptomatic and those with symptoms have differences in clinical presentations.

The minimal activation of DCs following exposure to ZIKV is similar to previous findings with tick-borne encephalitis virus, where DC maturation is inhibited through IRF-1 degradation (Robertson et al., 2014). Diminished up-regulation of MHC class II and CD40 molecules on splenic CD8α+ DCs was also observed following JEV infection in mice (Aleyas et al., 2010). In contrast to our findings with ZIKV, infection of human moDCs with the YFV vaccine strain, YF-17D, promotes DC maturation (Querec et al., 2006). The ability of YF-17D to activate human DCs may be explained through the loss of a viral antagonist during its attenuation process, or could represent a unique behavior

of certain flaviviruses. Indeed, infection of human moDCs with a pathogenic DENV serotype 2 strain also promotes the up-regulation of co-stimulatory and MHC molecules, along with pro-inflammatory cytokine secretion (Libraty et al., 2001). Combined, this work suggests members of Flaviviridae have evolved complementary, as well as unique strategies of targeting DCs to subvert the pressures of host immunity.

While infection with all four ZIKV strains induced type I IFN mRNA transcription, we detected minimal translation of type I or III IFN proteins. This was in contrast to RIG-I agonist treatment, which induced translation of both type I and III IFN proteins, despite similar levels of *IFNB1* transcription as observed during ZIKV infection. Indeed, ZIKV infection diminished RIG-I agonist-induced type I IFN production, suggesting ZIKV directly antagonizes type I IFN translation. We also observed a minor 2-3 fold enhancement in viral infection when type I IFN signaling was inhibited by antibody-mediated receptor blockade, further indicating type I IFN is secreted at only minimal levels during ZIKV infection. Previous work with DENV observed secretion of IFNα protein during infection of human moDCs, suggesting our findings may be unique to ZIKV infection. Despite the antagonism of type I or III IFN production, ZIKV infection up-regulated the expression of the RLRs, STAT proteins, and multiple antiviral effector proteins to similar levels observed following RIG-I agonist treatment. This suggests that the block in type I IFN translation is selective, and that much of the antiviral response induced during ZIKV infection of human DCs occurs independent of type I IFN signaling. Indeed, in the context of WNV infection, multiple antiviral effector genes are induced through an IFN independent, RLR signaling-dependent manner (Suthar et al., 2013a).

Recent work from multiple groups has analyzed ZIKV infection and immune responses from human clinical samples and in a variety of human cell types. During the acute phase of human ZIKV infection, multiple pro-inflammatory cytokines are increased within the blood, although the cellular sources of these responses remain unknown

(Tappe et al., 2016). Our findings suggest that infected DCs may not be an important source of these pro-inflammatory cytokines. In contrast to our work with DCs, ZIKV infection of A549 cells has been shown to induce IFNβ secretion, further suggesting cells other than DCs may be responsible for inducing inflammatory responses during ZIKV infection (Frumence et al., 2016). Indeed, ex vivo infection of primary human skin fibroblasts was found to induce transcriptional up-regulation of multiple pro-inflammatory mediators, although protein secretion was not explored (Hamel et al., 2015). In regards to congenital ZIKV infection, recent work has found both human fetal neural progenitor cells and placental HCs are poorly immunogenic, similar to our findings with adult DCs (see Chapter 4 and (Hanners et al., 2016)). In contrast, human embryonic cranial neural crest cells secrete cytokines following ZIKV infection at levels that were found to be harmful for neurodevelopment (Bayless et al., 2016). Together, different target cells of ZIKV have varying capacities to induce pro-inflammatory cytokine responses and further study is needed to determine the cell types responsible for initiating inflammatory responses during human infection.

Recent work has revealed that the NS5 protein of both MR-1947 and PR-2015 promotes the degradation of human STAT2 protein during infection, allowing ZIKV to evade type I IFN signaling downstream of type I IFN receptors (Grant et al., 2016). In agreement with this work, we found that while RIG-I agonist treatment potently restricted viral replication, type I IFN treatment was significantly less effective at blocking ZIKV infection. Mechanistically, we found infection with both contemporary and ancestral strains of ZIKV blocked phosphorylation of STAT1 and STAT2 downstream of type I IFN signaling in both human DCs and A549 cells. In contrast to previous findings, we did not observe significant STAT2 degradation in either human DCs or A549 cells (Grant et al., 2016). In fact, in most cases, we observed up-regulation of STAT2 protein during ZIKV infection. One possibility for this discrepancy may be differences in the cell types used

between the studies. Grant et al performed studies in Vero and 293 cells, while we conducted experiments in A549 cells and primary human DCs. We also used lower MOIs (0.1 and 1) for our A549 cell line infections than in their studies (MOI 5, 10, and 20) and did not perform viral protein overexpression studies. Although we did use an MOI of 10 for some of our DC work, the magnitude of infection is significant lower than in Vero or 293 cells and such differences in cell infectivity could also explain our differing findings. Nevertheless, we find that ZIKV antagonizes the type I IFN signaling pathway through blockade of STAT1 and STAT2 phosphorylation.

The ability of RIG-I agonist to efficiently block ZIKV replication is most likely attributed to an IFN-independent induction of antiviral effector molecules (Olagnier et al., 2014; Suthar et al., 2013a). Our observations that ZIKV infection induces an antiviral state in moDCs, despite viral antagonism of type I IFN responses, further suggests IFN-independent signaling pathways, such as RLR signaling through MAVS, are likely important for restriction of ZIKV replication. The ability of RIG-I agonist to potently restrict ZIKV replication across all four strains highlights the RLR signaling pathway as a potential target for antiviral therapy. Of note, small molecule agonists of the RLR pathway have gained recent attention as potential candidate vaccine adjuvants (Beljanski et al., 2015; Kulkarni et al., 2014) and for use in broad-spectrum antiviral therapy, including proof-of-principle studies showing potent activity against multiple flaviviruses (Olagnier et al., 2014; Pattabhi et al., 2015).

In summary, our work shows that human DCs are productively infected by currently circulating (PR-2015) and ancestral (P6-1966, MR-1947, and Dak-1984) strains of ZIKV. Each ZIKV strain exhibited unique replication kinetics and downstream effects on human DCs, including a unique ability of African lineage viruses to induce cell death. There was notable donor variability in viral replication across the ZIKV strains, highlighting the importance of both host and viral factors in influencing susceptibility

during infection. We observed minimal DC activation or secretion of inflammatory cytokines, as well as viral antagonism of type I IFN translation, despite strong induction of *IFNB1* at the RNA transcript level. Nevertheless, ZIKV-infected moDCs induced an antiviral state as noted by strong up-regulation of multiple antiviral effectors. RIG-I agonist treatment potently restricted ZIKV replication in human DCs, while type I IFN treatment had minimal effects. Mechanistically, all strains of ZIKV antagonized type I IFN-mediated phosphorylation of STAT1 and STAT2. Combined, our findings show that ZIKV efficiently evades type I IFN responses, but RLR signaling remains functional and may be a target for antiviral therapy in humans.

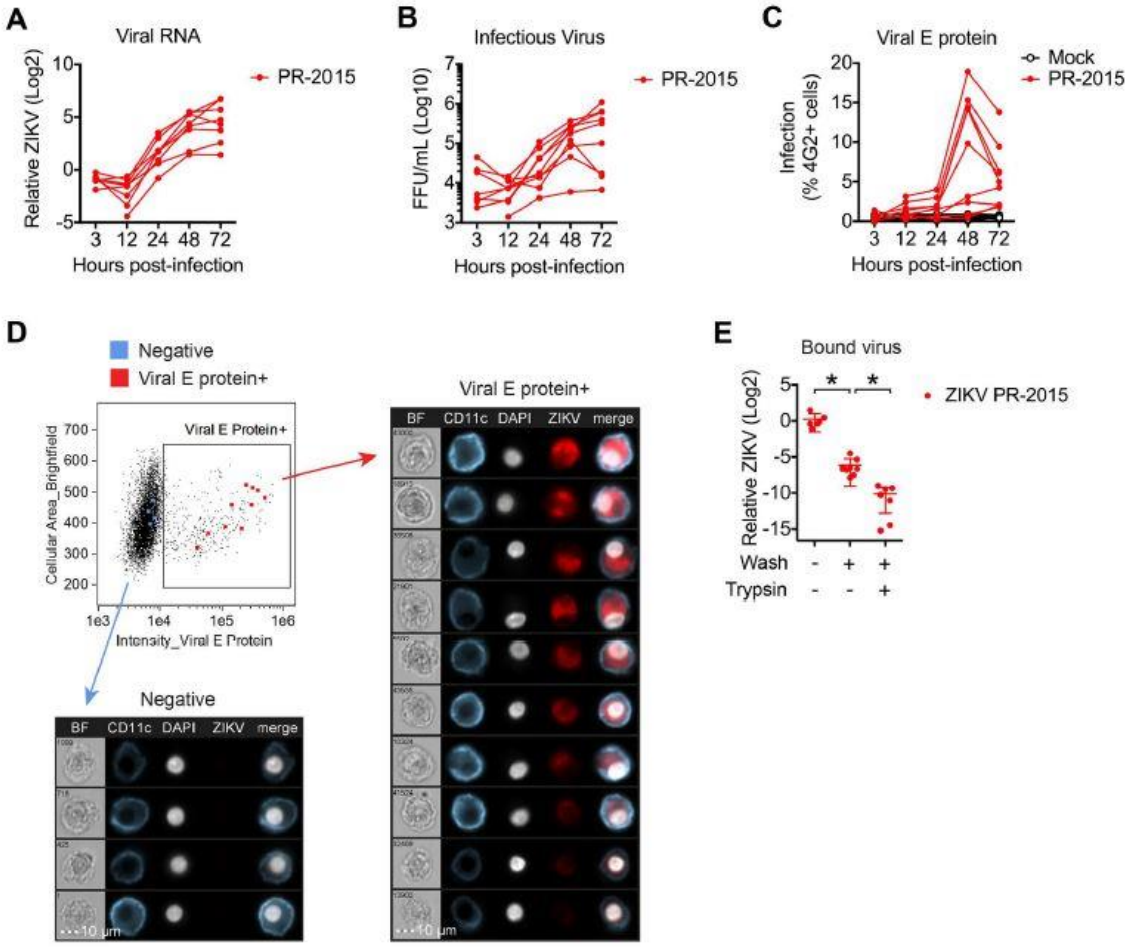

Figure 3-1: Contemporary Puerto Rican ZIKV isolate productively infects human DCs.

moDCs were infected with ZIKV PR-2015 at MOI of 1 and assessed for viral replication at indicated hours post-infection. **(A)** Viral RNA was detected in cell lysates by qRT-PCR for ZIKV E protein mRNA. Gene expression is shown as relative expression after normalization to *GAPDH* levels in each respective sample (n=7 donors). **(B)** Viral titers in supernatants of ZIKV-infected moDCs as determined by focus forming assay (n=8 donors). FFU, focus forming units. **(C)** Percent infected cells as assessed by ZIKV E protein staining (4G2-APC antibody) and flow cytometry (n=9 donors). **(D)** ImageStream analysis of ZIKV-infected moDCs labeled for viral E protein at 48hpi. Images of individual cells highlighted in the flow plot are represented and ordered according to E protein

staining intensity. **(E)** moDCs were infected with ZIKV PR-2015 at MOI of 1 for 1hr on ice, washed extensively, and bound virus was quantitated by qRT-PCR for ZIKV RNA. Gene expression is represented as relative expression after normalization to *GAPDH* levels in each respective sample and shown as the mean +/- SD from 5 donors.

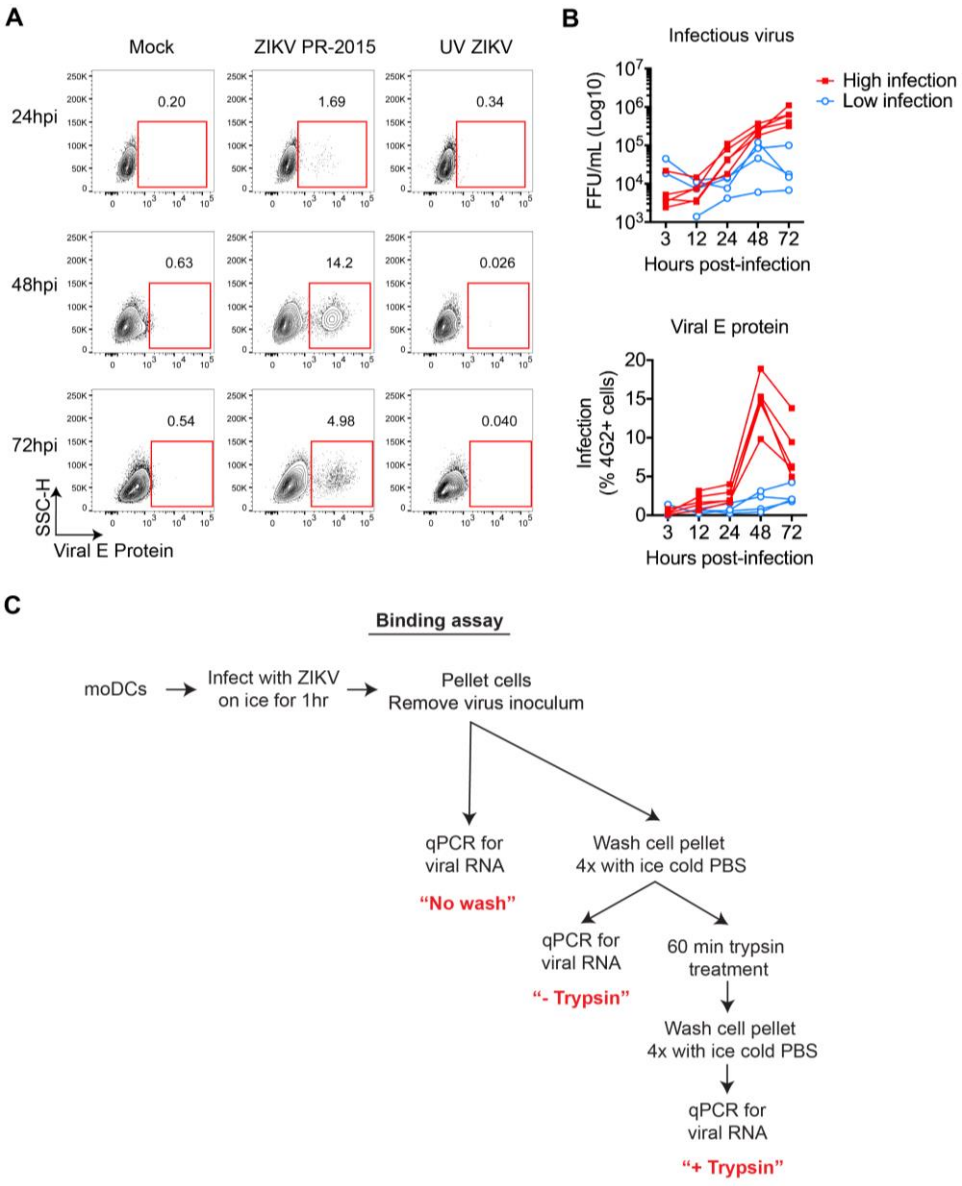

Figure 3-2: ZIKV PR-2015 productively infects moDCs.

(A) moDCs were mock-infected, infected with ZIKV PR-2015, or UV-inactivated PR-2015 ("UV ZIKV") at MOI of 1 and the percentage of infected cells assessed by ZIKV E protein

staining. ZIKV PR-2015 was inactivated by exposure to ultraviolet (UV) light for 1hr. hpi, hours post-infection. **(B)** Donors were stratified into “high” and “low” infection. **(C)** Experimental outline for ZIKV binding assay.

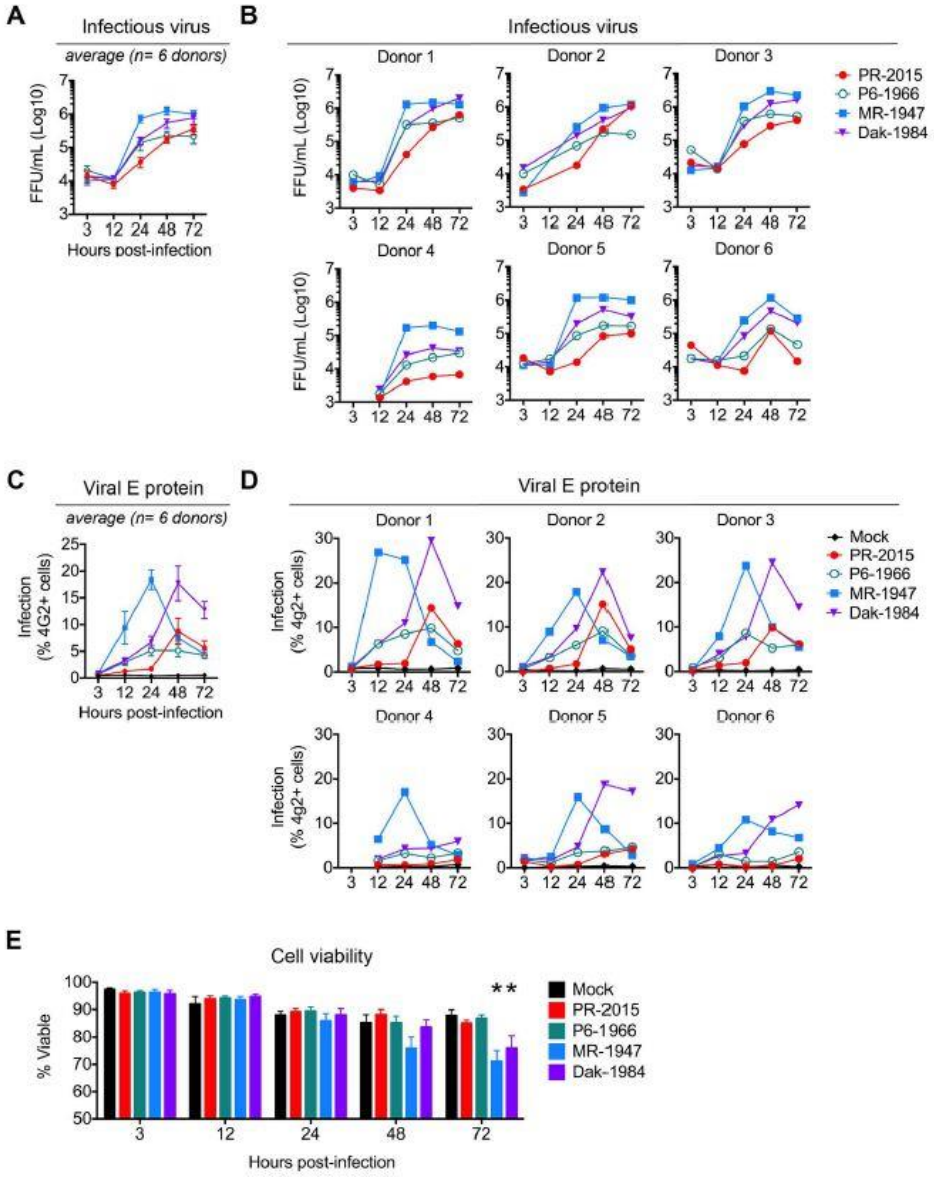

Figure 3-3: Differential infection of human DCs by evolutionarily distinct ZIKV strains.

moDCs were infected with PR-2015, P6-1966, MR-1947, or Dak-1984 at MOI of 1 and assessed for viral replication at the indicated hours post-infection. **(A)** Infectious virus

release into the supernatant was determined by FFA. Shown as the mean +/- SEM from 6-9 donors. **(B)** Infectious virus release for 6 of the individual donors summarized in panel A. **(C)** Percent infected cells assessed by ZIKV E protein staining and flow cytometry. Shown as the mean +/- SEM from 6-9 donors. **(D)** Percent infected cells in 6 of the individual donors summarized in panel C. **(E)** Cell viability of infected moDCs assessed by Ghost Red 780 (Tonbo) viability staining and flow cytometry. Shown as the mean +/- SEM from 6-9 donors. Statistical significance ($p < 0.05$) was determined using a two-way ANOVA with comparisons made to mock-infected cells. See also Table 1.

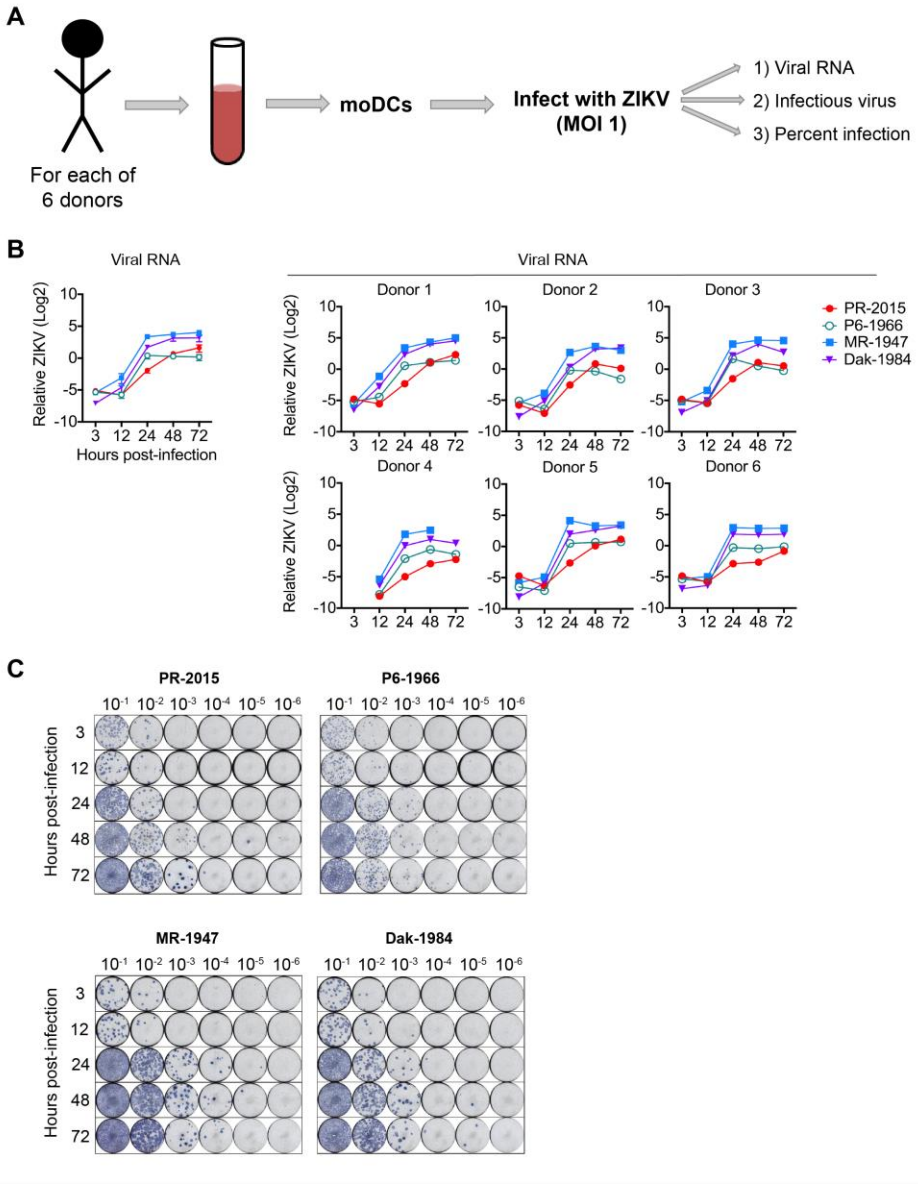

Figure 3-4: ZIKV strains have different replication characteristics.

(A) Experimental outline used to obtain data in Figure 3. moDCs were generated from healthy donors and infected with all four strains of ZIKV (n=6 donors). We performed parallel analysis of viral RNA, infectious virus release, and viral E protein staining from each of these samples. **(B)** Viral RNA was detected by qRT-PCR for ZIKV E protein mRNA. Gene expression is shown as relative expression after normalization to *GAPDH* levels in each respective sample (n=6 donors). **(C)** Representative FFA staining for the different ZIKV stains. Serial dilutions are indicated across the top.

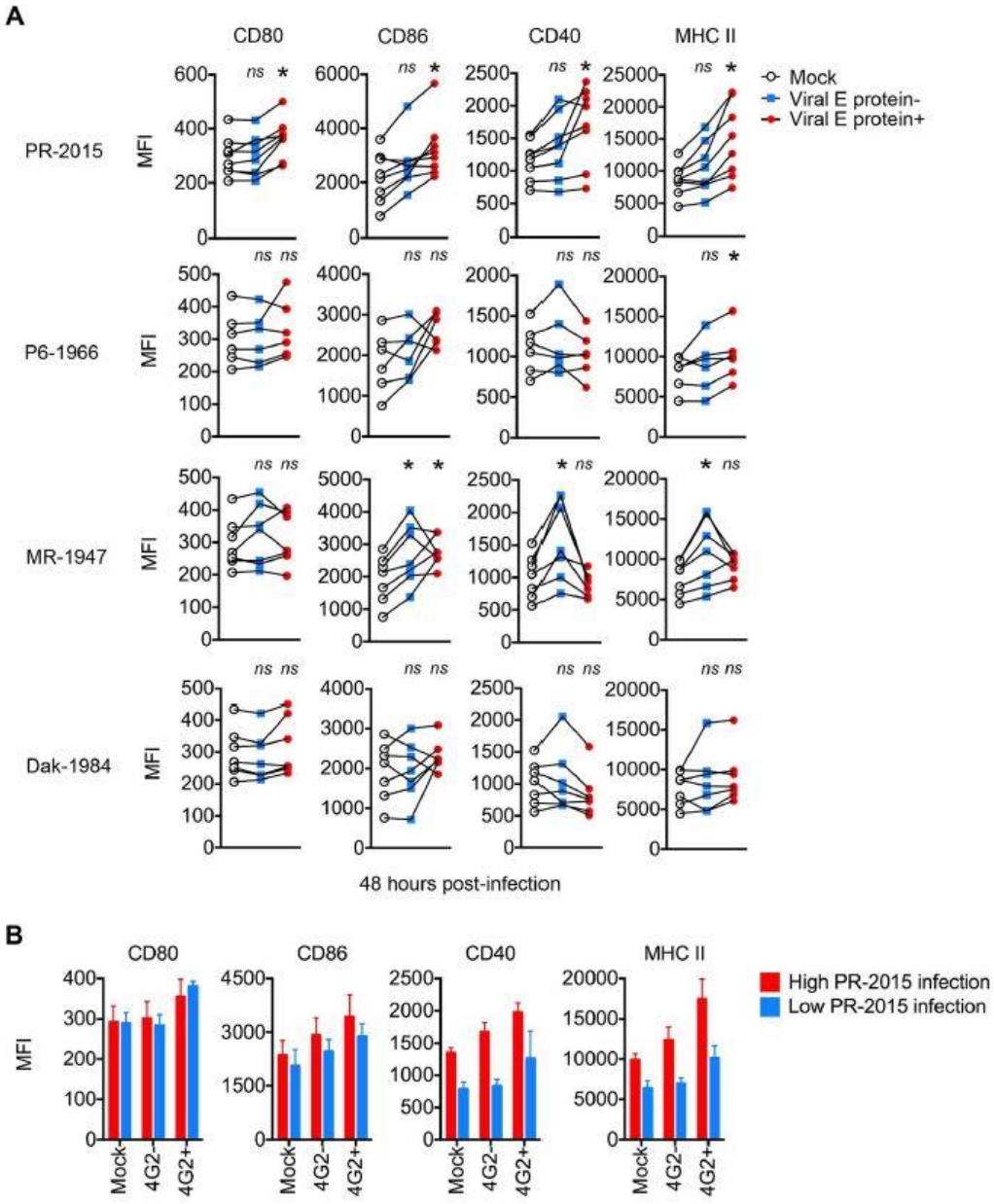

Figure 3-5: ZIKV infection minimally activates human DCs.

(A) moDCs were left uninfected ("Mock") or infected with PR-2015, P6-1966, MR-1947, or Dak-1984 at MOI of 1 (n=6-8 donors). Cells were collected at 48hpi and labeled for ZIKV E protein and indicated DC activation markers. Cells were categorized as being viral E protein- or viral E protein+ and activation marker surface expression quantitated by flow cytometry. Values are represented as median fluorescence intensity (MFI) for

each individual donor with uninfected and ZIKV infected samples from the same donor connected with a line. Statistical significance ($p < 0.05$) was determined using a Friedman test with comparisons made to donor-paired, uninfected cells. **(B)** moDCs infected with PR-2015 at MOI of 1 were stratified into “low” (n=3 donors) and “high” (n=5 donors) infection based on viral E protein staining. MFIs are shown as the mean +/- SD.

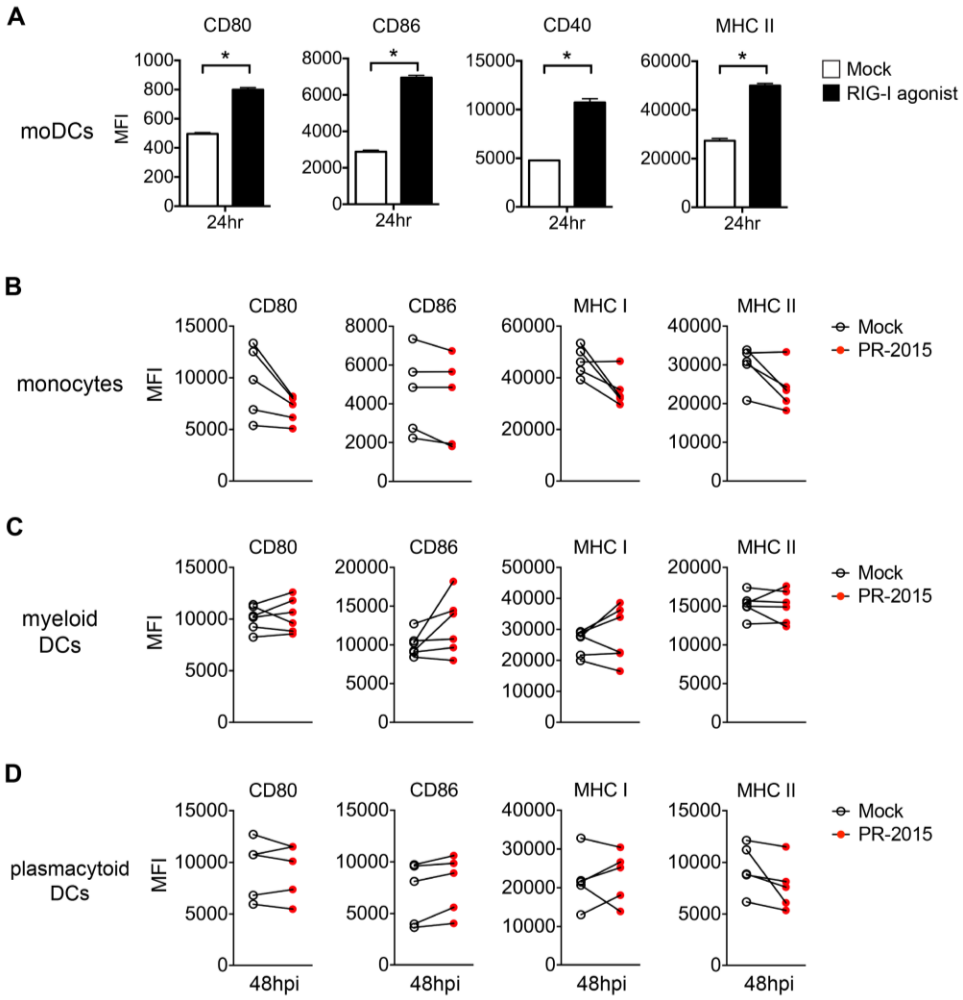

Figure 3-6: ZIKV PR-2015 does not induce activation of DC subsets.

(A) moDCs were treated with RIG-I agonist (10ng/1e5 cells) and collected 6, 12, and 24hr later. Cells were labeled for indicated DC activation markers and surface expression was quantitated by flow cytometry. Values are represented as the average

median fluorescence intensity (MFI) of three technical replicates. Error bars represent the SD. Statistical significance was determined as P<0.05 by a Mann Whitney U test. **(B)** Monocytes, **(C)** myeloid DCs (mDCs) and **(D)** plasmacytoid DCs (pDCs) were left untreated ("Mock") or infected with PR-2015 at MOI of 1 (n=5 donors). Cells were collected at 24hpi and labeled for indicated DC activation markers. Surface expression was quantitated by flow cytometry. Values for each donor are represented as the median fluorescence intensity (MFI), with mock and ZIKV infected samples from the same donor connected with a line. Statistical significance was determined as p<0.05 using a Wilcoxon signed-rank test **(B-D)**. Of note, no values were statistically significant in panels B-D.

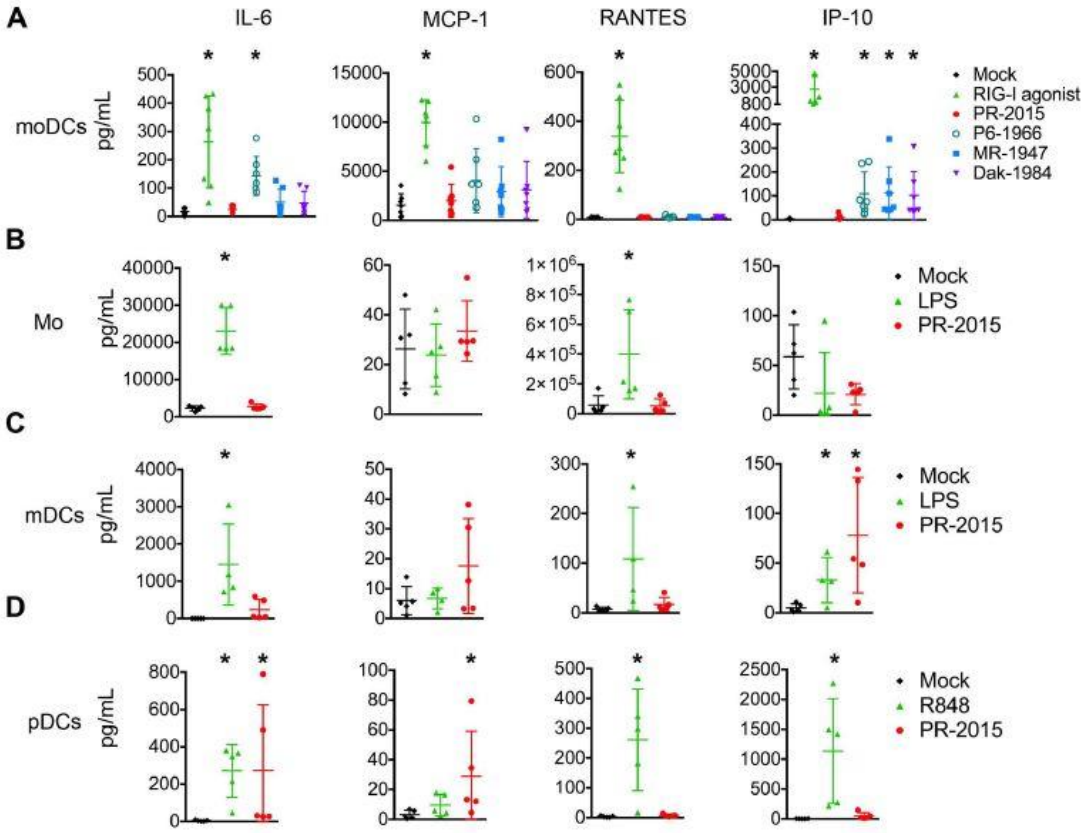

Figure 3-7: ZIKV infection induces minimal pro-inflammatory cytokine production by DCs.

(A) moDCs were left untreated (“Mock”), transfected with RIG-I agonist (10ng/1e5 cells), or infected with PR-2015, P6-1966, MR-1947, or Dak-1984 at MOI of 1 (n=7 donors). Supernatants were collected at 48hpi. **(B, C)** Monocytes (Mo) and myeloid DCs (mDCs) were left untreated (“Mock”), treated with LPS (100 ng/ml), or infected with PR-2015 at MOI of 1 (n=5 donors). Supernatants were collected at 24hpi. **(D)** Plasmacytoid DCs (pDCs) were left untreated (“Mock”), treated with R848 (1 µg/ml), or infected with PR-2015 at MOI of 1 (n=5 donors). Supernatants were collected at 24hpi. Cytokine production was assessed using multiplex bead array. Values for each individual donor are shown with the mean +/- SD. Statistical significance ($p < 0.05$) was determined using a Kruskal-Wallis test with comparisons made to untreated (“Mock”) cells.

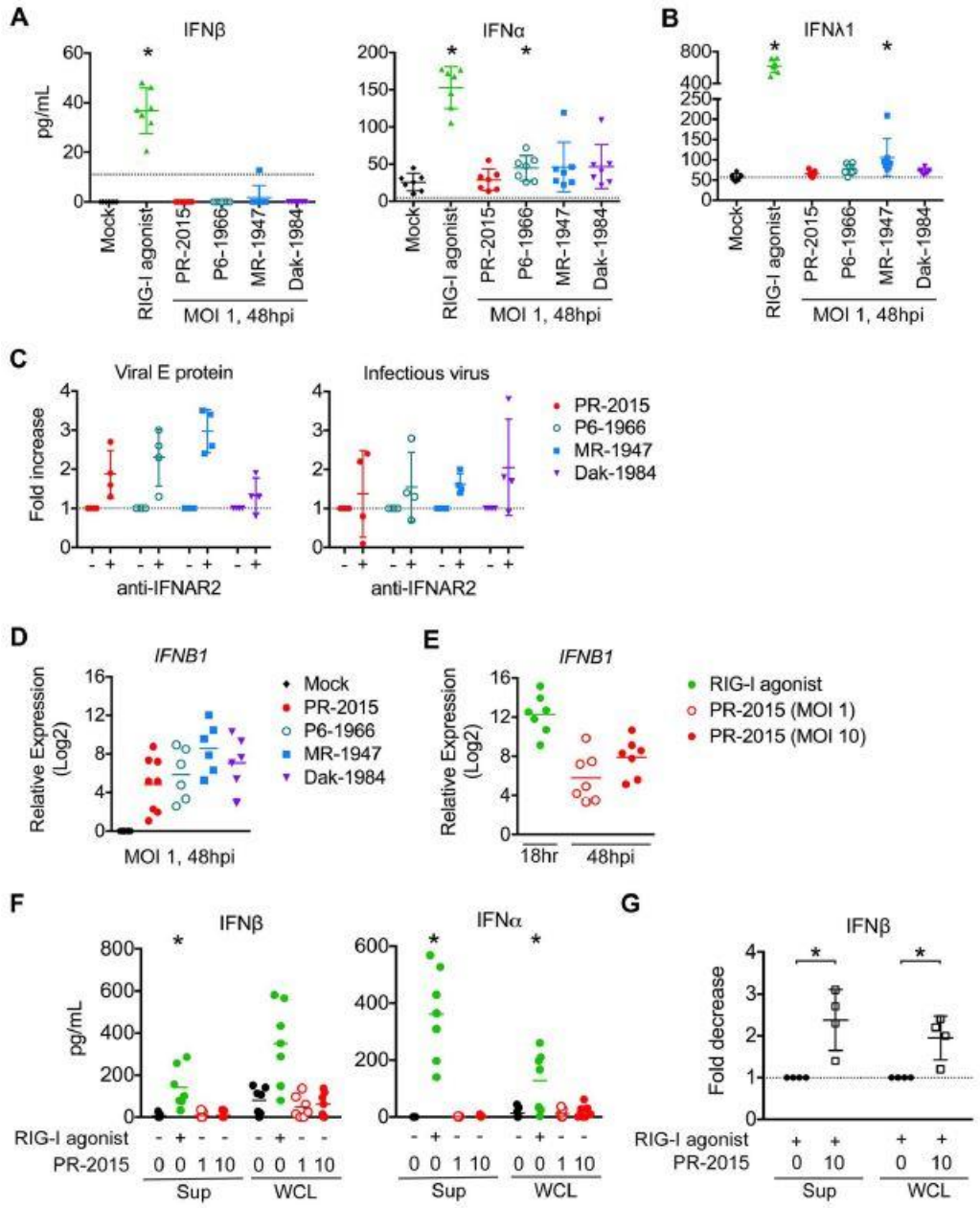

Figure 3-8: ZIKV infection induces type I IFN transcription but inhibits translation.

moDCs were left untreated ("Mock"), treated with RIG-I agonist (10ng/1e5 cells), or infected with PR-2015, P6-1966, MR-1947, or Dak-1984 at MOI of 1. Supernatants were collected 24hrs (RIG-I agonist treatment) or 48hrs (ZIKV infection) later and IFNβ and IFNα **(A)** or IFNλ1 **(B)** production was assessed via multiplex bead array. Values for each individual donor are shown with the mean +/- SD (n=7 donors). Statistical

significance ($p < 0.05$) was determined using a Friedman test with comparisons made to donor-paired mock-infected cells. A dashed line indicates the assay limit of detection. **(C)** moDCs were infected with ZIKV at MOI of 1 in the presence of anti-IFNAR2 blocking antibody. Cells were collected at 48hpi and labeled for ZIKV E protein, while release of infectious virus into the supernatants was determined by FFA. Values for each individual donor are shown with the mean +/- SD (n=4 donors). **(D)** RNA was harvested from cells treated the same as for cytokine analysis and *IFNB1* mRNA expression was determined by qRT-PCR. Gene expression was normalized to *GAPDH* transcript levels in each respective sample and represented as the fold increase above donor- and time-point matched untreated cells. Values for each individual donor are shown with the mean (n=6-8 donors). **(E)** moDCs were treated with RIG-I agonist (10ng/1e5 cells, 18hrs) or infected with ZIKV PR-2015 (MOI 1 and 10, 48hrs) and analyzed for *IFNB1* mRNA expression. Values for each individual donor are shown with the mean (n=7 donors) **(F)** IFNβ and IFNα were measured in the supernatant ("Sup") and whole cell lysate ("WCL") of moDCs treated the same as in E. Values for each individual donor are shown with the mean (n=7 donors). Statistical significance ($p < 0.05$) was determined using a Friedman test with comparisons made to donor-paired mock-infected cells. **(G)** Uninfected or ZIKV PR-2015-infected moDCs (MOI 10, 48hpi) were treated with RIG-I agonist (10ng/1e5 cells, 18hrs) and IFNβ and IFNα were measured as in F. The data is shown as the fold-decrease from RIG-I agonist treatment alone with significance ($P<0.05$) determined using a Mann Whitney Test (n= 4 donors). Error bars represent the mean +/- SD.

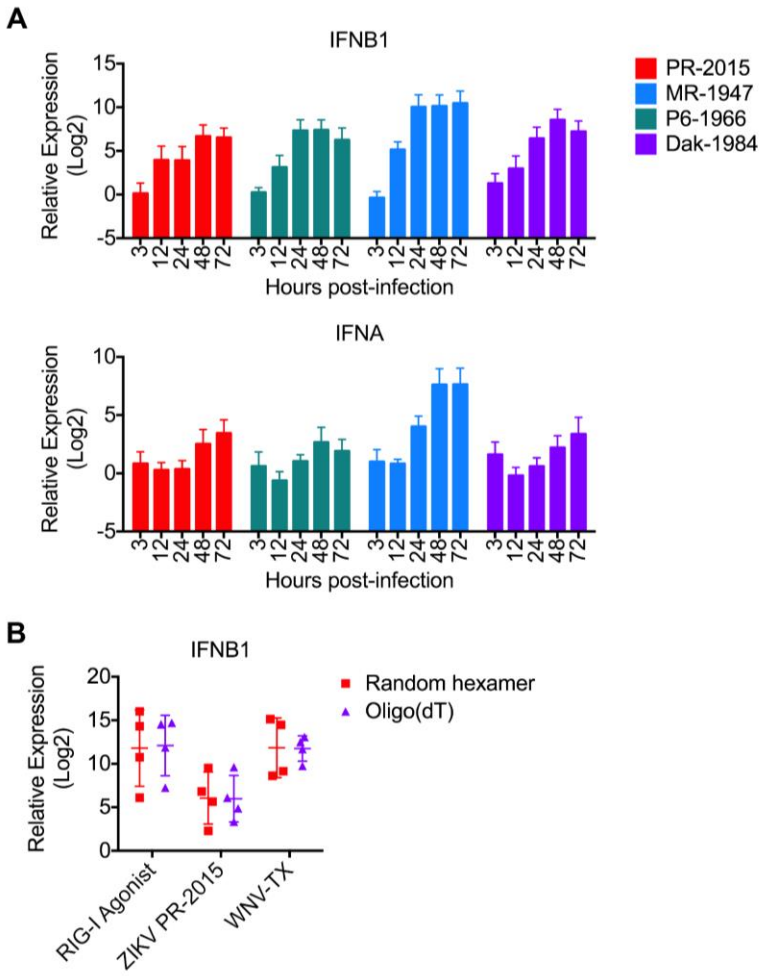

Figure 3-9: ZIKV induces type I IFN gene transcription.

(A) moDCs were infected with ZIKV PR-2015, P6-1966, MR-1947, or Dak-1984 at MOI of 1 (n=6-8 donors). Cells were collected at indicated hours-post infection and antiviral gene expression was determined by qRT-PCR. **(B)** moDCs were treated with RIG-I agonist (10ng/1e5 cells) or virally infected with ZIKV PR-2015 at MOI of 1 (n=4 donors). At 48hpi, RNA was isolated, reverse transcribed using either random hexamer or Oligo(dT) primers, and *IFNB1* expression was determined by qRT-PCR. All gene expression was normalized to *GAPDH* transcript levels in each respective sample and represented as the fold increase above donor and time-point matched uninfected cells. Error bars represent the mean +/- SD.

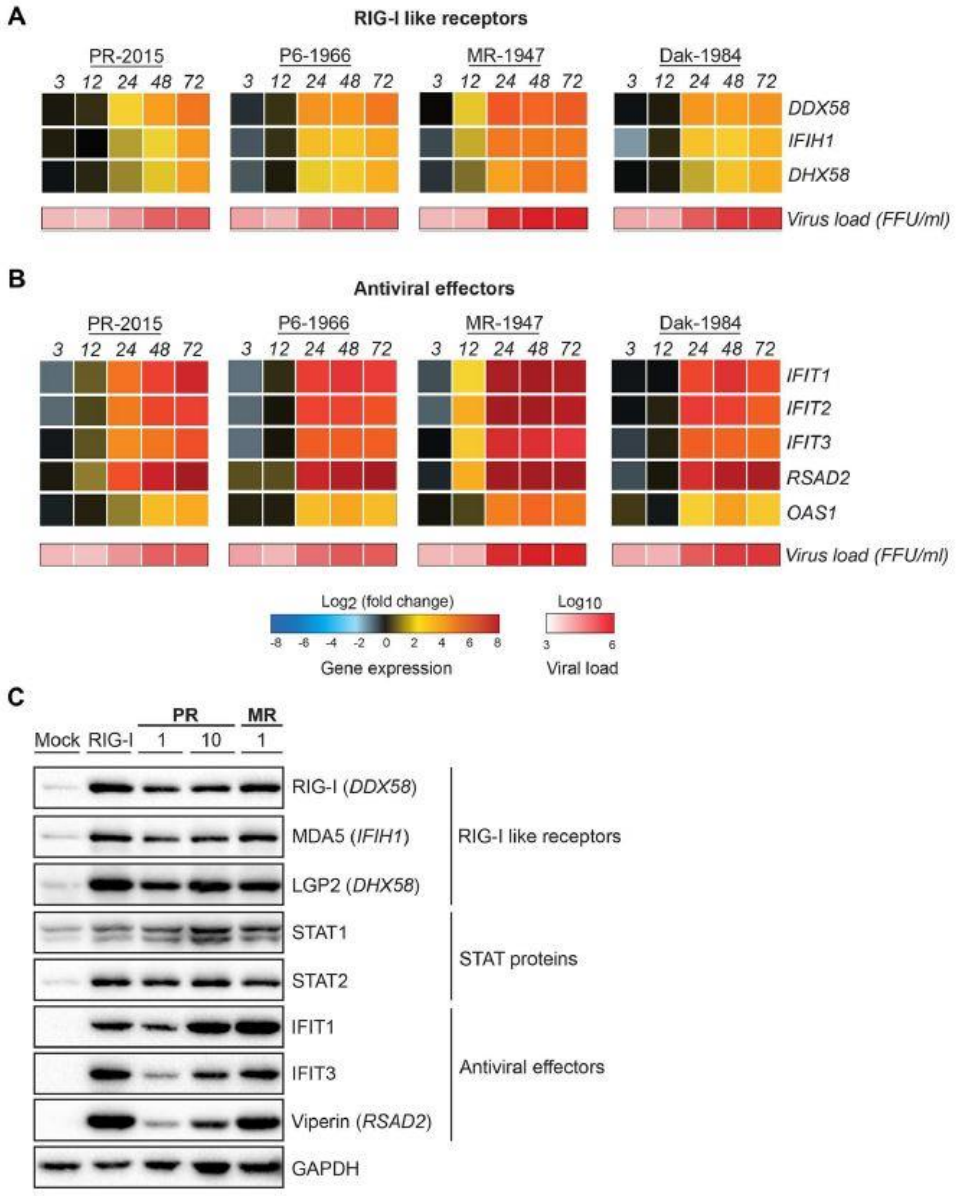

Figure 3-10: ZIKV infection induces an antiviral state within human DCs.

moDCs were infected with ZIKV PR-2015, P6-1966, MR-1947, or Dak-1984 at MOI of 1 (n=6-8 donors). Cells were collected at indicated hour-post infection and antiviral gene expression was determined by qRT-PCR. Gene expression was normalized to *GAPDH* transcript levels in each respective sample and represented as the averaged $\log_2$ normalized fold increase above donor and time-point matched uninfected cells. The averaged $\log_{10}$ normalized levels of infectious virus (FFU/mL) at each time point is

depicted beneath gene expression heat map. **(A)** RLR gene expression. **(B)** Antiviral effector gene expression. **(C)** moDCs were left untreated ("Mock"), treated with RIG-I agonist (10ng/1e5 cells), or infected with ZIKV PR-2015 (MOIs of 1 and 10) or MR-1947 (MOI 1). After 18hrs of agonist treatment or at 48hpi with ZIKV, WCL were collected for western blot analysis of host antiviral effector protein expression. Western blots are shown for a single donor and are representative of data obtained from two donors.

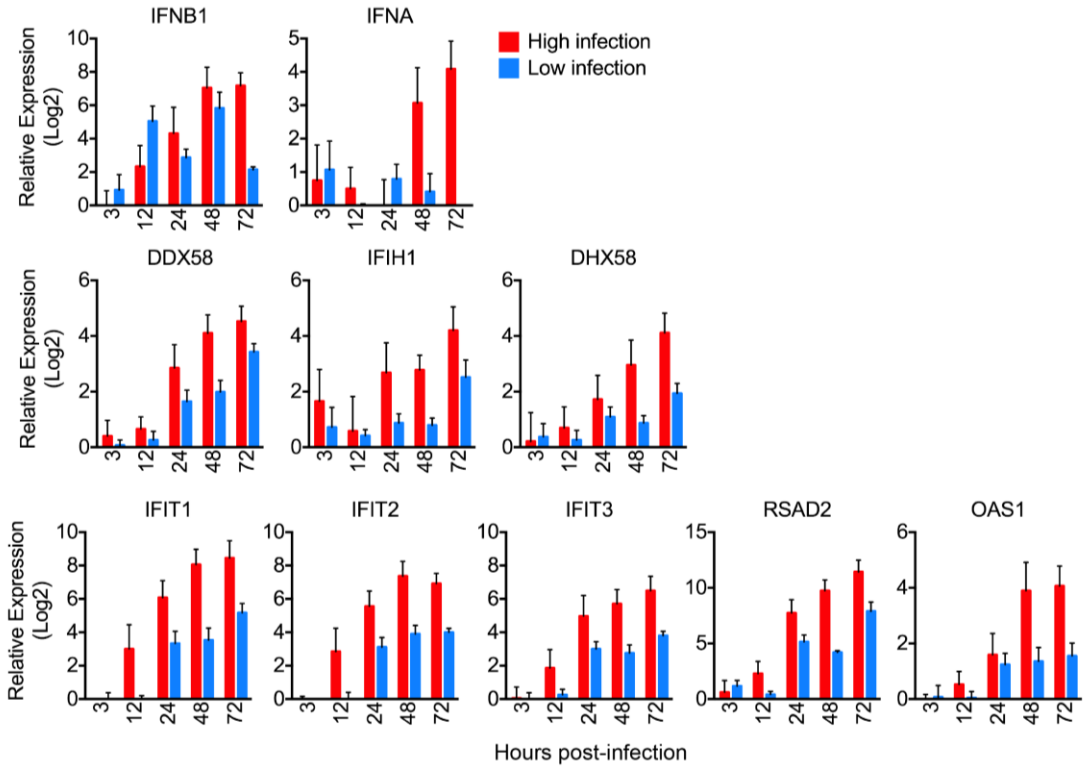

Figure 3-11: Antiviral effector gene expression corresponds with viral replication. moDCs from eight donors infected with ZIKV PR-2015 were separated into "high infection" (5 donors) and "low infection" (3 donors) on the basis of E protein staining as assessed by flow cytometry (see Figure 1C). Antiviral gene expression was determined by qRT-PCR. Gene expression was normalized to *GAPDH* transcript levels in each respective sample and represented as the averaged $\log_2$ normalized fold increase above donor and time-point matched, mock-infected cells. Error bars represent mean +/- SD.

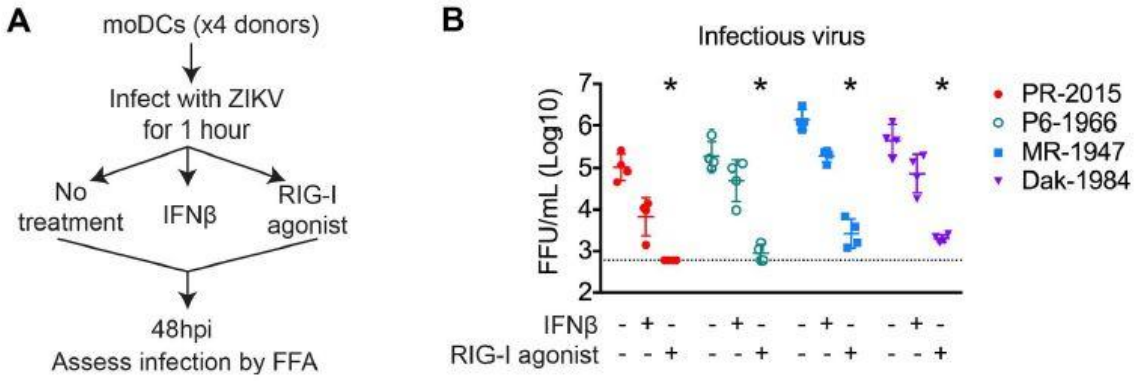

Figure 3-12: Innate immune signaling restricts ZIKV replication within human DCs. **(A)** moDCs were infected with PR-2015, P6-1966, MR-1947, or Dak-1984 at MOI of 1 (n=4 donors). After viral attachment and entry at 1hpi, cells were treated with RIG-I agonist (10ng/1e5 cells), treated with human IFN-β (100 IU/mL), or left untreated. **(B)** Supernatants were collected at 48hpi and assessed for infectious virus release by FFA. Values for each individual donor are shown with the mean +/- SD. Statistical significance ($p < 0.05$) was determined using a Friedman test with comparisons made to donor-paired untreated, ZIKV-infected cells. Assay limit of detection is indicated with a dashed line.

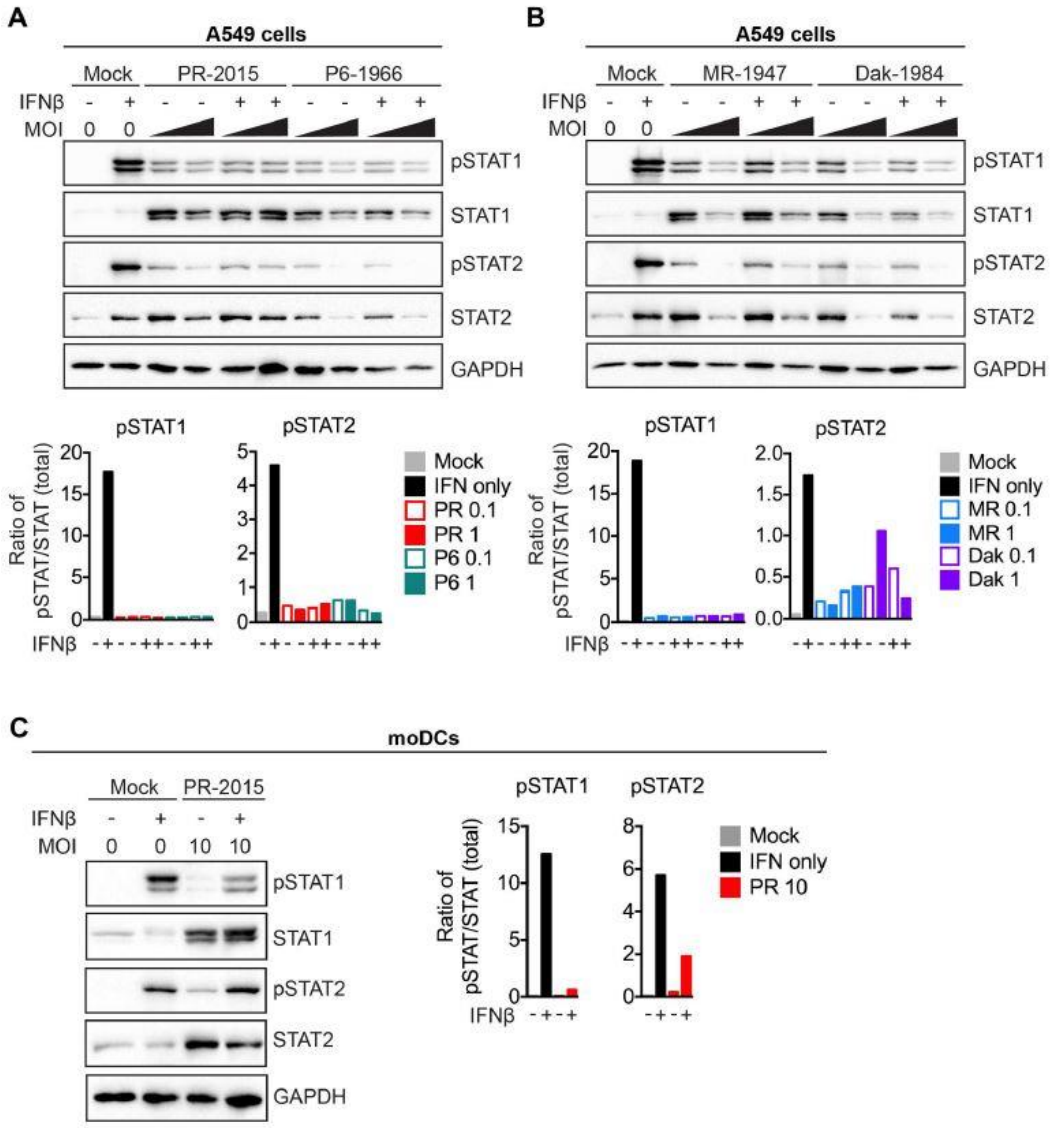

Figure 3-13: ZIKV antagonizes type I IFN signaling.

(A, B) A549 cells were infected with PR-2015, P6-1966, MR-1947, or Dak-1984 at MOIs of 0.1 and 1. At 48hpi, cells were pulse treated with 1000 IU/mL of recombinant human IFNβ for 30 minutes and whole-cell lysates were collected for western blot analysis of pSTAT1, pSTAT2, STAT1, STAT2, and GAPDH. Representative blots are shown from one of two independent experiments. Quantitation is shown below the representative blots. Intensity values were normalized to GAPDH levels on the same blot and then represented as the ratio of pSTAT:total STAT protein. **(C)** moDCs were infected with PR-

2015 (MOI 10) and STAT1 and STAT2 signaling was assessed as in A and B. Data is representative of three donors from two independent experiments. Quantitation is shown to the right of the representative blots. Intensity values are represented as the ratio of pSTAT:total STAT protein.

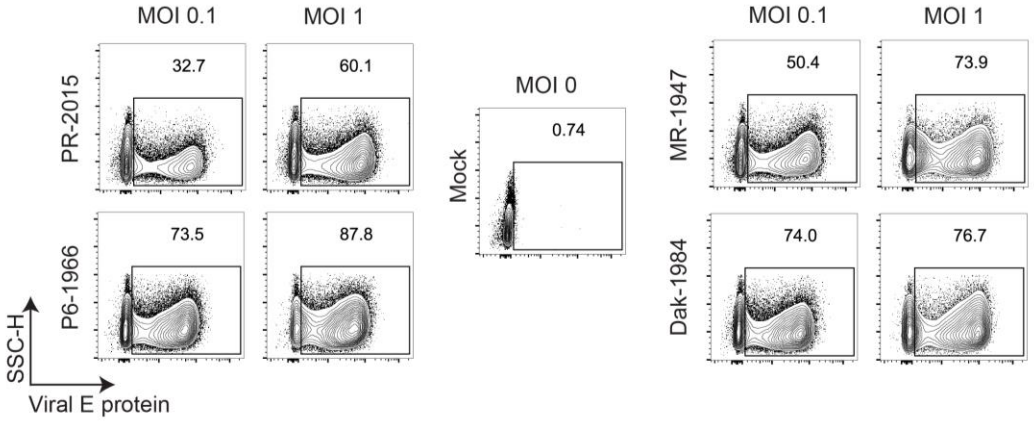

Figure 3-14: ZIKV infection of A549 cells.

Representative flow plots of A549 infected with ZIKV for 48hrs and labeled for viral E protein. Data is representative of two independent experiments.

Zika virus strain information

	PR-2015	P6-1966	MR-1947	Dak-1984
Strain	PRVABC59	P6-740	MR766	DakAr 41524
Accession	KX601168	KX601167	KX601169	KX601166
Lineage	Asian	Asian	East African	West African
Country	Puerto Rico	Malaysia	Uganda	Senegal
Date	2015	1966	1947	1984
Passages	V(4)	SM(6), V(3)	SM(149), V(3)	Ap61(1), C6(1), V(1)

Nucleotide similarity of the CDS between strains

	PR-2015	P6-1966	MR-1947	Dak-1984
PR-2015	100	95.5	88.6	88.6
P6-1966	95.5	100	89.9	89.9
MR-1947	88.6	89.9	100	93.4
Dak-1984	88.6	89.9	93.4	100

Amino acid changes as compared to PR-2015

		P6-1966		MR-1947		Dak-1984	
Protein	**Total AAs**	**# of changes**	**% changes**	**# of changes**	**% changes**	**# of changes**	**% changes**
ancC	**122**	1	0.8%	6	4.9%	5	4.1%
C	104	1	1.0%	4	3.8%	4	3.8%
anc	18	0	0.0%	2	11.1%	1	5.6%
preM	**168**	2	1.2%	10	6.0%	10	6.0%
pr	93	2	2.2%	7	7.5%	7	7.5%
M	75	0	0.0%	3	4.0%	3	4.0%
E	**504**	6	1.2%	19	3.8%	11	2.2%
NS1	**352**	2	0.6%	9	2.6%	7	2.0%
NS2A	**226**	2	0.9%	9	4.0%	10	4.4%
NS2B	**130**	0	0.0%	2	1.5%	2	1.5%
NS3	**617**	3	0.5%	10	1.6%	13	2.1%
NS4A	**127**	0	0.0%	1	0.8%	2	1.6%
2K	**23**	0	0.0%	0	0.0%	0	0.0%
NS4B	**251**	7	2.8%	10	4.0%	9	3.6%
NS5	**903**	16	1.8%	35	3.9%	35	3.9%
Structural	**794**	9	1.1%	35	4.4%	26	3.3%
Non-structural	**2629**	30	1.1%	76	2.9%	78	3.0%
Polyprotein	**3423**	39	1.1%	111	3.2%	104	3.0%

Table 3-1: ZIKV isolates used in this study.

(A) Information about the ZIKV strains used throughout these studies. **(B)** Nucleotide similarity between coding regions of ZIKV strain genomes. CDS, coding DNA sequence. **(C)** Amino acid differences between viral proteins of ZIKV strains. V- Vero cell, SM- suckling mouse brain, Ap61- Aedes pseudoscutellaris cell line, C6- Aedes albopictus clone C6/36 cell line.

Chapter 4: Zika Virus Infects Human Placental Macrophages

Kendra M. Quicke[1,2,¶], James R. Bowen[1,2,¶], Erica L. Johnson[1], Circe E. McDonald[1,2], Huailiang Ma[2,3], Justin T. O'Neal[1,2], Augustine Rajakumar[4], Jens Wrammert[1,2], Bassam H. Rimawi[4], Bali Pulendran[2,3], Raymond F. Schinazi[1,5,], Rana Chakraborty[1], Mehul S. Suthar[1,2]

[1]Department of Pediatrics, Division of Infectious Diseases, Emory University School of Medicine, Atlanta, GA 30322, USA.

[2]Emory Vaccine Center, Yerkes National Primate Research Center, Atlanta, GA 30329, USA.

[3]Department of Pathology and Laboratory Medicine, Emory University School of Medicine, Atlanta, GA 30329, USA

[4]Department of Gynecology and Obstetrics, Division of Maternal Fetal Medicine and Reproductive Infectious Diseases, Emory University School of Medicine, Atlanta, GA 30329, USA

[5]Center for AIDS Research, Laboratory of Biochemical Pharmacology, Emory University School of Medicine, Atlanta, GA 30322, USA

[¶]These authors contributed equally to this work.

*Originally published in *Cell Host & Microbe*: Quicke KM, Bowen JR, Johnson EL, McDonald CE, Ma H, O'Neal JT, Rajakumar A, Wrammert J, Rimawi BH, Pulendran B, Schinazi RF, Chakraborty R, Suthar MS. Zika virus infects human placental macrophages. *Cell Host & Microbe*. 2016 Jul 13;20(1):83-90.

Introduction

ZIKV is an emerging mosquito-borne flavivirus that has rapidly spread to over 30 countries in the Americas and causes illness with symptoms of fever, rash, joint pain and conjunctivitis (Lazear and Diamond, 2016; Petersen et al., 2016b). ZIKV is transmitted through several routes, including mosquito bites, sexual contact, and blood transfusion (Lazear and Diamond, 2016). Most notably, ZIKV can be vertically transmitted from an infected mother to the developing fetus *in utero*, resulting in adverse pregnancy outcomes that include fetal brain abnormalities and microcephaly, a condition characterized by a reduction in head circumference that is often associated with delayed or arrested brain development (Rasmussen et al., 2016). The mechanism by which ZIKV crosses the placenta to establish infection in the developing fetus is not well understood. Recent studies have identified ZIKV RNA in amniotic fluid, and fetal and newborn brain tissue (Calvet et al., 2016; Driggers et al., 2016; Martines et al., 2016) and ZIKV-specific IgM antibodies have been detected in newborn cerebrospinal fluid (Cordeiro et al., 2016). Additionally, ZIKV antigen was found in the chronic villi of a human placenta from a mother who gave birth to an infant with microcephaly, and ZIKV RNA has been isolated from placental tissue of mice infected with ZIKV (Jonathan J. Miner, 2016; Martines et al., 2016). Finally, a recent study detected ZIKV antigen in placental tissue from a mother diagnosed with ZIKV disease (Noronha et al., 2016). In particular, ZIKV antigen was detected in placental macrophages and histiocytes in the intervillous space.

Vertical transmission of ZIKV from an infected mother to the developing fetus *in utero* reflects tropism for placental cells. This organ is a target for a number of viruses by direct and contiguous infection of the cell layers, virion passage through a breach, or by cell-associated transport. Examples include rubella virus, cytomegalovirus, herpes simplex viruses, HIV-1, hepatitis B and C virus, and parvovirus B19 (Koi et al., 2001). The placenta is characterized by contact between the maternal blood and fetal chorionic

villi. Each villus is lined by trophoblasts, which encase the fetal blood supply and placental macrophages (HCs). Several studies have confirmed HCs are targets of viral infection *in vivo* (Lewis et al., 1990) and *in vitro* (Johnson and Chakraborty, 2012). In contrast, STBs (differentiated CTBs) have been shown to be resistant to infection by a wide range of viruses (Delorme-Axford et al., 2013). A recent study showed that STBs also appear to be resistant to infection by phylogenetically-related, historic ZIKV strains at early times following infection (24 and 48hpi) (Bayer et al., 2016).

Here we demonstrate that primary human HCs, and to a lesser extent CTBs, are permissive to productive infection by a contemporary strain of ZIKV, closely related to the strains currently circulating in Brazil. Upon infection, HCs are modestly activated and produce IFN-α and other pro-inflammatory cytokines. Analysis of antiviral gene expression shows up-regulation of RLR transcription as well as downstream antiviral effector genes, indicating that ZIKV induces an antiviral response in HCs and CTBs. Our results suggest that ZIKV gains access to the fetal compartment by infecting and proliferating in the cells of the placenta.

Methods

Ethics statement. Human Placenta: Term (>37 weeks gestation) placentae from HIV-1 seronegative and hepatitis B-uninfected women (>18 years of age) were obtained immediately following elective caesarian section without labor from Grady Memorial and Emory Midtown Hospitals in Atlanta, GA. Approval of the study was granted from the Emory University Institutional Review Board (IRB 00021715) and the Grady Research Oversight Committee. Written informed consent was obtained from donors before collection, and samples were de-identified prior to handling by laboratory personnel.

Isolation of primary placental cells. To isolate HCs and CTBs, membrane-free villous was dissected from the placenta, as previously described (Johnson and Chakraborty, 2012; Tang et al., 2011). The tissue was washed and mechanically dispersed in Hank's balanced salt solution (HBSS) to minimize peripheral blood contamination. For HC isolation, minced tissue was re-suspended in complete medium containing 10% Trypsin/EDTA (Sigma-Aldrich) for 1hr, followed by resuspension in media containing 1mg/ml collagenase A (Sigma-Aldrich), 10U/ml dispase (Worthington Biochemical Corp.), and 0.2mg/ml of DNase I (Sigma-Aldrich) and incubated in a shaking water bath at 37°C for 1hr. The digested tissue was washed with PBS and passed through gauze and a 70μm cell strainer (BD-Falcon Biosciences). The mononuclear cell population was isolated by density gradient centrifugation on Histopaque-1077 (Sigma-Aldrich). CD14+ Magnetic Cell separation was performed using anti-CD14 magnetic beads (Miltenyi Biotech) per the manufacturer's instructions. The purity of the HC population was assessed by CD14 staining and was on average greater than 97%. For CTB isolation, minced tissue was subjected to three sequential enzymatic digestions in a solution containing 0.25% trypsin

(Mediatech Inc.), 0.2% DNase I (Sigma-Aldrich), 25mM HEPES, 2mM CaCl2, and 0.8mM MgSO4 in HBSS at 37°C. Following each digestion, undigested tissue was removed by passage through gauze and 100μm cell strainer (BD) and washed with PBS. Supernatants from the second and third digestions were collected and the resulting cell pellets re-suspended in 1:1 DMEM/F12 supplemented with 10% FBS, 1mM L-glutamine, and 1% pen/strep (Sigma-Aldrich). The CTBs were isolated on a discontinuous gradient of Percoll (GE Healthcare) (50%/45%/35%/30%) by centrifugation. Cells migrating to the 35%/45% Percoll interface were recovered and immunopurified by negative selection with simultaneous treatment with anti-CD9 (to exclude EnC, FB, platelets, smooth muscle, extravillous trophoblast cells, B cells and monocytes) and anti-CD45RA (to

exclude leucocytes) antibodies and magnetic beads (Miltenyi Biotech) (Manoussaka et al., 2005). The purity of the CTB population was assessed by cytokeratin-7 staining and was on average greater than 97% (Chiuppesi et al., 2015). HCs were maintained in supplemented RPMI medium and CTBs were maintained in supplemented DMEM medium as described below.

To minimize maternal blood and decidual cell contamination, membrane-free villous tissue was macroscopically dissected from the fetal-facing surface of the placenta. The tissue was washed thoroughly with HBSS until the supernatant ran clear. Following the initial digest with trypsin, the remaining tissue is washed again thoroughly with PBS to further ensure removal of maternal blood. Similar to Tang et. al., our method of isolation (positive selection for CD14), ensures a pure population of placental macrophages, with negligible contamination of fibroblast or trophoblast. The placental macrophages isolated through this method express high levels of DC-SIGN and have a distinct morphology (Johnson and Chakraborty, 2012; Johnson et al., 2015), unlike other peripheral blood and tissue macrophages.

Cells. HCs were maintained in RPMI medium (Corning Cellgro) supplemented with 10% FBS, 2mM L-Glutamine (Corning Cellgro), 1mM sodium pyruvate (Corning Cellgro), 1x MEM Non-essential Amino Acids (Corning Cellgro), and 1x Antibiotics/Antimycotics (Corning Cellgro). CTBs and Vero cells were maintained in DMEM medium (Corning Cellgro) supplemented with 10% FBS, 2mM L-Glutamine (Corning Cellgro), 1mM HEPES (Corning Cellgro), 1mM sodium pyruvate (Corning Cellgro), 1x MEM Non-essential Amino Acids (Corning Cellgro), and 1x Antibiotics/Antimycotics (Corning Cellgro).

Viruses and infections. Zika virus strain PRVABC59 (ZIKV [PR 2015]) was isolated in 2015 from the serum of a patient who traveled to Puerto Rico, and passaged three times in Vero cells. PRVABC59 was obtained from the Centers for Disease Control and Prevention in Fort Collins, CO and passaged twice in Vero cells cultured in MEM (Gibco) supplemented with 10% FBS (Optima, Atlanta Biologics) to generate working viral stocks. Viral stocks were titered by plaque assay on Vero cells and stored in MEM with 20% FBS. Vero cells (ATCC) were maintained in complete DMEM medium (Supplemental Experimental Procedures). HCs or CTBs were allowed to rest for ~24h before infecting with ZIKV (PR 2015) at an MOI of 1 for 1hr at 37°C. Virus was washed off, cells were re-suspended in fresh complete media and incubated at 37°C for 3-96hr. MOI of 1 was based on results of plaque assays as well as a recent paper where DCs (a similar cell type to macrophages) were infected with ZIKV at an MOI of 1 (Hamel et al., 2015). All work with infectious ZIKV was performed in an approved BSL-3 facility.

Quantitative reverse transcription-PCR (qRT-PCR). Total RNA was purified from mock- or ZIKV-infected HCs or CTBs ($2x10^5$ cells per condition) using the ZR-96 Quick-RNA Kit (Zymo Research) per the manufacturer's instructions. Purified RNA was reverse transcribed using the High Capacity cDNA Reverse Transcription Kit (Applied Biosystems) using random hexamers. For quantitation of viral RNA and analysis of host gene expression, qRT-PCR was performed using TaqMan Gene Expression Master Mix (Applied Biosystems) per the manufactures instructions. For quantitation of viral RNA, each 12.5µl reaction contained 2.5pmol of TaqMan probe directed against the amplified ZIKV E gene region. Host gene expression was performed using SYBR green with appropriate primer sets. All qRT-PCR results were normalized to GAPDH.

Flow cytometry. The following mouse anti-human antibodies were purchased from BioLegend or Becton Dickinson: CD14 (M5E2), CD80 (2D10), CD86 (IT2.2), and HLA-DR (G46-6). Unconjugated 4G2 monoclonal antibody was kindly provided by Jens Wrammert and subsequently conjugated with APC (Novus Lightning-Link). $2x10^5$ HCs or CTBs were used per condition. Cells were blocked for 10min on ice in 25µl FACS buffer (PBS, 1mM EDTA, 0.5% BSA) with 0.25µl Human TruStain FcX (BioLegend) and then stained with 25µl surface staining mix (1:200 dilution of each antibody in FACS buffer) for 20min on ice. Cells were washed with PBS and re-suspended in 50µl PBS with 0.1µl Ghost Dye Red 780 viability dye (Tonbo Biosciences) and incubated on ice for 20min. Cells were washed with PBS and re-suspended in 100µl 1x Foxp3/Transcription Factor Fix/Perm buffer (Tonbo Biosciences) for 20min on ice. To perform intracellular staining of ZIKV E protein, fixed cells were washed twice with 1x Flow Cytometry Perm Buffer (Tonbo Biosciences) and re-suspended in 25µl intracellular Fc block (25µl Perm Buffer, 0.25µl Human TruStain FcX, 10% normal mouse serum) for 10min at RT. 25µl E protein staining mixture (25µl Perm Buffer, 0.25µg APC-conjugated 4G2 antibody) was added to cells for 20min at RT. Cells were washed twice in Perm Buffer and re-suspended in PBS prior to acquisition on a BD LSR II. All analysis was performed using FlowJo version 10.

Focus forming assay. Supernatants collected from mock- and ZIKV-infected HCs and CTBs (2x105 cells per condition) were diluted in DMEM supplemented with 1% FBS and used to infect Vero cells for 1hr at 37°C. Cells and inoculum were overlaid with methylcellulose (OptiMEM [Corning Cellgro], 1% Antibiotic/Antimycotic [Corning Cellgro], 2% FBS, 2% methylcellulose [Sigma Aldrich]) and incubated for 72hr at 37°C. Cells were washed with PBS and fixed with a 1:1 methanol/acetone mixture for 30min. Cells were blocked with 5% milk/PBS at RT for 20min and incubated with primary antibody (mouse 4G2 (Hamel et al., 2015)) at 1µg/ml in 5% milk for 2hr at RT. Cells were incubated with

secondary antibody (HRP-conjugated goat anti-mouse IgG) diluted 1:3000 in 5% milk for 1hr at RT. Foci were developed with TrueBlue Peroxidase Substrate (KPL). Plates were read on a CTL-ImmunoSpot S6 Micro Analyzer.

Multiplex bead array. Cytokine analysis was performed on supernatants from mock- or ZIKV-infected HCs or CTBs ($2x10^5$ cells per condition) using a human cytokine 25-plex panel (ThermoScientific), and a custom 2-plex panel with human IFNβ and IFNλ1 (eBioscience) per the manufacturer's instructions, and read on a Luminex 100 Analyzer.

Immunofluorescence and confocal microscopy. HCs and CTBs were grown on glass chamber slides (ThermoFisher Scientific) and infected with ZIKV (PR 2015) at an MOI of 1. At 72hpi, cells were fixed with 3.7% paraformaldehyde/PBS for 1hr, and permeabilized in 0.3% Triton X-100 for 30min at RT. Cells were blocked in 10% fetal bovine serum/PBS, and stained with primary (mouse 4G2 mAb) and secondary (donkey anti-mouse Alexa-488, ThermoFisher) antibodies in blocking buffer for 1hr, respectively. Cells were washed with PBS, stained with F-actin probe (BODIPY® 558/568 phalloidin, ThermoFisher) for 20min, and mounted with ProLong®Gold with DAPI (ThermoFisher). Fluorescence microscopy was performed with a Zeiss LSM 510 META confocal microscope at the Integrated Cellular Imaging Core of Emory University. Images were processed with ZEN imaging software (Zeiss). 3D images were acquired with Leica SP8 confocal microscopy at 100x magnification. Images were processed with ZEN (Zeiss) and Imaris version 8.1.2 (Bitplane) software for 3D reconstruction.

Statistical analysis. Sample size was dependent on the number of donors. HCs were isolated from 5 donors and CTBs were isolated from 3 of these donors. Experiments with HCs were repeated twice (3 donors in the first experiment, 2 donors in the second).

Experiments with CTBs were repeated once (3 donors in 1 experiment). All statistical analysis was performed in GraphPad Prism 6, with significance assessed by Mann Whitney U test with $p<0.05$. Infectivity as assessed by 4G2 staining utilized a 1-tailed test. Cell activation as assessed by surface staining utilized a 2-tailed test.

Results

Hofbauer cells and cytotrophoblasts are permissive to productive ZIKV infection

To determine whether human placental cells are permissive to ZIKV infection, we isolated primary HCs and CTBs from villous tissue of full-term placentae and infected with ZIKV (multiplicity of infection [MOI] 1). In this study, we used a low cell culture-passaged and sequence-verified ZIKV strain, PRVABC59 (PR 2015), isolated from the sera of an infected patient in Puerto Rico in December 2015. This strain is closely related to the epidemic strains circulating in the Americas that have been linked to *in utero* ZIKV infection (Faria et al., 2016). Through multiple virologic assays, we demonstrate that HCs, and to a lesser extent CTBs, are permissive to productive ZIKV infection (**Figure 1**). Following infection of HCs, we performed a focus forming assay (FFA) on Vero cells and observed a steady decline in viral titers from 3hpi through 24hpi that was immediately followed by log phase virus growth through 72hpi (**Figure 1A**). Notably, we observed donor-to-donor variation in viral kinetics and magnitude amongst HCs isolated from five donors. For donor 2, we detected an approximate 35-fold increase in virus in the supernatant between 3 - 48hpi. In contrast, donor 5 showed about a 2.5-fold increase in virus in the supernatant between 48 - 96hpi. We confirmed infection of HCs with viral qRT-PCR (**Figure 1B**) and immunofluorescence microscopy (**Figure 1C-E**). In HCs, viral RNA substantially increased in all donors between 48 - 72hpi, reflecting an increase in virus release into the supernatant (**Figure 1A**). Furthermore, we detected viral envelope (E) protein within infected HCs which localized

to distinct, perinuclear regions within the cell (**Figure 1C and D**). This pattern may be indicative of viral localization to the endoplasmic reticulum (ER), or ER-associated vesicles, a staining pattern consistent with virus assembly (Welsch et al., 2009). Finally, we observed between 4.9 - 7.2% infected cells by immunofluorescence staining using a pan-flavivirus antibody (**Figure 1E**).

In contrast, we observed minimal viral replication in CTBs at early times post-infection (3-72hpi; **Figure 2A**). Of note, we found evidence of productive infection at 96hpi with all three donors exhibiting approximately 5-fold increase in viral load between 72 - 96hpi, suggesting that CTBs may support productive virus infection, albeit at lower levels compared to HCs. We observed concurrent increases in viral RNA in all three donors between 72 - 96hpi as well (**Figure 2B**). Most notably, we detected persistent viral RNA in CTBs at all time points through 72hpi, further suggesting ZIKV infects and replicates in CTBs with delayed kinetics. Collectively, these findings demonstrate that HCs are permissive to ZIKV infection and represent a key target cell of ZIKV infection within the placenta.

To assess ZIKV replication in HCs at the single cell level, flow cytometry was utilized to detect intracellular expression of viral E protein. Consistent with peak production of viral RNA and infectious virus (**Figure 1**), we detected between 0.8 - 6.8% and 0.4 - 3.0% infected HCs at 48 and 72hpi, respectively (**Figure 3A**). Minimal background staining was observed in donor- and time-matched uninfected cells and in ZIKV-infected cells stained with an IgG isotype control (**Figure 4B**). Consistent with our FFA findings, HCs isolated from donor 2 were the most permissive to infection, with an average of 5.6% and 2.3% infected cells at 48 and 72hpi, respectively. This is consistent with infected cell counts observed by immunofluorescence microscopy (**Figure 1E**). In contrast to recent studies with neuronal progenitor cells (Garcez et al., 2016; Tang et al., 2016), we did not observe a significant loss of viability during ZIKV infection through

96hpi (**Figure 4C**), suggesting that these cells may be more resistant to virus-induced cell death or that ZIKV (PR 2015) is a less cytopathic virus in HCs.

Of note, percent infectivity and infectious virus production did not necessarily correspond to viral RNA levels (**Figure 1 and 3A**). Specifically, while donors 1 and 2 had a 6-fold difference in cellular infectivity at 48hpi and a consistent 1-log fold difference in infectious virus release between 24-96hpi, both had similar viral RNA levels present at 48 and 72hpi. Differences in infection between donor 1 and 2 may be explained by an enhanced rate of genome replication within HCs from donor 2, noted by an early increase in viral RNA at 24hpi in donor 2, but not donor 1 (**Figure 1**). Overall, we observed variable levels of viral RNA at 24 and 48hpi, despite similar levels of viral RNA at early (3hpi) and late (48 and 72hpi) time points, further supporting differential rates of genome replication between donors. Indeed, while donors 1, 3, and 4 had similar production of infectious virus at all time points assessed, notable differences in viral RNA levels were observed at 48hpi between these donors (**Figure 1**). Furthermore, while donor 5 showed minimal production of infectious virus, we observed comparable RNA levels to the more permissive donors, further highlighting discordance between genome replication and release of infectious virus. Together, these results suggest that different donors may have the capacity to differentially regulate ZIKV replication and may be restricting replication at different stages of the viral life cycle.

ZIKV infection induces modest activation of HCs

Next, to determine if ZIKV-infected HCs are poised to interact with T cells, we measured cell surface expression of the co-stimulatory molecules CD80, CD86, and MHC II. In ZIKV-infected HCs from all three donors, we observed minimal up-regulation of both CD80 and CD86 as compared to time-matched mock-infected cells between 48 - 72hpi (**Figure 3B-C**). Consistent with enhanced virus replication, ZIKV infection of HCs from

donor 2 led to up-regulation of both CD80 and CD86 by 72hpi. Additionally, significant up-regulation of MHC II was only observed with donor 2 between 48 - 72hpi (**Figure 3D**). Overall, there appears to be donor-to-donor variability in terms of up-regulation of co-stimulatory molecules, however, enhanced virus replication led to greater activation of HCs. These data suggest that ZIKV infection has the potential to program HCs for antigen presentation and T cell priming.

Type I IFN and pro-inflammatory cytokines are produced in response to ZIKV infection

When cells are infected with virus, pattern recognition receptors (PRRs) within the cell recognize the viral genetic material and trigger a potent innate immune response to control viral replication and spread. Upon binding viral RNA, PRRs initiate signaling cascades that result in the production of type I IFNs, pro-inflammatory cytokines and expression of antiviral effector genes that serve to limit virus replication. In order to further assess the immunostimulatory potential of HCs, we measured pro-inflammatory cytokines and chemokines in supernatants from infected cells by multiplex bead array. Following ZIKV infection, we observed increased IFNα secretion, but not IFNβ or IFNλ1 (IL-29; **Figure 5 and data not shown**). We also found increased secretion of the pro-inflammatory cytokine IL-6 and chemokines MCP-1, involved in monocyte infiltration, and IP-10, involved in recruitment of activated effector T cells. Though these cytokines were induced in all five donors, there were individual differences in the magnitude of production. Donor 2, which had the highest viral load at 48 and 72hpi (**Figure 1A**), tended to exhibit the highest overall levels of IFN-α, IL-6, MCP-1 and IP-10, however, donor 2 was not consistently the lead producer of cytokines over mock-infected controls. Of note, donor 5, which had the lowest viral load at 48 and 72hpi, did not consistently show the lowest levels of cytokines, but did exhibit reduced induction over mock-infected

controls at 72hpi. No discernable patterns could be confidently drawn with CXCL-8, MIP-1α, MIP-1β or IL-1RA. In contrast to HCs, we observed limited induction of type I IFN, IL-6 and IP-10, and no detectable type III IFN in CTBs at the time points assessed (**Figure 6A and data not shown**). Donor 1, while slightly less permissive to viral infection and replication (**Figure 2**), did not have correspondingly lower levels of cytokine production compared to donors 2 and 3. We did observe however that donor 1 tended to have reduced production of cytokines over mock-infected control cells at 72hpi. These findings demonstrate that HCs are capable of initiating an inflammatory response to ZIKV infection.

ZIKV infection provokes an antiviral immune response in HCs and CTBs

To evaluate the antiviral potential of HCs and CTBs, we examined the expression of several antiviral effector genes. We observed increased expression of *IFNA* transcripts as early as 24hpi in HCs (**Figure 7A**), concordant with increased IFNα secretion (**Figure 5**). While we did not observe IFNβ secretion, we detected an increase in *IFNB1* transcripts over time-matched mock cells as early as 24hpi (**Figure 7A**), suggesting possible discordance between transcript levels and translation/secretion of IFNβ (Schulz et al., 2010). In contrast, both *IFNA* and *IFNB1* were induced at low levels in CTBs (**Figure 6B**). We next measured expression of the RLRs, a family of PRRs known to recognize flavivirus RNA and induce production of Type I IFNs and pro-inflammatory cytokines (Daffis et al., 2009; Loo et al., 2008; Suthar et al., 2013b; Suthar et al., 2010). Expression of *DDX58* (RIG-I), *IFIH1* (MDA5) and *DHX58* (LGP2) transcripts are induced above time-matched mock-infected HCs across all donors by 72hpi and remain highly expressed through 96hpi (**Figure 7B**). RLR expression corresponds to kinetics of virus replication, suggesting that RLRs are induced in response to ZIKV infection of HCs. In CTBs, RLR transcription is modestly induced and both *IFIH1* and *DHX58* return to near

basal levels by 96hpi, though *DDX58* expression remains slightly elevated through 96hpi (**Figure 6B**). We also evaluated expression of several antiviral genes produced downstream of the RLR and type I IFN signaling axes and found that *RSAD2*, *IFIT1*, *IFIT2*, *IFIT3 and OAS1* were all induced by 72hpi in HCs and remained elevated through 96hpi (**Figure 7C**). In CTBs, these genes were modestly induced through 72hpi (**Figure 6B**), likely corresponding to the low level of viral replication during this time period (**Figure 1**). By 96hpi, a time point at which we observed productive virus replication, these cells also initiate an antiviral immune response. Importantly, we observed low levels of *IFNA* and ISG expression in mock-infected HCs and CTBs, likely induced by the cell isolation procedure, which may limit the percent of infected cells we see in our *in vitro* system. Taken together, these results show that both HCs and CTBs respond to ZIKV infection through initiation of antiviral signaling pathways.

The kinetics of the antiviral response are complex and variable and we observed donor-to-donor variation in induction of antiviral gene expression. Of note, HCs from donor 2, which exhibited the highest viral loads, and donor 5, which exhibited the lowest viral loads, induced similar levels of antiviral effector genes by 96hpi, although genes in donor 2 were induced at a faster rate (**Figure 7**). This may reflect the higher rate of replication and viral output by HCs from this donor (**Figure 1**). There is likely a multifactorial rationale for why viral load does not correlate with antiviral gene expression that likely encompasses differences in individual genetics and the antagonistic capabilities of the virus.

Discussion

The present data demonstrate that primary HCs and CTBs isolated from full-term placentae are permissive to productive ZIKV infection by a contemporary strain currently circulating in the Americas. We also found that HCs respond to infection by triggering

antiviral defense programs in the absence of overt cell death. In this limited study of five donors, we observed individual variability in kinetics and magnitude of virus replication, inflammation and antiviral gene expression, likely reflecting differences in individual genetics (Querec et al., 2009; Thio, 2008). Though unlikely given the low number of cell passages PR 2015 has undergone, it is possible that minor cell culture adaptations or quasi species may also be playing a role in donor-to-donor variability. These observations suggest that donors may have the capacity to restrict ZIKV at different stages of the viral replication cycle. This may also relate to observed differences in intrauterine transmission efficiency, where more susceptible HCs from a pregnant mother may support higher levels of virus replication and subsequent spread to the developing fetal nervous system. Additionally, it will be important in future studies to characterize when HCs and CTBs are most susceptible to ZIKV infection (i.e. first, second or third trimester). Recent projections from the CDC based on data from Brazil indicate that virus infection during the first trimester or early in the second trimester of pregnancy is temporally associated with the observed increase in infants born with microcephaly (Reefhuis et al., 2016).

A recent study reported that primary STBs isolated from full-term placentae are resistant to ZIKV infection through a potential mechanism involving type III IFN-mediated antiviral immunity (Bayer et al., 2016). Similarly, in CTBs we observed a lack of productive virus replication through 48hpi, however, we did observe persistent viral RNA through 72hpi. By 96hpi, we observed low level virus replication as well as induction of antiviral effector genes, suggesting that ZIKV infects and persists in CTBs but is efficiently controlled at early times post-infection. Additionally, while Bayer et al. was able to identify IFN-λ (Type III IFN) in the supernatant of uninfected STBs, we did not detect the presence of IFN-λ in the supernatants of ZIKV-infected HCs or CTBs. The discordance between these two studies may be attributed to differences in time points

assessed and viral isolates used in each study (FSS13025 and MR766 as compared to PR 2015).

What are the possible mechanisms by which ZIKV crosses the placental barrier and infects HCs? One explanation is that ZIKV may initially infect trophoblasts and productively replicate and disseminate locally within the placenta to involve HCs, which then support more efficient ZIKV replication than CTBs. An alternative hypothesis is that non-neutralizing, cross-reactive antibodies bind ZIKV and traffic across the placenta, through a neonatal Fc-receptor-mediated mechanism, to infect placental macrophages. ZIKV crossing the placenta and replication in/release from HCs likely results in viral dissemination through the cord blood with subsequent infection of neural progenitor cells. At this time, it is uncertain whether maternal macrophages are infected or play a role in allowing ZIKV to cross the placental barrier. However, a recent report has directly identified the presence of viral antigen through immunohistochemistry in the placenta from a mother with an infant who developed ZIKV-related fetal anomalies (Martines et al., 2016). Of note, ZIKV viral antigen was detected within the chorionic villi and not in the maternal decidua. Based on these findings, it does not appear that decidual macrophages are key players in ZIKV transmission at the placenta.

HCs are likely programmed to limit inflammation following virus infection, a mechanism that is consistent with the immune tolerant environment of the placenta and which would support higher infection of HCs compared to maternal macrophages. An alternative hypothesis is that the relative paucity of effector cells in the placenta that would otherwise readily kill infected macrophages (e.g. CD8+ T cells), contributes to a permissive environment for ZIKV infection and replication in HCs. Altogether, our data support the notion that HCs represent a key target cell within the placenta. These findings stress the importance of developing antiviral therapies directed against ZIKV replication within placental cells as a means to reduce vertical transmission in the

mother-infant dyad and the incidence of adverse pregnancy outcomes and fetal abnormalities.

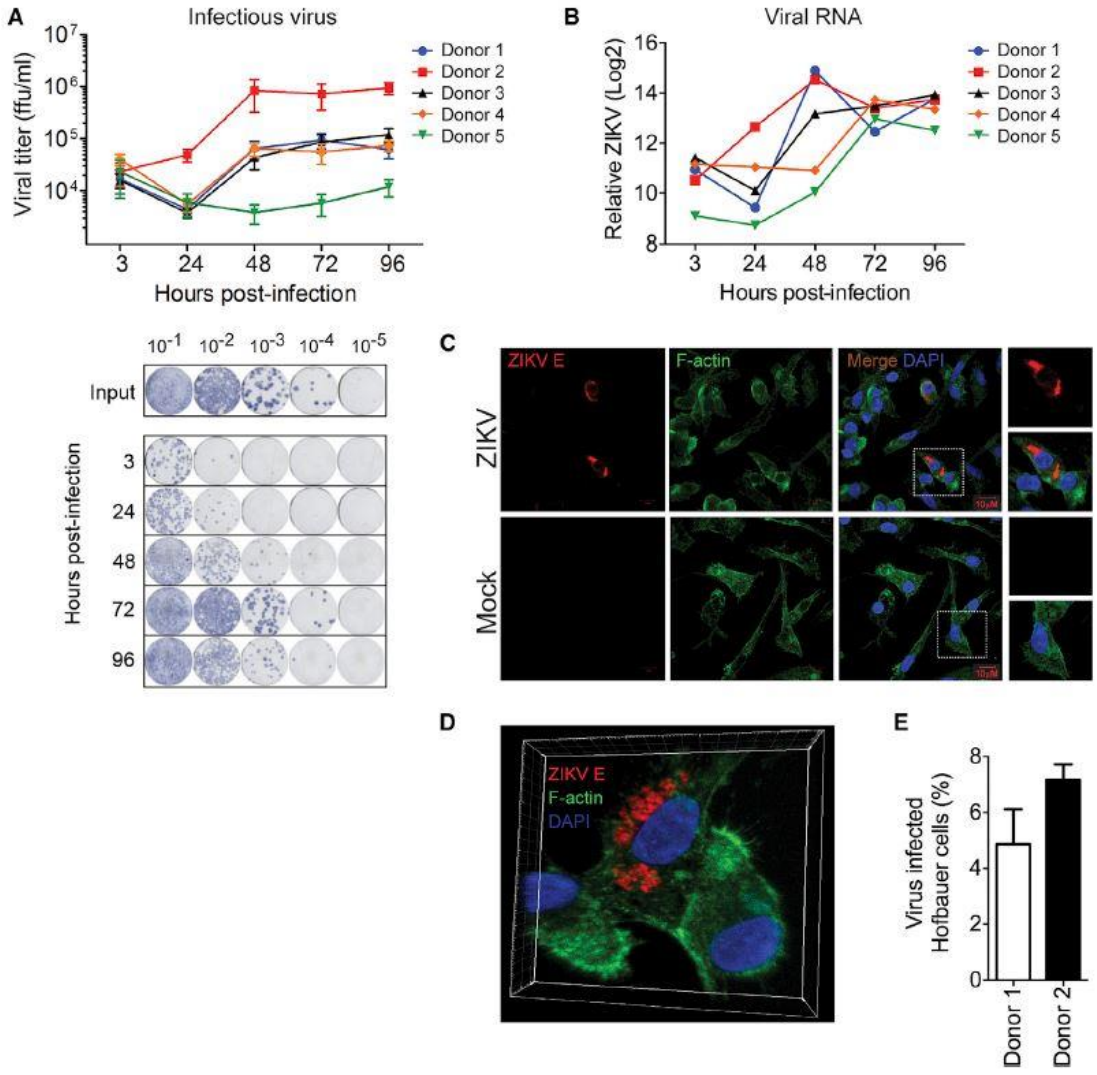

Figure 4-1: Hofbauer cells are permissive to ZIKV infection.

(A) HCs from five donors were infected with ZIKV (PR 2015) at an MOI of 1 and viral titers in supernatants determined by FFA. Viral inoculum for all donors was $1x10^6$ffu/ml. Data are represented as the mean of four technical replicates +/- SD (top). Representative FFA staining (bottom). ffu, focus forming units. **(B)** Viral RNA detected by qRT-PCR in HCs infected with ZIKV (PR 2015). Data are relative to GAPDH control and mock-infected cells ($\Delta\Delta C_T$). **(C, D, E)** Confocal microscopy of mock- and ZIKV (PR 2015)-infected HCs at 72hpi. **(D)** 3D reconstruction. **(E)** Percent infected cells determined from 5 fields of view. Data are represented as mean +/- SD.

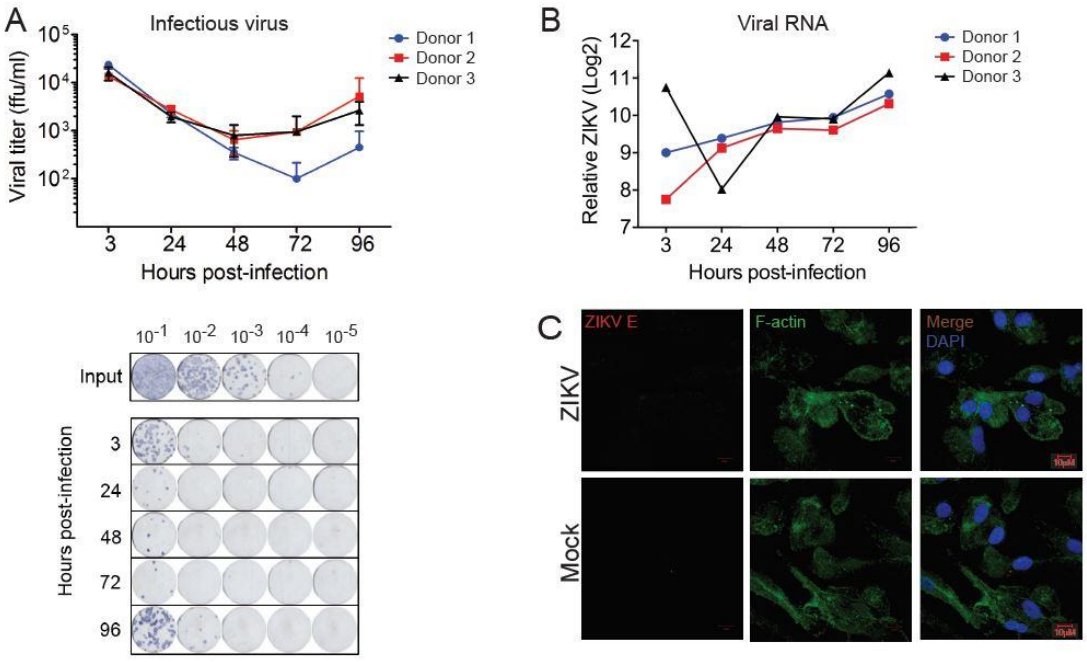

Figure 4-2: Cytotrophoblasts are permissive to ZIKV infection.

(A) CTBs from three donors were infected with ZIKV (PR 2015) at an MOI of 1 and viral titers in supernatants determined by FFA. Data are represented as the mean of four technical replicates +/- SD (top). Representative FFA staining (bottom). ffu, focus forming units. **(B)** Viral RNA detected by qRT-PCR in CTBs infected with ZIKV (PR 2015). Data are relative to GAPDH control and mock infected cells ($\Delta\Delta C_T$). **(C)** Confocal microscopy of mock- and ZIKV (PR 2015)-infected CTBs at 72hpi.

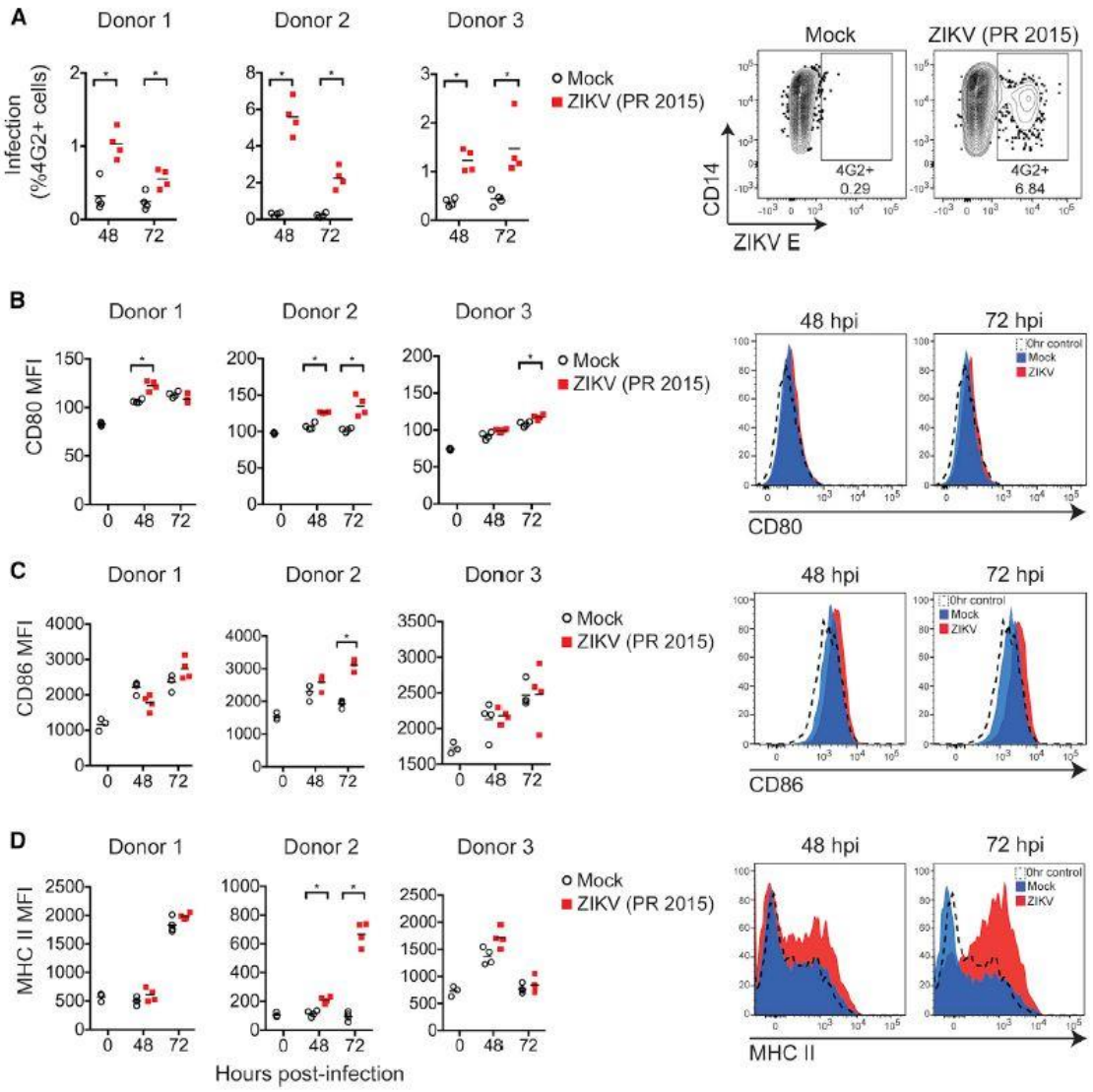

Figure 4-3: ZIKV infection induces activation of HCs.

(A) HCs from three donors were infected with ZIKV (PR 2015) at an MOI of 1 or mock-infected. Percentages of infected cells at 48 and 72hpi were determined by intracellular viral E protein staining and flow cytometry (left panels). Horizontal bars indicate the mean of four technical replicates. (**B, C, D**) Surface expression of CD80, CD86, and MHC II was determined by flow cytometry. Data are represented as median fluorescence intensity (MFI). Horizontal bars indicate the mean of four technical replicates. Representative histograms are provided (right panels). hpi, hours post-infection.

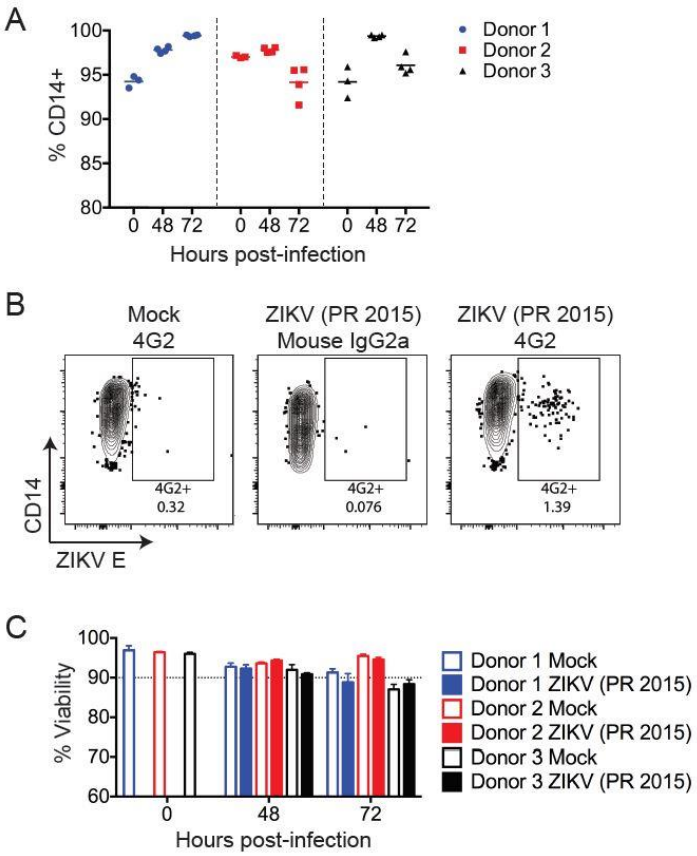

Figure 4-4: Controls for HC flow cytometry analysis.

(A) HCs used in these experiments were on average >95% pure by CD14 staining. Horizontal bars indicate the mean. For 0hpi, n=3; for 48 and 72hpi, n=4. **(B)** No ZIKV E protein was detected by mouse 4G2 antibody in mock-infected cells, or by mouse IgG2A isotype control in ZIKV-infected cells. **(C)** Both mock- and ZIKV-infected HCs retained ~90% or better viability over the time course as determined by Ghost Dye Red 780 staining. Data are represented as the mean +/- SD.

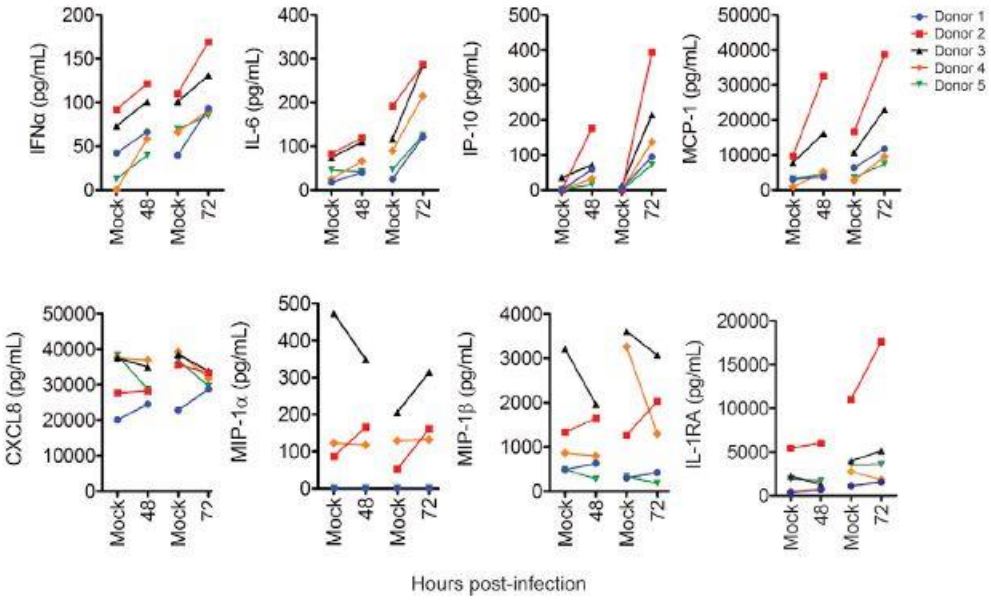

Figure 4-5: ZIKV infection of HCs induces type I IFN and inflammatory cytokines.

HCs from five donors were infected with ZIKV (PR 2015) at an MOI of 1 or mock-infected. Cytokine levels in the supernatants were determined by multiplex bead array. All values are represented in “pg/ml” and shown with a connecting line between ZIKV-infected samples (48 and 72hpi) and their respective donor- and time-matched mock-infected samples.

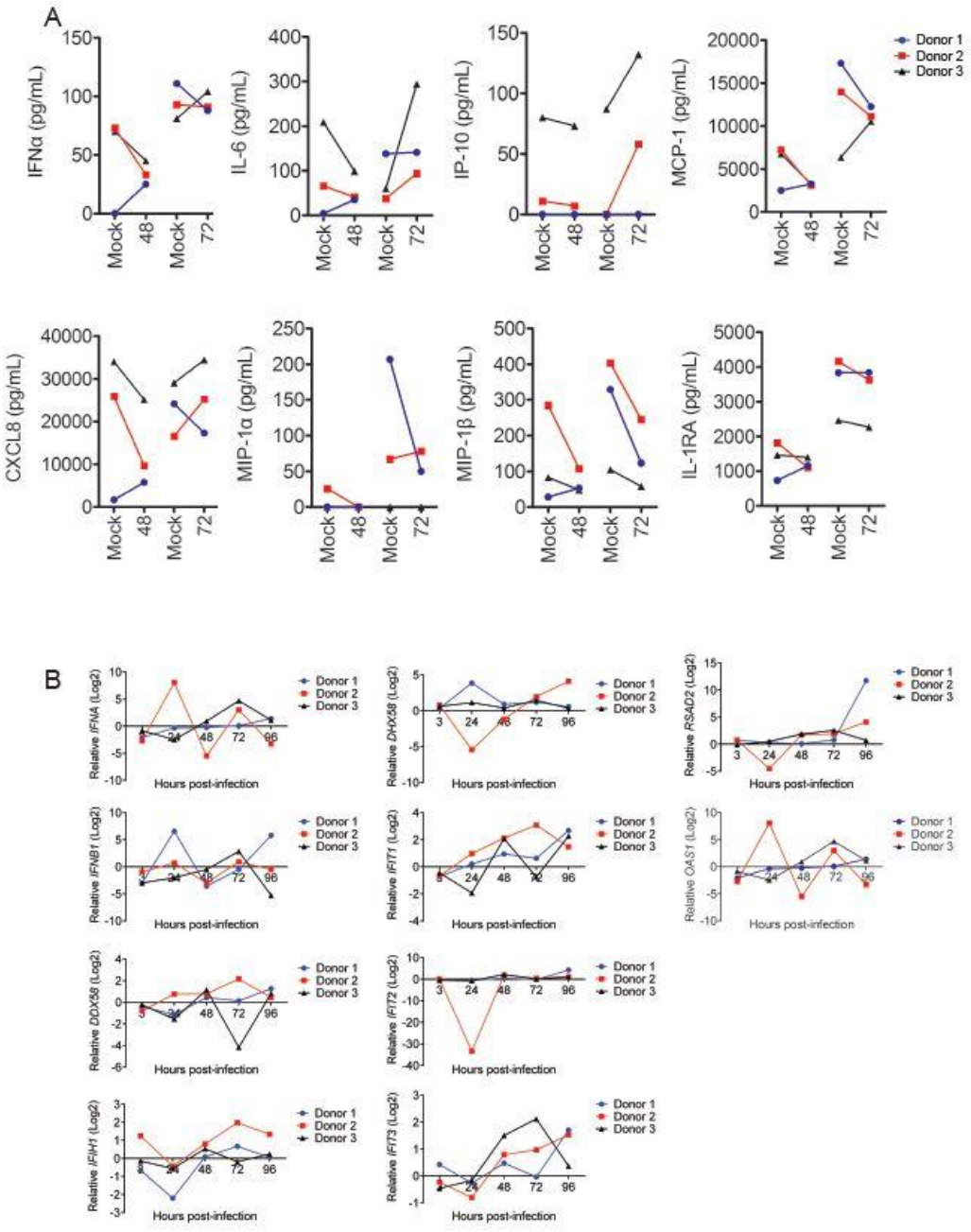

Figure 4-6: ZIKV infection of CTBs induces limited type I IFN and pro-inflammatory cytokine response.

(A) CTBs isolated from three donors were infected with ZIKV (PR 2015) at an MOI of 1 or mock-infected. Cytokine levels in the supernatants were determined by multiplex bead array. All values are represented in “pg/ml” and shown with a connecting line between ZIKV-infected samples (48 and 72hpi) and their respective donor- and time-matched

mock-infected samples. **(B)** Antiviral gene expression determined by qRT-PCR in CTBs (three donors) infected with ZIKV (PR 2015). Gene expression data are represented as fold change relative to time-matched mock-infected controls (gene expression normalized to GAPDH - $\Delta\Delta C_T$ method).

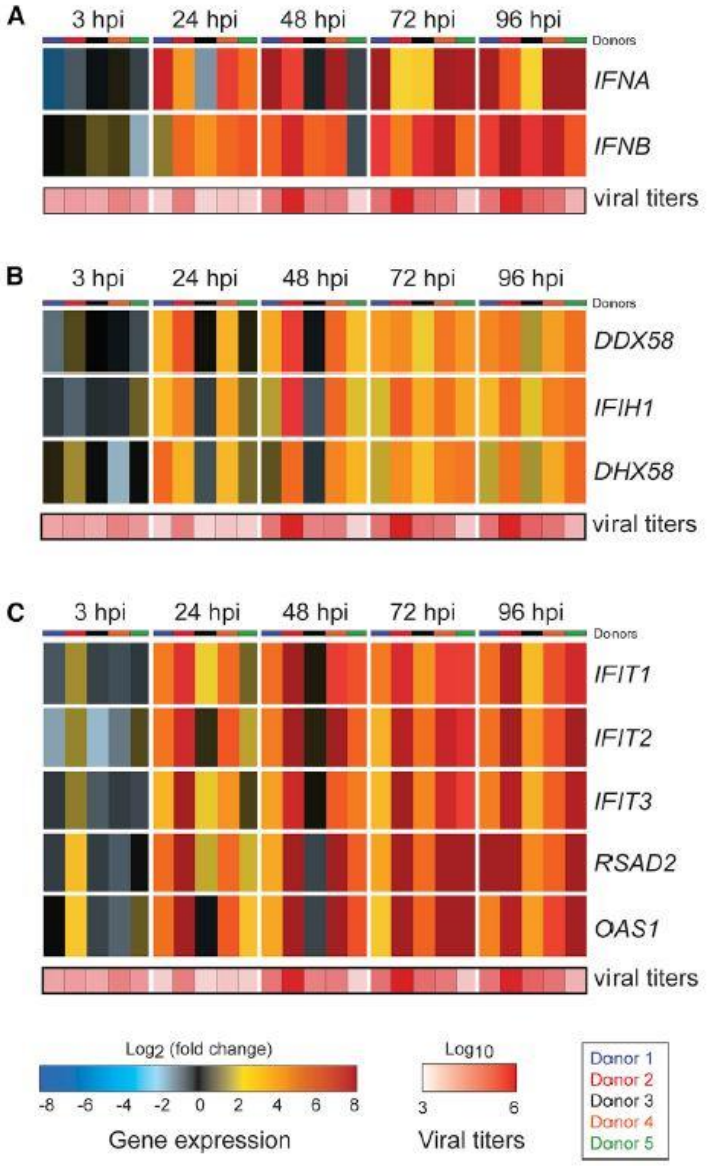

Figure 4-7: ZIKV infection induces an antiviral response in HCs.

HCs from five donors were infected with ZIKV (PR 2015) at an MOI of 1 and antiviral gene expression determined by qRT-PCR. Gene expression data are represented as

fold change relative to time-matched mock-infected controls (gene expression normalized to GAPDH - $\Delta\Delta C_T$ method). Individual donors are depicted as separate bars, organized from donor 1 to donor 5, within each time point block. Viral titers determined in Figure 1 are represented as a separate heat map below each group of genes. **(A)** Type I IFNs. **(B)** RLRs. **(C)** Antiviral effector genes. hpi, hours post-infection.

Chapter 5: Human Antibody Responses After Dengue Virus Infection are Highly Cross-Reactive to Zika Virus

Lalita Priyamvada[1, ¶], Kendra M. Quicke[1, ¶], William Hudson[2], Nattawat Onlamoon[3], Jaturong Sewatanon[2,4], Srilatha Edupuganti[5], Kovit Pattanapanyasat[3], Kulkanya Chokephaibulkit[6], Mark J. Mulligan[5], Patrick Wilson[7], Rafi Ahmed[2], Mehul S. Suthar[1], Jens Wrammert[1]

[1]Emory Vaccine Center, Emory University School of Medicine, Atlanta, GA 30322; Division of Infectious Disease, Department of Pediatrics, Emory University School of Medicine, Atlanta, GA 30322.

[2]Emory Vaccine Center, Emory University School of Medicine, Atlanta, GA 30322; Department of Microbiology and Immunology, Emory University School of Medicine, Atlanta, GA 30322.

[3]Department of Research and Development, Faculty of Medicine Siriraj Hospital, Mahidol University, Bangkok 10700, Thailand.

[4]Department of Microbiology, Faculty of Medicine Siriraj Hospital, Mahidol University, Bangkok 10700, Thailand.

[5]The Hope Clinic of the Emory Vaccine Center, Emory University School of Medicine, Atlanta, GA 30322; Department of Medicine, Division of Infectious Diseases, Emory University School of Medicine, Atlanta, GA 30322.

[6]Department of Pediatrics, Faculty of Medicine Siriraj Hospital, Mahidol University, Bangkok 10700, Thailand.

[7]Section of Rheumatology, The Knapp Center for Lupus and Immunology Research, Department of Medicine, University of Chicago, Chicago, IL 60637.

¶These authors contributed equally to this work.

*Data originally published in the *Proceedings of the National Academy of Science*: Priyamvada L, Quicke KM, Hudson WH, Onlamoon N, Sewatanon J, Edupuganti S, Pattanapanyasat K, Chokephaibulkit K, Mulligan MJ, Wilson PC, Ahmed R, Suthar MS, Wrammert J. Human antibody responses after dengue virus infection are highly cross-reactive to Zika virus. *PNAS*. 2016 Jul 12;113(28):7852-7.

Introduction

ZIKV is a mosquito-borne virus belonging to the *Flaviviridae* family of single-stranded, positive-sense RNA viruses. Until its appearance in French Polynesia in 2013 and more recently in Brazil in 2015, ZIKV infection was primarily associated with mild self-limiting illness, with symptoms resembling and often milder than DENV or Chikungunya virus (CHIKV) infections (Duffy et al., 2009; Ioos et al., 2014; Musso and Gubler, 2016). However, the more recent outbreaks have caused severe neurological complications including Guillain-Barré Syndrome in adults as well as congenital microcephaly and other adverse birth outcomes in Brazil (Cao-Lormeau et al., 2016; Mlakar et al., 2016; Rasmussen et al., 2016). The Pan American Health Organization reported that as of May 2016, local transmission of ZIKV had spread to over 38 countries or territories in the Americas. In addition, a recent World Health Organization (WHO) report states that 44 new countries are experiencing their first ZIKV outbreak since 2015. Despite improving surveillance of the virus, accurate diagnosis has been challenging given the similarities in the clinical presentation of ZIKV to other arboviral infections endemic in these regions, among other factors.

During the viremic period, ZIKV can be detected in patient blood, saliva, urine and other bodily fluids early after symptom onset (Fonseca et al., 2014; Lanciotti et al., 2008; Musso et al., 2015a). During the Yap Islands epidemic in 2007, anti-ZIKV IgM ELISAs and ZIKV plaque reduction neutralization tests (PRNT) were performed to confirm infection in RT-PCR negative cases (Duffy et al., 2009; Lanciotti et al., 2008). However, as these studies showed, the cross-reactivity between ZIKV and other flaviviruses makes confirmation of infection difficult, especially when patients may have had flavivirus exposures prior to their suspected ZIKV infection (Duffy et al., 2009; Lanciotti et al., 2008). Given the overlapping presence of DENV and other flaviviruses in

a majority of ZIKV epidemic regions (Bhatt et al., 2013), there are great challenges for serology-based testing of flavivirus immune patients (Dasgupta et al., 2016).

The DENV envelope (E) protein, considered a major imunodominant target for antibody responses in dengue patients (Beltramello et al., 2010; Priyamvada et al., 2016; Xu et al., 2012), bears greater than 50% homology to ZIKV E protein (Sirohi et al., 2016). In addition to complicating the serology-based diagnosis of ZIKV infection, this raises an intriguing question about the biological implications of this observed cross-reactivity on protection, virulence, and immunopathology during ZIKV infections. At present, the effect of pre-existing immunity to DENV or other flaviviruses on immune responses induced by ZIKV is unknown. To this end, we were interested in determining the degree to which dengue-induced antibodies cross-react with ZIKV in terms of binding, virus neutralization and antibody dependent enhancement (ADE) of ZIKV infection, both at the serum and single cell level.

In this study, we provide an analysis of the cross-reactivity of acute and convalescent dengue immune sera against ZIKV. The sera were collected from nine patients admitted to Siriraj Hospital in Bangkok, Thailand with confirmed DENV infection. Both acute and convalescent sera showed high binding titers to ZIKV lysate, and could also neutralize ZIKV *in vitro.* To understand the origin and characteristics of these cross-reactive serum responses we also analyzed a panel of plasmablast-derived DENV-reactive monoclonal antibodies (mAbs). Of the 47 mAbs tested nearly half (22/47) bound to ZIKV lysate, and an additional four to whole virus. Seven of these mAbs also neutralized ZIKV *in vitro*. Five sera and a subset of the mAbs were also tested for ADE activity using the FcγR-bearing monocytic U937 cell line. All sera and ZIKV-reactive mAbs tested enhanced infection *in vitro,* while two DENV-specific but ZIKV non-reactive mAbs did not. The data presented here have important implications for clinical diagnosis given that the current ZIKV outbreak in the Americas and the Caribbean is largely

ongoing in dengue endemic areas. Equally important, these findings set the stage for more in-depth studies that explore how pre-existing flavivirus immunity may shape immune responses to ZIKV infection.

Methods

Patient samples. The dengue serum samples in this study were collected at Siriraj Hospital in Bangkok, Thailand. All patients were diagnosed with DENV infection by serotype-specific RT-PCR (17) and serum samples were collected during acute infection and/or convalescence. From four of these patients, a panel of mAbs was derived from single cell sorted plasmablasts (13). Two flavivirus-naïve sera were also included as controls. These studies were pre-approved by the Faculty of Medicine at Siriraj Hospital and the Emory institutional review board (IRB) #IRB00015730.

Viruses and viral antigens. ZIKV PRVABC59 (KU501215.1) was passaged by infecting Vero cells (ATCC; CRL-1586) at an MOI of 0.1 in serum-free MEM (Life Technologies Gibco). After a 1 h infection at 37°C, MEM supplemented with 10% FBS and 1% antibiotic/antimycotic (Corning) was added to the cells and virus inoculum. Upon observation of severe CPE, supernatants were collected and spun down at 2000 rpm for 10 min at 4°C. Supernatant containing virus was supplemented with an additional 10% FBS before freezing at -80°C. The titer of the passaged virus was determined by plaque assay. To prepare ZIKV lysate, the remaining adherent cells and cell pellet from the virus-containing supernatant were washed twice with PBS and then re-suspended in RIPA Buffer (10mM Tris, 150mM NaCl, 1% sodium deoxycholate, 1% Triton X-100, pH 7.4) supplemented with protease inhibitor (ThermoFisher Scientific; 87785) and phosphatase inhibitor (Biovision; K275-1). Mock lysate was prepared in a similar fashion with uninfected cells. Bradford assay was performed to quantitate total protein yield.

DENV2 Tonga/74 (AY744147.1) was gifted by Dr. Stephen S. Whitehead: NIH/NIAID, Bethesda, MD. DENV2 viral stocks were made by infecting Vero cells at an MOI of 0.01 in Opti-Pro SF media (Invitrogen; 12309019). Virus-containing supernatant was collected at day 5 post infection after appearance of CPE and frozen after addition of 10% SPG stabilizer as previously described (18). Viral stocks were titrated by FFA prior to use.

Preparation of 4G2 antibody. A hybridoma expressing a pan-flavivirus mouse monoclonal (D1-4G2-4-15; ATCC HB-112) was grown in RPMI supplemented with 2% FBS, antibiotics and L-glutamine until terminal density. Clarified supernatant was filtered through a 0.2 μm filter, purified over a protein G column according to manufacturer recommendations, and stored in PBS with sodium azide.

Sequence and structure alignment. To visualize structural similarity between the DENV and ZIKV E proteins, their structures (19, 20) (PDB accession codes 3J27 and 5IRE, respectively) were aligned and secondary structure assigned in Chimera (21). Chimera is developed by the Resource for Biocomputing, Visualization, and Informatics at the University of California, San Francisco. Structural figures were made using the PyMOL Molecular Graphics System, Version 1.7 (Schrödinger, LLC). Sequences were aligned using Geneious (Biomatters, Ltd.) using GenBank accession numbers AY744147.1 and KU501215.1 for DENV and ZIKV E proteins, respectively. Envelope domains (ED) I-III (22), the hinge (23), fusion loop (24), and transmembrane helices (25) were designated as previously described. For the fusion loop alignment, GenBank accession numbers used were EF623988.1 (JEV), M12294.2 (West Nile), KF769016.1 (Asibi), JX949181.1 (17D).

Western blot. ZIKV and mock lysate samples (20 µg per lane) were prepared with β-ME-containing loading buffer and boiled for 15 min at 95°C. Lysates were run by SDS-PAGE on a 10% polyacrylamide gel and transferred to nitrocellulose membrane. Blots were blocked for 30 min in 5% milk in PBS with 0.1% Tween and probed for ZIKV E protein using the mouse anti-flavivirus 4G2 primary antibody for 30 min. Blots were washed and incubated with HRP-conjugated goat anti-mouse secondary antibody (Southern Biotech; 1030-05) for 10 min. Blots were developed using SuperSignaling West Femto Maximum Sensitivity Substrate (ThermoFisher Scientific; 34096) on a Bio-Rad Molecular Imager ChemiDoc XRS+.

ELISA. For lysate ELISA, NUNC Maxisorp plates (eBioscience; 44-2404) were coated overnight at 4°C with ZIKV or mock lysates diluted in PBS. Plates were washed with PBS containing 0.05% Tween (PBS-T) and blocked with PBS with 10% FBS and 0.05% Tween (PBS-T-FBS) for 1.5 h. Subsequently, mAbs or serum was serially diluted in PBS-T-FBS and added to the plates for 1 h. A peroxidase-conjugated anti-human IgG antibody (Jackson ImmunoResearch; 109-036-098) was added for 1.5 h before developing the plates using an o-phenylenediamine substrate (Sigma; P8787).

For virus capture ELISA, plates were coated overnight at 4°C with 4G2 at a concentration of 0.25 µg/well. After blocking with PBS-T-FBS for 1.5 h, ZIKV was added for 1 h. Plates were washed with PBS-T, and serially diluted mAbs or serum was added. The addition of the secondary antibody and developing steps were performed as described above. For all ELISA experiments, the serum dilution factor or mAb concentration was plotted versus their respective OD values at 490 nm. The endpoint titer/ minimum effective concentration was determined as the concentration required for three times the background signal of flavivirus-naive serum/ irrelevant mAb.

Viral neutralization assay. The neutralization potential of mAbs and serum samples was determined by a focus reduction neutralization test (FRNT) as previously described (13) with select modifications. Serially diluted mAbs or heat inactivated sera were incubated with a previously titrated amount of virus (60-100 focus forming units) of ZIKV or DENV2 for 1 h at 37°C. Vero cell monolayers in 96 well plates were subsequently infected with the mixture for 1 h at 37°C. An overlay containing 2% methylcellulose (Sigma; M0512-2506) was added to the cells. After incubating 3 days at 37°C, the cells were washed, and fixed with a 1:1 mixture of acetone and methanol. Foci were stained using 4G2 for 2 h followed by HRP-linked anti-mouse IgG (Cell Signaling; 7076S) for 1h and were developed using TrueBlue Peroxidase substrate (KPL; 50-78-02). Foci were imaged using a CTL-Immunospot S6 Micro Analyzer. FRNT50 was determined as the concentration or dilution factor of sample required for 50% neutralization of virus.

Antibody dependent enhancement assay. Serially diluted sera or mAbs were incubated with 104 ffu ZIKV for 1 h at 37°C. The virus and serum/mAb mixture was then added to a 96 well plate containing 2x104 U937 cells (ATCC; CRL-1593.2) per well in RPMI containing 10% FBS, antibiotics and L-glutamine. Cells were infected for 24 h at 37°C. Infected cells were washed, and then fixed/ permeabilized using BD intracellular staining reagents (Fix/Perm Solution (BD; 51-2090KZ) and Perm/Wash Buffer (BD; 51-2091KZ)) according to the manufacturer's protocol. Cells were stained using 4G2 for 1 h followed by anti-mouse IgG Alexa Fluor 488 (Life Technologies; A11029) for 25 min. The frequency of infected cells was determined using flow cytometry, defined as the percentage of 4G2+ cells.

Results

Sera from DENV infected patients are highly cross-reactive to ZIKV lysate

A recently published study reported high structural similarity between the E proteins of ZIKV and other flaviviruses including DENV (Sirohi et al., 2016). We compared the ZIKV and DENV2 strains used in our study, ZIKV PRVABC59 and DENV2 Tonga/74, to determine the homology between their E proteins and identify potential targets for cross-reactive immune responses. The DENV2 and ZIKV E proteins share an extremely similar, superimposable structure (RMSD 1.1 Å; **Figure 1A and B**), with an overall 53.9% amino acid sequence identity (**Figure 2A and C**). Envelope domain I (EDI) and EDII exhibit slightly higher conservation (59.1 and 56.6% identity, respectively), including the fusion loop of EDII, which is perfectly conserved between the two proteins (**Figure 2B and C**). To assess the degree of cross-reactivity of DENV-specific B cell responses against ZIKV, mock- and ZIKV-infected Vero cell lysates were generated for use in binding assays. The lysates were tested by Western blot and probed for the presence of E protein using the mouse pan-flavivirus antibody 4G2. A band consistent with the size of ZIKV E protein was observed in ZIKV lysate, and absent in the mock lysate (**Figure 3A**). We then measured binding of both acute and convalescent dengue sera, as well as naive sera, using the ZIKV lysate by IgG ELISA (**Figure 3B and C, Table 1**).

The nine dengue patients in this study were all confirmed for DENV infection by RT-PCR. Serum samples were collected once during the acute phase (n=9) and for five patients, a second time at convalescence (n=5) (**Table 1**). Sera from two flavivirus-naïve donors were also included in our analyses as a comparison to dengue sera (**Table 1**). All 14 dengue serum samples showed high ZIKV-specific IgG endpoint dilution titers, with median values of 177,400 and 125,000 for acute and convalescent samples respectively (**Figure 3B and C, Table 1**). All sera showed negligible titers against mock lysate (endpoint dilution < 250). The flavivirus-naïve samples were essentially negative against both the ZIKV-infected and the mock lysates (**Figure 3C, Table 1**). These data illustrate

that ZIKV cross-reactive antibodies can be readily detected in the serum of dengue patients living a highly dengue endemic country like Thailand.

Dengue immune sera exhibit high neutralization potency against ZIKV

To determine whether the dengue sera could also neutralize ZIKV *in vitro*, we performed focus reduction neutralization tests (FRNT) on all 14 dengue sera against ZIKV. A representative example of the ZIKV neutralization assay with two dengue acute sera (#33 and #39) and one flavivirus-naïve serum sample (#21) is shown in **Figure 4A**. The ZIKV FRNT50 titers of the acute dengue samples ranged from 60 (#60) to 23,109 (#79), with a median value of 770. The convalescent dengue sera ranged in FRNT50 titers from 126 (#60R) to 50,346 (#79R), with a median titer of 350. While neutralization titers increased between the acute and convalescent bleeds for three patients, convalescent titers for patients #55 and #67 were lower than their acute titers (**Figure 4B, Table 1**). Of note, the convalescent samples for these two donors were obtained at a much later time-point after fever onset (61-100 days) than the other three convalescent sera (**Table 1**). These data show that dengue immune sera are can neutralize ZIKV *in vitro*. The impact of these neutralizing titers on either protective immunity or disease severity after ZIKV infection remains to be defined.

Monoclonal antibodies derived from dengue-induced plasmablasts are highly cross-reactive to ZIKV

While analysis of polyclonal sera from the dengue patients clearly illustrates ample cross-reactivity of dengue immune sera against ZIKV, serum analyses alone cannot determine the origin of these cross-reactive antibodies. In other words, whether the serum cross-reactivity was caused by two individual pools of antibodies, one DENV-specific and the other ZIKV-specific, or by antibodies that recognize both viruses, can

only be conclusively determined by analyzing functional cross-reactivity at the monoclonal level. To dissect the cross-reactivity between DENV infection-induced antibodies and ZIKV, we characterized the binding and neutralization activity of a panel of plasmablast-derived mAbs against ZIKV. These mAbs were generated from *in vivo* activated, single cell sorted plasmablasts isolated during ongoing infection from four DENV2 patients and were previously shown to be DENV-reactive either in binding, or in both binding and neutralization (Priyamvada et al., 2016).

Of the 47 mAbs tested, 22 bound with high affinity to ZIKV lysate (**Figure 5A**). An additional four ZIKV cross-reactive mAbs were identified using a whole virus capture ELISA (**Figure 5B, Table 2**). A majority of the ZIKV-specific mAbs (20/26) came from the plasmablasts of donors #31 and #39. Only a handful of mAbs from donors #32 and #33 cross-reacted with ZIKV, with several of these recognizing only whole ZIKV. While nearly half of all DENV-reactive mAbs bound ZIKV lysate or whole virus, only seven of the mAbs neutralized ZIKV *in vitro* (**Figure 5C and 5D, Table 2**). Six of these seven mAbs exhibited moderate neutralizing activity against ZIKV, with FRNT50 titers ranging between 5 µg/mL and 1 µg/mL. In contrast, mAb 33.3A06 was highly potent in ZIKV neutralization with a ZIKV FRNT50 titer of 0.03 µg/mL. Interestingly, despite the overall lower frequency of ZIKV-binding mAbs isolated from #32 and #33, half of all ZIKV neutralizing mAbs in the panel, including the three most potently neutralizing mAbs, were derived from these two patients. Repertoire analysis of the cross-reactive mAbs showed broad VJ gene usage and junctional diversity. The cross-reactive cells were also highly mutated, illustrating that these responses were likely the result of multiple previous DENV exposures (**Table 2**).

Dengue-induced antibodies can enhance ZIKV infection of an FcγR-bearing monocytic cell line in vitro

We tested the ability of five dengue sera and 11 plasmablast-derived mAbs to enhance ZIKV infection using a human FcγR-bearing monocytic cell line, U937. The U937 cell line is widely used to study ADE of DENV infection, and it is not typically permissive to high levels of DENV infection in the absence of enhancing antibodies (Smith et al., 2012). The five dengue sera tested were all acute samples from DENV2-infected patients, including patients #31, #32, #33 and #39 from whose plasmablasts the mAbs in this study were derived. The mAbs tested included seven ZIKV-neutralizing mAbs, of which six were intermediate in neutralization ($ELISA^{+}/Neut^{int}$) and one potent ($ELISA^{+}/Neut^{++}$), two ZIKV-reactive but non-neutralizing mAbs ($ELISA^{+}/Neut^{neg}$), and two mAbs that bound DENV, but did not cross-react with ZIKV ($ELISA^{-}/Neut^{neg}$). In addition to the dengue sera and mAbs, one flavivirus-naïve serum sample (#21) and two irrelevant mAbs (cholera and influenza-specific) were also tested for ZIKV ADE activity. A representative example of the flow cytometry-based assay showing ADE activity of mAb 31.3F01 is provided in **Figure 6A**. Each of the five dengue sera tested was able to enhance ZIKV infection of U937 cells, with peak percent infection between 27% (#31) to 66% (#55). The bell-shaped ADE curves observed with this assay generally seemed to shift to lower dilutions as the neutralizing potency of the serum sample increased (**Figure 6B, Table 1**), presumably due to complete neutralization of the virus at higher concentrations. The flavivirus-naïve serum sample did not enhance ZIKV infection of U937 cells (**Figure 6B**).

The six $ELISA^{+}/Neut^{int}$ mAbs enhanced ZIKV infection at the maximum concentration tested (10 μg/mL), while the potent neutralizer 33.3A06 exhibited minimal ADE above 2 μg/mL, again potentially due to complete viral neutralization. At lower concentrations, however, the mAb facilitated the infection of U937 cells, reaching a maximal percent infection of 81% (**Figure 6C**). The two ZIKV $ELISA^{+}/Neut^{neg}$ mAbs also enhanced ZIKV infection, similar to the neutralizing mAbs. Two mAbs that were

previously shown to be DENV1-specific (Priyamvada et al., 2016) and were ZIKV non-reactive (**Figure 5**) did not enhance ZIKV infection (**Figure 6C**). These data demonstrate that ZIKV-reactive antibodies can potentiate infection of FcγR-bearing human monocytic cells *in vitro* and that both maximal infection and the effective concentration range of individual antibodies varies significantly.

Discussion

The emerging ZIKV shares a high degree of sequence and structural homology with other flaviviruses, including DENV (Sirohi et al., 2016). For the current outbreak in the Americas and the Caribbean this is of major public health concern. It is not clear how pre-existing antibody titers to other flaviviruses might affect the quality of immune responses generated to ZIKV infection, and equally important, whether cross-reactive antibodies provide protective immunity or impact disease severity in infected adults (Olagnier et al., 2016). In the study presented here, we have determined the degree by which dengue-induced antibodies cross-react with ZIKV, both at a serum level as well as at a single cell level.

We characterized the ZIKV binding and neutralization potential of sera obtained from PCR-confirmed dengue patients sampled during acute disease and at convalescence. Both acute and convalescent sera had high IgG binding titers to ZIKV and potently neutralized the virus *in vitro* (**Figure 3C and 4B, Table 1**). While no obvious correlation was observed between DENV2- and ZIKV-specific neutralization titers in the same patients (**Table 1**), it is evident that a significant proportion of serum antibodies present after DENV infection cross-react with ZIKV. Although a majority of the dengue sera tested neutralized DENV2 more potently than ZIKV, sera from patients #55 and #79 had higher FRNT50 titers to ZIKV compared to DENV2 (**Table 1**). For patient #79, the lower dengue titers could simply be attributed to the mismatch between the serotype of

infection (DENV1) and the virus tested (DENV2). For patient #55, this could have been caused by genetic differences between the lab-adapted DENV2 strain used in our study and the infecting DENV2 strain. An alternative possibility is that these patients were previously exposed to ZIKV, and thus had ZIKV-reactive antibodies in their sera as a result. In fact, in the past few years, isolated cases of ZIKV transmission in Thailand have been reported (Fonseca et al., 2014; Tappe et al., 2014; Wikan et al., 2016). Although there is no evidence of previous ZIKV epidemics in Thailand, the possibility that the patients in our study are ZIKV-immune, and that the extensive cross-reactivity of their sera against ZIKV is due to pre-existing ZIKV-induced antibodies cannot be formally ruled out. To definitively conclude that antibodies induced by DENV infection cross-react with ZIKV, it is important to demonstrate this cross-reactivity at the monoclonal level as well. In addition, from the serum data it is unclear whether the observed cross-reactivity is caused by a small number of highly potent, cross-reactive antibodies, or if this is the result of a broader, low level cross-reactivity.

To deconstruct the cross-reactivity observed at the serum level, we analyzed the ZIKV binding and neutralization activities of plasmablast-derived mAbs generated from four acutely infected DENV2 patients. We found that over half of the DENV-reactive mAbs bound with high affinity to ZIKV (**Figure 5A and B**). At least 23 of the 26 ZIKV cross-reactive mAbs were E protein specific, as they were previously shown to bind recombinant DENV E protein (Priyamvada et al., 2016). Although cross-reactive binding was abundant, and all 26 ZIKV reactive mAbs neutralized DENV2, less than a third neutralized ZIKV *in vitro*. Furthermore, of the seven ZIKV-neutralizing mAbs, only one displayed potent neutralization activity (**Figure 5C**). Therefore, even though a large number of dengue patient mAbs were able to bind viral epitopes, the capacity to cross-neutralize ZIKV was restricted to a select few. Additionally, a majority of these DENV-reactive mAbs were previously shown to neutralize more than one DENV serotype

(**Table 2**) (Priyamvada et al., 2016). Hence, for a large proportion of our mAb panel, the ability to cross-neutralize virus did not extend beyond the DENV species to ZIKV. Lastly, no obvious patterns in terms of VH gene usage or dominant clones were observed for the ZIKV-reactive mAbs (**Table 2**) (Priyamvada et al., 2016). Thus, the cross-reactivity observed at the serum level, at least for these four patients, appears to be caused by a diverse repertoire of B cells.

The ZIKV E protein shares a high degree of homology with the E protein of other flaviviruses including DENV (Sirohi et al., 2016). We compared the E proteins of the ZIKV and DENV2 strains used in our study and found an overall sequence identity of 54% (**Figure 2A and C**). EDI and EDII were relatively more conserved than EDIII, which had a lower sequence identity of 44.6% (**Figure 2C**). Notably, the fusion loop is 100% conserved between the two viruses, and also when compared to other flaviviruses including yellow fever virus, West Nile virus, and Japanese encephalitis virus (**Figure 2B**). The fusion loop has been described as a target for broadly cross-reactive antibodies against DENV (Costin et al., 2013; Lai et al., 2008) as well as other flaviviruses (Park et al., 2011; Sultana et al., 2009; Vogt et al., 2011), and could be one of the epitopes targeted by the cross-reactive antibodies described in our study. In addition, despite the amino acid differences between the DENV2 and ZIKV E proteins compared, the two proteins share nearly identical structures (**Figure 1A**). This could have important implications for antibodies against conformationally sensitive epitopes, which depend on the quaternary structure of the E protein for recognition and binding (de Alwis et al., 2012; Dejnirattisai et al., 2015; Gallichotte et al., 2015). In fact, 4 out of 7 ZIKV neutralizing antibodies characterized in this study bound to whole virus, but failed to bind ZIKV lysate, suggesting that they recognize a conformational epitope. Efforts to map the binding sites of some of the antibodies described above are ongoing, focused especially on the potent ZIKV neutralizer 33.3A06. Identifying potential targets for

broadly cross-neutralizing antibody responses could inform the design of vaccines or antibody-based therapies in the future.

Since the current ZIKV outbreak is largely localized within dengue endemic areas, the potential for pre-existing dengue-induced antibodies to enhance ZIKV infection is of concern. ADE is hypothesized to contribute to the increased disease severity often observed in secondary DENV infections (Kliks et al., 1989). ADE is thought to occur when pre-existing cross-reactive antibodies form virus-antibody complexes that then facilitate the infection of FcγR-bearing cells (Halstead, 2003). This may increase the number of infected cells and cause higher serum viral loads, which have been shown to positively correlate with higher disease severity (Libraty et al., 2002; Vaughn et al., 2000). To determine whether dengue antibodies can enhance ZIKV infection *in vitro*, we infected the FcγR-bearing U937 monocytic cell line in the presence of five acute sera and 11 dengue mAbs. All five sera and the nine ZIKV-cross-reactive mAbs tested ($ELISA^{+}$) enhanced ZIKV infection *in vitro* (**Figure 6B and C**). Two DENV1-specific mAbs that did not react with ZIKV by binding or neutralization assays failed to enhance ZIKV infection in this system (**Figure 6C**). These data clearly illustrate that ZIKV-cross reactive antibodies induced after DENV infection can enhance ZIKV infection *in vitro*. However, it is important to point out that the physiological relevance of this mechanism must be carefully examined *in vivo* to determine its importance in the context of ZIKV infection of flavivirus-immune patients.

Our findings raise important questions regarding the role of cross-reactive antibodies in protective immunity, as well as their potential impact on ZIKV pathogenesis and disease severity. The data presented suggest that ZIKV infection may have the potential to reactivate cross-reactive dengue-induced memory responses in patients with prior DENV exposures. There may thus be interesting differences between the immunological responses of DENV-immune patients vs. those of a flavivirus-naïve

individual to ZIKV. To address these issues, ongoing comparative studies of immune responses, disease severity and clinical outcomes in ZIKV infected patients both in flavivirus-endemic and non-endemic areas are required. One of the most critical aspects of the current ZIKV virus outbreak is the ability of the virus to cause congenital microcephaly (Mlakar et al., 2016; Rasmussen et al., 2016). It will be essential to determine if the pre-existing cross-reactive antibodies may be involved in the context of maternal-fetal transmission of ZIKV. Equally important, studying cross-reactivity against multiple ZIKV isolates, derived from both recent and previous epidemics, might shed light on the cause for the increased disease severity observed in the current outbreak. Finally, as additional ZIKV-reactive human plasmablast and memory B cell-derived mAbs are identified, characterizing their *in vivo* properties in murine and macaque models will be an important step in generating potential prophylactic/therapeutic treatments. Such studies will also improve our understanding of the immunobiology of ZIKV infection and how pre-existing antibodies to DENV or other flaviviruses might modulate the ZIKV immune response.

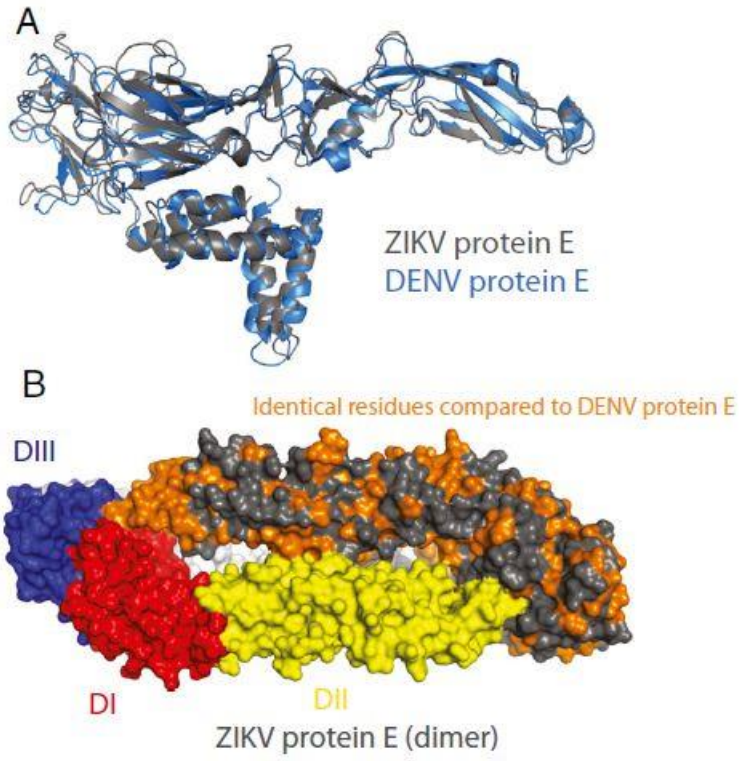

Figure 5-1: The DENV2 and ZIKV E proteins share a highly similar fold and 54% sequence identity.

(A) Overlay of DENV2 (blue) and ZIKV (gray) E protein structures (16, 19). **(B)** Structure of the ZIKV E protein dimer. The left monomer is colored by its domain structure. At right, amino acids conserved between the ZIKV PRVABC59 and DENV2 Tonga/74 envelope proteins are colored orange on a gray ZIKV backbone.

C

E protein region	Sequence identity
Total E protein	53.9%
EDI	59.1%
EDII	56.6%
EDIII	44.6%
TM	51.5%
Fusion loop	100%

Figure 5-2: ZIKV and DENV2 E proteins share high sequence identity, especially in the fusion loop.

(A) Sequence alignment of the ZIKV (gray) and DENV2 (blue) E proteins, which share 53.9% identical amino acids. The fusion loop and hinge regions are shown in green and magenta, respectively. **(B)** The fusion loop is perfectly conserved among other flaviviruses. DENV2 (blue) and ZIKV (gray) have been compared to isolate 057434 of JEV, the WNV strain WN 956 D117 3B and the 17D and Asibi strains of YFV. **(C)** Sequence identity of the ZIKV and DENV2 E protein sequences. TM: trans-membrane domain.

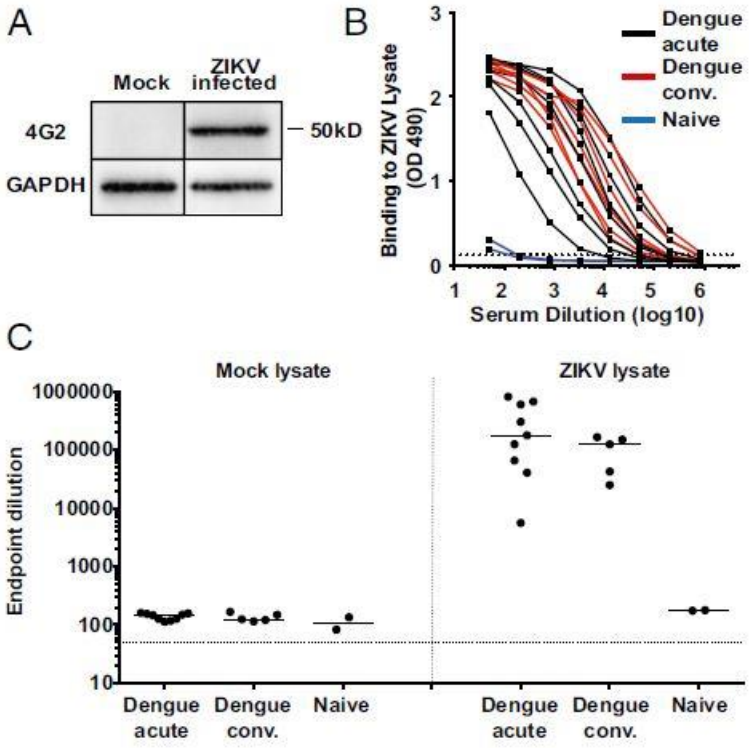

Figure 5-3: Sera from patients with secondary DENV infection exhibit potent cross-reactivity against ZIKV.

(A) Western blot of lysates from mock- or ZIKV- infected Vero cells. The pan-flavivirus reactive mAb 4G2 was used to probe for E protein. **(B)** Binding of acute (black) and convalescent (red) dengue immune and flavivirus-naïve (blue) sera to ZIKV lysate. Dotted line represents three times the background signal of plain blocking buffer. **(C)** Summary of binding of serum samples to lysates from mock- or ZIKV-infected Vero cells determined by ELISA. Acute (n=9) and convalescent (n=5) dengue and two control sera were tested. Median endpoint IgG titers for each set of sera are indicated. The dotted line represents the initial serum dilution (1/60). The binding data shown in panels B and C are the result of two independent experiments and the mean value is plotted.

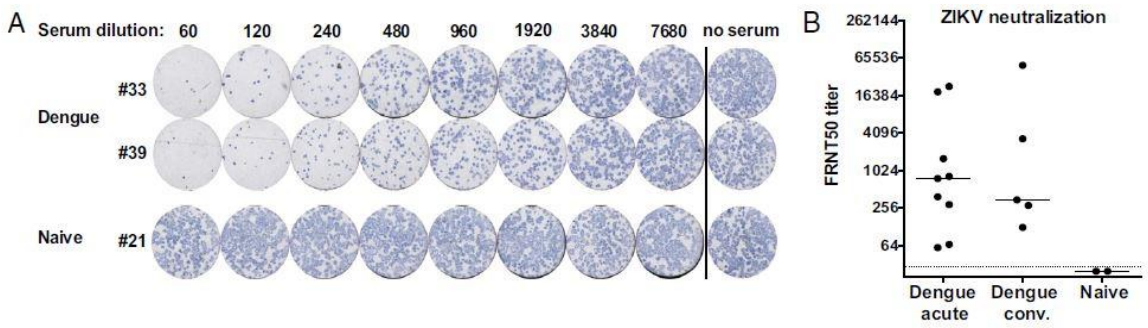

Figure 5-4: Sera from acute and convalescent dengue patients neutralizes ZIKV.

(A) Representative panel of FRNT assay showing neutralization of ZIKV by acute dengue sera (#33, #39) and one flavivirus-naïve serum sample (#21). **(B)** Neutralization activity of serum samples against ZIKV. The FRNT50 titers of flavivirus-naïve (n=2) sera and acute (n=9) and convalescent (n=5) dengue sera were determined by FRNT assay as previously described (13). The FRNT assay for each sample was repeated in two or more independent experiments. The solid line represents median FRNT50 value, and dotted line represents the initial serum dilution (1/30).

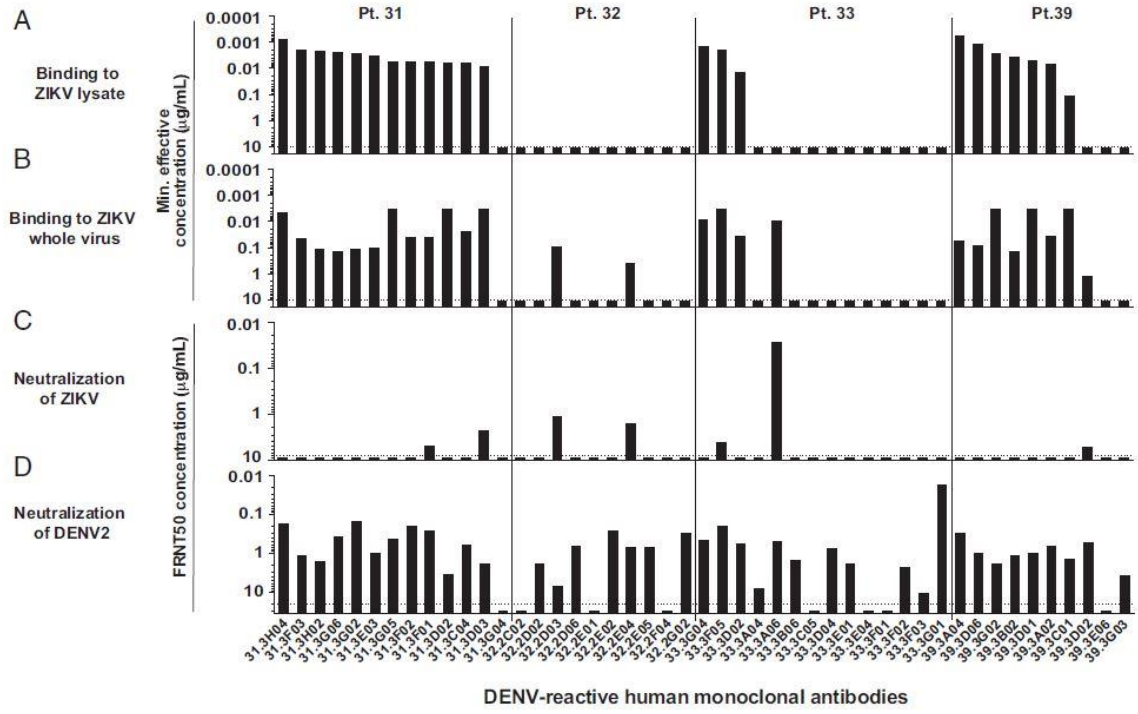

Figure 5-5: A subset of DENV-specific plasmablast-derived mAbs cross-react to ZIKV both by binding and neutralization.

Binding of DENV-reactive mAbs (n=47) to **(A)** ZIKV lysate or **(B)** whole ZIKV. The mAbs are grouped by patient (Pt.). Values plotted represent the minimum concentration required for three times the background signal from an irrelevant mAb. Dotted line represents the maximum concentration of mAb tested in ELISA: 10 µg/mL. FRNT50 of DENV-reactive mAbs against ZIKV **(C)** and DENV2 **(D)**. Dotted line represents the maximum concentration of mAb tested: 8 µg/mL (ZIKV FRNT) and 20 µg/mL (DENV FRNT). The DENV2 neutralization data in D has been adapted from previously published data (13). All experimental data shown is the result of two or more independent experiments.

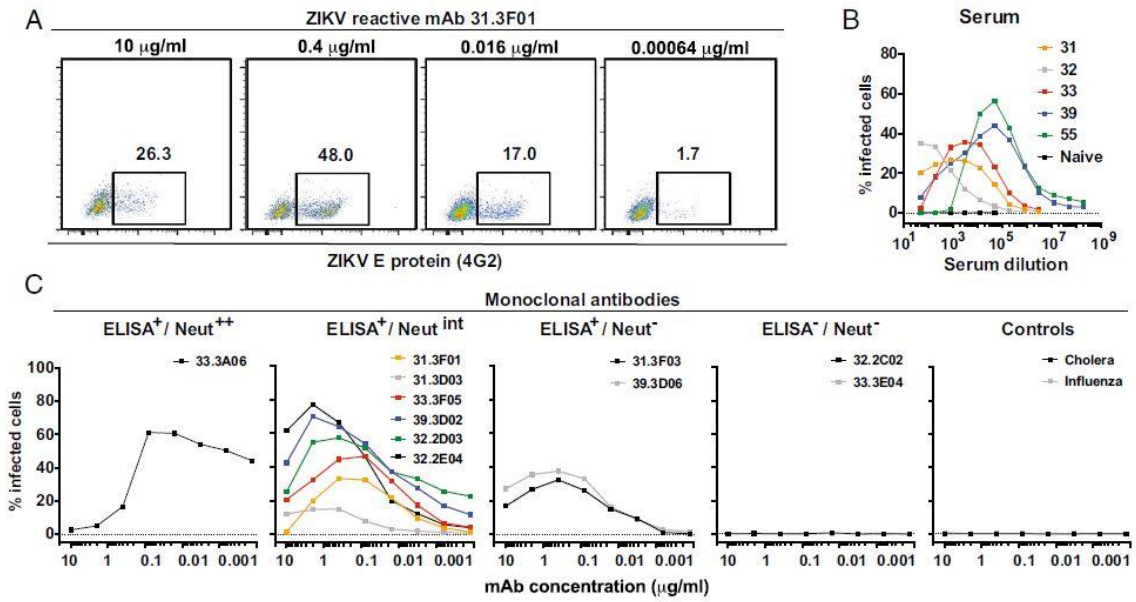

Figure 5-6: Sera and mAbs from DENV-infected patients can enhance ZIKV infection of U937 cells.

(A) Representative flow cytometry panel of mAb 31.3F01 showing percent infection at a range of mAb concentrations. **(B)** ADE activity of five dengue sera and one flavivirus-naïve serum sample. **(C)** ADE activity of dengue patient-derived (n=11) and control (n=2) mAbs. The antibodies are grouped by ZIKV cross-reactivity phenotype. ELISA+/- refers to binding activity to ZIKV by capture virus ELISA while Neut++/+/neg refers to ZIKV neutralization activity. Infected cells were identified by 4G2 staining. The dotted line in panels B and C represents percent infection in the absence of antibody (virus only). Data shown is representative of two or more independently performed experiments.

Sample	Day after fever onset*	Infection type	ZIKV endpoint dilution†	FRNT50‡	
				DENV2	ZIKV
31	4	DENV2	600,000	1,653	392
32	3	DENV2	5,600	1,355	294
33	5	DENV2	40,600	1,318	1,602
39	6	DENV2	819,200	2,286	770
55	4	DENV2	675,000	1,373	18,940
55R§	100		25,000	218	3,344
60	6	DENV3	302,400	7,614	60
60R§	40		150,000	14,807	126
67	6	DENV1	125,000	2,858	832
67R§	61		42,500	1,880	285
79	4	DENV1	65,600	528	23,109
79R§	37		165,000	470	50,346
86	6	DENV3	177,400	322	67
86R§	41		125,000	263	350
21		HC¶	175	<30	<30
22		HC¶	179	<30	<30

*Number of days post-fever onset at which blood was collected.
†IgG ELISA measuring endpoint titer for binding to ZIKV-infected lysate. The signal from mock lysate was <250 for all samples.
‡50% focus reduction neutralization titer.
§Convalescent sample.
¶Healthy control.

Table 5-1: Summary of serum binding and neutralization.

											Rearrangement						
		Binding to ZIKV†		Neutralization—FRNT50 titer‡, μg/mL					Ig isotype		Heavy chain			Light chain			
Patient*	Ab	Lysate	Whole virus	ZIKV	DENV1	DENV2	DENV3	DENV4	Heavy chain§	Light chain	V	J	Mutations	V	J	Mutations	
31	3H04	+	+	—	1.3	0.2	0.4	0.4	IgG1	Igκ	4–30	4	16	1–12	1	13	
	3F03	+	+	—	—	1.2	—	—	IgG1	Igλ	3–43	4	22	7–43	2	19	
	3H02	+	+	—	—	1.6	—	1.8	IgG1	Igκ	3–30	4	22	3–11	2	9	
	3G06	+	+	—	7.5	0.4	—	2.5	IgG1	Igλ	3–30	4	18	2–23	2	19	
	3G02	+	+	—	—	0.2	1.8	1.2	IgG1	Igκ	3–13	4	15	2–30	4	6	
	3E03	+	+	—	—	1.0	6.2	4.5	IgG1	Igλ	3–43	4	19	7–43	2	14	
	3G05	+	+	—	—	0.4	0.5	3.0	IgG1	Igκ	3–23	4	25	3–20	3	16	
	3F02	+	+	—	—	0.2	0.9	0.5	IgG1	Igκ	3–30	4	29	2–30	2	2	
	3F01	+	+	5.0	—	0.3	—	—	IgG1	Igκ	3–30	4	23	2–30	4	11	
	3D02	+	+	—	—	3.5	—	—	IgG1	Igκ	3–23	4	23	3–20	3	14	
	3C04	+	+	—	—	0.6	—	3.1	IgG1	Igκ	1–2	4	16	3–20	4	11	
	3D03	+	+	2.3	—	1.9	4.1	—	IgG1	Igκ	4–4	3	5	1–5	2	7	
32	2D03	—	+	1.1	0.8	7.0	4.3	—	IgG1	Igκ	3–21	3	12	1–5	2	20	
	2E04	—	+	1.6	1.0	0.7	4.0	—	IgG1	Igκ	1–46	6	17	2–28	2	5	
33	3G04	+	+	—	3.1	0.5	—	2.9	IgG1	Igλ	3–21	4	14	1–44	3	6	
	3F05	+	+	4.3	—	0.2	—	1.2	IgG1	Igκ	3–11	4	10	1–33	1	10	
	3D02	+	+	—	2.1	0.6	2.2	0.5	IgG1	Igκ	3–15	4	12	3–20	2	8	
	3A06	—	+	0.03	0.2	0.5	1.4	—	IgG1	Igλ	4–61	5	35	1–44	3	18	
39	3A04	+	+	—	7.7	0.3	4.7	1.6	IgG1	Igλ	4–39	4	24	2–14	2	12	
	3D06	+	+	—	—	1.0	—	7.2	IgG1	Igλ	7–4	4	16	7–43	3	32	
	3G02	+	+	—	2.9	1.9	6.3	—	IgG1	Igλ	3–30	4	24	1–9	4	21	
	3B02	+	+	—	—	1.2	—	—	IgG1	Igλ	3–21	4	7	1–47	3	12	
	3D01	+	+	—	—	1.0	0.5	1.1	IgG1	Igλ	3–21	4	20	1–47	3	13	
	3A02	+	+	—	3.6	0.7	3.5	2.1	IgG1	Igλ	3–7	3	31	2–14	2	23	
	3C01	+	+	—	4.2	1.4	4.4	—	IgG1	Igλ	1–69	6	24	1–51	2	8	
	3D02	—	+	5.2	0.8	0.6	—	—	IgG1	Igλ	4–59	5	9	1–44	3	12	

*All patients were infected with DENV2.
†Maximum mAb concentration tested = 10 μg/mL.
‡FRNT50 values below 8 μg/mL are shown.
§All mAbs were cloned into heavy chain expression vectors containing the IgG1 constant region.

Table 5-2: Summary of characteristics of mAbs.

Chapter 6: Cross-reactive dengue virus antibodies augment Zika virus infection of human placental macrophages

Matthew G. Zimmerman [1, 2, ¶], Kendra M. Quicke [1, 2, ¶], Justin T. O'Neal[1, 2], Nitin Arora[3], Lalita Priyamvada[1, 2], Robert C. Kauffman[1, 2], Emery Register[1, 2], Dominika Swieboda[1], Erica L. Johnson[1], Sarah Cordes[3], Lisa Haddad[3], Rana Chakraborty[1], Carolyn B. Coyne[3,4], Jens Wrammert[1, 2], Mehul S. Suthar[1, 2]

[1]Department of Pediatrics, Division of Infectious Disease, Emory University School of Medicine, Atlanta, GA 30322, USA.

[2]Emory Vaccine Center, Yerkes National Primate Research Center, Atlanta, GA 30329, USA.

[3]Department of Pediatrics, University of Pittsburgh School of Medicine, Pittsburgh, PA 15224, USA.

[4]Center for Microbial Pathogenesis, Children's Hospital of Pittsburgh of UPMC (University of Pittsburgh Medical Center), Pittsburgh, PA 15224, USA.

[5]Department of Gynecology and Obstetrics, Emory University, School of Medicine, Atlanta, Georgia 30322, USA.

[¶]These authors contributed equally to this work.

*Manuscript in preparation.

Introduction

ZIKV is a mosquito-borne flavivirus responsible for continuing epidemics of fetal congenital malformations within the Americas since its introduction to Brazil in 2015 (de Oliveira et al., 2017; Melo et al., 2017; Rasmussen et al., 2016). ZIKV is primarily transmitted through bites from infected *Aedes* mosquitos but can also be transmitted through sexual contact and blood transfusion (Lazear and Diamond, 2016). Notably, vertical transmission of ZIKV from mother to child *in utero* has been implicated in the rise of congenital microcephaly among neonates in ZIKV-endemic regions (Coyne and Lazear, 2016). Additionally, recent studies have discovered some infants with normal head circumference developed post-natal onset microcephaly, eye abnormalities, joint disorders, and sensorineural hearing loss following congenital ZIKV infection (Delaney et al., 2018; Fitzgerald et al., 2018; van der Linden et al., 2016). These studies demonstrate that congenital ZIKV infection has wide-ranging effects on infected fetuses, emphasizing the importance of understanding the mechanisms of vertical transmission.

We and others have shown that ZIKV productively infects placental cell types within the fetal-derived chorionic villi, including macrophages (HCs) and, to a lesser extent, CTBs (see Chapter 4 and (Jurado et al., 2016; Tabata et al., 2016)). Upon gaining access to the placenta, ZIKV primarily infects HCs and persists within the placenta and fetal brain throughout pregnancy (Bhatnagar et al., 2017). However, the mechanisms of transplacental transmission of ZIKV and seeding of the placenta are not well understood. STBs, the outermost layer of the chorionic villi, maintain resistance to ZIKV infection through the constitutive secretion of IFN-λ, a type III IFN known for providing immunologic protection at anatomic barriers (e.g. blood-brain barrier, placenta, epithelial surfaces) during viral infection (Bayer et al., 2016; Lazear et al., 2015a; Lazear et al., 2015b). In mice, the IFN-λ-dependent antiviral response correlates with gestational age, specifically the development of the mature trophoblast barrier at later

stages of pregnancy (Jagger et al., 2017). The inability of ZIKV to directly infect STBs suggests alternative routes for ZIKV transplacental transmission.

The emergence of ZIKV in the Americas overlaps with the regional distribution of DENV seroprevalence, a related flavivirus that infects 50-100 million people per year (Bhatt et al., 2013). DENV exists as four serotypes (DENV1-4) that differ by 30-35% in amino acid sequence of the envelope protein. Infection with one DENV serotype confers life-long immunity to that serotype but not to subsequent infections with heterologous serotypes (Bhatt et al., 2013; Culshaw et al., 2017). In fact, immunity to previous DENV serotypes has been demonstrated to augment secondary DENV infections and induce dengue hemorrhagic fever/dengue shock syndrome (DHF/DSS) as a result of antibody-dependent enhancement (ADE) (Katzelnick et al., 2017). ADE occurs when non-neutralizing or sub-neutralizing concentrations of antibodies towards one DENV serotype bind to a different DENV serotype, allowing for Fcγ receptor (FcγR)-mediated opsonization and enhanced infection of myeloid cells (Taylor et al., 2015). Numerous studies have shown that cross-reactive DENV antibodies can bind ZIKV, which differs from DENV by 41-46% in the envelope protein, resulting in enhanced ZIKV infection in FcγR-expressing cells (see Chapter 5 and (Dejnirattisai et al., 2016; Paul et al., 2016)). Others have demonstrated that immunodeficient mice treated with convalescent human serum containing cross-reactive DENV or WNV antibodies exhibit increased mortality and broader tissue tropism after ZIKV challenge (Bardina et al., 2017). However, it is not clear what role DENV-induced cross-reactive antibodies play in mediating transplacental transmission of ZIKV.

Here we evaluate the impact of cross-reactive DENV antibodies on ZIKV infection of the placenta. We demonstrate that the presence of DENV mAbs increased ZIKV infection of HCs from approximately 5-10% to over 80% of cells infected in culture. Despite enhanced ZIKV infection, we failed to observe substantial induction of cellular

activation, pro-inflammatory cytokines, or type I IFN. In addition, immune complex-infected cells displayed low levels of IRF3- and IFN-regulated antiviral gene expression. Notably, we found that exogenous type I, but not type III IFN, significantly restricted ZIKV replication within ZIKV- and immune complex-infected HCs. Using mAbs with the identical binding site shuffled onto different IgG scaffolds, we determined that ZIKV complexed with IgG1 and IgG3 resulted in higher infection of HCs compared to IgG2 and IgG4. Finally, we performed viral infection studies in a human mid-gestation placental explant model and found that immune-complexed ZIKV was more efficient at infecting the tissue than non-complexed virus and that this enhancement occurred in an IgG subclass-dependent manner. Collectively, these findings support a mechanism by which cross-reactive DENV antibodies may facilitate viral vertical transmission across the placental barrier and enhancement of ZIKV infection in HCs.

Methods

Ethics statement. Human term placentae (>37 weeks gestation) were collected from hepatitis B, HIV-1 seronegative women (>18 years of age) immediately after elective cesarean section without labor from Emory Midtown Hospital, Atlanta, GA. This study was approved by the Emory University Institutional Review Board (IRB 000217715). Written informed consent was acquired from all donors before cesarean section and sample collection. Samples were de-identified before being transferred to laboratory personnel for primary HC isolation.

Isolation of primary Hofbauer cells. HCs were isolated from membrane-free villous placenta, as previously described (Johnson and Chakraborty, 2012). HCs were separated by density gradient centrifugation and purified using the MojoSort Human CD14 positive selection kit per the manufacturer's instructions (BioLegend). The purity of

the CD14+ HC fraction was determined by CD14 and CD163 staining and flow cytometry. On average, the purity was >95%. After isolation, HCs were cultured in complete RPMI medium consisting of 1x RPMI (Corning Cellgro), 10% FBS (Optima, Atlanta Biologics), 2mM L-glutamine (Corning Cellgro), 1mM sodium pyruvate (Corning Cellgro), 1x Non-essential Amino Acids (Corning Cellgro), 1x antibiotics (penicillin, streptomycin, amphotericin B; Corning Cellgro).

Isolation of human placental explants. Second trimester human placentae were obtained from consented donors who elected to terminate normal pregnancies. Tissues were received from the University of Pittsburgh Health Sciences Tissue Bank via an honest broker system as approved by the University of Pittsburgh Institutional Review Board and in accordance with the University of Pittsburgh anatomical tissue procurement guidelines. Chorionic villi were dissected from placental tissue and maintained in DMEM/F12 medium with 10% FBS and penicillin/streptomycin. Villi were separated into individual wells of a 48-well plate each containing 800ul of DMEM/F12 medium for subsequent experiments.

Viruses and cells. ZIKV strain PRVABC59 was used for all experiments. PRVABC59 was initially isolated in 2015 from a patient infected while in Puerto Rico. We obtained this strain from the Centers for Disease Control and Prevention in Fort Collins, CO. The virus used in these experiments has undergone a total of 5 passages in Vero cells. Viral titers were determined by plaque assay on Vero cells (ATCC). ZIKV was UV-inactivated (UV-ZIKV) by exposing virus to UV light in a Spectroline UV Crosslinker for 1 hour. Vero cells were cultured in complete DMEM medium consisting of 1x DMEM (Corning Cellgro), 10% FBS, 25mM HEPES Buffer (Corning Cellgro), 2mM L-glutamine, 1mM sodium pyruvate, 1x Non-essential Amino Acids, and 1x antibiotics.

Antibodies. The human mAbs used in these experiments were generated essentially as previously described (see Chapter 5). Briefly, plasmablasts were isolated from DENV-infected patients and single cell sorted for use in expression cloning. Immunoglobulin (Ig) genes were amplified by RT-PCR and inserted into IgG1 expression vectors. IgG1 vectors were transiently expressed in expi293F cells and secreted IgG antibodies were purified from supernatants using protein A coupled sepharose beads (Pierce). Antibodies were stored in 1x PBS with 0.05% sodium azide. The pan-flavivirus anti-envelope protein 4G2 mAb (mouse IgG1) was isolated from the supernatant of mouse hybridoma D1-4G2-4-15 (ATCC; HB-112) using a protein G column (GE Life Sciences). IgG2, IgG3, and IgG4 variants of mAb 33.3A06 were generated by subcloning the heavy chain variable domain into the appropriate IgG subclass vector by restriction digest (AgeI and SalI) and ligation. IgG3 antibodies were purified using protein G coupled sepharose beads (Pierce). The IgG1-LALA variant of mAb 33.3A06 was generated by replacing the constant region of the wild-type IgG1 heavy chain expression vector with a gene synthesized construct (Integrated DNA Technologies), containing a leucine (L) to alanine (A) substitution at amino acid positions 234 and 235 of the IgG1 constant region by restriction digest (SalI and HindIII) and ligation.

Infections and interferon treatment. HCs were infected immediately following isolation. mAbs were diluted in 1x PBS to the desired concentrations and mixed 1:1 with ZIKV at MOI of 1. No antibody (Ab-) conditions received 1x PBS; no virus (ZIKV-) conditions received RPMI. mAb:ZIKV immune complexes were incubated at 37°C for 1 hour. HCs were then infected in 200ul mAb:ZIKV complexes, or with ZIKV alone at MOI of 1 or 10, as indicated, at 37°C for 1 hour. HCs were washed once with warm RPMI to remove residual immune complexes and re-suspended in complete RPMI medium.

Infected cells were incubated at 37°C. For IFN treatment experiments, IFN-β (PBL Assay Science) and IFN-λ (PBL Assay Science) were diluted in complete RPMI medium and added to HCs at 10IU/ml or 100IU/ml following the 1-hour infection incubation. For infection of human placental explants, diluted mAbs were mixed 1:1 with $5x10^5$pfu/ml ZIKV, as MOI cannot be calculated. After the 1 hour incubation, 200ul of explant medium was removed from each well before addition of 200ul mAb:ZIKV complexes. Tissues were incubated at 37°C for 2 hours then washed 2x with warm complete DMEM/F12 medium to remove residual immune complexes and re-supplied with 800ul complete DMEM/F12 medium. Infected explant tissues were incubated at 37°C.

Flow cytometry. Most conditions were run with biological triplicate samples, and $2x10^5$ HCs were used per sample. HCs were blocked for 10min on ice with 0.25ul/sample Human TruStain FcX (BioLegend) in FACS buffer (1x PBS, 0.1% BSA, 1mM EDTA) and stained for surface markers for 20min on ice using 0.25ul/sample of the following anti-human antibodies from BioLegend in FACS buffer: CD14 (M5E2), CD80 (2D10), CD86 (IT2.2), CD40 (5C3), and HLA-DR (G46-6; BD Biosciences); or CD16 (3G8), CD32 (FUN-2), CD64 (10.1), and Ms IgG Isotype Control (C1.18.4; TONBO Biosciences). Cells were also live/dead stained for 20min on ice with 0.1ul/sample either Ghost 780 of Ghost 510 viability dye (TONBO Biosciences) in 1x PBS. HCs were fixed with 1x Transcription Factor Fix/Perm (diluted in Transcription Factor Fix/Perm Diluent; TONBO Biosciences) for 20min on ice and permeabilized by washing twice with 1x Flow Cytometry Perm Buffer (diluted in ddiH_2O; TONBO Biosciences). HCs were re-blocked for 5min on ice with 0.25ul/sample Human TruStain FcX and 0.25ul/sample normal mouse serum (ThermoFisher Scientific) in Perm Buffer and stained for ZIKV E protein for 20min on ice using 0.5ul/sample of a 4G2-APC antibody in Perm Buffer. Unconjugated monoclonal 4G2 antibody was conjugated to APC using a Novus Lighting-

Link kit per the manufacturer's instructions. Flow cytometry samples were re-suspended in 1x PBS and run on an LSR-II flow cytometry machine.

Focus-forming assay. Focus-forming assay (FFA) was performed on Vero cells with supernatants from ADE-ZIKV-infected HCs ($2x10^5$ cells per condition) or human placental explants and accompanying controls. Supernatants were initially diluted 1:10 in DMEM with 1% FBS followed by 10-fold serial dilution. Vero cells were plated in a 96-well plate and infected with 50ul diluted supernatant for 1 hour at 37°C. Cells and inoculum were then overlaid with methylcellulose (DMEM [Corning Cellgro], 1% antibiotic, 2% FBS, 2% methylcellulose [Sigma Aldrich]) and incubated at 37°C for 72 hours. Methylcellulose was aspirated, and cells were washed 3x with 1x PBS and fixed/permeabilized with a 1:1 mixture of acetone and methanol. Cells were washed once with 1x PBS and blocked with 5% milk in 1x PBS for 20min at RT. Cells were incubated with primary mouse 4G2 antibody (1µg/mL) in 5% milk in 1x PBS for 2 hours at RT and washed 2x with 1x PBS. Goat anti-mouse HRP-conjugated secondary antibody was applied at 1:3000 dilution in 5% milk in 1x PBS for 1 hour at RT. Cells were washed 2x with 1x PBS and foci were developed with TrueBlue Peroxidase Substrate (KPL). Plates were read on a CTL50 ImmunoSpot S6 Micro Analyzer and spots were counted manually using ImageJ.

Multiplex bead assay. Type I IFN and cytokine concentrations in the supernatants of ADE-ZIKV-infected HCs ($2x10^5$ cells per condition) and accompanying controls were assessed using a human cytokine 25-plex panel (Novex) and a ProcartaPlex human IFN-beta simplex kit (Invitrogen) per the manufacturers' instructions. Plates were read on a Luminex 100 Analyzer.

Quantitative real time-PCR (qRT-PCR). HCs infected with mAb:ZIKV immune complexes and control cells ($1x10^5$ cells per condition) were lysed in RNA Lysis Buffer. Total RNA was isolated from cells using the Quick-RNA MiniPrep Kit (Zymo Research) per the manufacturer's instructions. For human placental explants, tissues infected with mAb:ZIKV immune complexes and control conditions were suspended in TRI reagent and mechanically homogenized using ceramic bead tubes (Omni International) on a Beadruptor Homogenizer. Total RNA was isolated from homogenized tissues using the Direct-zol RNA MiniPrep Plus Kit (Zymo Research) per the manufacturer's instructions. Purified RNA was reverse transcribed using random primers with the High-Capacity cDNA Reverse Transcription Kit (Applied Biosystems). HC gene expression and ZIKV viral RNA levels were quantified by qRT-PCR using PrimeTime Gene Expression Master Mix (Integrated DNA Technologies), ZIKV-specific primers and probe set (**Table 1**) (Lanciotti et al., 2008) and TaqMan gene expression assays (ThermoFisher) for host genes: Gapdh (Hs02758991_g1), Ifna2 (Hs00265051_s1), Ifnb1 (Hs01077958_s1), Ifnl1 (Hs00601677_g1), Ifit1 (Hs03027069_s1), Ifit2 (Hs01922738_s1), Ifit3 (Hs01922752_s1), Ddx58 (Hs01061436_m1), Ifih1 (Hs00223420_m1), Dhx58 (Hs01597843_m1), Oas1 (Hs00973637_m1), and Rsad2 (Hs00369813_m1). C_T values were normalized to the reference gene *Gapdh* and represented as fold change over values from time-matched mock samples using the formula $2^{-\Delta\Delta CT}$. All primers and probes were purchased from Integrated DNA Technologies (IDT). qRT-PCR was performed in 384-well plates and run on an Applied Biosystems 7500 HT Real-Time PCR System.

ZIKV strand-specific qRT-PCR. Purified RNA was reverse transcribed using oligo(dT) and a ZIKV-specific cDNA primer. The two ZIKV-specific cDNA primers are complementary to either the positive-strand or negative-strand and include a unique 5'

tag (**Table 1**). Two cDNA and qRT-PCR reactions were run for each sample, one for positive-strand and one for negative-strand. For ZIKV strand-specific detection, a ZIKV-specific primer and tag-specific primer were used for targeted amplification of the tagged cDNA in addition to the ZIKV-specific probe. C_T values were normalized to the reference gene *Gapdh* and represented as fold change over values from time-matched mock samples using the formula $2^{-\Delta\Delta CT}$.

qRT-PCR on viral RNA from supernatants. Total RNA was isolated from the supernatants of infected HCs and human placental explants using the QIAamp Viral RNA Mini Kit (QIAGEN) per the manufacturer's instructions. ZIKV RNA standard was generated by annealing two oligonucleotides spanning the target ZIKV prM-E gene region and performing *in vitro* transcription using the MEGAscript SP6 Transcription Kit (Ambion). For ZIKV RNA quantification in supernatants, a standard curve was generated using tenfold serial dilutions of ZIKV RNA standard, and qRT-PCR was performed using ZIKV-specific primers and probe (**Table 1**) (Lanciotti et al., 2008) Viral RNA copies were interpolated from the standard curve using the sample C_T value and represented as copies per mL of supernatant.

Western blot. ADE-ZIKV-infected HCs and control cells ($1.2x10^6$ cells per condition) were washed 2x with 1x PBS with 1mM EDTA and lysed with modified RIPA buffer (10mM Tris, 150mM NaCl, 1% NA-deoxycholate, 1% Triton X-100, 1x protease inhibitor cocktail [ThermoFisher Scientific], 1x phosphatase inhibitor cocktail [ThermoFisher Scientific]). Protein concentrations were determined by Bradford assay – 2ul cell lysate in 200ul 1x Bradford Reagent (BioRad) and read on a SynergyH1 Hybrid Reader (BioTek). Proteins were denatured with 1x loading buffer (0.25M Tris, 40% glycerol, 20% β-ME, 9.2% SDS, 0.04% Bromophenol Blue) and boiling for 15min. Lysates were then

run on SDS-PAGE gel and transferred to nitrocellulose membrane for Western blotting. Blots were blocked in 5% milk in PBST (1xPBS, 0.1% Tween-20) and rinsed with ddiH_2O. Blots were incubated with the following primary antibodies in PBST with 10% FBS: Rb anti-IFIT1 (1:1000; Cell Signaling), Ms anti-IFIT2 (1:1000; Cell Signaling), Rb anti-IFIT3 (1:10,000; kindly provided by Dr. Ganes Sen), Rb anti-RIG-I (1:1000; Cell Signaling), Rb anti-MDA5 (1:1000; Cell Signaling), Rb anti-LGP2 (1:100; IBL), Rb anti-Viperin (1:1000; Cell Signaling), and Rb anti-GAPDH (1:2500; Cell Signaling). Blots were washed with PBST and incubated for 10min with anti-mouse or anti-rabbit HRP-conjugated secondary antibodies at 1:750 dilution in PBST with 1% FBS. Blots were washed again with PBST and developed with ThermoScientific SuperSignal West Femto Maximum Sensitivity Substrate. Blots were imaged on a BioRad ChemiDocXRS+.

Binding and entry assay. mAb:ZIKV immune complexes were prepared as described above and incubated for 1 hour at 37°C. mAb:ZIKV complexes and HCs were then chilled on ice for 1 hour prior to infection. HCs were infected with mAb:ZIKV complexes for 1 hour on ice and then washed 4x with ice cold 1x PBS. To assess virus binding to the cell surface, HCs were immediately lysed in RNA lysis buffer after washes. To assess viral entry into cells, HCs were re-suspended in pre-warmed complete RPMI medium and incubated at 37°C for 2 hours. HCs were then washed 4x with ice cold 1x PBS and lysed in RNA lysis buffer. ZIKV genomic RNA levels were assessed by qRT-PCR as described above.

Statistical analyses. All figures are representative of at least three independent experiments and at least three individual donors. Cytokine protein data (multiplex bead assay) and viral binding/entry data were analyzed by 1-way ANOVA followed by Tukey's test for multiple comparisons, $p<0.05$. Interferon treatment data were analyzed by 2-way

ANOVA followed by Tukey's test for multiple comparisons, $p<0.05$. All statistical analysis was performed using GraphPad Prism software.

Results

Cross-reactive DENV antibodies enhance ZIKV infection of HCs

Due to structural similarities between the ZIKV and DENV E proteins, anti-DENV human mAbs can cross-react and enhance ZIKV infection in FcγR-expressing human monocytic cell lines (see Chapter 5 and (Sirohi et al., 2016)). Thus, we determined whether DENV cross-reactive antibodies can enhance ZIKV infection of HCs. We isolated primary HCs from full-term placenta and infected them with ZIKV (PRVABC59) alone or complexed with anti-DENV2 mAbs (IgG1 subclass). These DENV mAbs were previously isolated from plasmablasts collected from patients acutely infected with DENV2 (Priyamvada et al., 2016), and were previously characterized with regards to their cross-reactivity to ZIKV (see Chapter 5). We evaluated four DENV2 mAbs, which vary based on ZIKV binding and neutralization capabilities, along with a non-specific control mAb originally isolated from a patient with acute influenza infection (Wrammert et al., 2011) (**Figure 1A**). We observed that the three ZIKV cross-reactive DENV mAbs robustly enhanced ZIKV infection with >70% of cells infected at the highest mAb concentration (10μg/mL) as compared to cells infected with ZIKV alone at an MOI of 1 (4%) or 10 (21%; **Figure 1B**). We found the most dramatic enhancement of ZIKV infection in HCs treated with the 33.3A06 mAb at 10μg/mL (83.5%) as compared to the 31.3F03 (76.3%) and 33.3F05 (75.7%) mAbs. As previously reported, the non-cross-reactive 33.3E04 mAb and the non-specific control mAb (influenza virus EM4CO4 mAb) failed to enhance ZIKV infection (see Chapter 5). We performed additional titrations with the 33.3A06 mAb and observed a dose-dependent decrease in ZIKV infection, beginning at 1.6×10^{-2} μg/mL and reaching similar levels as ZIKV infection alone (MOI 1) by 1.28×10^{-4} μg/mL mAb

(**Figure 1C**). We measured release of infectious virus by focus-forming assay (FFA) and similarly observed the highest levels of infectious virus in HC supernatants under conditions where ZIKV immune complexes were generated with $4x10^{-1}$ to $1.6X10^{-2}$ µg/mL of 33.3A06 mAb (**Figure 1D-E**). We also measured cell surface expression of costimulatory markers (CD80, CD86, CD40) in the presence of ZIKV complexed with 33.3A06 mAb (92.7% ZIKV E+ cells; **Figure 2A**). Compared to ZIKV infection alone (MOI 1 or 10) or ZIKV infection in the presence of the non-specific control mAb, we observed very little change in CD40, CD80, and CD86 upon ADE-ZIKV infection of HCs (**Figure 2B-D**). This is consistent with our previous observations that ZIKV induces a modest increase in co-stimulatory molecule expression on HCs (see Chapter 4). Similar to our previous findings, we did not observe a substantial increase in cell death with either ZIKV infection alone or following infection with immune-complexed ZIKV as compared to mock infected cells (**Figure 2E**). Altogether, these findings demonstrate that cross-reactive DENV antibodies augment ZIKV infection of HCs with minimal effects on cellular activation or cell death.

DENV mAb immune complexes increase ZIKV binding and entry in HCs

To date, the mechanisms of ADE during flavivirus infection remain incompletely understood; however, it is hypothesized that enhancement of viral infection can involve two different, but not mutually exclusive, mechanisms: extrinsic or intrinsic ADE (Taylor et al., 2015). Extrinsic ADE is defined as sub-neutralizing concentrations of antibody binding to a virus and subsequently increasing attachment and entry into cells expressing Fc receptors. Intrinsic ADE involves negative regulation of innate immune signaling following binding of immune complexes to surface Fc receptors, thus making the cells more permissive to viral infection (Taylor et al., 2015). To establish the mechanism of ADE of ZIKV infection in HCs, we performed viral binding and entry

assays on HCs infected with ZIKV alone (MOI 1 or 10) or in the presence of cross-reactive and non-specific mAbs (**Figure 3A**). As expected, we observed a log-fold increase in viral binding and entry in HCs between ZIKV at an MOI of 1 and 10 (**Figure 3B**). In ADE-ZIKV-infected HCs, we observed significantly increased viral binding as compared ZIKV infection of HCs in the presence of the non-specific control mAb. Similarly, we also observed a log-fold increase in viral entry in ADE-ZIKV-infected cells as compared to ZIKV alone at an MOI of 1 or in the presence of non-specific control mAb. Despite similar levels of viral entry between cells infected with ZIKV at an MOI of 10 and ADE-ZIKV-infected cells, we consistently observed higher levels of infected cells as measured by viral E protein staining in ADE-ZIKV-infected HCs (**Figure 1**). These findings suggest that extrinsic ADE, and to a lesser extent intrinsic ADE, plays a significant role in enhancing ZIKV infection of HCs.

ADE of ZIKV infection induces IFN gene expression but dampens antiviral responses in HCs

We previously reported that ZIKV infection of HCs triggers expression of antiviral effector genes in the absence of detectable type I IFN (see Chapter 4). Thus, we next determined whether there were differences in the induction of innate immune responses between non-ADE- and ADE-ZIKV-infected HCs. We evaluated the expression of type I and type III IFNs following ZIKV infection of HCs. HCs infected with ZIKV alone (MOI of 1 or 10) or in the presence of the non-specific control mAb displayed robust induction of type I and III IFN mRNAs, which corresponded with increased viral RNA as compared to time-matched mock-infected controls (**Figure 4A**). Similarly, robust increases in IFN-β (630-fold), IFN-α (267-fold) and IFN-λ (209-fold) transcript expression were observed in the highest ADE-ZIKV infected HCs ($1.24x10^6$ ZIKV RNA) as compared to time-matched mock-infected controls. Notably, we failed to detect IFN-β protein in the supernatants of

HCs infected under any condition (non-ADE and ADE-ZIKV infected HCs; **Figure 4B**). This finding is consistent with our previous observations in ZIKV-infected HCs and moDCs, in which we failed to observe IFN-β protein in cells or in the supernatants despite robust induction of IFN-β transcripts (see Chapters 3 and 4). We did observe basal IFN-α protein in the supernatants of mock-infected cells. Notably, we observed a significant reduction in IFN-α protein in ADE-ZIKV-infected HCs as compared to HCs infected with ZIKV alone (MOI 1) or in the presence of the non-specific control mAb (**Figure 4B**). These results indicate that ZIKV infection potently triggers transcription of type I and III IFNs but blocks the translation/secretion of type I IFNs into the supernatant.

Next, we evaluated the effect of ADE-ZIKV infection on the induction of pro-inflammatory cytokines/chemokines. For this analysis, we performed a multi-plex cytokine/chemokine analysis on supernatants following ZIKV infection of HCs (non-ADE and ADE). Infection of HCs with ZIKV at MOI 1 resulted in significant increases in MCP-1, MIP-1α and MIP-1β, and modest increases in IL-2R and IL-1Rα over mock-infected controls (**Figure 5**). Despite high levels of infection, we observed a lack of induction of MCP-1, MIP-1α, MIP-1β, IL-2R and IL-1Rα as well as other pro-inflammatory cytokines/chemokines (**data not shown**) in ADE-ZIKV-infected HCs over mock-infected cells. MCP-1 (CCL2), MIP-1α (CCL3), and MIP-1β (CCL4) are important for trafficking and infiltration of inflammatory myeloid cells and leukocytes to sites of flavivirus infection (Michlmayr and Lim, 2014). Notably, levels of IL-8, a cytokine canonically associated with neutrophil trafficking and degranulation but also non-inflammatory placental angiogenesis in HCs (Schliefsteiner et al., 2017), was reduced in ADE-ZIKV-infected HCs compared to mock infected controls (**Figure 5**). Furthermore, we failed to detect IL-10, which has been implicated in contributing to intrinsic ADE (Tsai et al., 2014), in either mock-infected cells or following ZIKV infection of HCs (**data not shown**).

We next measured the expression of the RLRs, which play a critical role in triggering an innate immune response following ZIKV infection and antiviral effector genes that restrict ZIKV infection (see Chapter 3). At the transcript level, we observed that *DDX58* (RIG-I), *IFIH1* (MDA5), and *DHX58* (LGP2) expressions were induced in HCs infected with ZIKV alone (MOI of 1 and 10) or in the presence of the non-specific control mAb as compared to time-matched mock-infected controls (**Figure 4C**). However, at the highest concentrations of 33.3A06 mAb immune-complexed ZIKV, which corresponded with robust ZIKV replication, we observed minimal induction of *DDX58* (3.4-fold), *IFIH1* (3.1-fold), and *DHX58* (2.8-fold) as compared to time-matched mock-infected controls. In a similar manner, we observed minimal induction of antiviral effector genes *IFIT1* (8.0-fold), *IFIT2* (31.4-fold), *IFIT3* (4.9-fold), *RSAD2* (5.0-fold) and *OAS1* (1.1-fold) in ADE-ZIKV-infected HCs as compared to cells infected with ZIKV alone (MOI of 1 and 10) or in the presence of the non-specific control mAb (**Figure 4C**). To determine whether ZIKV also blocks the translation of antiviral effector genes, we performed Western blot analysis on a parallel set of infected HC samples. ZIKV infection alone (MOI of 1 and 10) showed robust increases in expression of the RLRs, IFIT proteins, Viperin and OAS1 over mock-infected controls (**Figure 4D**). However, we observed a lack of RLRs and antiviral effector proteins in ADE-ZIKV-infected cells as compared to mock-infected cells. As a control, we did not observe any changes in GAPDH protein across the various conditions of infected HCs. Combined, these findings demonstrate that ZIKV antagonizes type I IFN signaling by inhibiting translation or secretion of IFN-α/β. Furthermore, these findings suggest that when cells are infected with immune-complexed ZIKV, this allows for efficient blockade of type I IFN signaling, such as inhibition of STAT phosphorylation (see Chapter 3) and/or STAT2 degradation (Grant et al., 2016), or that immune-complexed ZIKV binding to Fc receptors triggers a negative signal within HCs that prevents the induction of antiviral effector genes.

Type I IFN, but not Type III IFN, restricts ADE-ZIKV infection in HCs

Treatment of cells with type I IFN has been shown to restrict ZIKV replication in human moDCs (see Chapter 3). Similarly, type III IFN was shown to be critical for preventing ZIKV infection and replication in the STB layer of the placenta (Bayer et al., 2016; Delorme-Axford et al., 2013). We next determined whether type I or III IFN can restrict ADE of ZIKV infection in HCs by performing an interferon inhibition assay. In this assay, we infected HCs with ZIKV immune complexes for 1h followed by treatment with recombinant human IFN-λ1 or IFN-β (10 IU/mL or 100 IU/mL) for 24h. We then measured both ZIKV infection by intracellular viral E protein staining and infectious virus production by FFA. Following IFN-λ1 treatment (10 IU/mL and 100 IU/mL), we observed a modest, yet significant, increase in the percentage of ZIKV-infected cells as compared to untreated cells (**Figure 6A**). Notably, we observed this increase in both non-ADE- and ADE-ZIKV-infected cells (**Figure 6C**). However, we did not observe an increase in infectious virus release following IFN-λ1 treatment (**Figure 6A**). In contrast to IFN-λ1, IFN-β treatment resulted in significant reduction in both the percentage of ZIKV infected cells and infectious virus in the supernatants (**Figure 6B**). This reduction was consistent across non-ADE- and ADE-ZIKV-infected HCs (**Figure 6C**). These results indicate that HCs are highly responsive to IFN-β treatment and that IFN-β inhibits ZIKV replication in HCs despite the high levels of infection seen with ADE. Notably, IFN-λ1, a cytokine considered to have similar antiviral properties as type I IFN, enhanced ZIKV infection of HCs.

IgG subclass influences infectivity of HCs during ADE

Given that our work thus far used an IgG1 subclass mAb, we next determined whether similar levels of enhanced ZIKV infection were observed across various IgG subclasses.

Earlier studies with full-term placental villous tissue found that HCs preferentially express FcγRI (CD64) and FcγRII (CD32) with variable expression of FcγRIII (CD16) (Kameda et al., 1991; Kristoffersen et al., 1990; Simister and Story, 1997). We performed flow cytometry analysis on HCs isolated from full-term placenta and found that these cells express CD16, CD32 and CD64, albeit to varying levels (**Figure 7A**). We observed that >98% of HCs expressed CD32 and CD64; however, <2% of cells expressed CD16. FcγRs bind to the Fc portion of different IgG subclasses with varying affinities (Smith and Clatworthy, 2010); therefore we assessed the ability of ZIKV complexed with IgG1, IgG2, IgG3 and IgG4 to infect HCs. We generated a panel of mAbs containing the Fab region from the cross-reactive 33.3A06 mAb but interchanged the Fc regions with the four human IgG subclasses. We also generated a mutant form of IgG1 containing a "LALA" modification in the Fc region, which is known to substantially inhibit FcγRI, FcγRII, and FcγRIII binding (Beltramello et al., 2010; Hessell et al., 2007). We generated ZIKV immune complexes using this panel of mAbs and observed similar levels of infection with IgG1, IgG3, and IgG4 subclasses with substantially reduced infection with IgG2 at the highest antibody concentration (**Figure 7B**). However, at lower Ab concentrations ($1.6x10^{-2}$, $3.2x10^{-3}$ µg/mL), we observed distinct differences in viral infection using the panel of 33.3A06 IgG subclasses. At $1.6x10^{-2}$ µg/mL, IgG1 and IgG3 immune complexes displayed a higher percentage of infected cells (76.9% and 82% 4G2+ cells, respectively); IgG4 had an intermediate phenotype (64.5% 4G2+ cells), and IgG2 displayed low levels of infection (4.38% 4G2+ cells; **Figure 7B**). As previously shown, ADE of ZIKV infection is lost at the 6^{th}-7^{th} mAb dilution for the entire panel of 33.3A06 mAb IgG subclasses. ZIKV immune complexes generated with the 33.3A06 IgG1-LALA mAb variant showed reduced infection across all antibody concentrations and reached similar levels as cells infected with ZIKV alone (MOI 1) or in the presence of non-specific control mAb. This demonstrates that ADE-ZIKV occurs through an Fc receptor-

dependent mechanism. Collectively, the results demonstrate that HCs express specific FcγRs that promote binding of viral immune complexes and augment ZIKV infection in an IgG subclass-specific manner.

Cross-reactive DENV mAbs enhance ZIKV infection of human mid-gestation placental explants

We next determined the ability of cross-reactive DENV mAbs to enhance ZIKV infection of human mid-gestation placental explants. For these studies, we generated ZIKV immune complexes using the panel of 33.3A06 IgG subclasses as well as the IgG1-LALA mutant and infected second-trimester human placental villous explants with the immune complexes, ZIKV alone, or in the presence of non-specific control mAb. Virus was pre-adsorbed to the explants for 2 hours, washed with PBS, and explants incubated for 24 or 48 hours. To measure virus replication, we performed strand-specific qRT-PCR, wherein we used a tagged primer approach to measure both positive- and negative-sense ZIKV RNA (Lanciotti et al., 2008). In explants treated with the 33.3A06 mAb immune complexes, we detected increased levels of positive- and negative-sense ZIKV RNA as compared to ZIKV infection alone or in the presence of non-specific control mAb (**Figure 8A**). Specifically, we found that infection with IgG1 and IgG3 displayed increased infection as compared to IgG4 and IgG2 (**Figure 8A, top**). We observed an mAb dose-dependent increase in ZIKV replication as ZIKV immune complexes generated with low 33.3A06 mAb concentrations (0.001 μg/mL) displayed similar levels of viral RNA detection as that of ZIKV alone, or in the presence of IgG1-LALA or non-specific control mAbs (**Figure 8A, bottom**). Furthermore, we observed minimal positive-sense and no detectable negative-sense ZIKV RNA in the UV-inactivated control samples (**Figure 8A, bottom**). We also measured virus release in supernatants from explants by qRT-PCR and FFA. Consistent with the strand-specific

qRT-PCR results, we detected higher levels of total ZIKV RNA in supernatants from explants infected with IgG1- and IgG3-ZIKV immune complexes (**Figure 8B**). Compared to the control samples, we observed a 1 log-fold increase in ZIKV RNA in 33.3A06 IgG1 immune complex-infected explants and a 1.5 log-fold increase with IgG3-ZIKV immune complexes. Similarly, we found increasing levels of infectious virus release in placental explants infected with IgG1-ZIKV immune complexes but not in the explants treated with ZIKV alone or in the presence of the non-specific control mAb (**Figure 8C**). Altogether, these data show that cross-reactive DENV mAbs, particularly IgG1 and IgG3 subclasses, enhance ZIKV infection of human placental explants.

Discussion

Our findings demonstrate that cross-reactive DENV mAbs can augment ZIKV infection of HCs isolated from full-term placenta in a dose-dependent manner. Mechanistically, we determined that cross-reactive DENV mAb immune complexes enhanced viral binding to HCs and increased viral entry. However, despite the high levels of infection seen in ADE-ZIKV-infected HCs, we observed minimal up-regulation of costimulatory markers and pro-inflammatory cytokines. Although HCs induce type I and III IFN transcript during ADE-ZIKV infection, IFN protein secretion as well as expression of key antiviral effectors were severely diminished in ADE-ZIKV-infected cells. Notably, ADE-ZIKV infection was significantly reduced upon IFN-β treatment; however, we unexpectedly observed that IFN-λ treatment slightly increased infection in both ADE-ZIKV-infected HCs and ZIKV-infected controls. We also found that enhancement of ZIKV infection in HCs is dependent on the IgG subclass of the cross-reactive antibody with the strongest enhancement observed in the presence of IgG1 and IgG3 immune complexes. Consistent with these results, we observed enhanced ZIKV infection in human mid-gestation placental explants in an IgG subclass-specific manner.

Although HCs have been found to be the primary cell type infected during ZIKV infection (see Chapter 4 and (Bhatnagar et al., 2017; Jurado et al., 2016)), a limitation of our study is the relevance of the observed immune complex-mediated increase of ZIKV infection in isolated human HCs *in vitro*. To address this limitation and more accurately model the effect of DENV cross-reactive mAbs on ZIKV infection, we employed *ex vivo* human second-trimester placental explants. The human placental explant system allowed us to observe the ability of viral immune complexes to enhance ZIKV infection in tissues that retain the architecture of the chorionic villi. Recent work has demonstrated that ZIKV replicates and persists within the placentas of ZIKV-infected women as well as the brains of the developing fetuses (Bhatnagar et al., 2017). In addition, in situ hybridization (ISH) probes for negative-strand replicating RNA were detected within HCs in the placentas of ZIKV-infected women (75%; n=12) with adverse pregnancy outcomes during the first or second trimester. Although it is unclear whether patients had previous flavivirus exposure or seropositivity, the entire cohort had traveled to or resided within DENV-endemic regions. Given that ZIKV infection induces minimal HC death (**Figure 2E**) and that ZIKV persists in HCs throughout pregnancy, continuous spillover of ZIKV into the fetal bloodstream could lead to continuous viral seeding of the fetus. However, the role of previous flavivirus immunity on pregnancy outcomes remains controversial.

More recent work in a cohort of pregnant women with possible ZIKV exposure showed that over half of the women with previous anti-flavivirus immunity who successfully gave birth were positive for ZIKV RNA in placental tissues (Reagan-Steiner et al., 2017). Others have found that the presence of DENV IgG in ZIKV-infected pregnant women did not significantly increase the incidence of abnormal birth outcomes compared to DENV-IgG negative patients (Halai et al., 2017). However, this study examined the role of previous flavivirus immunity on adverse pregnancy outcomes, not viral seeding of the placenta. Neither of these studies categorized the flavivirus-exposed,

ZIKV-infected women based on DENV IgG titers nor prevalence of individual DENV IgG subclasses. Identifying these parameters could increase the observed incidence of viral seeding of the placenta and adverse pregnancy outcomes during ZIKV infection in flavivirus-exposed women. Our observations in human placental explants suggest that cross-reactive antibodies enhance ZIKV infection in an IgG subclass-specific manner, most likely by delivery of mAb:ZIKV immune complexes to the villous core, where the virus can establish persistent infection in HCs. However, the specific cell type(s) targeted by these complexes in human tissue remain unclear. Given that our data point to a specific role for enhanced infection in HCs, it is possible that these complexes bypass the STB layer via Fc-mediated transport and are delivered to HCs and possibly other placental cell types. Altogether, our data support that previous flavivirus immunity could influence viral seeding of the placenta. More extensive studies are needed to determine whether flavivirus-exposed pregnant women show increased rates of viral seeding of the placenta and subsequent congenital disease during ZIKV infection.

DENV infection initiates a robust IgG response with peak levels occurring a few weeks after infection and persisting for a decade or longer (Wahala and Silva, 2011). Further characterization of this IgG response has described skewed production of IgG1 and IgG3 in individuals who develop symptomatic dengue fever (Koraka et al., 2001). It has also been shown that titers of DENV-specific IgG1 are over 100-fold higher compared to DENV-specific IgG4 within the cord blood of infants born to DENV-experienced mothers (Castanha et al., 2016). This correlates with our findings that higher levels of negative-sense ZIKV RNA and infectious virus release were detected in HCs and placental explants treated with cross-reactive IgG1 and IgG3 mAbs complexed to ZIKV compared to IgG4 and IgG2 mAb subclasses (**Figure 8A-B**). Translocation of IgG across the placenta is a normal physiologic process facilitated by the neonatal Fc receptor (FcRn), a specialized Fc receptor expressed on STBs, to provide passive

immunity to the developing fetus (Coyne and Lazear, 2016; Simister and Story, 1997; Simister et al., 1996b; Story et al., 1994). Our results could reflect that FcRn preferentially binds immune complexes comprised of specific IgG subclasses. Studies examining the kinetics of monomeric human IgG binding to human FcRn have determined that IgG1 binds with greater affinity to FcRn compared to IgG3, IgG4 and to a lesser extent than IgG2 (Abdiche et al., 2015; Ober et al., 2001). This corresponds to our observations that the highest levels of viral enhancement were observed in IgG1 and IgG3 immune complexes. Altogether, our results, along with previous studies, suggest that DENV-specific IgG1 and IgG3 are found to a higher degree during DENV infection and that ZIKV immune complexes containing these IgG subclasses could be transcytosed across the placenta and result in viral seeding of the placenta. However, more extensive work must be done to understand the relative binding affinities of FcRn to various IgG subclass immune complexes in the context of viral infection.

In a mouse model of ZIKV infection, type I IFN signaling inhibits ZIKV infection, but also causes fetal resorption of immunocompetent *Ifnar+/-* mice conceived within *Ifnar-/-* dams (Yockey et al., 2018). Type III IFN signaling, on the other hand, is continually secreted by STBs, generating a constitutively potent antiviral state at the trophoblast layer (Bayer et al., 2016). Treatment with IFN-λ decreased viral burden within the murine placenta and dams and provided protection from ZIKV infection in human maternal and fetal tissue (Jagger et al., 2017). In contrast, we observed increased infection of HCs treated with IFN-λ (10IU/mL and 100IU/mL) at higher 33.3A06 mAb concentrations and no effect on infection at lower 33.3A06 concentrations. Higher levels of infection were seen in IFN-λ-treated HCs even during ZIKV infection alone at MOI 1 and 10. In contrast, IFN-β treatment significantly reduced ZIKV infection in both ADE-ZIKV- and non-ADE-infected HCs at all mAb concentrations (**Figure 6A-C**). These results are consistent with recent work done in THP-1 cells, a human monocytic

cell line, in which treatment with conditioned media containing type III IFN increased ZIKV infection (Corry et al., 2017). IFN-β and IFN-λ activate the Janus kinases JAK1 and TYK2, leading to phosphorylation and nuclear translocation of STAT1 and STAT2 followed by transcription of antiviral effector genes that serve to restrict viral replication (Lazear et al., 2015b). However, we found that IFN-λ failed to control ZIKV replication in HCs. This strongly suggests that type I and III IFNs play a cell-specific role in promoting antiviral responses and that there is likely a bifurcation in type I and III IFN signaling. Consistent with this, type I IFNs induce placental damage in human tissue, which was not observed with type III IFNs (Yockey et al., 2018). It is plausible that IFN-λ plays an immunomodulatory role in HCs within the villous stroma while simultaneously promoting an antiviral state in STBs. IFN-λ has been shown to skew macrophage differentiation toward a more pro-inflammatory state and increase their sensitivity to IFN-λ (Egli et al., 2014). However, HCs are fetal in origin and may be evolutionarily programmed to upregulate homeostatic processes and anti-inflammatory effectors in response to IFN-λ to protect the fetus from overwhelming inflammation in the context of viral infection. Because STBs continually secrete IFN-λ, the inability of IFN-λ to control ADE-ZIKV infection of HCs could also reflect desensitization of HCs to IFN-λ (Corry et al., 2017; Coyne and Lazear, 2016; Delorme-Axford et al., 2013). Moreover, although it is clear that STBs secrete type III IFNs from the apical domain, it remains unclear whether there is also secretion from the basolateral surface into the villous stroma, which would impact HCs. Further investigation is needed to fully define the roles of type III IFN signaling in HCs in the context of viral infection.

Mechanistically, we observed that DENV mAb:ZIKV immune complexes increased viral infection by promoting increased viral binding and entry in HCs, a phenomenon known as “extrinsic ADE” (**Figure 3B**). Earlier work from our group showed that ZIKV infection in HCs leads to robust antiviral responses corresponding to increases

in viral load (Chapter 4). In this study, we discovered that with increasing cross-reactive DENV mAb concentration, the ZIKV viral load dramatically increased while, in contrast, expression of RLRs (DDX58, IFIH1, DHX58) as well as key antiviral effectors (IFIT1, IFIT2, IFIT3, OAS1, RSAD2) was dramatically downregulated (**Figure 4**). Although this might reflect viral antagonism of antiviral gene transcription, an alternative hypothesis is that binding of cross-reactive DENV mAb immune complexes to FcγRs on HCs dampens innate immune responses through "intrinsic ADE." FcγRII, which is highly expressed on HCs (**Figure 7A**), is differentiated into two subclasses, FcγRIIa and FcγRIIb, each of which express cytoplasmic Ig gene family tyrosine activation or inhibitory motifs (ITAMs and ITIMS), respectively (Smith and Clatworthy, 2010). Previous studies have demonstrated that binding of DENV Ab-antigen complexes to FcγRIIa, but not FcγRIIb, resulted in ADE, and that, upon modification of the ITAM to an ITIM domain, ADE of DENV infection was eliminated (Boonnak et al., 2013). However, the downstream effects of switching the ITAM and ITIM domains on antiviral immune responses are still unclear. Our findings in HCs, revealed that IgG subclass affects infection levels: (highest to lowest) 33.3A06 IgG3>IgG1>IgG4>>IgG1-LALA> IgG2 (**Figure 7B**). These results are similar to the optimal Ab binding affinities of FcγRIIb, which is known to exert downstream inhibitory signals through its ITIM cytoplasmic domain (Smith and Clatworthy, 2010). Inhibition of FcγRIIb signaling in the presence of activating immune complexes drives robust type I IFN responses and induces DC activation (Dhodapkar et al., 2007). This suggests that intrinsic ADE, in addition to extrinsic ADE, may be an important determinant in antibody-mediated augmentation of ZIKV infection in HCs.

Altogether, our data indicate that cross-reactive DENV mAbs can enhance ZIKV infection in HCs and human mid-gestation placental explants. This suggests that pre-existing anti-flavivirus immunity could play a role in viral seeding of the fetus through

enhanced infection of HCs. The high occurrence of DENV-seroprevalence in ZIKV-endemic regions and the recent discovery that WNV and Powassan virus (POWV) are also capable of infecting human placental explants (Platt et al., 2018) may indicate that antibody-mediated enhancement of flavivirus infection of the placenta occurs more frequently than currently appreciated. In addition, our study has broad implications for the continuing effort to produce effective vaccines against DENV, WNV, and ZIKV. Vaccinations for these flaviviruses could induce antibody responses that may lead to increased viral seeding of the placenta and enhanced ZIKV infection of HCs in pregnant women. Our results presented here, along with previous studies concerning neurotropic flavivirus infection during pregnancy, underpin the importance of furthering our understanding of the effects of antibody-mediated viral transport in the placenta and the developing fetus.

A.

mAb	Specificity	Subtype	ZIKV Binding	ZIKV Neutralization
33.3A06	DENV2	IgG1	+	+++
33.3F05	DENV2	IgG1	+	+
31.3F03	DENV2	IgG1	+	-
33.3E04	DENV2	IgG1	-	-
EM4CO4	Influenza virus	IgG1	Non-binding	Non-neutralizing

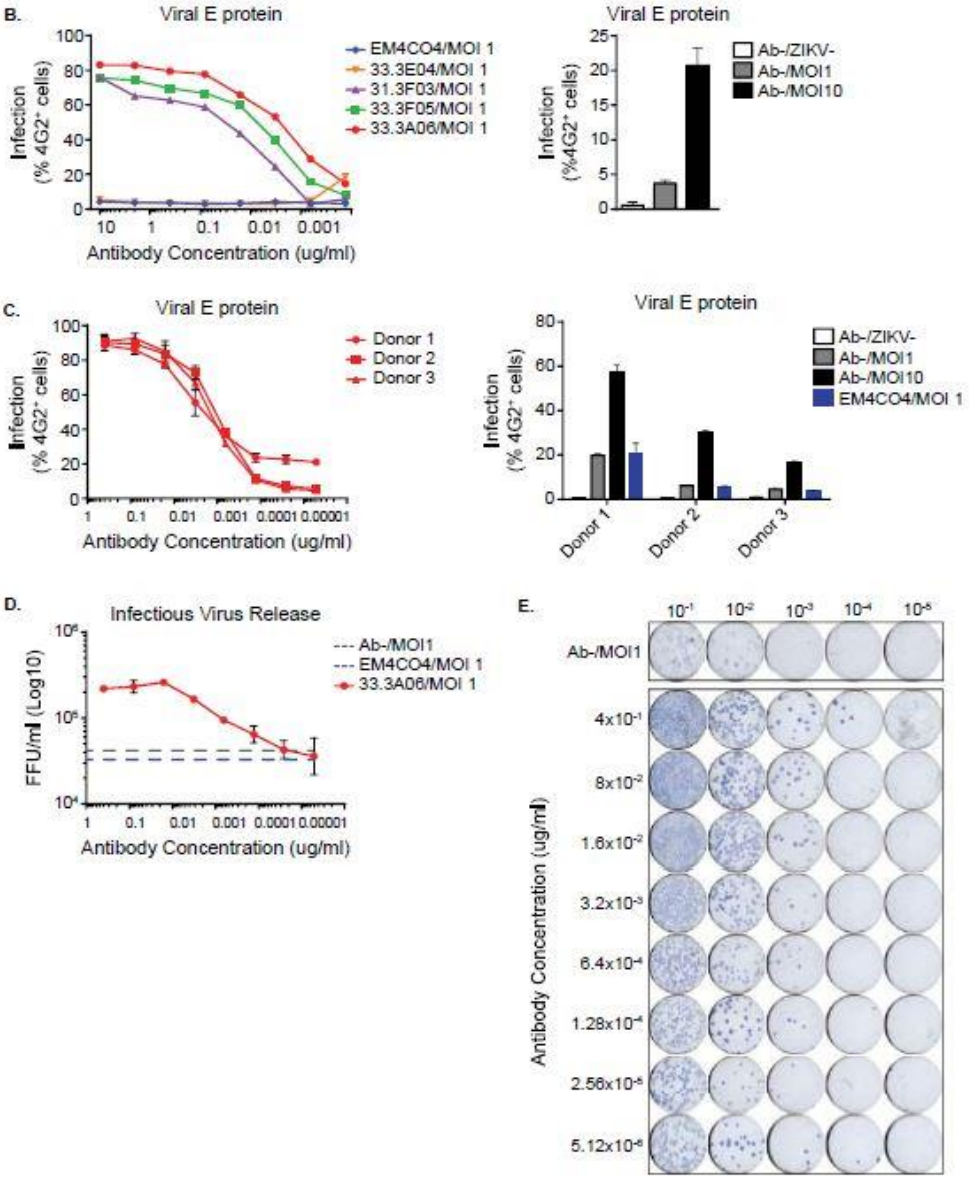

Figure 6-1: Cross-reactive DENV mAbs enhance ZIKV infection of human placental macrophages (HCs).

(A) Binding and neutralization properties of mAbs. **(B)** HCs were infected with ZIKV (MOI 1) in the presence of DENV cross-reactive mAbs or non-specific control (EM4CO4;

10, 2, $4x10^{-1}$, $8x10^{-2}$, $1.6x10^{-2}$, $3.2x10^{-3}$, $6.4x10^{-4}$, $1.28x10^{-4}$ µg/mL). Intracellular ZIKV E protein in ADE-ZIKV-infected (left) and controls (right) was assessed by 4G2 staining and flow cytometry at 24 hours post-infection (hpi). Antibody dilutions were performed in singlicate. Control conditions are shown as the average of biological triplicates ±SD. Ab^-, no mAb. $ZIKV^-$, no ZIKV. **(C)** HCs (n=3 donors) were infected with ZIKV (MOI 1) in the presence of mAb 33.3A06 ($4x10^{-1}$, $8x10^{-2}$, $1.6x10^{-2}$, $3.2x10^{-3}$, $6.4x10^{-4}$, $1.28x10^{-4}$, $2.56x10^{-5}$, $5.12x10^{-6}$ µg/mL) or EM4CO4 ($4x10^{-1}$ ug/mL). Intracellular ZIKV E protein in ADE-ZIKV-infected (left) and controls (right) was assessed at 24hpi as in (B). All conditions are shown as the average of biological triplicates ±SD. **(D)** HCs were infected as in (C). Release of infectious virus into the supernatant was assessed by focus-forming assay (FFA) at 24hpi. Data are shown as the average of biological triplicates ±SD. FFU, focus-forming units. **(E)** Representative FFA illustrating increased foci formation in the presence of 33.3A06 mAb. Supernatant dilutions indicated across the top.

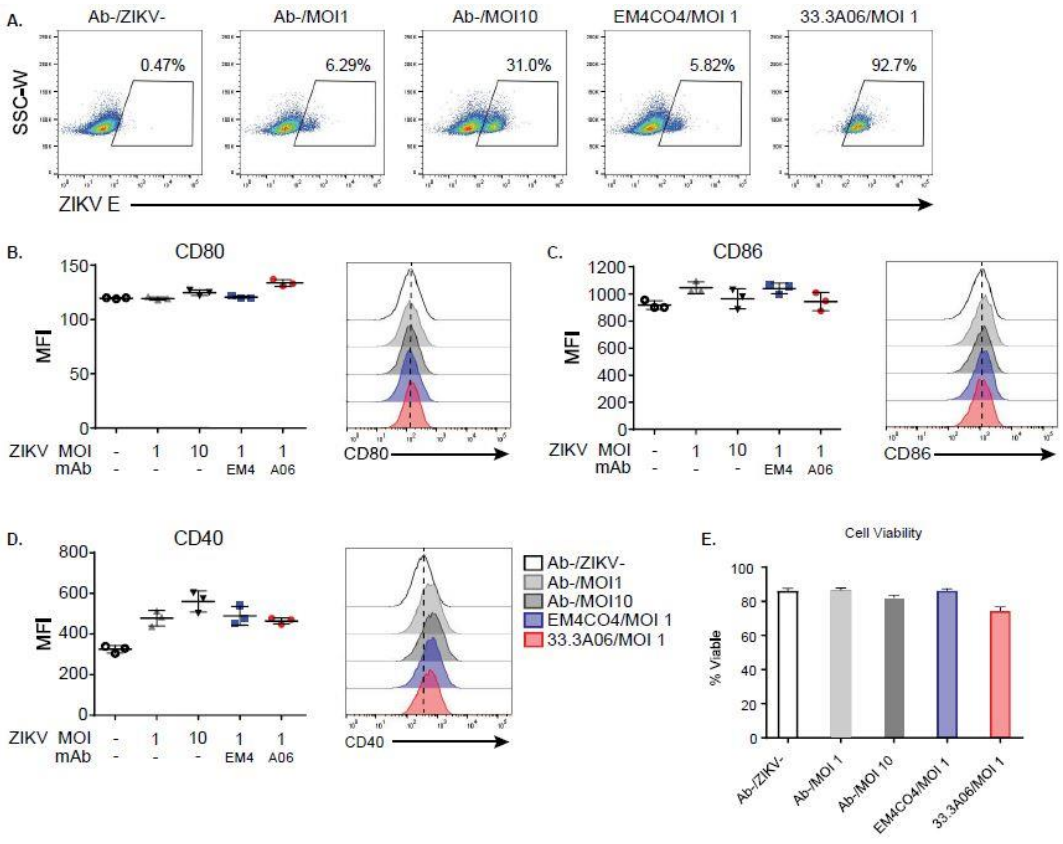

Figure 6-2: HCs are modestly activated upon infection with mAb:ZIKV immune complexes.

(A) Representative flow plots of percent infected HCs ($4G2^{+}$) under control and ADE-ZIKV-infected conditions. 33.3A06 and EM4CO4 were used at 0.4µg/mL. Ab^{-}, no mAb. $ZIKV^{-}$, no ZIKV. **(B)** Mean fluorescence intensity (MFI) of CD80 surface expression and representative histograms (right) of ADE-ZIKV-infected HCs and controls. EM4CO4 and 33.3A06 were used at 0.4µg/mL. All conditions are shown as the average of biological triplicates ±SD. **(C)** MFI of CD86 surface expression and representative histograms (right). Conditions are identical to those in (B). **(D)** MFI of CD40 surface expression and representative histograms (right). Conditions are identical to those in (B). **(E)** Viability of HCs is not affected by ADE-ZIKV infection. Conditions are identical to those in (B). Percent viable cells was determined by Ghost dye staining and flow cytometry. Data are shown as the average of biological triplicates ±SD.

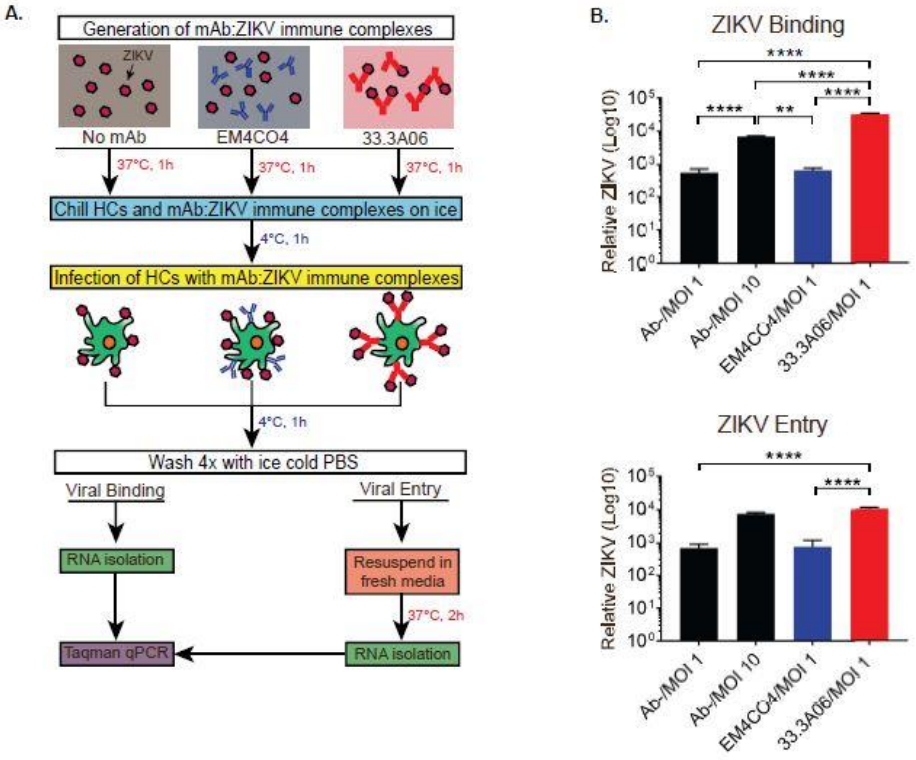

Figure 6-3: Infection with ZIKV in the presence of mAb 33.3A06 results in increased viral binding and entry of HCs.

(A) Binding/entry assay procedure. mAb:ZIKV (MOI 1) immune complexes were chilled on ice and used to infect HCs for 1h on ice. Cells were then washed with ice cold PBS and either immediately lysed for RNA (binding) or incubated in fresh media for 2h at 37°C before lysing for RNA (entry). EM4CO4 and 33.3A06 mAbs were used at 0.4µg/mL. **(B)** ZIKV genomic RNA from bound virus (top) or internalized virus (bottom) was measured by qRT-PCR. Viral RNA expression was normalized to *GAPDH* and is shown as the average Log_{10} fold change over time-matched $Ab^-/ZIKV^-$ control of biological triplicates ±SD. Data were analyzed by 1-way ANOVA and Tukey's multiple comparison test, **p<0.01, ***p<0.001, ****p<0.0001.

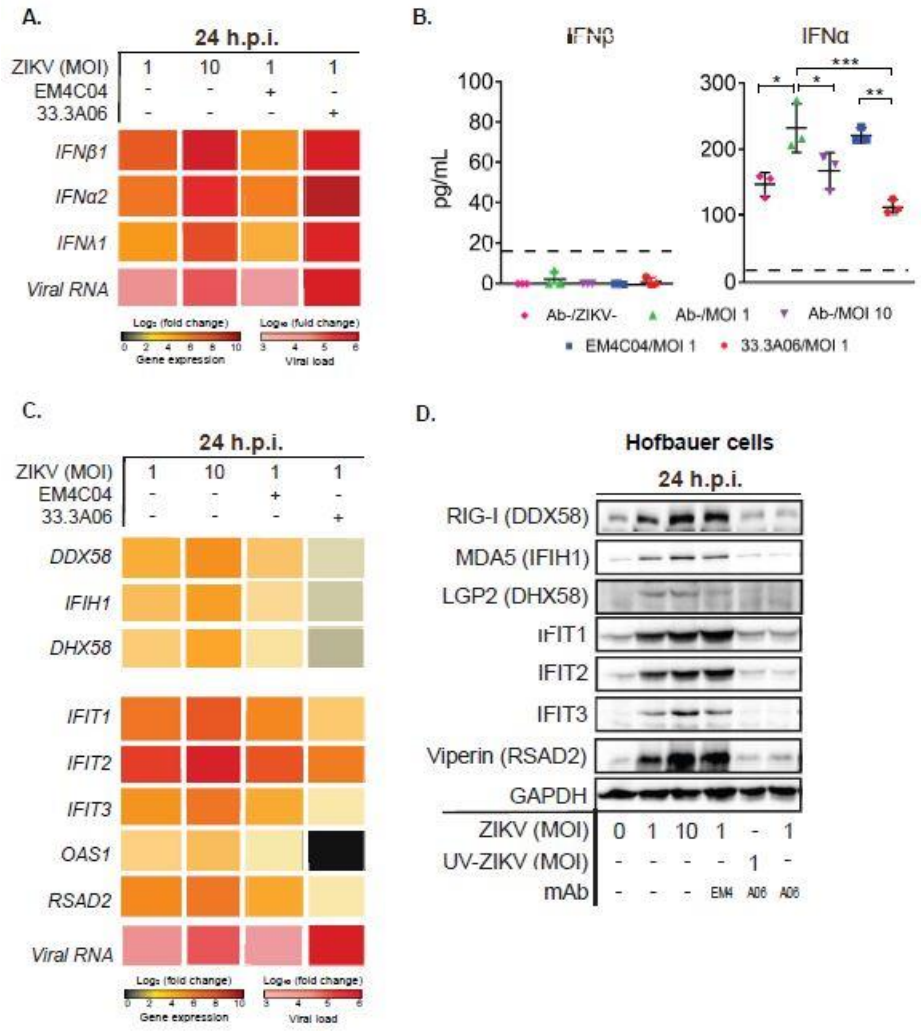

Figure 6-4: HCs infected with mAb:ZIKV immune complexes induce type I IFN and ISG transcription, but not protein translation.

(A) HC gene expression of type I and type III IFNs at 24hpi with ZIKV alone (MOI 1 and 10) or mAb:ZIKV (MOI 1) immune complexes. 33.3A06 and EM4CO4 were used at 0.4µg/mL. Host gene expression was normalized to *GAPDH* and is shown as Log_2 fold change over time-matched $Ab^-/ZIKV^-$ control. ZIKV RNA in these cells was normalized to *GAPDH* and is shown at the bottom as Log_{10} fold change over time-matched $Ab^-/ZIKV^-$ control. **(B)** HC protein secretion of type I IFNs at 24hpi. Cells were infected as in (A). Dashed line indicates lower limit of detection. Data are shown as the average of

biological triplicates ±SD analyzed by 1-way ANOVA and Tukey's multiple comparison test, *p<0.05, **p<0.01, ***p<0.001. Ab^-, no mAb. $ZIKV^-$, no ZIKV. **(C)** HC gene expression of ISGs at 24hpi. Cells were infected and analyzed as in (A). **(D)** Protein expression of ISGs in HCs at 24hpi. Cells were infected as in (A), with the addition of mAb (0.4µg/mL):UV-inactivated ZIKV control (UV-ZIKV; MOI 1) immune complexes.

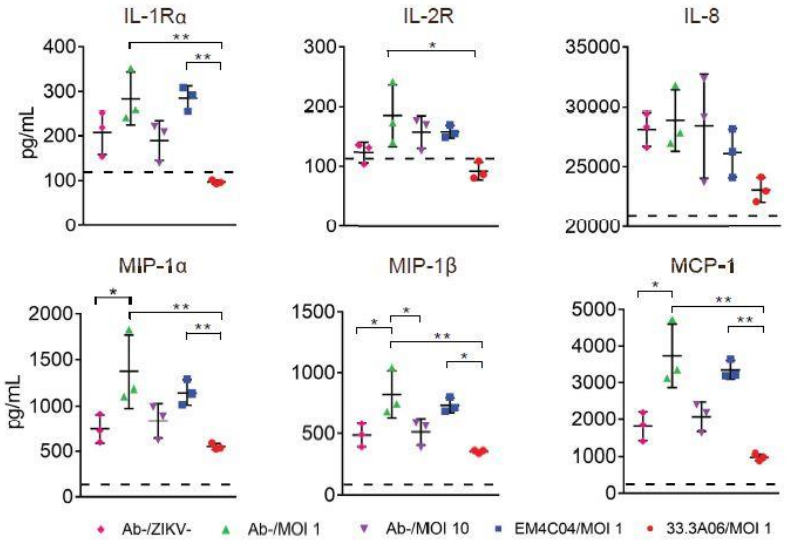

Figure 6-5: HCs infected with mAb:ZIKV immune complexes fail to secrete pro-inflammatory cytokines.

Cytokine concentrations in the supernatant of ADE-ZIKV-infected and control HCs were assessed by multiplex bead assay at 24hpi. 33.3A06 and EM4CO4 were used at 0.4µg/mL with ZIKV at MOI 1. Data are shown as the average of biological triplicates ±SD analyzed by 1-way ANOVA and Tukey's test, *p<0.05, **p<0.01. Dashed line represents lower limit of detection; IL-8: dashed line represents upper limit of detection. Ab^-, no mAb. $ZIKV^-$, no ZIKV.

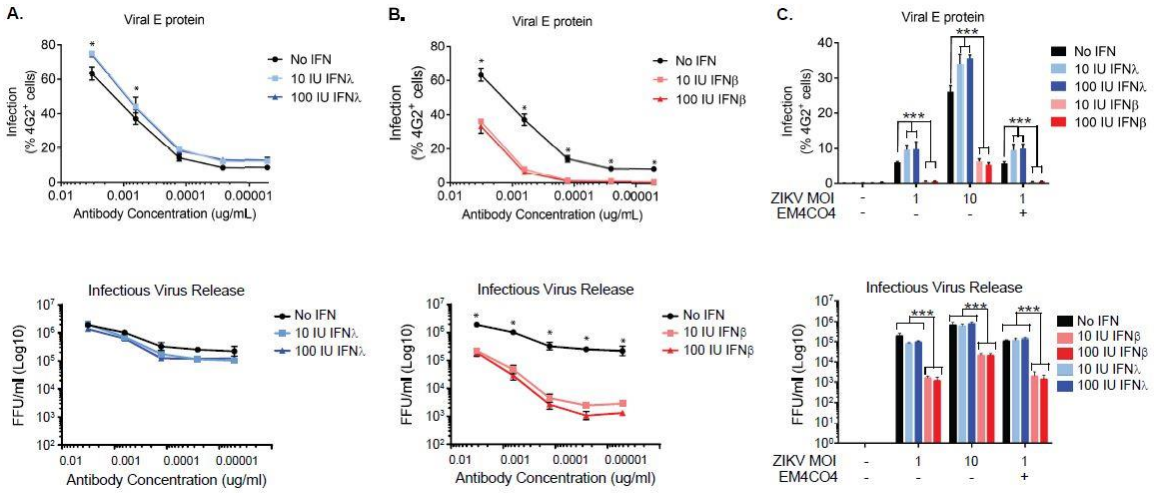

Figure 6-6: ADE-ZIKV infection of HCs is slightly enhanced by IFN-λ treatment.

(A) HCs were infected with ZIKV (MOI 1) in the presence of 33.3A06 mAb ($3.2x10^{-3}$, $6.4x10^{-4}$, $1.28x10^{-4}$, $2.56x10^{-5}$, $5.12x10^{-6}$ µg/mL) and subsequently treated with 10 or 100IU/ml of IFN-λ (blue) or left untreated (black). Upper panel: Intracellular ZIKV E protein was evaluated by 4G2 staining and flow cytometry at 24hpi. Lower panel: Supernatants from infected HCs were collected 24hpi and infectious virus release assessed by FFA. Data are shown as the average of biological triplicates ±SD analyzed by 2-way ANOVA and Tukey's test, *p<0.05. FFU, focus-forming units. **(B)** HCs were infected as in (A) and subsequently treated with 10 or 100IU/ml of IFN-β (red) or left untreated (black). Intracellular ZIKV E protein (upper panel) and infectious virus release (lower panel) were assessed and analyzed as in (A). *p<0.05 **(C)** HCs were infected with ZIKV alone at MOI 1 or 10, or in the presence of EM4CO4 ($3.2x10^{-3}$ µg/mL). Cells were subsequently treated with 10 or 100IU/ml of IFN-λ (blue) or IFN-β (red) or left untreated (black). Intracellular ZIKV E protein (upper panel) and infectious virus release (lower panel) were assessed and analyzed as in (A). *p<0.05, ***p<0.001.

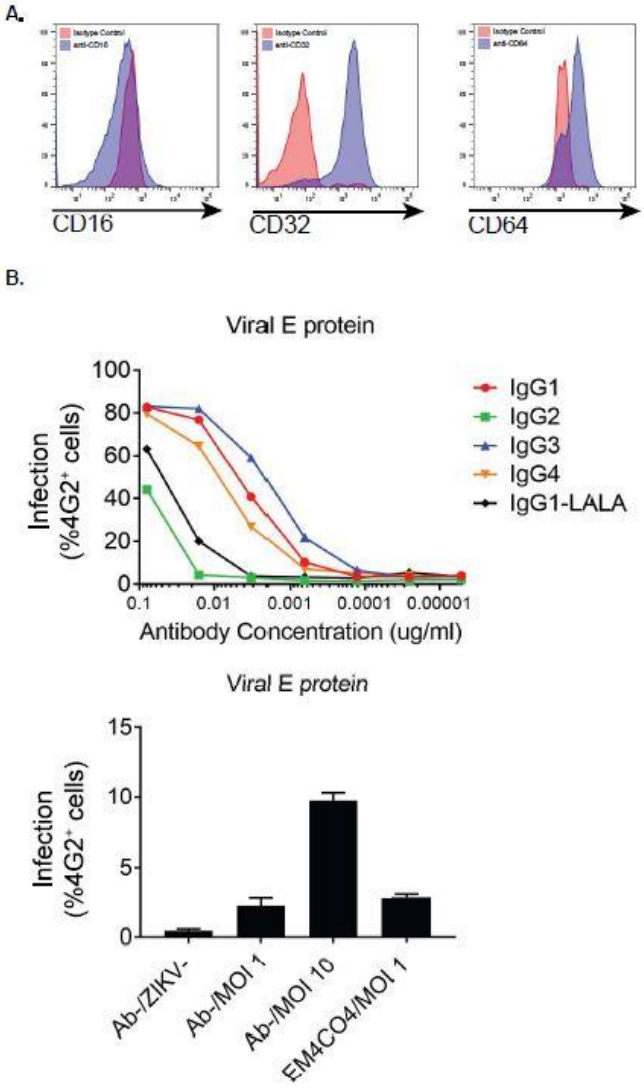

Figure 6-7: IgG subclass affects enhancement of HC infection by ZIKV.

(A) Representative flow cytometry histograms illustrating expression of FcγRIII (CD16), FcγRII (CD32), and FcγRI (CD64) on the surface of uninfected HCs immediately following HC isolation. **(B)** HCs were infected with ZIKV (MOI 1) in the presence of different 33.3A06 IgG subclasses ($8x10^{-2}$, $1.6x10^{-2}$, $3.2x10^{-3}$, $6.4x10^{-4}$, $1.28x10^{-4}$, $2.56x10^{-5}$, $5.12x10^{-6}$ µg/mL). Intracellular ZIKV E protein was assessed by 4G2 staining and flow cytometry at 24hpi. mAb:ZIKV conditions were performed in singlicate (upper panel). Controls are shown as the average of biological triplicates ±SD (lower panel). Ab^-, no mAb. $ZIKV^-$, no ZIKV.

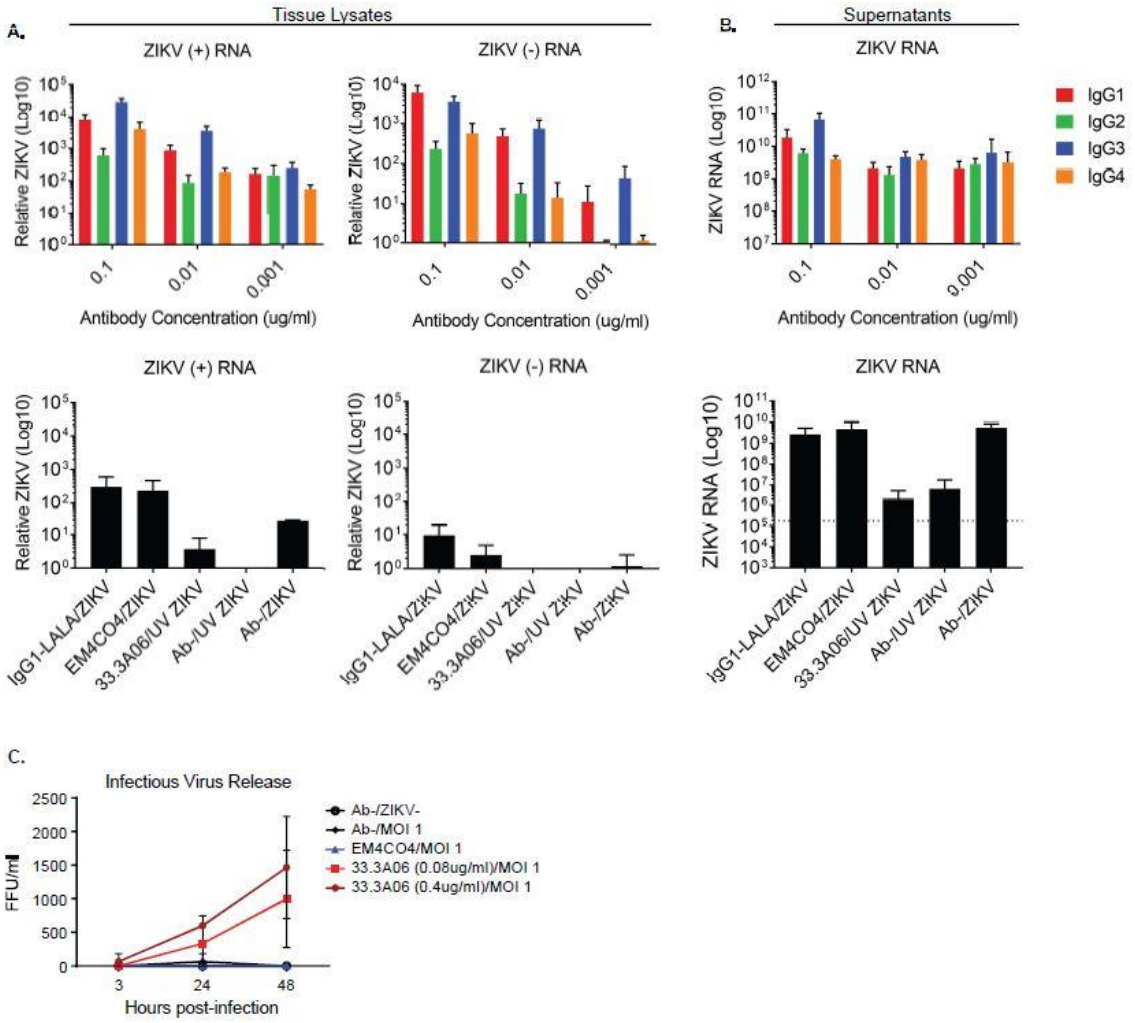

Figure 6-8: The IgG1 and IgG3 subclasses preferentially enhance ZIKV infection of human placental explants.

(A) Human placental explants were infected with ZIKV ($5x10^5$pfu/ml) in the presence of 33.3A06 mAb IgG subclasses (0.1, 0.01, 0.001µg/mL). Viral replication within tissues was assessed by strand-specific qRT-PCR at 24hpi. ZIKV RNA expression was normalized to *GAPDH* and is shown as the average Log_{10} fold change over time-matched $Ab^-/ZIKV^-$ controls of biological triplicates ±SD (n. Controls are shown below with ZIKV alone and UV-ZIKV at $5x10^5$pfu/ml and mAbs at 0.1ug/mL. UV, UV-inactivated ZIKV. **(B)** Supernatants from human placental explants infected as in (A) were collected

at 24hpi and ZIKV genomic RNA measured by qRT-PCR. RNA expression was normalized to ZIKV RNA standards and is shown as the average Log_{10} fold change over time-matched $Ab^-/ZIKV^-$ controls of biological triplicates ±SD. Controls are shown below. **(C)** Human placental explants were infected with ZIKV alone ($5x10^5$pfu/ml) or in the presence of 33.3A06 mAb (0.4 and 0.08µg/mL) or EM4CO4 (0.4µg/mL). Supernatants were collected at 3, 24, and 48hpi and infectious virus release assessed by FFA. FFU, focus-forming units. Ab^-, no mAb. $ZIKV^-$, no ZIKV.

	Reaction	Name	Assay Target	Genome Position	Sequence (5' → 3')
ZIKV	qPCR primer 1	ZIKV_907	prM-E	907-929	TTGGTCATGATACTGCTGATTGC
	qPCR primer 2	ZIKV_983c	prM-E	983-962	CCTTCCACAAAGTCCCTATTGC
	Probe	ZIKV_932 FAM-NFQ	prM-E	932-958	CGGCATACAGCATCAGGTGCATAGGAG
ZIKV (+) strand	cDNA primer	T7_ZIKV_983c	prM-E (+)	983-962	GCGTAATACGACTCACTATACCTTCCACAAAGTCCCTATTGC
	qPCR primer 1	ZIKV_907	prM-E (+)	907-929	TTGGTCATGATACTGCTGATTGC
	qPCR primer 2	T7tag	prM-E (+)		GCGTAATACGACTCACTATA
	Probe	ZIKV_932 FAM-NFQ	prM-E (+)	932-958	CGGCATACAGCATCAGGTGCATAGGAG
ZIKV (–) strand	cDNA primer	GVA_ZIKV_907	prM-E (–)	907-929	TTTGCTAGCTTTAGGACCTACTATATCTACCTTTGGTCATGATACTGCTGATTGC
	qPCR primer 1	ZIKV_983c	prM-E (–)	983-962	CCTTCCACAAAGTCCCTATTGC
	qPCR primer 2	GVAtag	prM-E (–)		TTTGCTAGCTTTAGGACCTACTATATCTACCT
	Probe	ZIKV_932 FAM-NFQ	prM-E (–)	932-958	CGGCATACAGCATCAGGTGCATAGGAG

Table 6-1: ZIKV-specific primer/probe sequences used for qRT-PCR.

ZIKV-specific primer and probe sequences adapted from Lanciotti et al. (2008) and used for ZIKV RNA qRT-PCR and ZIKV strand-specific qRT-PCR. Genome position is in reference to Zika virus strain ZIKV/Homo Sapiens/PRI/PRVABC59/2015 (GenBank accession number: KX601168.1). Unique 5' tag sequences are underlined.

Chapter 7: Discussion

Written by Kendra M. Quicke

Summary of LGP2 study findings

In this work, we have confirmed that LGP2 is a negative regulator of RIG-I signaling, using the RIG-I-specific HCV PAMP RNA and the RIG-I-targeted virus SeV in murine BM-DCs from pure C57BL/6J background mice and the HEK293 model human cell line. Contrary to previous findings by other groups, we demonstrated that LGP2 inhibits RIG-I signaling in RNA binding- and ATP hydrolysis-independent manner, and that the CTD of LGP2 is similarly dispensable. Instead, we showed that LGP2 prevents the activating K63-polyubiquitination of the RIG-I N-terminal CARDs by inhibiting the E3 ligase activity of TRIM25. It is possible that LGP2 plays a broader role in preventing ubiquitination of multiple targets throughout the cell. In addition to TRIM25, our mass spectroscopy results identified interactions between LGP2 and several other ubiquitin machinery components, including the E3 ubiquitin ligases STUB1 and RNF8 (unpublished data). We also observe a cell-wide decrease in ubiquitin expression in certain experiments (**Figure 8E**, WCL). Furthermore, Parisien and colleagues have shown that LGP2 inhibits the ubiquitin ligase activity of the TRAF family proteins (Parisien et al., 2018). RNA binding, ATP hydrolysis and the CTD of LGP2 are dispensable for this inhibitory function of LGP2, in concordance with our findings shown here. These observations suggest that LGP2 may have the ability to inhibit the activities of a broader range of E3 ubiquitin ligases.

Potential factors influencing disparate results

Our understanding of LGP2 function has in part been confounded by the differing phenotypes observed in LGP2$^{-/-}$ mice, and cells derived from these mice (Satoh et al., 2010; Suthar et al., 2012b; Venkataraman et al., 2007). This may be due to several factors, including the genetic background of the mice, the global knockout of LGP2 in

these mice, the specificity of agonists used, and, during virus infection, the presence of viral factors that antagonize innate immune signaling pathways.

LGP2$^{-/-}$ mice have been generated on three separate occasions. The first strain was made on a mixed background of C57BL/6J and 129SvEv (Venkataraman et al., 2007). These mice were born at the normal Mendelian ratio and exhibited normal development, but their genetic make-up was 50% C57BL/6J and 50% 129SvEv. Experiments with these mice suggested a negative regulatory role for LGP2 during NDV-induced RIG-I signaling, and a positive regulatory role for LGP2 during EMCV-induced MDA5 signaling. The second LGP2$^{-/-}$ mouse strain was made on a mixed background of C57BL/6 and GSI-1 (Satoh et al., 2010). These mice were not born at the normal Mendelian ratio, and female LGP2$^{-/-}$ mice exhibited enlarged uteruses and vaginal atresia. In these experiments, LGP2 appeared to be required to positively regulate both RIG-I- and MDA5-mediated antiviral responses. The third mouse strain was on a pure C57BL/6J background (Suthar et al., 2012b). These mice were born at the normal Mendelian ratio and did not exhibit any health defects. Experiments suggested that LGP2 was necessary for survival and IFN-β production during infection with WNV, but that LGP2 had no effect on downstream ISG expression or peripheral innate immune responses. However, it should be noted that WNV is targeted by both RIG-I and MDA5, making it difficult to assess the effect of LGP2 on RIG-I-specific signaling.

The role of genetics on individual immune responses is becoming a more appreciated phenomenon. Studies in humans and in mice have found that individual genetics and passenger mutations can influence protein function and immune responses to infection (Bowen et al., 2016; Querec et al., 2009; Thio, 2008; Vanden Berghe et al., 2015). Genetic variations between human subjects have been shown to impact the immune responses to the yellow fever virus vaccine (YF-17D) and may in fact be used to predict the efficacy of the vaccine (Querec et al., 2009). Similarly, several groups have

observed that slight differences in individual genes can influence the response to HCV infection, and may determine whether the virus is cleared or becomes a chronic infection leading to liver disease (reviewed in (Thio, 2008)). Other human studies have revealed single nucleotide polymorphisms (SNPs) within innate immune genes that can influence susceptibility to viral infection or autoimmunity (reviewed in (Bowen et al., 2016)). For instance, a frameshift mutation within NOD2 corresponded to an increase in the negative regulatory activity of NOD2 and subsequent dampening of RIG-I antiviral signaling (Morosky et al., 2011). Additionally, one study analyzed the genomes of congenic mice generated using embryonic stem cells (ESCs) from the 129 strain and recipient adults from the C57BL/6J strain (Vanden Berghe et al., 2015). The majority of these congenic mouse strains harbored mutations in the target gene that were carried over from the 129 ESCs ('passenger mutations'). Many of these mutations resulted in unintentional phenotypic differences. This illustrates that mice generated on a mixed genetic background to study gene function may exhibit phenotypes that do not accurately represent the role of the protein of interest. Generating mouse strains on a pure genetic background – using ESCs and recipients from the same mouse strain – should reduce the incidence of passenger mutations and mitigate the appearance of misleading results.

The global nature of the LGP2 gene knockout in these three mouse strains is another factor that may confound results of *in vivo* experiments. It is probable that LGP2 functions in a cell type-specific manner, and/or performs multiple functions within the same cell type depending on the cellular conditions. Thus, while gene function may be confidently studied in highly controlled *in vitro* experiments using primary cells isolated from these mice, ascertaining a cell-specific phenotype in a mouse where LGP2 is absent in every tissue can be challenging. This challenge is highlighted by the expanding number of processes LGP2 has been implicated in (Komuro et al., 2016; Suthar et al., 2012b; van der Veen et al., 2018; Widau et al., 2014). A more reliable

model would be a Cre/lox system in which LGP2 can be knocked out in specific cell types within a mouse. The use of such conditionally gene-targeted mice would enhance our understanding of LGP2 function in the RLR pathway within key innate immune cells, including DCs, monocytes, and macrophages, and could be used to examine the role of LGP2 in other tissues as well. Specifically, our group aims to utilize CD11c-floxed mice in future experiments to better define the role of LGP2 in DCs *in vivo* during virus infection.

In addition to selecting an appropriate model system, it is important to carefully consider the choice of agonist used. This is of particular necessity in studies regarding the mechanism of LGP2 regulation of the RLR pathway, since LGP2 appears to differentially regulate RIG-I- (negatively) and MDA5-mediated (positively) antiviral responses. For instance, it has been demonstrated that both RIG-I and MDA5 recognize and respond to transfected poly(I:C), a dsRNA agonist (Yoneyama et al., 2005; Yoneyama et al., 2004). Since the finding that RIG-I and MDA5 preferentially bind dsRNA ligands of different lengths (Kato et al., 2008), low molecular weight (LMW; <1kb) and high molecular weight (HMW; >1.5kb) versions of poly(I:C) have been created. However, this distinction is not always taken into account and the specificity of these agonists is incomplete, making it difficult to draw conclusions on the effects of LGP2 on RIG-I- or MDA5-specific signaling. Similarly, many viruses are targeted by RIG-I and MDA5, with signaling by both RLRs being required for adequate innate immune responses to infection (Fredericksen et al., 2008; Kato et al., 2008; Loo et al., 2008). Use of such viruses to stimulate RLR signaling can again confound conclusions related to the LGP2-mediated regulation of RIG-I- or MDA5-specific signaling. Thus it is important to utilize highly specific RIG-I and MDA5 agonists, such as the HCV PAMP RNA employed in our experiments (Saito et al., 2008), or viruses that are reliably

targeted by either RIG-I (e.g. SeV; (Yoneyama et al., 2005)) or MDA5 (e.g. EMCV; (Kato et al., 2006) alone.

Of course, using virus infection to study the mechanisms of innate immune signaling, while more biologically relevant, carries its own set of experimental complications. Viruses inherently introduce factors responsible for antagonizing antiviral signaling, and several have been shown to target proteins in the RLR pathway (reviewed in (Chan and Gack, 2016)). Disruption of RLR signaling by a viral factor could adversely affect phenotypes related to the regulation of the pathway, particularly the effects of host-derived negative regulatory proteins. In the context of RIG-I signaling, we and others have demonstrated that LGP2 is one such negative regulator (Rothenfusser et al., 2005; Saito et al., 2007; Venkataraman et al., 2007; Yoneyama et al., 2005). If a viral factor strongly inhibits RIG-I signaling upstream or downstream of LGP2 activity, the loss of LGP2 would likely result in no change, or a very modest phenotype compared to WT cells, making it appear as though LGP2 plays a dispensable role in the RIG-I antiviral pathway. Alternatively, if a viral factor inhibits RIG-I signaling at the same step where LGP2 exerts its activity, knocking out LGP2 may reduce competition for binding to the host protein, enhancing the inhibitory effect of the viral factor and resulting in lower antiviral signaling readouts that in WT cells. Such a phenotype would make it appear as though LGP2 is required to upregulate antiviral responses. To mitigate these issues, it may be necessary to include analyses using synthetic or virus-derived agonists that can be introduced without other viral components. Additionally, modified viruses or virus strains defective in innate immune signaling antagonism, such as influenza virus ΔNS1 (Kato et al., 2006) or non-pathogenic WNV-MAD (Madagascar strain; (Suthar et al., 2012a)), could be employed to assess pathway regulation during virus infection.

The conundrum of LGP2 function during WNV infection

Our group specifically studies immune responses to WNV and ZIKV infection. While the role of LGP2 during ZIKV infection has yet to be explored, we have previously shown that LGP2 is involved in regulating responses to WNV infection. Suthar and colleagues found that upon infection with pathogenic WNV, LGP2$^{-/-}$ mice exhibited higher mortality than WT mice (87.5% and 13%, respectively) (Suthar et al., 2012b). However, there were no detectible differences in viral load between LGP2$^{-/-}$ and WT mice in either the popliteal draining lymph node (pDLN) or the spleen through 8 days post-infection (dpi). Additionally, no difference was found in either IFN-β or ISG transcript or protein levels in the pDLN or spleen over a similar time course, which seems to suggest that while LGP2 is necessary for overall survival, it is not playing an overt role in the peripheral innate immune response to WNV infection *in vivo*. Initial innate immune responses are largely driven by DCs and macrophages, which are also known cell targets for WNV infection *in vivo* (reviewed in (Samuel and Diamond, 2006)). Bone marrow-derived DCs and macrophages from LGP2$^{-/-}$ mice showed increased WNV replication at 24 hours post-infection (hpi) compared to WT cells (Suthar et al., 2012b). Additionally, LGP2$^{-/-}$ DCs and macrophages exhibited decreased IFN-β production, but no differences were observed in downstream ISG protein expression, including RIG-I, MDA5, IFIT2 and IFIT3. This appears to indicate a potential positive regulatory role for LGP2 during initial innate immune responses, but also that LGP2 is largely nonessential in the context of WNV infection.

As noted previously, WNV RNA replication products are recognized and bound by both RIG-I and MDA5 (Fredericksen et al., 2008). This alone presents a complicating factor in the study of LGP2 function during WNV infection, as LGP2 negatively regulates RIG-I signaling (see Chapter 2) but is necessary for enhancement of MDA5 signaling (Bruns et al., 2014; Bruns et al., 2013; Childs et al., 2013). It may be that the decrease in

IFN-β production by LGP2$^{-/-}$ DCs is the result of a drop in MDA5 signaling in the absence of LGP2 positive regulation, and that this phenotype is eclipsing any effect that may be wrought on the RIG-I signaling pathway. We could evaluate this hypothesis by generating LGP2$^{-/-}$xMDA5$^{-/-}$ double knockout (DKO) mice. Barring effects due to viral antagonism, we would expect that the phenotypes observed in BM-DCs from these mice would illustrate the regulatory effect of LGP2 on RIG-I-specific responses during WNV infection, as the responsibility for antiviral signaling would fall on RIG-I alone. Additionally, we could use the HEK293 human cell model system to generate shRNA-mediated knockdown, or CRISPR/Cas9-mediated knockout, cell lines lacking combinations of LGP2, RIG-I and MDA5. This would allow us to assess the relationship of LGP2 with RIG-I and MDA5 during WNV infection via IFN-β promoter luciferase assays and exogenous expression rescue studies.

An alternative hypothesis to the apparently contradictory results described by Suthar and colleagues, is that WNV produces a viral factor that antagonizes the RIG-I pathway at the same point where LGP2 exerts its negative regulatory function. Based on our findings, this would occur by WNV targeting the activity of TRIM25. If the WNV factor competes with LGP2 for interaction with TRIM25, and inhibits TRIM25 activity more efficiently than LGP2, it would follow that in the absence of LGP2, more of the viral factor would have access to TRIM25, resulting in even greater reduction of RIG-I signaling than in WT cells. Indeed, several viruses have been shown to antagonize TRIM25 activity to inhibit RLR signaling. DENV, a flavivirus like WNV, produces a subgenomic flavivirus RNA (sfRNA) that has been implicated in preventing TRIM25 activation and subsequent RIG-I signaling (Manokaran et al., 2015). In this case, DENV sfRNA was found to interact with endogenous TRIM25 and prevent the de-ubiquitination of TRIM25 that is required for activation. Through this mechanism, the sfRNA alone was able to reduce IFN-β expression in Huh7 cells transfected with poly(I:C). Furthermore, siRNA

knockdown of TRIM25 did not enhance DENV replication in Huh7 cells. WNV likewise produces an sfRNA that has been implicated in viral evasion of antiviral responses (Pijlman et al., 2008; Schuessler et al., 2012), though the precise mechanism is not well understood. It is possible that WNV sfRNA has a similar inhibitory mechanism to that of DENV sfRNA.

Similarly, the E6 proteins of multiple human papillomaviruses (HPV) were found to bind to the TRIM25 B-box domains, inhibiting TRIM25 de-ubiquitination and resulting in greater TRIM25 degradation (Chiang et al., 2018). This inhibition of TRIM25 activation subsequently prevented the TRIM25-mediated ubiquitination of N-RIG (RIG-I CARDs), N-RIG interaction with MAVS, and downstream RIG-I signaling. Mechanistically, HPV E6 appears to compete with TRIM25 for de-ubiquitination by USP15. Co-expression of HPV E6 and USP15 resulted in E6 de-ubiquitination which stabilized expression of the viral protein. Influenza virus NS1 was found to interact directly with the coiled-coil domain (CCD) of TRIM25 and prevent TRIM25 multimerization (Gack et al., 2009). Multimerization of TRIM25 was required for the polyubiquitination of RIG-I. Thus, NS1 inhibited the TRIM25-mediated ubiquitination of RIG-I that is required for RIG-I activation and interaction with MAVS. This phenotype was consistent in HEK293T cells expression NS1 alone or infected with influenza virus. However, cells infected with an influenza virus lacking NS1 (ΔNS1) exhibited no defect in RIG-I ubiquitination or downstream signaling. Additionally, paramyxovirus V proteins from Nipah virus (NiV), measles virus (MeV), SeV, and parainfluenza virus type 5 (PIV5) were all found to interact with TRIM25 and RIG-I (Sanchez-Aparicio et al., 2018). NiV V protein was further determined to interact with the SPRY domain of TRIM25 and the N-terminal CARDs of RIG-I, the domains required for the interaction between TRIM25 and RIG-I. However, this interaction was not disrupted by V protein binding. Instead, NiV, MeV and PIV5 V proteins inhibited ubiquitination N-RIG (RIG-I CARDs) and prevented N-RIG interaction

with MAVS. TRIM25-enhanced RIG-I signaling was also reduced by NiV and MeV V proteins.

We could test for WNV interference at the TRIM25 activation step and whether viral factors compete with LGP2 for TRIM25 regulation. Initially, we could exogenously co-express individual viral proteins with TRIM25 in a model cell line, such as HEK293 cells, to determine whether any WNV proteins interact with TRIM25. We could also infect cells with WNV and immunoprecipitate the endogenous host proteins TRIM25 and LGP2 and probe a Western blot for viral proteins to confirm whether interactions occur in the context of infection. If we discover such an interaction, we can then determine the downstream effects on TRIM25 and RIG-I activation, and whether the viral protein disrupts the interaction between TRIM25 and LGP2. We could then generate a mutant WNV lacking the viral protein and use this to infect WT and LGP2$^{-/-}$ BM-DCs to see whether this results in increased innate immune responses in LGP2$^{-/-}$ cells. Alternatively, if no viral protein is identified, we can test the role of WNV sfRNA by infecting WT and LGP2$^{-/-}$ BM-DCs with a WNV defective in producing sfRNA (Schuessler et al., 2012). If this results in increased innate immune responses in LGP2$^{-/-}$ cells compared to WT cells, then we can subsequently use HEK293 cells to test for an interaction between WNV sfRNA and TRIM25 or USP15, and whether sfRNA adversely affects TRIM25 and RIG-I activation.

LGP2 conclusion: RLR agonists as vaccine adjuvants

It is becoming increasingly important to understand how innate and adaptive immune responses are regulated. RLR agonists are now being developed and considered as potential broad-spectrum antiviral therapeutics (Martinez-Gil et al., 2013; Olagnier et al., 2014) and as adjuvants to enhance immunogenicity during vaccination (Chakravarthy et al., 2010; Saito et al., 2008). Therefore, it is crucial to understand how the RLR signaling

pathway is regulated in order to successfully augment immunogenicity and prevent cytokine-mediated tissue damage (Clyde et al., 2006; Oldstone and Rosen, 2014; Sun et al., 2012). As a key regulator of RLR signaling, LGP2 is central to understanding the regulation of innate and adaptive immune responses. A more complete understanding of LGP2 function would aid in developing novel antiviral therapies and vaccines, or additional treatments to improve the efficacy of existing anti-cancer therapies.

Summary of ZIKV study findings

In Chapters 3-6, we expand on the fields of ZIKV tropism and immunogenicity. We show that African and Asian lineage strains of ZIKV target primary human moDCs for infection. ZIKV infection induced expression of RLRs and antiviral effectors, but elicited minimal DC activation and pro-inflammatory cytokine secretion. Viral antagonism was observed at multiple levels, as ZIKV (PRVABC59) blocked translation of IFN-β and inhibited phosphorylation of STAT1 and STAT2. ZIKV PRVABC59 was also able to productively infect primary human HCs, the fetal-derived placental macrophages, and CTBs. Infection elicited modest HC activation, but did result in production of pro-inflammatory cytokines and induction of RLR and antiviral effector genes. Serum and monoclonal antibodies isolated from DENV-infected patients were able to cross-react with and neutralize ZIKV (PRVABC59) to varying degrees. Several of these monoclonal antibodies were able to enhance ZIKV infection of U937 cells (monocytic cell line). We were also able to show enhanced ZIKV infection of primary HCs and second semester human placental explants in the presence of DENV cross-reactive antibodies. Enhancement was IgG subtype-dependent and seemed to involve both increased binding and entry of virus to cells and downregulation of RLR and antiviral effector expression.

Further advances in ZIKV tropism and immunology

While much remains to be discovered in the realms of cellular tropism, innate immune responses, and the consequences of pre-existing flavivirus immunity, the body of work on ZIKV has expanded rapidly since early 2016. Several other groups have corroborated our findings on the ability of ZIKV to productively infect human DCs (Sun et al., 2017; Vielle et al., 2018) and placental macrophages (Bhatnagar et al., 2017; El Costa et al., 2016; Jurado et al., 2016; Noronha et al., 2016) and CTBs (Aagaard et al., 2017; El Costa et al., 2016; Sheridan et al., 2017; Tabata et al., 2016). Sun and colleagues detected ZIKV RNA in myeloid DCs isolated from two ZIKV-infected patients (Sun et al., 2017). Viral RNA was not detected in plasmacytoid DCs (pDCs), natural killer (NK) cells, T cells or B cells isolated from the same patients. Another study demonstrated *in vitro* infection of $CD14^+$ blood monocytes by both African and Asian lineage ZIKV strains (Foo et al., 2017). Among placental cell types, isolated human primary HCs are now confirmed to support ZIKV replication (El Costa et al., 2016; Jurado et al., 2016). Infection has also been observed in HCs and CTBs within human placental explants, which retain much of the fetal chorionic villi architecture (Jurado et al., 2016; Tabata et al., 2016; Weisblum et al., 2017), and in maternal decidual explant tissues (El Costa et al., 2016; Weisblum et al., 2017). El Costa and colleagues also found that ZIKV infects and replicates in maternal decidual macrophages, suggesting these cells may play a role in ZIKV transmission at the placenta (El Costa et al., 2016). Furthermore, HCs within the chorionic villi of placental tissues from ZIKV-infected women were found to contain evidence of replicating ZIKV (Bhatnagar et al., 2017; Noronha et al., 2016). Some studies have failed to find ZIKV infection of CTBs (Jurado et al., 2016), however, this may be due to the lower level of infection in these cells compared to HCs, as observed by us and others (Tabata et al., 2016), or differentiation in culture into more resistant STB-like cells. Sheridan and colleagues described an embryonic stem cell (ESC)-

derived trophoblast model that can be differentiated into CTBs and STBs, and appears to be representative of the early placental barrier formed within the first seven days of pregnancy (Sheridan et al., 2017). Surprisingly, ESC-derived STBs were susceptible to ZIKV infection in addition to CTBs. STBs are generally considered resistant to infection due to the constitutive release of IFN-λ (Bayer et al., 2016; Corry et al., 2017; Delorme-Axford et al., 2013; Tabata et al., 2016; Weisblum et al., 2017). However, another group has also described ZIKV infection of multinucleated CTBs (El Costa et al., 2016). Together these findings suggest that STBs may not be as impervious to viral infection as is currently thought.

Studies on innate immune responses in ZIKV-susceptible cells continue to report variable results based on cell type. Similar to our findings, Vielle and colleagues report induction of type I IFN and ISG transcription in response to ZIKV infection of DCs (Vielle et al., 2018). THP-1 monocytes were also found to increase expression of type I IFN and cytokine genes (Luo et al., 2018). In contrast, mDCs isolated from ZIKV-infected patients exhibited down-regulation of PRR, transcription factor, type I, II, and III IFN, and ISG transcripts, though differences between infected and uninfected *in vitro*-derived mDCs were more modest (Sun et al., 2017). However, information regarding the innate immune responses within DC subtypes is still very sparse. $CD14^+$ monocytes infected *in vitro* with an Asian lineage ZIKV exhibited a shift toward an immunosuppressive phenotype with inhibition of type I IFN signaling (Foo et al., 2017). This shift was even more pronounced in cells isolated from pregnant women. Somewhat expectedly, due to the immune tolerant nature of the placenta, we and others have found that innate immune responses in primary placental cells are generally unenthusiastic (Rosenberg et al., 2017; Schwartz, 2017; Weisblum et al., 2017), with the exception of IFN-λ secretion by STBs (Bayer et al., 2016; Corry et al., 2017; Tabata et al., 2016; Weisblum et al., 2017).

Progress has been made on identifying specific antiviral factors involved in controlling ZIKV infection. IFITM3 and viperin were quickly recognized as important antiviral effectors in the response to ZIKV (Savidis et al., 2016; Van der Hoek et al., 2017). The role of viperin was confirmed in HEK293T cells, where it was found to interact with individually expressed ZIKV NS3 and mediate proteasomal degradation of the viral protein (Panayiotou et al., 2018). Wang and colleagues described the induction of the NLRP3 inflammasome upon ZIKV infection (Wang et al., 2018). The activation of IL-1β can be promoted by the NLRP3 inflammasome and helps promote antiviral inflammatory responses. IL-1β protein levels were increased in the sera of ZIKV-infected human patients and A129 mice, as well as within human PBMCs, THP-1 macrophages, and mouse BM-DCs. The knockdown of NLRP3 in THP-1 cells and the knockout of NLRP3 in C57BL/6 mice attenuated IL-1β secretion and maturation, suggesting a role for NLRP3 in the response to ZIKV. Furthermore, several members of the RLR signaling pathway were shown to inhibit ZIKV replication (Hertzog et al., 2018; Piret et al., 2018). ZIKV-infected MAVS$^{-/-}$ mice exhibited higher viremia and lower type I IFN and cytokine protein levels in the spleen than WT or TRIF$^{-/-}$ mice (Piret et al., 2018). MAVS is the central adaptor protein for the RLR signaling pathway, while TRIF is the adaptor protein for TLR3, suggesting that RLR signaling contributes more effectively to the innate response to ZIKV infection. More specifically, RNAs generated during ZIKV infection were shown to activate signaling by RIG-I, and to a lesser extent MDA5, indicating that ZIKV is likely recognized primarily by RIG-I (Hertzog et al., 2018). The implication of RLRs in the innate immune response to ZIKV is consistent with our data showing increased transcription and translation of RLRs in moDCs and HCs (**Chapter 3, Figure 10; Chapter 4, Figure 7**).

In addition, multiple studies have now described cross-reactivity between DENV antibodies and ZIKV, though there is some uncertainty about whether these antibodies

are protective against ZIKV infection (Dai et al., 2016; Fernandez et al., 2017; Swanstrom et al., 2016) or whether they enhance infection and increase the risk of symptomatic disease or trans-placental transmission (Bardina et al., 2017; Charles and Christofferson, 2016; Dejnirattisai et al., 2016; Paul et al., 2016; Stettler et al., 2016). In confirmation of our results, others have since found that human sera and monoclonal antibodies from DENV-infected patients can cross-react and neutralize ZIKV with some variability (Barba-Spaeth et al., 2016; Bardina et al., 2017; Dejnirattisai et al., 2016; Fernandez et al., 2017; Paul et al., 2016; Stettler et al., 2016). Antibody-dependent enhancement (ADE) of ZIKV infection by DENV antibodies has also been shown by other groups in cell culture models, including THP-1, U937, and K562 cells (Bardina et al., 2017; Charles and Christofferson, 2016; Dejnirattisai et al., 2016; McCracken et al., 2017; Pantoja et al., 2017; Paul et al., 2016; Stettler et al., 2016). However, few have demonstrated ADE in primary cell types as we did in Chapter 6. One study went on to demonstrate enhanced morbidity and mortality in ZIKV-infected $STAT2^{-/-}$ mice that were pre-treated with plasma from DENV-infected patients (Bardina et al., 2017). Another showed enhanced morbidity and mortality in AG129 mice infected with ZIKV or DENV in the presence of DENV mAb or ZIKV mAb, respectively, indicating that ZIKV immunity may adversely affect DENV disease as well (Stettler et al., 2016). However, when the impact of pre-exiting flavivirus antibodies on ZIKV infection was tested in animal models, results often suggested either no effect (McCracken et al., 2017; Pantoja et al., 2017), or a protective effect against ZIKV (Dai et al., 2016; Fernandez et al., 2017; Swanstrom et al., 2016). In immunocompromised mice infected with ZIKV, treatment with human DENV monoclonal antibodies reduced mortality and viral loads (Dai et al., 2016; Fernandez et al., 2017; Swanstrom et al., 2016). In addition, ZIKV-infected pregnant mice treated with these antibodies experienced lower viral loads in fetal tissues and less fetal demise (Fernandez et al., 2017). Two studies using rhesus macaque models

reported that while DENV-experienced sera resulted in ADE of ZIKV infection *in vitro*, there was no effect *in vivo* on ZIKV disease in these animals (McCracken et al., 2017; Pantoja et al., 2017). This highlights the necessity for testing this ADE concept in primary cells, and especially *in vivo*. It will also be crucial to determine whether enhancement of infection occurs naturally in humans, or if pre-existing flavivirus antibodies can influence other tropism or transmission characteristics of ZIKV, as we suggest in Chapter 6.

Once ZIKV gains access to placental tissues, the lack of a strong antiviral response in fetal-derived cells, along with the innate abilities of ZIKV to suppress IFN signaling at multiple levels (Grant et al., 2016; Kumar et al., 2016; Wu et al., 2017), may provide a niche in which ZIKV can persist within the host. The possibility of ZIKV persistence in placental tissues has been suggested by findings both in humans and in rhesus macaques (Bhatnagar et al., 2017; Driggers et al., 2016; Dudley et al., 2016; Rosenberg et al., 2017). Cases evaluating the placentas from women infected with ZIKV during pregnancy have identified ZIKV RNA upon birth, regardless of when infection occurred. Others have observed heightened proliferation of HCs in placentas from ZIKV-infected women, which could increase the number of host cells available for ZIKV replication (Noronha et al., 2016; Rosenberg et al., 2017; Schwartz, 2017). Such an environment could easily increase the risk of ZIKV transmission to the fetus, as well as re-infection of the mother, by allowing for greater amplification of the virus and providing a wider temporal window for transmission to occur.

Vertical transmission of other flaviviruses

ZIKV currently seems unique among flaviviruses in its ability to be transmitted across the placenta. However, this characteristic of the virus was not identified until the outbreaks in the Americas, and then later observed retrospectively during the outbreaks in French

Polynesia (Cauchemez et al., 2016). One potential reason for this is lack of reporting during previous outbreaks, or the small number of cases comprising outbreaks until 2007. In this context, it may be that other flaviviruses are also capable of vertical transmission, but that reports are lacking due to small numbers of cases or failure to associate fetal outcomes with flavivirus infection during pregnancy. Indeed, Platt and colleagues recently described trans-placental transmission in mice and infection of human placental explants with WNV and Powassan virus (POWV), a tick-borne flavivirus (Platt et al., 2018). WNV and POWV are both neurotropic and have caused fewer human cases than the ZIKV outbreaks of the Western hemisphere. In immunocompetent WT mice infected with WNV (3000.0259) or POWV (Spooner strain), viral RNA was found in the placenta and fetal head, and resulted in ~50% fetal demise. More specifically, WNV RNA was detected in both the maternal and fetal tissues of the placenta, but no damage to placental structure was observed. In second trimester human placental explants, WNV and POWV were both able to replicate in the maternal decidua and the fetal chorionic villi, as was ZIKV (Paraiba strain).

WNV has been detected in the placentas of mice by other groups as well (Cordoba et al., 2007; Julander et al., 2005; Julander et al., 2006), and a handful of studies have attempted to examine the potential for WNV trans-placental transmission and the effects of in utero WNV infection in humans, with mixed results. Alpert and colleagues described the first documented case of WNV congenital infection (Alpert et al., 2003). The mother was diagnosed with WNV in the third trimester, and the fetus was found to have ocular and brain pathologies. Blood and cerebrospinal fluid (CSF) from the infant was positive for WNV IgM antibodies. As IgM does not cross the placenta, this suggests WNV vertical transmission and infection of the developing fetus. Another broader study evaluated fetal outcomes of 77 women infected with WNV during pregnancy (O'Leary et al., 2006). The women were determined to have been infected at

a range of gestational ages (1st, 2nd or 3rd trimester) and exhibited a wide range of symptoms, from asymptomatic viremia to WNV neuroinvasive disease. Of the infants that were successfully delivered, none had conclusive evidence of in utero WNV infection, though the number of severe birth defects in this cohort was higher than expected (7/66 infants). There were three cases of possible WNV congenital infection. In all cases, mothers had symptomatic WNV infection late in the third trimester, and infants were either born with WNV symptoms or developed symptoms soon after birth. Two were found to have WNV IgM in the CSF, and one had detectible WNV IgM in the serum at one month after birth. However, only 1/50 placentas tested was positive for WNV RNA, and viral RNA was detected in fetal, but not maternal placental tissues. Others have also failed to detect significant differences in growth or neural/cognitive development in children born to WNV-infected mothers compared to those born to uninfected mothers (Paisley et al., 2006; Pridjian et al., 2016; Sirois et al., 2014). Thus, the question of WNV trans-placental transmission has not been resolved.

WNV infection causes disease in immunocompetent WT mice, indicating that, unlike ZIKV, WNV is able to overcome type I IFN signaling in this model. However, it could be that WNV is sensitive to type III IFN, in particular human IFN-λ1, which is secreted by the STBs that form the protective outer layer of the placenta (Bayer et al., 2016). Also, in the four potential cases of vertical transmission described above, mothers were diagnosed with WNV during the third trimester. Later in the third trimester of pregnancy, the CTB layer becomes inconsistent as more CTBs are needed to supply differentiated cells to the now large STB layer (Coyne and Lazear, 2016). It is possible that the maternal immune response to WNV could damage the thinned outer layers of the placenta, providing WNV with easier access to HCs. HCs would likely be more susceptible to infection as macrophages and DCs are known targets of WNV infection (Suthar et al., 2013b). Thus, WNV could represent a more opportunistic infection of the

fetal compartment than natural tropism for placental or fetal tissues. However, upon reaching the fetal brain, the neurotropism of WNV would likely allow it to replicate efficiently and cause subsequent tissue damage.

Unanswered questions

Despite the veritable explosion of work surrounding ZIKV in the last two years, there is still much that remains unknown. For instance, what was it about the outbreaks in French Polynesia and the Americas that led to the connection of ZIKV with congenic infection and microcephaly when this had not been observed in previous outbreaks? It is possible that there were ZIKV-associated cases of microcephaly in previous outbreaks, but due to lack of testing/reporting for ZIKV infection, the association went undocumented. In contrast, both ZIKV infections and pregnancy outcomes were well documented during the outbreak in Brazil. In a similar vein, it may be that ZIKV-associated microcephaly was observed in these outbreaks simply because of the large number of cases. Microcephaly is observed in about 1-17% of cases, depending on geographical location and assumed percentage of pregnant women infected (Cauchemez et al., 2016; Coelho and Crovella, 2017; Jaenisch et al., 2017), and before 2007, ZIKV outbreaks were very limited (Hayes, 2009). Thus, ZIKV may always have been capable of causing microcephaly, there were just never enough infected pregnant women in previous outbreaks for it to manifest.

Others, however, have hypothesized that changes in the viral genome resulted in the evolution of more virulent ZIKV strains. Differences between African and Asian lineage viruses have been demonstrated and several genomic variations have been identified between ancestral Asian lineage viruses and those strains isolated from the French Polynesian and American epidemics (Faria et al., 2016; Haddow et al., 2012; Zhu et al., 2016), some of which resulted in amino acid changes within viral proteins

(Pettersson et al., 2016; Wang et al., 2016). Yuan and colleagues observed that contemporary ZIKV isolates are more neuro-pathogenic than an ancestral Asian strain from Cambodia (FSS13025) (Yuan et al., 2017). A previous study identified a S139N amino acid change in the genomes of several recently isolated ZIKV strains, that corresponded to position 17 in the prM protein (Pettersson et al., 2016). When this substitution was introduced in the ZIKV FSS13025 prM protein, the mutant virus exhibited enhanced replication in human and mouse NPCs and resulted in more severe microcephaly in mice compared to the WT ZIKV FSS13025 (Yuan et al., 2017). Additionally, when this natural amino acid change in the 2016 Venezuelan ZIKV isolate (GZ01) was reversed (N139S), the mutant virus became phenotypically similar to ZIKV FSS13025, with lower mortality rates in mice than the WT ZIKV GZ01 strain. The S139N substitution occurred just before the ZIKV outbreak in French Polynesia, the first outbreak in which ZIKV was associated with fetal microcephaly, suggesting it may increase the neuro-pathogenesis of the virus compared to more historical stains. Another study identified a number of amino acid changes in the NS4b protein of Brazilian lineage viruses compared to African lineage viruses (Jun et al., 2017). These changes increased the potential of NS4b to be phosphorylated, which may interfere with fetal brain development pathways. It is possible that other amino acid changes could enhance the ability of newer Asian strains to cross the placenta. If this were the case, easier access to the fetal compartment could result in more frequent transmission to the fetus and an increase in adverse neurological outcomes.

The risk factors for trans-placental transmission and subsequent developmental abnormalities are also still unclear. It is believed that gestational age during ZIKV infection likely affects the outcome, as the developing fetus and the placental architecture are more vulnerable at early times during pregnancy. However, there is still some debate as to which time period represents the greatest risk (Cauchemez et al.,

2016; Faria et al., 2016; Hoen et al., 2018; Honein et al., 2017), and others have failed to observe a significant correlation between gestational age at infection and adverse fetal outcomes (Brasil et al., 2016a; Shapiro-Mendoza et al., 2017). The route of infection should also be considered. ZIKV transmission most often occurs from the bite of an infected mosquito, but instances of sexual transmission have also been reported (Foy et al., 2011; McCarthy, 2016; Musso et al., 2015b). Sexual transmission may increase the risk of vertical transmission from a pregnant mother to her developing fetus and thus increase the risk of congenital ZIKV infection. Infection of vaginal tissues could provide a more direct route for ZIKV infection of the placenta and trans-placental transmission. Indeed, vaginal inoculation of WT immunocompetent mice was able to produce detectible ZIKV replication in the vaginal tract (Yockey et al., 2016), whereas subcutaneous inoculation (representative of transmission via mosquito bite) does not result in productive infection (Lazear et al., 2016). Several case and cohort studies have implicated ZIKV infection in the first trimester as a risk factor for congenital infection and microcephaly or other developmental abnormalities (Cauchemez et al., 2016; Hoen et al., 2018). Another group described an *in vitro* model that reflected the earliest stages of placental development and found that these cells were particularly susceptible to infection (Sheridan et al., 2017). Infection at this early stage could easily occur if the virus were sexually transmitted. Additionally, symptomatic versus asymptomatic maternal ZIKV disease during pregnancy should be evaluated. The majority of studies conducted thus far have evaluated fetal outcomes from ZIKV-infected cohorts with non-infected women as controls. However, there is evidence that microcephaly and other potentially ZIKV-related neuro-pathologies can occur following asymptomatic infection of pregnant women (Franca et al., 2016; Pacheco et al., 2016).

ZIKV conclusion: A lingering threat

Understanding the virology, immunology and transmission of ZIKV will be essential for guiding future efforts to combat this emerging pathogen. ZIKV is now endemic across much of South and Central America, as well as in Puerto Rico (Adams et al., 2016; Lozier et al., 2016; Petersen et al., 2016a). There have been multiple travel-associated cases identified within non-endemic countries, including the United States (Armstrong et al., 2016; Leta et al., 2018; Meaney-Delman et al., 2016), and even some instances of subsequent autochthonous transmission, presumably by mosquito vectors (Likos et al., 2016). A number of *Aedes* spp. mosquitoes, including *Aedes aegypti* and *Aedes albopictus*, that have been shown to transmit ZIKV have territories that include regions of the US, which increases the risk that ZIKV could become endemic in this country as well (Leta et al., 2018; Petersen et al., 2016a; Weaver et al., 2016). ZIKV can also be spread through sexual contact, and has been shown to remain viable in semen for up to two weeks after symptoms have resolved (Mansuy et al., 2016; Musso et al., 2015b), further enhancing the transmission potential of the virus.

Specifically, knowledge of the tropism, initial innate antiviral responses, and potential consequences of flavivirus cross-reactive antibodies during ZIKV infection will be essential for developing vaccines and therapeutics targeting ZIKV. Ideally, a treatment would stimulate those antiviral pathways shown to successfully activate innate immune cells, such as DCs and macrophages, and control ZIKV infection and would evoke a ZIKV-specific antibody response. The immunogenic properties of ZIKV may also affect ongoing research into other flavivirus vaccines. For instance, there has been great progress in the effort to develop an effective vaccine against DENV. The most promising candidate at this time is a quadrivalent vaccine that contains epitopes from all four DENV serotypes, in an effort to produce an antibody repertoire that can efficiently neutralize subsequent infection by any DENV serotype, reducing the risk of ADE (Diaz et

al., 2018; Olivera-Botello et al., 2016). The efficacy of this and other vaccines may be complicated if ZIKV-specific antibodies can cross-react with DENV.

Concluding thoughts

We and others have observed up-regulation of RLR gene and protein expression in response to ZIKV infection (Luo et al., 2018; Vielle et al., 2018), and several members of the RLR signaling pathway have been specifically implicated in controlling virus replication (Hertzog et al., 2018; Piret et al., 2018). Indeed, we and others have found that treating cells with type I IFN after infection is established has little effect on viral titers (Frumence et al., 2016; Hamel et al., 2015), however we also showed that post-infection treatment with a RIG-I specific agonist could significantly reduce infectious virus release (**Chapter 3, Figure 12B**). Together these results indicate that the RLR signaling pathway is a critical component of the antiviral response to ZIKV. Thus, LGP2 likely plays a central role in regulating this response. LGP2 mRNA expression is induced in ZIKV-infected moDCs (**Chapter 3, Figure 10A**) and HCs (**Chapter 4, Figure 7B**), and protein levels are similarly increased in moDCs (**Chapter 3, Figure 10C**) and HCs (**Chapter 6, Figure 4D**) during ZIKV infection, further supporting the involvement of LGP2. As mentioned above, it is necessary to understand the innate immune responses to ZIKV in its natural cell targets in order to design effective vaccines and therapeutics. Integral to this is understanding how these innate responses are regulated. It will be necessary to identify whether RIG-I or MDA5 specifically recognize and target ZIKV, or if both proteins are required to initiate an adequate response, as LGP2 differentially regulates these RLRs. It should also be investigated whether ZIKV possesses any antagonistic mechanisms that target proteins in the RLR pathway, specifically TRIM25, as this could impact the function of LGP2 during ZIKV infection. Also mentioned above is the consideration of RLR agonists as vaccine adjuvants. This may be particularly

effective against ZIKV, given our findings (**Chapter 3, Figure 12B**). However, if this approach is to be considered, it will be essential to understand the LGP2-mediated regulation of this pathway.

Works Cited

Aagaard, K.M., A. Lahon, M.A. Suter, R.P. Arya, M.D. Seferovic, M.B. Vogt, M. Hu, F. Stossi, M.A. Mancini, R.A. Harris, M. Kahr, C. Eppes, M. Rac, M.A. Belfort, C.S. Park, D. Lacorazza, and R. Rico-Hesse. 2017. Primary Human Placental Trophoblasts are Permissive for Zika Virus (ZIKV) Replication. *Sci Rep* 7:41389.

Abdiche, Y.N., Y.A. Yeung, J. Chaparro-Riggers, I. Barman, P. Strop, S.M. Chin, A. Pham, G. Bolton, D. McDonough, K. Lindquist, J. Pons, and A. Rajpal. 2015. The neonatal Fc receptor (FcRn) binds independently to both sites of the IgG homodimer with identical affinity. *MAbs* 7:331-343.

Ablasser, A., F. Bauernfeind, G. Hartmann, E. Latz, K.A. Fitzgerald, and V. Hornung. 2009. RIG-I-dependent sensing of poly(dA:dT) through the induction of an RNA polymerase III-transcribed RNA intermediate. *Nat Immunol* 10:1065-1072.

Adams, L., M. Bello-Pagan, M. Lozier, K.R. Ryff, C. Espinet, J. Torres, J. Perez-Padilla, M.F. Febo, E. Dirlikov, A. Martinez, J. Munoz-Jordan, M. Garcia, M.O. Segarra, G. Malave, A. Rivera, C. Shapiro-Mendoza, A. Rosinger, M.J. Kuehnert, K.W. Chung, L.L. Pate, A. Harris, R.R. Hemme, A. Lenhart, G. Aquino, S. Zaki, J.S. Read, S.H. Waterman, L.I. Alvarado, F. Alvarado-Ramy, M. Valencia-Prado, D. Thomas, T.M. Sharp, and B. Rivera-Garcia. 2016. Update: Ongoing Zika Virus Transmission - Puerto Rico, November 1, 2015-July 7, 2016. *MMWR Morb Mortal Wkly Rep* 65:774-779.

Aleyas, A.G., Y.W. Han, J.A. George, B. Kim, K. Kim, C.K. Lee, and S.K. Eo. 2010. Multifront assault on antigen presentation by Japanese encephalitis virus subverts CD8+ T cell responses. *J Immunol* 185:1429-1441.

Aliota, M.T., E.A. Caine, E.C. Walker, K.E. Larkin, E. Camacho, and J.E. Osorio. 2016. Characterization of Lethal Zika Virus Infection in AG129 Mice. *PLoS Negl Trop Dis* 10:e0004682.

Alpert, S.G., J. Fergerson, and L.P. Noel. 2003. Intrauterine West Nile virus: ocular and systemic findings. *Am J Ophthalmol* 136:733-735.

Andrejeva, J., K.S. Childs, D.F. Young, T.S. Carlos, N. Stock, S. Goodbourn, and R.E. Randall. 2004. The V proteins of paramyxoviruses bind the IFN-inducible RNA helicase, mda-5, and inhibit its activation of the IFN-beta promoter. *Proc Natl Acad Sci U S A* 101:17264-17269.

Anglero-Rodriguez, Y.I., P. Pantoja, and C.A. Sariol. 2014. Dengue virus subverts the interferon induction pathway via NS2B/3 protease-IkappaB kinase epsilon interaction. *Clin Vaccine Immunol* 21:29-38.

Arimoto, K., H. Takahashi, T. Hishiki, H. Konishi, T. Fujita, and K. Shimotohno. 2007. Negative regulation of the RIG-I signaling by the ubiquitin ligase RNF125. *Proc Natl Acad Sci U S A* 104:7500-7505.

Armstrong, P., M. Hennessey, M. Adams, C. Cherry, S. Chiu, A. Harrist, N. Kwit, L. Lewis, D.O. McGuire, T. Oduyebo, K. Russell, P. Talley, M. Tanner, C. Williams, E. Zika Virus Response, and T. Laboratory. 2016. Travel-Associated Zika Virus Disease Cases Among U.S. Residents--United States, January 2015-February 2016. *MMWR Morb Mortal Wkly Rep* 65:286-289.

Arora, N., Y. Sadovsky, T.S. Dermody, and C.B. Coyne. 2017. Microbial Vertical Transmission during Human Pregnancy. *Cell Host Microbe* 21:561-567.

Bamming, D., and C.M. Horvath. 2009. Regulation of signal transduction by enzymatically inactive antiviral RNA helicase proteins MDA5, RIG-I, and LGP2. *J Biol Chem* 284:9700-9712.

Barba-Spaeth, G., W. Dejnirattisai, A. Rouvinski, M.C. Vaney, I. Medits, A. Sharma, E. Simon-Loriere, A. Sakuntabhai, V.M. Cao-Lormeau, A. Haouz, P. England, K. Stiasny, J. Mongkolsapaya, F.X. Heinz, G.R. Screaton, and F.A. Rey. 2016. Structural basis of potent Zika-dengue virus antibody cross-neutralization. *Nature* 536:48-53.

Bardina, S.V., P. Bunduc, S. Tripathi, J. Duehr, J.J. Frere, J.A. Brown, R. Nachbagauer, G.A. Foster, D. Krysztof, D. Tortorella, S.L. Stramer, A. Garcia-Sastre, F. Krammer, and J.K. Lim. 2017. Enhancement of Zika virus pathogenesis by preexisting antiflavivirus immunity. *Science* 356:175-180.

Bayer, A., N.J. Lennemann, Y. Ouyang, J.C. Bramley, S. Morosky, E.T. Marques, Jr., S. Cherry, Y. Sadovsky, and C.B. Coyne. 2016. Type III Interferons Produced by Human Placental Trophoblasts Confer Protection against Zika Virus Infection. *Cell Host Microbe* 19:705-712.

Bayless, N.L., R.S. Greenberg, T. Swigut, J. Wysocka, and C.A. Blish. 2016. Zika Virus Infection Induces Cranial Neural Crest Cells to Produce Cytokines at Levels Detrimental for Neurogenesis. *Cell Host Microbe* 20:423-428.

Beljanski, V., C. Chiang, G.A. Kirchenbaum, D. Olagnier, C.E. Bloom, T. Wong, E.K. Haddad, L. Trautmann, T.M. Ross, and J. Hiscott. 2015. Enhanced Influenza Virus-Like Particle Vaccination with a Structurally Optimized RIG-I Agonist as Adjuvant. *J Virol* 89:10612-10624.

Beltramello, M., K.L. Williams, C.P. Simmons, A. Macagno, L. Simonelli, N.T. Quyen, S. Sukupolvi-Petty, E. Navarro-Sanchez, P.R. Young, A.M. de Silva, F.A. Rey, L. Varani, S.S. Whitehead, M.S. Diamond, E. Harris, A. Lanzavecchia, and F. Sallusto. 2010. The human immune response to Dengue virus is dominated by highly cross-reactive antibodies endowed with neutralizing and enhancing activity. *Cell Host Microbe* 8:271-283.

Besnard, M., S. Lastere, A. Teissier, V. Cao-Lormeau, and D. Musso. 2014. Evidence of perinatal transmission of Zika virus, French Polynesia, December 2013 and February 2014. *Euro Surveill* 19:

Best, S.M., K.L. Morris, J.G. Shannon, S.J. Robertson, D.N. Mitzel, G.S. Park, E. Boer, J.B. Wolfinbarger, and M.E. Bloom. 2005. Inhibition of interferon-stimulated JAK-STAT signaling by a tick-borne flavivirus and identification of NS5 as an interferon antagonist. *J Virol* 79:12828-12839.

Bhatnagar, J., D.B. Rabeneck, R.B. Martines, S. Reagan-Steiner, Y. Ermias, L.B. Estetter, T. Suzuki, J. Ritter, M.K. Keating, G. Hale, J. Gary, A. Muehlenbachs, A. Lambert, R. Lanciotti, T. Oduyebo, D. Meaney-Delman, F. Bolanos, E.A. Saad, W.J. Shieh, and S.R. Zaki. 2017. Zika Virus RNA Replication and Persistence in Brain and Placental Tissue. *Emerg Infect Dis* 23:405-414.

Bhatt, S., P.W. Gething, O.J. Brady, J.P. Messina, A.W. Farlow, C.L. Moyes, J.M. Drake, J.S. Brownstein, A.G. Hoen, O. Sankoh, M.F. Myers, D.B. George, T. Jaenisch, G.R. Wint, C.P. Simmons, T.W. Scott, J.J. Farrar, and S.I. Hay. 2013. The global distribution and burden of dengue. *Nature* 496:504-507.

Bol, S.M., Y. van Remmerden, J.G. Sietzema, N.A. Kootstra, H. Schuitemaker, and A.B. van't Wout. 2009. Donor variation in in vitro HIV-1 susceptibility of monocyte-derived macrophages. *Virology* 390:205-211.

Boonnak, K., B.M. Slike, G.C. Donofrio, and M.A. Marovich. 2013. Human FcgammaRII cytoplasmic domains differentially influence antibody-mediated dengue virus infection. *J Immunol* 190:5659-5665.

Bouchier-Hayes, L., and S.J. Martin. 2002. CARD games in apoptosis and immunity. *EMBO Rep* 3:616-621.

Bowen, J.R., M.T. Ferris, and M.S. Suthar. 2016. Systems biology: A tool for charting the antiviral landscape. *Virus Res* 218:2-9.

Brasil, P., J.P. Pereira, Jr., M.E. Moreira, R.M. Ribeiro Nogueira, L. Damasceno, M. Wakimoto, R.S. Rabello, S.G. Valderramos, U.A. Halai, T.S. Salles, A.A. Zin, D. Horovitz, P. Daltro, M. Boechat, C. Raja Gabaglia, P. Carvalho de Sequeira, J.H. Pilotto, R. Medialdea-Carrera, D. Cotrim da Cunha, L.M. Abreu de Carvalho, M. Pone, A. Machado Siqueira, G.A. Calvet, A.E. Rodrigues Baiao, E.S. Neves, P.R. Nassar de Carvalho, R.H. Hasue, P.B. Marschik, C. Einspieler, C. Janzen, J.D. Cherry, A.M. Bispo de Filippis, and K. Nielsen-Saines. 2016a. Zika Virus Infection in Pregnant Women in Rio de Janeiro. *N Engl J Med* 375:2321-2334.

Brasil, P., J.P. Pereira, Jr., C. Raja Gabaglia, L. Damasceno, M. Wakimoto, R.M. Ribeiro Nogueira, P. Carvalho de Sequeira, A. Machado Siqueira, L.M. Abreu de Carvalho, D. Cotrim da Cunha, G.A. Calvet, E.S. Neves, M.E. Moreira, A.E. Rodrigues Baiao, P.R. Nassar de Carvalho, C. Janzen, S.G. Valderramos, J.D. Cherry, A.M. Bispo de Filippis, and K. Nielsen-Saines. 2016b. Zika Virus Infection in Pregnant Women in Rio de Janeiro - Preliminary Report. *N Engl J Med*

Brasil, P., P.C. Sequeira, A.D. Freitas, H.E. Zogbi, G.A. Calvet, R.V. de Souza, A.M. Siqueira, M.C. de Mendonca, R.M. Nogueira, A.M. de Filippis, and T. Solomon. 2016c. Guillain-Barre syndrome associated with Zika virus infection. *Lancet* 387:1482.

Bruns, A.M., and C.M. Horvath. 2012. Activation of RIG-I-like receptor signal transduction. *Crit Rev Biochem Mol Biol* 47:194-206.

Bruns, A.M., G.P. Leser, R.A. Lamb, and C.M. Horvath. 2014. The innate immune sensor LGP2 activates antiviral signaling by regulating MDA5-RNA interaction and filament assembly. *Mol Cell* 55:771-781.

Bruns, A.M., D. Pollpeter, N. Hadizadeh, S. Myong, J.F. Marko, and C.M. Horvath. 2013. ATP hydrolysis enhances RNA recognition and antiviral signal transduction by the innate immune sensor, laboratory of genetics and physiology 2 (LGP2). *J Biol Chem* 288:938-946.

Calvet, G., R.S. Aguiar, A.S.O. Melo, S.A. Sampaio, I. de Filippis, A. Fabri, E.S.M. Araujo, P.C. de Sequeira, M.C.L. de Mendonca, L. de Oliveira, D.A. Tschoeke, C.G. Schrago, F.L. Thompson, P. Brasil, F.B. Dos Santos, R.M.R. Nogueira, A. Tanuri, and A.M.B. de Filippis. 2016. Detection and sequencing of Zika virus from amniotic fluid of fetuses with microcephaly in Brazil: a case study. *Lancet Infect Dis* 16:653-660.

Campos, G.S., A.C. Bandeira, and S.I. Sardi. 2015. Zika Virus Outbreak, Bahia, Brazil. *Emerg Infect Dis* 21:1885-1886.

Cao-Lormeau, V.M., A. Blake, S. Mons, S. Lastere, C. Roche, J. Vanhomwegen, T. Dub, L. Baudouin, A. Teissier, P. Larre, A.L. Vial, C. Decam, V. Choumet, S.K. Halstead, H.J. Willison, L. Musset, J.C. Manuguerra, P. Despres, E. Fournier, H.P. Mallet, D. Musso, A. Fontanet, J. Neil, and F. Ghawche. 2016. Guillain-Barre Syndrome outbreak associated with Zika virus infection in French Polynesia: a case-control study. *Lancet* 387:1531-1539.

Castanha, P.M., C. Braga, M.T. Cordeiro, A.I. Souza, C.D. Silva, Jr., C.M. Martelli, W.G. van Panhuis, E.J. Nascimento, and E.T. Marques. 2016. Placental Transfer of Dengue Virus (DENV)-Specific Antibodies and Kinetics of DENV Infection-Enhancing Activity in Brazilian Infants. *J Infect Dis* 214:265-272.

Castanier, C., N. Zemirli, A. Portier, D. Garcin, N. Bidere, A. Vazquez, and D. Arnoult. 2012. MAVS ubiquitination by the E3 ligase TRIM25 and degradation by the

proteasome is involved in type I interferon production after activation of the antiviral RIG-I-like receptors. *BMC Biol* 10:44.

Cauchemez, S., M. Besnard, P. Bompard, T. Dub, P. Guillemette-Artur, D. Eyrolle-Guignot, H. Salje, M.D. Van Kerkhove, V. Abadie, C. Garel, A. Fontanet, and H.P. Mallet. 2016. Association between Zika virus and microcephaly in French Polynesia, 2013-15: a retrospective study. *Lancet* 387:2125-2132.

Cerny, D., M. Haniffa, A. Shin, P. Bigliardi, B.K. Tan, B. Lee, M. Poidinger, E.Y. Tan, F. Ginhoux, and K. Fink. 2014. Selective susceptibility of human skin antigen presenting cells to productive dengue virus infection. *PLoS Pathog* 10:e1004548.

Chakravarthy, K.V., A.C. Bonoiu, W.G. Davis, P. Ranjan, H. Ding, R. Hu, J.B. Bowzard, E.J. Bergey, J.M. Katz, P.R. Knight, S. Sambhara, and P.N. Prasad. 2010. Gold nanorod delivery of an ssRNA immune activator inhibits pandemic H1N1 influenza viral replication. *Proceedings of the National Academy of Sciences of the United States of America* 107:10172-10177.

Chambers, T.J., M. Halevy, A. Nestorowicz, C.M. Rice, and S. Lustig. 1998. West Nile virus envelope proteins: nucleotide sequence analysis of strains differing in mouse neuroinvasiveness. *J Gen Virol* 79 (Pt 10):2375-2380.

Chan, Y.K., and M.U. Gack. 2016. Viral evasion of intracellular DNA and RNA sensing. *Nat Rev Microbiol* 14:360-373.

Charles, A.S., and R.C. Christofferson. 2016. Utility of a Dengue-Derived Monoclonal Antibody to Enhance Zika Infection In Vitro. *PLoS Curr* 8:

Chaudhary, V., K.S. Yuen, J.F. Chan, C.P. Chan, P.H. Wang, J.P. Cai, S. Zhang, M. Liang, K.H. Kok, C.P. Chan, K.Y. Yuen, and D.Y. Jin. 2017. Selective Activation of Type II Interferon Signaling by Zika Virus NS5 Protein. *J Virol* 91:

Chiang, C., E.K. Pauli, J. Biryukov, K.F. Feister, M. Meng, E.A. White, K. Munger, P.M. Howley, C. Meyers, and M.U. Gack. 2018. The Human Papillomavirus E6 Oncoprotein Targets USP15 and TRIM25 To Suppress RIG-I-Mediated Innate Immune Signaling. *J Virol* 92:

Childs, K.S., R.E. Randall, and S. Goodbourn. 2013. LGP2 plays a critical role in sensitizing mda-5 to activation by double-stranded RNA. *PLoS One* 8:e64202.

Chiu, Y.H., J.B. Macmillan, and Z.J. Chen. 2009. RNA polymerase III detects cytosolic DNA and induces type I interferons through the RIG-I pathway. *Cell* 138:576-591.

Chiuppesi, F., F. Wussow, E. Johnson, C. Bian, M. Zhuo, A. Rajakumar, P.A. Barry, W.J. Britt, R. Chakraborty, and D.J. Diamond. 2015. Vaccine-Derived Neutralizing Antibodies to the Human Cytomegalovirus gH/gL Pentamer Potently Block Primary Cytotrophoblast Infection. *J Virol* 89:11884-11898.

Clyde, K., J.L. Kyle, and E. Harris. 2006. Recent advances in deciphering viral and host determinants of dengue virus replication and pathogenesis. *J Virol* 80:11418-11431.

Coelho, A.V.C., and S. Crovella. 2017. Microcephaly Prevalence in Infants Born to Zika Virus-Infected Women: A Systematic Review and Meta-Analysis. *Int J Mol Sci* 18:

Cordeiro, M.T., L.J. Pena, C.A. Brito, L.H. Gil, and E.T. Marques. 2016. Positive IgM for Zika virus in the cerebrospinal fluid of 30 neonates with microcephaly in Brazil. *Lancet*

Cordin, O., J. Banroques, N.K. Tanner, and P. Linder. 2006. The DEAD-box protein family of RNA helicases. *Gene* 367:17-37.

Cordoba, L., E. Escribano-Romero, A. Garmendia, and J.C. Saiz. 2007. Pregnancy increases the risk of mortality in West Nile virus-infected mice. *J Gen Virol* 88:476-480.

Corry, J., N. Arora, C.A. Good, Y. Sadovsky, and C.B. Coyne. 2017. Organotypic models of type III interferon-mediated protection from Zika virus infections at the maternal-fetal interface. *Proc Natl Acad Sci U S A* 114:9433-9438.

Costin, J.M., E. Zaitseva, K.M. Kahle, C.O. Nicholson, D.K. Rowe, A.S. Graham, L.E. Bazzone, G. Hogancamp, M. Figueroa Sierra, R.H. Fong, S.T. Yang, L. Lin, J.E. Robinson, B.J. Doranz, L.V. Chernomordik, S.F. Michael, J.S. Schieffelin, and S. Isern. 2013. Mechanistic study of broadly neutralizing human monoclonal antibodies against dengue virus that target the fusion loop. *J Virol* 87:52-66.

Coyne, C.B., and H.M. Lazear. 2016. Zika virus - reigniting the TORCH. *Nat Rev Microbiol* 14:707-715.

Cugola, F.R., I.R. Fernandes, F.B. Russo, B.C. Freitas, J.L.M. Dias, K.P. Guimarães, C. Benazzato, N. Almeida, G.C. Pignatari, S. Romero, C.M. Polonio, I. Cunha, C.L. Freitas, W.N. Brandão, C. Rossato, D.G. Andrade, D.d.P. Faria, A.T. Garcez, C.A. Buchpigel, C.T. Braconi, E. Mendes, A.A. Sall, P.M.d.A. Zanotto, J.P.S. Peron, A.R. Muotri, and P.C.B. Beltrão-Braga. 2016. The Brazilian Zika virus strain causes birth defects in experimental models. *Nature*

Cui, S., K. Eisenacher, A. Kirchhofer, K. Brzozka, A. Lammens, K. Lammens, T. Fujita, K.K. Conzelmann, A. Krug, and K.P. Hopfner. 2008. The C-terminal regulatory domain is the RNA 5'-triphosphate sensor of RIG-I. *Mol Cell* 29:169-179.

Cui, Y., M. Li, K.D. Walton, K. Sun, J.A. Hanover, P.A. Furth, and L. Hennighausen. 2001. The Stat3/5 locus encodes novel endoplasmic reticulum and helicase-like proteins that are preferentially expressed in normal and neoplastic mammary tissue. *Genomics* 78:129-134.

Culshaw, A., J. Mongkolsapaya, and G.R. Screaton. 2017. The immunopathology of dengue and Zika virus infections. *Curr Opin Immunol* 48:1-6.

D'Ortenzio, E., S. Matheron, Y. Yazdanpanah, X. de Lamballerie, B. Hubert, G. Piorkowski, M. Maquart, D. Descamps, F. Damond, and I. Leparc-Goffart. 2016. Evidence of Sexual Transmission of Zika Virus. *N Engl J Med* 374:2195-2198.

Daffis, S., M.S. Suthar, K.J. Szretter, M. Gale, Jr., and M.S. Diamond. 2009. Induction of IFN-beta and the innate antiviral response in myeloid cells occurs through an IPS-1-dependent signal that does not require IRF-3 and IRF-7. *PLoS Pathog* 5:e1000607.

Dai, L., J. Song, X. Lu, Y.Q. Deng, A.M. Musyoki, H. Cheng, Y. Zhang, Y. Yuan, H. Song, J. Haywood, H. Xiao, J. Yan, Y. Shi, C.F. Qin, J. Qi, and G.F. Gao. 2016. Structures of the Zika Virus Envelope Protein and Its Complex with a Flavivirus Broadly Protective Antibody. *Cell Host Microbe* 19:696-704.

Dang, J., S.K. Tiwari, G. Lichinchi, Y. Qin, V.S. Patil, A.M. Eroshkin, and T.M. Rana. 2016. Zika Virus Depletes Neural Progenitors in Human Cerebral Organoids through Activation of the Innate Immune Receptor TLR3. *Cell Stem Cell*

Dasgupta, S., S. Reagan-Steiner, D. Goodenough, K. Russell, M. Tanner, L. Lewis, E.E. Petersen, A.M. Powers, K. Kniss, D. Meaney-Delman, T. Oduyebo, D. O'Leary, S. Chiu, P. Talley, M. Hennessey, S. Hills, A. Cohn, C. Gregory, E. Zika Virus Response, T. Laboratory, Cdc, and Cdc. 2016. Patterns in Zika Virus Testing and Infection, by Report of Symptoms and Pregnancy Status - United States, January 3-March 5, 2016. *MMWR Morb Mortal Wkly Rep* 65:395-399.

Davidson, A., S. Slavinski, K. Komoto, J. Rakeman, and D. Weiss. 2016. Suspected Female-to-Male Sexual Transmission of Zika Virus - New York City, 2016. *MMWR Morb Mortal Wkly Rep* 65:716-717.

de Alwis, R., S.A. Smith, N.P. Olivarez, W.B. Messer, J.P. Huynh, W.M. Wahala, L.J. White, M.S. Diamond, R.S. Baric, J.E. Crowe, Jr., and A.M. de Silva. 2012.

Identification of human neutralizing antibodies that bind to complex epitopes on dengue virions. *Proc Natl Acad Sci U S A* 109:7439-7444.

de Oliveira, W.K., G.V.A. de Franca, E.H. Carmo, B.B. Duncan, R. de Souza Kuchenbecker, and M.I. Schmidt. 2017. Infection-related microcephaly after the 2015 and 2016 Zika virus outbreaks in Brazil: a surveillance-based analysis. *Lancet* 390:861-870.

Dejnirattisai, W., P. Supasa, W. Wongwiwat, A. Rouvinski, G. Barba-Spaeth, T. Duangchinda, A. Sakuntabhai, V.M. Cao-Lormeau, P. Malasit, F.A. Rey, J. Mongkolsapaya, and G.R. Screaton. 2016. Dengue virus sero-cross-reactivity drives antibody-dependent enhancement of infection with zika virus. *Nat Immunol* 17:1102-1108.

Dejnirattisai, W., W. Wongwiwat, S. Supasa, X. Zhang, X. Dai, A. Rouvinski, A. Jumnainsong, C. Edwards, N.T. Quyen, T. Duangchinda, J.M. Grimes, W.Y. Tsai, C.Y. Lai, W.K. Wang, P. Malasit, J. Farrar, C.P. Simmons, Z.H. Zhou, F.A. Rey, J. Mongkolsapaya, and G.R. Screaton. 2015. A new class of highly potent, broadly neutralizing antibodies isolated from viremic patients infected with dengue virus. *Nat Immunol* 16:170-177.

Delaloye, J., T. Roger, Q.G. Steiner-Tardivel, D. Le Roy, M. Knaup Reymond, S. Akira, V. Petrilli, C.E. Gomez, B. Perdiguero, J. Tschopp, G. Pantaleo, M. Esteban, and T. Calandra. 2009. Innate immune sensing of modified vaccinia virus Ankara (MVA) is mediated by TLR2-TLR6, MDA-5 and the NALP3 inflammasome. *PLoS Pathog* 5:e1000480.

Delaney, A., C. Mai, A. Smoots, J. Cragan, S. Ellington, P. Langlois, R. Breidenbach, J. Fornoff, J. Dunn, M. Yazdy, N. Scotto-Rosato, J. Sweatlock, D. Fox, J. Palacios, N. Forestieri, V. Leedom, M. Smiley, A. Nance, H. Lake-Burger, P. Romitti, C. Fall, M.V. Prado, J. Barton, J.M. Bryan, W. Arias, S.V. Brown, J. Kimura, S. Mann, B. Martin, L. Orantes, A. Taylor, J. Nahabedian, A. Akosa, Z. Song, S. Martin, R. Ramlal, C. Shapiro-Mendoza, J. Isenburg, C.A. Moore, S. Gilboa, and M.A. Honein. 2018. Population-Based Surveillance of Birth Defects Potentially Related to Zika Virus Infection - 15 States and U.S. Territories, 2016. *MMWR Morb Mortal Wkly Rep* 67:91-96.

Delorme-Axford, E., R.B. Donker, J.F. Mouillet, T. Chu, A. Bayer, Y. Ouyang, T. Wang, D.B. Stolz, S.N. Sarkar, A.E. Morelli, Y. Sadovsky, and C.B. Coyne. 2013. Human placental trophoblasts confer viral resistance to recipient cells. *Proc Natl Acad Sci U S A* 110:12048-12053.

Deng, Y.Q., J.X. Dai, G.H. Ji, T. Jiang, H.J. Wang, H.O. Yang, W.L. Tan, R. Liu, M. Yu, B.X. Ge, Q.Y. Zhu, E.D. Qin, Y.J. Guo, and C.F. Qin. 2011. A broadly flavivirus cross-neutralizing monoclonal antibody that recognizes a novel epitope within the fusion loop of E protein. *PLoS One* 6:e16059.

Dhodapkar, K.M., D. Banerjee, J. Connolly, A. Kukreja, E. Matayeva, M.C. Veri, J.V. Ravetch, R.M. Steinman, and M.V. Dhodapkar. 2007. Selective blockade of the inhibitory Fcgamma receptor (FcgammaRIIB) in human dendritic cells and monocytes induces a type I interferon response program. *J Exp Med* 204:1359-1369.

Diaz, C., L. Lin, L.J. Martinez, K.H. Eckels, M. Campos, R.G. Jarman, R. De La Barrera, E. Lepine, J.F. Toussaint, I. Febo, B.L. Innis, S.J. Thomas, and A.C. Schmidt. 2018. Phase 1 Randomized Study of a Tetravalent Dengue Purified Inactivated Vaccine in Healthy Adults from Puerto Rico. *Am J Trop Med Hyg*

Dick, G.W., S.F. Kitchen, and A.J. Haddow. 1952. Zika virus. I. Isolations and serological specificity. *Trans R Soc Trop Med Hyg* 46:509-520.

Dowall, S.D., V.A. Graham, E. Rayner, B. Atkinson, G. Hall, R.J. Watson, A. Bosworth, L.C. Bonney, S. Kitchen, and R. Hewson. 2016. A Susceptible Mouse Model for Zika Virus Infection. *PLoS Negl Trop Dis* 10:e0004658.

Dowd, K.A., C.R. DeMaso, R.S. Pelc, S.D. Speer, A.R.Y. Smith, L. Goo, D.J. Platt, J.R. Mascola, B.S. Graham, M.J. Mulligan, M.S. Diamond, J.E. Ledgerwood, and T.C. Pierson. 2016. Broadly Neutralizing Activity of Zika Virus-Immune Sera Identifies a Single Viral Serotype. *Cell Rep* 16:1485-1491.

Driggers, R.W., C.Y. Ho, E.M. Korhonen, S. Kuivanen, A.J. Jaaskelainen, T. Smura, A. Rosenberg, D.A. Hill, R.L. DeBiasi, G. Vezina, J. Timofeev, F.J. Rodriguez, L. Levanov, J. Razak, P. Iyengar, A. Hennenfent, R. Kennedy, R. Lanciotti, A. du Plessis, and O. Vapalahti. 2016. Zika Virus Infection with Prolonged Maternal Viremia and Fetal Brain Abnormalities. *N Engl J Med* 374:2142-2151.

Dudley, D.M., M.T. Aliota, E.L. Mohr, A.M. Weiler, G. Lehrer-Brey, K.L. Weisgrau, M.S. Mohns, M.E. Breitbach, M.N. Rasheed, C.M. Newman, D.D. Gellerup, L.H. Moncla, J. Post, N. Schultz-Darken, M.L. Schotzko, J.M. Hayes, J.A. Eudailey, M.A. Moody, S.R. Permar, S.L. O'Connor, E.G. Rakasz, H.A. Simmons, S. Capuano, T.G. Golos, J.E. Osorio, T.C. Friedrich, and D.H. O'Connor. 2016. A rhesus macaque model of Asian-lineage Zika virus infection. *Nat Commun* 7:12204.

Duffy, M.R., T.H. Chen, W.T. Hancock, A.M. Powers, J.L. Kool, R.S. Lanciotti, M. Pretrick, M. Marfel, S. Holzbauer, C. Dubray, L. Guillaumot, A. Griggs, M. Bel, A.J. Lambert, J. Laven, O. Kosoy, A. Panella, B.J. Biggerstaff, M. Fischer, and E.B. Hayes. 2009. Zika virus outbreak on Yap Island, Federated States of Micronesia. *N Engl J Med* 360:2536-2543.

Egli, A., D.M. Santer, D. O'Shea, D.L. Tyrrell, and M. Houghton. 2014. The impact of the interferon-lambda family on the innate and adaptive immune response to viral infections. *Emerg Microbes Infect* 3:e51.

El Costa, H., J. Gouilly, J.M. Mansuy, Q. Chen, C. Levy, G. Cartron, F. Veas, R. Al-Daccak, J. Izopet, and N. Jabrane-Ferrat. 2016. ZIKA virus reveals broad tissue and cell tropism during the first trimester of pregnancy. *Sci Rep* 6:35296.

Errett, J.S., M.S. Suthar, A. McMillan, M.S. Diamond, and M. Gale, Jr. 2013. The essential, nonredundant roles of RIG-I and MDA5 in detecting and controlling West Nile virus infection. *J Virol* 87:11416-11425.

Faria, N.R., R. Azevedo, M.U.G. Kraemer, R. Souza, M.S. Cunha, S.C. Hill, J. Theze, M.B. Bonsall, T.A. Bowden, I. Rissanen, I.M. Rocco, J.S. Nogueira, A.Y. Maeda, F. Vasami, F.L.L. Macedo, A. Suzuki, S.G. Rodrigues, A.C.R. Cruz, B.T. Nunes, D.B.A. Medeiros, D.S.G. Rodrigues, A.L.N. Queiroz, E.V.P. da Silva, D.F. Henriques, E.S.T. da Rosa, C.S. de Oliveira, L.C. Martins, H.B. Vasconcelos, L.M.N. Casseb, D.B. Simith, J.P. Messina, L. Abade, J. Lourenco, L.C.J. Alcantara, M.M. de Lima, M. Giovanetti, S.I. Hay, R.S. de Oliveira, P.D.S. Lemos, L.F. de Oliveira, C.P.S. de Lima, S.P. da Silva, J.M. de Vasconcelos, L. Franco, J.F. Cardoso, J. Vianez-Junior, D. Mir, G. Bello, E. Delatorre, K. Khan, M. Creatore, G.E. Coelho, W.K. de Oliveira, R. Tesh, O.G. Pybus, M.R.T. Nunes, and P.F.C. Vasconcelos. 2016. Zika virus in the Americas: Early epidemiological and genetic findings. *Science* 352:345-349.

Fernandez, E., W. Dejnirattisai, B. Cao, S.M. Scheaffer, P. Supasa, W. Wongwiwat, P. Esakky, A. Drury, J. Mongkolsapaya, K.H. Moley, I.U. Mysorekar, G.R. Screaton, and M.S. Diamond. 2017. Human antibodies to the dengue virus E-dimer epitope have therapeutic activity against Zika virus infection. *Nat Immunol* 18:1261-1269.

Fitzgerald, B., C. Boyle, and M.A. Honein. 2018. Birth Defects Potentially Related to Zika Virus Infection During Pregnancy in the United States. *JAMA*

Flipse, J., M.A. Diosa-Toro, T.E. Hoornweg, D.P. van de Pol, S. Urcuqui-Inchima, and J.M. Smit. 2016. Antibody-Dependent Enhancement of Dengue Virus Infection in Primary Human Macrophages; Balancing Higher Fusion against Antiviral Responses. *Sci Rep* 6:29201.

Fonseca, K., B. Meatherall, D. Zarra, M. Drebot, J. MacDonald, K. Pabbaraju, S. Wong, P. Webster, R. Lindsay, and R. Tellier. 2014. First case of Zika virus infection in a returning Canadian traveler. *Am J Trop Med Hyg* 91:1035-1038.

Foo, S.S., W. Chen, Y. Chan, J.W. Bowman, L.C. Chang, Y. Choi, J.S. Yoo, J. Ge, G. Cheng, A. Bonnin, K. Nielsen-Saines, P. Brasil, and J.U. Jung. 2017. Asian Zika virus strains target CD14(+) blood monocytes and induce M2-skewed immunosuppression during pregnancy. *Nat Microbiol* 2:1558-1570.

Foy, B.D., K.C. Kobylinski, J.L. Chilson Foy, B.J. Blitvich, A. Travassos da Rosa, A.D. Haddow, R.S. Lanciotti, and R.B. Tesh. 2011. Probable non-vector-borne transmission of Zika virus, Colorado, USA. *Emerg Infect Dis* 17:880-882.

Franca, G.V., L. Schuler-Faccini, W.K. Oliveira, C.M. Henriques, E.H. Carmo, V.D. Pedi, M.L. Nunes, M.C. Castro, S. Serruya, M.F. Silveira, F.C. Barros, and C.G. Victora. 2016. Congenital Zika virus syndrome in Brazil: a case series of the first 1501 livebirths with complete investigation. *Lancet* 388:891-897.

Fredericksen, B.L., B.C. Keller, J. Fornek, M.G. Katze, and M. Gale, Jr. 2008. Establishment and maintenance of the innate antiviral response to West Nile Virus involves both RIG-I and MDA5 signaling through IPS-1. *J Virol* 82:609-616.

Frumence, E., M. Roche, P. Krejbich-Trotot, C. El-Kalamouni, B. Nativel, P. Rondeau, D. Misse, G. Gadea, W. Viranaicken, and P. Despres. 2016. The South Pacific epidemic strain of Zika virus replicates efficiently in human epithelial A549 cells leading to IFN-beta production and apoptosis induction. *Virology* 493:217-226.

Gack, M.U., R.A. Albrecht, T. Urano, K.S. Inn, I.C. Huang, E. Carnero, M. Farzan, S. Inoue, J.U. Jung, and A. Garcia-Sastre. 2009. Influenza A virus NS1 targets the ubiquitin ligase TRIM25 to evade recognition by the host viral RNA sensor RIG-I. *Cell Host Microbe* 5:439-449.

Gack, M.U., E. Nistal-Villan, K.S. Inn, A. Garcia-Sastre, and J.U. Jung. 2010. Phosphorylation-mediated negative regulation of RIG-I antiviral activity. *J Virol* 84:3220-3229.

Gack, M.U., Y.C. Shin, C.H. Joo, T. Urano, C. Liang, L. Sun, O. Takeuchi, S. Akira, Z. Chen, S. Inoue, and J.U. Jung. 2007. TRIM25 RING-finger E3 ubiquitin ligase is essential for RIG-I-mediated antiviral activity. *Nature* 446:916-920.

Gallichotte, E.N., D.G. Widman, B.L. Yount, W.M. Wahala, A. Durbin, S. Whitehead, C.A. Sariol, J.E. Crowe, Jr., A.M. de Silva, and R.S. Baric. 2015. A new quaternary structure epitope on dengue virus serotype 2 is the target of durable type-specific neutralizing antibodies. *MBio* 6:e01461-01415.

Garcez, P.P., E.C. Loiola, R. Madeiro da Costa, L.M. Higa, P. Trindade, R. Delvecchio, J.M. Nascimento, R. Brindeiro, A. Tanuri, and S.K. Rehen. 2016. Zika virus impairs growth in human neurospheres and brain organoids. *Science* 352:816-818.

Goulet, M.L., D. Olagnier, Z. Xu, S. Paz, S.M. Belgnaoui, E.I. Lafferty, V. Janelle, M. Arguello, M. Paquet, K. Ghneim, S. Richards, A. Smith, P. Wilkinson, M. Cameron, U. Kalinke, S. Qureshi, A. Lamarre, E.K. Haddad, R.P. Sekaly, S. Peri, S. Balachandran, R. Lin, and J. Hiscott. 2013. Systems analysis of a RIG-I agonist inducing broad spectrum inhibition of virus infectivity. *PLoS Pathog* 9:e1003298.

Govero, J., P. Esakky, S.M. Scheaffer, E. Fernandez, A. Drury, D.J. Platt, M.J. Gorman, J.M. Richner, E.A. Caine, V. Salazar, K.H. Moley, and M.S. Diamond. 2016. Zika virus infection damages the testes in mice. *Nature*

Graham, J.B., S. Thomas, J. Swarts, A.A. McMillan, M.T. Ferris, M.S. Suthar, P.M. Treuting, R. Ireton, M. Gale, Jr., and J.M. Lund. 2015. Genetic diversity in the collaborative cross model recapitulates human West Nile virus disease outcomes. *MBio* 6:e00493-00415.

Grant, A., S.S. Ponia, S. Tripathi, V. Balasubramaniam, L. Miorin, M. Sourisseau, M.C. Schwarz, M.P. Sanchez-Seco, M.J. Evans, S.M. Best, and A. Garcia-Sastre. 2016. Zika Virus Targets Human STAT2 to Inhibit Type I Interferon Signaling. *Cell Host Microbe* 19:882-890.

Guo, B., and G. Cheng. 2007. Modulation of the interferon antiviral response by the TBK1/IKKi adaptor protein TANK. *J Biol Chem* 282:11817-11826.

Haddow, A.D., A.J. Schuh, C.Y. Yasuda, M.R. Kasper, V. Heang, R. Huy, H. Guzman, R.B. Tesh, and S.C. Weaver. 2012. Genetic characterization of Zika virus strains: geographic expansion of the Asian lineage. *PLoS Negl Trop Dis* 6:e1477.

Haddow, A.J., M.C. Williams, J.P. Woodall, D.I. Simpson, and L.K. Goma. 1964. Twelve Isolations of Zika Virus from Aedes (Stegomyia) Africanus (Theobald) Taken in and above a Uganda Forest. *Bull World Health Organ* 31:57-69.

Halai, U.A., K. Nielsen-Saines, M.L. Moreira, P.C. de Sequeira, J.P. Pereira, A.A. Zin, J. Cherry, C.R. Gabaglia, S.L. Gaw, K. Adachi, I. Tsui, J.H. Pilotto, R.R. Nogueira, A.M.B. de Filippis, and P. Brasil. 2017. Maternal Zika Virus Disease Severity, Virus Load, Prior Dengue Antibodies, and Their Relationship to Birth Outcomes. *Clin Infect Dis* 65:877-883.

Halstead, S.B. 2003. Neutralization and antibody-dependent enhancement of dengue viruses. *Advances in virus research* 60:421-467.

Hamel, R., O. Dejarnac, S. Wichit, P. Ekchariyawat, A. Neyret, N. Luplertlop, M. Perera-Lecoin, P. Surasombatpattana, L. Talignani, F. Thomas, V.M. Cao-Lormeau, V. Choumet, L. Briant, P. Despres, A. Amara, H. Yssel, and D. Misse. 2015. Biology of Zika Virus Infection in Human Skin Cells. *J Virol* 89:8880-8896.

Hanners, N.W., J.L. Eitson, N. Usui, R.B. Richardson, E.M. Wexler, G. Konopka, and J.W. Schoggins. 2016. Western Zika Virus in Human Fetal Neural Progenitors Persists Long Term with Partial Cytopathic and Limited Immunogenic Effects. *Cell Rep* 15:2315-2322.

Hayes, E.B. 2009. Zika virus outside Africa. *Emerg Infect Dis* 15:1347-1350.

Hertzog, J., A.G. Dias Junior, R.E. Rigby, C.L. Donald, A. Mayer, E. Sezgin, C. Song, B. Jin, P. Hublitz, C. Eggeling, A. Kohl, and J. Rehwinkel. 2018. Infection with a Brazilian isolate of Zika virus generates RIG-I stimulatory RNA and the viral NS5 protein blocks type I IFN induction and signaling. *Eur J Immunol*

Hessell, A.J., L. Hangartner, M. Hunter, C.E. Havenith, F.J. Beurskens, J.M. Bakker, C.M. Lanigan, G. Landucci, D.N. Forthal, P.W. Parren, P.A. Marx, and D.R. Burton. 2007. Fc receptor but not complement binding is important in antibody protection against HIV. *Nature* 449:101-104.

Hoen, B., B. Schaub, A.L. Funk, V. Ardillon, M. Boullard, A. Cabie, C. Callier, G. Carles, S. Cassadou, R. Cesaire, M. Douine, C. Herrmann-Storck, P. Kadhel, C. Laouenan, Y. Madec, A. Monthieux, M. Nacher, F. Najioullah, D. Rousset, C. Ryan, K. Schepers, S. Stegmann-Planchard, B. Tressieres, J.L. Volumenie, S. Yassinguezo, E. Janky, and A. Fontanet. 2018. Pregnancy Outcomes after ZIKV Infection in French Territories in the Americas. *N Engl J Med* 378:985-994.

Honein, M.A., A.L. Dawson, E.E. Petersen, A.M. Jones, E.H. Lee, M.M. Yazdy, N. Ahmad, J. Macdonald, N. Evert, A. Bingham, S.R. Ellington, C.K. Shapiro-

Mendoza, T. Oduyebo, A.D. Fine, C.M. Brown, J.N. Sommer, J. Gupta, P. Cavicchia, S. Slavinski, J.L. White, S.M. Owen, L.R. Petersen, C. Boyle, D. Meaney-Delman, D.J. Jamieson, and U.S.Z.P.R. Collaboration. 2017. Birth Defects Among Fetuses and Infants of US Women With Evidence of Possible Zika Virus Infection During Pregnancy. *JAMA* 317:59-68.

Horner, S.M., H.M. Liu, H.S. Park, J. Briley, and M. Gale, Jr. 2011. Mitochondrial-associated endoplasmic reticulum membranes (MAM) form innate immune synapses and are targeted by hepatitis C virus. *Proc Natl Acad Sci U S A* 108:14590-14595.

Horner, S.M., H.S. Park, and M. Gale, Jr. 2012. Control of innate immune signaling and membrane targeting by the Hepatitis C virus NS3/4A protease are governed by the NS3 helix alpha0. *J Virol* 86:3112-3120.

Hornung, V., J. Ellegast, S. Kim, K. Brzozka, A. Jung, H. Kato, H. Poeck, S. Akira, K.K. Conzelmann, M. Schlee, S. Endres, and G. Hartmann. 2006. 5'-Triphosphate RNA is the ligand for RIG-I. *Science* 314:994-997.

Hou, W., N. Armstrong, L.A. Obwolo, M. Thomas, X. Pang, K.S. Jones, and Q. Tang. 2017. Determination of the Cell Permissiveness Spectrum, Mode of RNA Replication, and RNA-Protein Interaction of Zika Virus. *BMC Infect Dis* 17:239.

Hugot, J.P., M. Chamaillard, H. Zouali, S. Lesage, J.P. Cezard, J. Belaiche, S. Almer, C. Tysk, C.A. O'Morain, M. Gassull, V. Binder, Y. Finkel, A. Cortot, R. Modigliani, P. Laurent-Puig, C. Gower-Rousseau, J. Macry, J.F. Colombel, M. Sahbatou, and G. Thomas. 2001. Association of NOD2 leucine-rich repeat variants with susceptibility to Crohn's disease. *Nature* 411:599-603.

Imaizumi, T., S. Aratani, T. Nakajima, M. Carlson, T. Matsumiya, K. Tanji, K. Ookawa, H. Yoshida, S. Tsuchida, T.M. McIntyre, S.M. Prescott, G.A. Zimmerman, and K. Satoh. 2002. Retinoic acid-inducible gene-I is induced in endothelial cells by LPS and regulates expression of COX-2. *Biochem Biophys Res Commun* 292:274-279.

Ioos, S., H.P. Mallet, I. Leparc Goffart, V. Gauthier, T. Cardoso, and M. Herida. 2014. Current Zika virus epidemiology and recent epidemics. *Med Mal Infect* 44:302-307.

Jaenisch, T., K.D. Rosenberger, C. Brito, O. Brady, P. Brasil, and E.T. Marques. 2017. Risk of microcephaly after Zika virus infection in Brazil, 2015 to 2016. *Bull World Health Organ* 95:191-198.

Jagger, B.W., J.J. Miner, B. Cao, N. Arora, A.M. Smith, A. Kovacs, I.U. Mysorekar, C.B. Coyne, and M.S. Diamond. 2017. Gestational Stage and IFN-lambda Signaling Regulate ZIKV Infection In Utero. *Cell Host Microbe* 22:366-376 e363.

Johnson, E.L., and R. Chakraborty. 2012. Placental Hofbauer cells limit HIV-1 replication and potentially offset mother to child transmission (MTCT) by induction of immunoregulatory cytokines. *Retrovirology* 9:101.

Johnson, E.L., H. Chu, S.N. Byrareddy, P. Spearman, and R. Chakraborty. 2015. Placental Hofbauer cells assemble and sequester HIV-1 in tetraspanin-positive compartments that are accessible to broadly neutralizing antibodies. *J Int AIDS Soc* 18:19385.

Jonathan J. Miner, B.C., Jennifer Govero, Amber M. Smith, Estefania Fernandez, Omar H. Cabrera, Charise Garber, Michelle Noll, Robyn S. Klein, Kevin K. Noguchi, Indira U. Mysorekar, Michael S. Diamond. 2016. Zika Virus Infection during Pregnancy in Mice Causes Placental Damage and Fetal Demise. *Cell*

Julander, J.G., Q.A. Winger, A.L. Olsen, C.W. Day, R.W. Sidwell, and J.D. Morrey. 2005. Treatment of West Nile virus-infected mice with reactive immunoglobulin reduces fetal titers and increases dam survival. *Antiviral Res* 65:79-85.

Julander, J.G., Q.A. Winger, L.F. Rickords, P.Y. Shi, M. Tilgner, I. Binduga-Gajewska, R.W. Sidwell, and J.D. Morrey. 2006. West Nile virus infection of the placenta. *Virology* 347:175-182.

Jun, S.R., T.M. Wassenaar, V. Wanchai, P. Patumcharoenpol, I. Nookaew, and D.W. Ussery. 2017. Suggested mechanisms for Zika virus causing microcephaly: what do the genomes tell us? *BMC Bioinformatics* 18:471.

Jurado, K.A., M.K. Simoni, Z. Tang, R. Uraki, J. Hwang, S. Householder, M. Wu, B.D. Lindenbach, V.M. Abrahams, S. Guller, and E. Fikrig. 2016. Zika virus productively infects primary human placenta-specific macrophages. *JCI Insight* 1:

Kameda, T., M. Koyama, N. Matsuzaki, T. Taniguchi, F. Saji, and O. Tanizawa. 1991. Localization of three subtypes of Fc gamma receptors in human placenta by immunohistochemical analysis. *Placenta* 12:15-26.

Kato, H., O. Takeuchi, E. Mikamo-Satoh, R. Hirai, T. Kawai, K. Matsushita, A. Hiiragi, T.S. Dermody, T. Fujita, and S. Akira. 2008. Length-dependent recognition of double-stranded ribonucleic acids by retinoic acid-inducible gene-I and melanoma differentiation-associated gene 5. *J Exp Med* 205:1601-1610.

Kato, H., O. Takeuchi, S. Sato, M. Yoneyama, M. Yamamoto, K. Matsui, S. Uematsu, A. Jung, T. Kawai, K.J. Ishii, O. Yamaguchi, K. Otsu, T. Tsujimura, C.S. Koh, C. Reis e Sousa, Y. Matsuura, T. Fujita, and S. Akira. 2006. Differential roles of MDA5 and RIG-I helicases in the recognition of RNA viruses. *Nature* 441:101-105.

Katzelnick, L.C., L. Gresh, M.E. Halloran, J.C. Mercado, G. Kuan, A. Gordon, A. Balmaseda, and E. Harris. 2017. Antibody-dependent enhancement of severe dengue disease in humans. *Science* 358:929-932.

Kaul, A., I. Woerz, P. Meuleman, G. Leroux-Roels, and R. Bartenschlager. 2007. Cell culture adaptation of hepatitis C virus and in vivo viability of an adapted variant. *J Virol* 81:13168-13179.

Keller, B.C., B.L. Fredericksen, M.A. Samuel, R.E. Mock, P.W. Mason, M.S. Diamond, and M. Gale, Jr. 2006. Resistance to alpha/beta interferon is a determinant of West Nile virus replication fitness and virulence. *J Virol* 80:9424-9434.

Kliks, S.C., A. Nisalak, W.E. Brandt, L. Wahl, and D.S. Burke. 1989. Antibody-dependent enhancement of dengue virus growth in human monocytes as a risk factor for dengue hemorrhagic fever. *Am J Trop Med Hyg* 40:444-451.

Klimstra, W.B., K.D. Ryman, and R.E. Johnston. 1998. Adaptation of Sindbis virus to BHK cells selects for use of heparan sulfate as an attachment receptor. *Journal of virology* 72:7357-7366.

Koi, H., J. Zhang, and S. Parry. 2001. The mechanisms of placental viral infection. *Ann N Y Acad Sci* 943:148-156.

Komuro, A., Y. Homma, T. Negoro, G.N. Barber, and C.M. Horvath. 2016. The TAR-RNA binding protein is required for immunoresponses triggered by Cardiovirus infection. *Biochem Biophys Res Commun* 480:187-193.

Komuro, A., and C.M. Horvath. 2006. RNA- and virus-independent inhibition of antiviral signaling by RNA helicase LGP2. *J Virol* 80:12332-12342.

Koraka, P., C. Suharti, T.E. Setiati, A.T. Mairuhu, E. Van Gorp, C.E. Hack, M. Juffrie, J. Sutaryo, G.M. Van Der Meer, J. Groen, and A.D. Osterhaus. 2001. Kinetics of dengue virus-specific serum immunoglobulin classes and subclasses correlate with clinical outcome of infection. *J Clin Microbiol* 39:4332-4338.

Kristoffersen, E.K., E. Ulvestad, C.A. Vedeler, and R. Matre. 1990. Fc gamma receptor heterogeneity in the human placenta. *Scand J Immunol* 32:561-564.

Kulkarni, R.R., M.A. Rasheed, S.K. Bhaumik, P. Ranjan, W. Cao, C. Davis, K. Marisetti, S. Thomas, S. Gangappa, S. Sambhara, and K. Murali-Krishna. 2014. Activation

of the RIG-I pathway during influenza vaccination enhances the germinal center reaction, promotes T follicular helper cell induction, and provides a dose-sparing effect and protective immunity. *J Virol* 88:13990-14001.

Kumar, A., S. Hou, A.M. Airo, D. Limonta, V. Mancinelli, W. Branton, C. Power, and T.C. Hobman. 2016. Zika virus inhibits type-I interferon production and downstream signaling. *EMBO Rep* 17:1766-1775.

Lai, C.Y., W.Y. Tsai, S.R. Lin, C.L. Kao, H.P. Hu, C.C. King, H.C. Wu, G.J. Chang, and W.K. Wang. 2008. Antibodies to envelope glycoprotein of dengue virus during the natural course of infection are predominantly cross-reactive and recognize epitopes containing highly conserved residues at the fusion loop of domain II. *Journal of virology* 82:6631-6643.

Lanciotti, R.S., O.L. Kosoy, J.J. Laven, J.O. Velez, A.J. Lambert, A.J. Johnson, S.M. Stanfield, and M.R. Duffy. 2008. Genetic and serologic properties of Zika virus associated with an epidemic, Yap State, Micronesia, 2007. *Emerg Infect Dis* 14:1232-1239.

Lanciotti, R.S., A.J. Lambert, M. Holodniy, S. Saavedra, and C. Signor Ldel. 2016. Phylogeny of Zika Virus in Western Hemisphere, 2015. *Emerg Infect Dis* 22:933-935.

Lang, X., T. Tang, T. Jin, C. Ding, R. Zhou, and W. Jiang. 2017. TRIM65-catalized ubiquitination is essential for MDA5-mediated antiviral innate immunity. *J Exp Med* 214:459-473.

Laurent-Rolle, M., E.F. Boer, K.J. Lubick, J.B. Wolfinbarger, A.B. Carmody, B. Rockx, W. Liu, J. Ashour, W.L. Shupert, M.R. Holbrook, A.D. Barrett, P.W. Mason, M.E. Bloom, A. Garcia-Sastre, A.A. Khromykh, and S.M. Best. 2010. The NS5 protein of the virulent West Nile virus NY99 strain is a potent antagonist of type I interferon-mediated JAK-STAT signaling. *J Virol* 84:3503-3515.

Laurent-Rolle, M., J. Morrison, R. Rajsbaum, J.M. Macleod, G. Pisanelli, A. Pham, J. Ayllon, L. Miorin, C. Martinez-Romero, B.R. tenOever, and A. Garcia-Sastre. 2014. The interferon signaling antagonist function of yellow fever virus NS5 protein is activated by type I interferon. *Cell Host Microbe* 16:314-327.

Lazear, H.M., B.P. Daniels, A.K. Pinto, A.C. Huang, S.C. Vick, S.E. Doyle, M. Gale, Jr., R.S. Klein, and M.S. Diamond. 2015a. Interferon-lambda restricts West Nile virus neuroinvasion by tightening the blood-brain barrier. *Sci Transl Med* 7:284ra259.

Lazear, H.M., and M.S. Diamond. 2016. Zika Virus: New Clinical Syndromes and Its Emergence in the Western Hemisphere. *J Virol* 90:4864-4875.

Lazear, H.M., J. Govero, A.M. Smith, D.J. Platt, E. Fernandez, J.J. Miner, and M.S. Diamond. 2016. A Mouse Model of Zika Virus Pathogenesis. *Cell Host Microbe* 19:720-730.

Lazear, H.M., T.J. Nice, and M.S. Diamond. 2015b. Interferon-lambda: Immune Functions at Barrier Surfaces and Beyond. *Immunity* 43:15-28.

Lazear, H.M., A.K. Pinto, M.R. Vogt, M. Gale, Jr., and M.S. Diamond. 2011. Beta interferon controls West Nile virus infection and pathogenesis in mice. *J Virol* 85:7186-7194.

Lenardo, M.J., C.M. Fan, T. Maniatis, and D. Baltimore. 1989. The involvement of NF-kappa B in beta-interferon gene regulation reveals its role as widely inducible mediator of signal transduction. *Cell* 57:287-294.

Lesniewska, E., and M. Boguta. 2017. Novel layers of RNA polymerase III control affecting tRNA gene transcription in eukaryotes. *Open Biol* 7:

Leta, S., T.J. Beyene, E.M. De Clercq, K. Amenu, M.U.G. Kraemer, and C.W. Revie. 2018. Global risk mapping for major diseases transmitted by Aedes aegypti and Aedes albopictus. *Int J Infect Dis* 67:25-35.

Lewis, S.H., H.E. Fox, C. Reynolds-Kohler, and J.A. Nelson. 1990. HIV-1 in trophoblastic and villous Hofbauer cells, and haematological precursors in eight-week fetuses. *The Lancet* 335:565-568.

Li, C., D. Xu, Q. Ye, S. Hong, Y. Jiang, X. Liu, N. Zhang, L. Shi, C.F. Qin, and Z. Xu. 2016a. Zika Virus Disrupts Neural Progenitor Development and Leads to Microcephaly in Mice. *Cell Stem Cell*

Li, X., C. Lu, M. Stewart, H. Xu, R.K. Strong, T. Igumenova, and P. Li. 2009a. Structural basis of double-stranded RNA recognition by the RIG-I like receptor MDA5. *Arch Biochem Biophys* 488:23-33.

Li, X., C.T. Ranjith-Kumar, M.T. Brooks, S. Dharmaiah, A.B. Herr, C. Kao, and P. Li. 2009b. The RIG-I-like receptor LGP2 recognizes the termini of double-stranded RNA. *J Biol Chem* 284:13881-13891.

Li, X.F., H.L. Dong, X.Y. Huang, Y.F. Qiu, H.J. Wang, Y.Q. Deng, N.N. Zhang, Q. Ye, H. Zhao, Z.Y. Liu, H. Fan, X.P. An, S.H. Sun, B. Gao, Y.Z. Fa, Y.G. Tong, F.C. Zhang, G.F. Gao, W.C. Cao, P.Y. Shi, and C.F. Qin. 2016b. Characterization of a 2016 Clinical Isolate of Zika Virus in Non-human Primates. *EBioMedicine* 12:170-177.

Libraty, D.H., T.P. Endy, H.S. Houng, S. Green, S. Kalayanarooj, S. Suntayakorn, W. Chansiriwongs, D.W. Vaughn, A. Nisalak, F.A. Ennis, and A.L. Rothman. 2002. Differing influences of virus burden and immune activation on disease severity in secondary dengue-3 virus infections. *J Infect Dis* 185:1213-1221.

Libraty, D.H., S. Pichyangkul, C. Ajariyakhajorn, T.P. Endy, and F.A. Ennis. 2001. Human dendritic cells are activated by dengue virus infection: enhancement by gamma interferon and implications for disease pathogenesis. *J Virol* 75:3501-3508.

Likos, A., I. Griffin, A.M. Bingham, D. Stanek, M. Fischer, S. White, J. Hamilton, L. Eisenstein, D. Atrubin, P. Mulay, B. Scott, P. Jenkins, D. Fernandez, E. Rico, L. Gillis, R. Jean, M. Cone, C. Blackmore, J. McAllister, C. Vasquez, L. Rivera, and C. Philip. 2016. Local Mosquito-Borne Transmission of Zika Virus - Miami-Dade and Broward Counties, Florida, June-August 2016. *MMWR Morb Mortal Wkly Rep* 65:1032-1038.

Liu, H.M., Y.M. Loo, S.M. Horner, G.A. Zornetzer, M.G. Katze, and M. Gale, Jr. 2012. The mitochondrial targeting chaperone 14-3-3epsilon regulates a RIG-I translocon that mediates membrane association and innate antiviral immunity. *Cell Host Microbe* 11:528-537.

Liu, S., X. Cai, J. Wu, Q. Cong, X. Chen, T. Li, F. Du, J. Ren, Y.T. Wu, N.V. Grishin, and Z.J. Chen. 2015. Phosphorylation of innate immune adaptor proteins MAVS, STING, and TRIF induces IRF3 activation. *Science* 347:aaa2630.

Liu, S., L.J. DeLalio, B.E. Isakson, and T.T. Wang. 2016. AXL-Mediated Productive Infection of Human Endothelial Cells by Zika Virus. *Circ Res* 119:1183-1189.

Loo, Y.M., J. Fornek, N. Crochet, G. Bajwa, O. Perwitasari, L. Martinez-Sobrido, S. Akira, M.A. Gill, A. Garcia-Sastre, M.G. Katze, and M. Gale, Jr. 2008. Distinct RIG-I and MDA5 signaling by RNA viruses in innate immunity. *J Virol* 82:335-345.

Loo, Y.M., and M. Gale, Jr. 2011. Immune signaling by RIG-I-like receptors. *Immunity* 34:680-692.

Love, M.I., W. Huber, and S. Anders. 2014. Moderated estimation of fold change and dispersion for RNA-seq data with DESeq2. *Genome Biol* 15:550.

Lozier, M., L. Adams, M.F. Febo, J. Torres-Aponte, M. Bello-Pagan, K.R. Ryff, J. Munoz-Jordan, M. Garcia, A. Rivera, J.S. Read, S.H. Waterman, T.M. Sharp, and B. Rivera-Garcia. 2016. Incidence of Zika Virus Disease by Age and Sex - Puerto

Rico, November 1, 2015-October 20, 2016. *MMWR Morb Mortal Wkly Rep* 65:1219-1223.

Lu, C., H. Xu, C.T. Ranjith-Kumar, M.T. Brooks, T.Y. Hou, F. Hu, A.B. Herr, R.K. Strong, C.C. Kao, and P. Li. 2010. The structural basis of 5' triphosphate double-stranded RNA recognition by RIG-I C-terminal domain. *Structure* 18:1032-1043.

Luo, H., E.R. Winkelmann, I. Fernandez-Salas, L. Li, S.V. Mayer, R. Danis-Lozano, R.M. Sanchez-Casas, N. Vasilakis, R. Tesh, A.D. Barrett, S.C. Weaver, and T. Wang. 2018. Zika, dengue and yellow fever viruses induce differential anti-viral immune responses in human monocytic and first trimester trophoblast cells. *Antiviral Res* 151:55-62.

Macnamara, F.N. 1954. Zika virus: a report on three cases of human infection during an epidemic of jaundice in Nigeria. *Trans R Soc Trop Med Hyg* 48:139-145.

Maharaj, N.P., E. Wies, A. Stoll, and M.U. Gack. 2012. Conventional protein kinase C-alpha (PKC-alpha) and PKC-beta negatively regulate RIG-I antiviral signal transduction. *J Virol* 86:1358-1371.

Malur, M., M. Gale, Jr., and R.M. Krug. 2012. LGP2 downregulates interferon production during infection with seasonal human influenza A viruses that activate interferon regulatory factor 3. *J Virol* 86:10733-10738.

Manokaran, G., E. Finol, C. Wang, J. Gunaratne, J. Bahl, E.Z. Ong, H.C. Tan, O.M. Sessions, A.M. Ward, D.J. Gubler, E. Harris, M.A. Garcia-Blanco, and E.E. Ooi. 2015. Dengue subgenomic RNA binds TRIM25 to inhibit interferon expression for epidemiological fitness. *Science* 350:217-221.

Manoussaka, M.S., D.J. Jackson, R.J. Lock, S.R. Sooranna, and B.M. Kumpel. 2005. Flow cytometric characterisation of cells of differing densities isolated from human term placentae and enrichment of villous trophoblast cells. *Placenta* 26:308-318.

Mansuy, J.M., M. Dutertre, C. Mengelle, C. Fourcade, B. Marchou, P. Delobel, J. Izopet, and G. Martin-Blondel. 2016. Zika virus: high infectious viral load in semen, a new sexually transmitted pathogen? *Lancet Infect Dis* 16:405.

Marchette, N.J., R. Garcia, and A. Rudnick. 1969. Isolation of Zika virus from Aedes aegypti mosquitoes in Malaysia. *Am J Trop Med Hyg* 18:411-415.

Martines, R.B., J. Bhatnagar, M.K. Keating, L. Silva-Flannery, A. Muehlenbachs, J. Gary, C. Goldsmith, G. Hale, J. Ritter, D. Rollin, W.J. Shieh, K.G. Luz, A.M. Ramos, H.P. Davi, W. Kleber de Oliveria, R. Lanciotti, A. Lambert, and S. Zaki. 2016. Notes from the Field: Evidence of Zika Virus Infection in Brain and Placental Tissues from Two Congenitally Infected Newborns and Two Fetal Losses--Brazil, 2015. *MMWR Morb Mortal Wkly Rep* 65:159-160.

Martinez-Gil, L., P.H. Goff, R. Hai, A. Garcia-Sastre, M.L. Shaw, and P. Palese. 2013. A Sendai virus-derived RNA agonist of RIG-I as a virus vaccine adjuvant. *Journal of virology* 87:1290-1300.

McCarthy, M. 2016. Zika virus was transmitted by sexual contact in Texas, health officials report. *BMJ* 352:i720.

McCracken, M.K., G.D. Gromowski, H.L. Friberg, X. Lin, P. Abbink, R. De La Barrera, K.H. Eckles, L.S. Garver, M. Boyd, D. Jetton, D.H. Barouch, M.C. Wise, B.S. Lewis, J.R. Currier, K. Modjarrad, M. Milazzo, M. Liu, A.B. Mullins, J.R. Putnak, N.L. Michael, R.G. Jarman, and S.J. Thomas. 2017. Impact of prior flavivirus immunity on Zika virus infection in rhesus macaques. *PLoS Pathog* 13:e1006487.

Meaney-Delman, D., S.L. Hills, C. Williams, R.R. Galang, P. Iyengar, A.K. Hennenfent, I.B. Rabe, A. Panella, T. Oduyebo, M.A. Honein, S. Zaki, N. Lindsey, J.A. Lehman, N. Kwit, J. Bertolli, S. Ellington, I. Igbinosa, A.A. Minta, E.E. Petersen,

P. Mead, S.A. Rasmussen, and D.J. Jamieson. 2016. Zika Virus Infection Among U.S. Pregnant Travelers - August 2015-February 2016. *MMWR Morb Mortal Wkly Rep* 65:211-214.

Melo, A.S.O., L. Chimelli, and A. Tanuri. 2017. Congenital Zika Virus Infection: Beyond Neonatal Microcephaly-Reply. *JAMA Neurol* 74:610-611.

Mibayashi, M., L. Martinez-Sobrido, Y.M. Loo, W.B. Cardenas, M. Gale, Jr., and A. Garcia-Sastre. 2007. Inhibition of retinoic acid-inducible gene I-mediated induction of beta interferon by the NS1 protein of influenza A virus. *J Virol* 81:514-524.

Michlmayr, D., and J.K. Lim. 2014. Chemokine receptors as important regulators of pathogenesis during arboviral encephalitis. *Front Cell Neurosci* 8:264.

Miner, J.J., B. Cao, J. Govero, A.M. Smith, E. Fernandez, O.H. Cabrera, C. Garber, M. Noll, R.S. Klein, K.K. Noguchi, I.U. Mysorekar, and M.S. Diamond. 2016. Zika Virus Infection during Pregnancy in Mice Causes Placental Damage and Fetal Demise. *Cell* 165:1081-1091.

Miner, J.J., and M.S. Diamond. 2017. Zika Virus Pathogenesis and Tissue Tropism. *Cell Host Microbe* 21:134-142.

Miorin, L., A.M. Maestre, A. Fernandez-Sesma, and A. Garcia-Sastre. 2017. Antagonism of type I interferon by flaviviruses. *Biochem Biophys Res Commun* 492:587-596.

Mlakar, J., M. Korva, N. Tul, M. Popovic, M. Poljsak-Prijatelj, J. Mraz, M. Kolenc, K. Resman Rus, T. Vesnaver Vipotnik, V. Fabjan Vodusek, A. Vizjak, J. Pizem, M. Petrovec, and T. Avsic Zupanc. 2016. Zika Virus Associated with Microcephaly. *N Engl J Med* 374:951-958.

Morosky, S.A., J. Zhu, A. Mukherjee, S.N. Sarkar, and C.B. Coyne. 2011. Retinoic acid-induced gene-I (RIG-I) associates with nucleotide-binding oligomerization domain-2 (NOD2) to negatively regulate inflammatory signaling. *J Biol Chem* 286:28574-28583.

Moser, L.A., L. Ramirez-Carvajal, V. Puri, S.J. Pauszek, K. Matthews, K.A. Dilley, C. Mullan, J. McGraw, M. Khayat, K. Beeri, A. Yee, V. Dugan, M.T. Heise, M.B. Frieman, L.L. Rodriguez, K.A. Bernard, D.E. Wentworth, T.B. Stockwell, and R.S. Shabman. 2016. A Universal Next-Generation Sequencing Protocol To Generate Noninfectious Barcoded cDNA Libraries from High-Containment RNA Viruses. *mSystems* 1:15.

Motta, I.J., B.R. Spencer, S.G. Cordeiro da Silva, M.B. Arruda, J.A. Dobbin, Y.B. Gonzaga, I.P. Arcuri, R.C. Tavares, E.H. Atta, R.F. Fernandes, D.A. Costa, L.J. Ribeiro, F. Limonte, L.M. Higa, C.M. Voloch, R.M. Brindeiro, A. Tanuri, and O.C. Ferreira, Jr. 2016. Evidence for Transmission of Zika Virus by Platelet Transfusion. *N Engl J Med*

Mukhopadhyay, S., B.S. Kim, P.R. Chipman, M.G. Rossmann, and R.J. Kuhn. 2003. Structure of West Nile virus. *Science* 302:248.

Murali, A., X. Li, C.T. Ranjith-Kumar, K. Bhardwaj, A. Holzenburg, P. Li, and C.C. Kao. 2008. Structure and function of LGP2, a DEX(D/H) helicase that regulates the innate immunity response. *J Biol Chem* 283:15825-15833.

Musso, D., and D.J. Gubler. 2016. Zika Virus. *Clin Microbiol Rev* 29:487-524.

Musso, D., C. Roche, T.X. Nhan, E. Robin, A. Teissier, and V.M. Cao-Lormeau. 2015a. Detection of Zika virus in saliva. *J Clin Virol* 68:53-55.

Musso, D., C. Roche, E. Robin, T. Nhan, A. Teissier, and V.M. Cao-Lormeau. 2015b. Potential sexual transmission of Zika virus. *Emerg Infect Dis* 21:359-361.

Napolitano, L.M., E.G. Jaffray, R.T. Hay, and G. Meroni. 2011. Functional interactions between ubiquitin E2 enzymes and TRIM proteins. *Biochem J* 434:309-319.

Noronha, L., C. Zanluca, M.L. Azevedo, K.G. Luz, and C.N. Santos. 2016. Zika virus damages the human placental barrier and presents marked fetal neurotropism. *Mem Inst Oswaldo Cruz* 111:287-293.

Nybakken, G.E., T. Oliphant, S. Johnson, S. Burke, M.S. Diamond, and D.H. Fremont. 2005. Structural basis of West Nile virus neutralization by a therapeutic antibody. *Nature* 437:764-769.

O'Leary, D.R., S. Kuhn, K.L. Kniss, A.F. Hinckley, S.A. Rasmussen, W.J. Pape, L.K. Kightlinger, B.D. Beecham, T.K. Miller, D.F. Neitzel, S.R. Michaels, G.L. Campbell, R.S. Lanciotti, and E.B. Hayes. 2006. Birth outcomes following West Nile Virus infection of pregnant women in the United States: 2003-2004. *Pediatrics* 117:e537-545.

Ober, R.J., C.G. Radu, V. Ghetie, and E.S. Ward. 2001. Differences in promiscuity for antibody-FcRn interactions across species: implications for therapeutic antibodies. *Int Immunol* 13:1551-1559.

Oehler, E., L. Watrin, P. Larre, I. Leparc-Goffart, S. Lastere, F. Valour, L. Baudouin, H. Mallet, D. Musso, and F. Ghawche. 2014. Zika virus infection complicated by Guillain-Barre syndrome--case report, French Polynesia, December 2013. *Euro Surveill* 19:

Ogura, Y., D.K. Bonen, N. Inohara, D.L. Nicolae, F.F. Chen, R. Ramos, H. Britton, T. Moran, R. Karaliuskas, R.H. Duerr, J.P. Achkar, S.R. Brant, T.M. Bayless, B.S. Kirschner, S.B. Hanauer, G. Nunez, and J.H. Cho. 2001. A frameshift mutation in NOD2 associated with susceptibility to Crohn's disease. *Nature* 411:603-606.

Olagnier, D., D. Amatore, L. Castiello, M. Ferrari, E. Palermo, M.S. Diamond, A.T. Palamara, and J. Hiscott. 2016. Dengue Virus Immunopathogenesis: Lessons Applicable to the Emergence of Zika Virus. *J Mol Biol*

Olagnier, D., F.E. Scholte, C. Chiang, I.C. Albulescu, C. Nichols, Z. He, R. Lin, E.J. Snijder, M.J. van Hemert, and J. Hiscott. 2014. Inhibition of dengue and chikungunya virus infections by RIG-I-mediated type I interferon-independent stimulation of the innate antiviral response. *J Virol* 88:4180-4194.

Oldstone, M.B., and H. Rosen. 2014. Cytokine storm plays a direct role in the morbidity and mortality from influenza virus infection and is chemically treatable with a single sphingosine-1-phosphate agonist molecule. *Curr Top Microbiol Immunol* 378:129-147.

Oliphant, T., M. Engle, G.E. Nybakken, C. Doane, S. Johnson, L. Huang, S. Gorlatov, E. Mehlhop, A. Marri, K.M. Chung, G.D. Ebel, L.D. Kramer, D.H. Fremont, and M.S. Diamond. 2005. Development of a humanized monoclonal antibody with therapeutic potential against West Nile virus. *Nat Med* 11:522-530.

Olivas, W.M., D. Muhlrad, and R. Parker. 1997. Analysis of the yeast genome: identification of new non-coding and small ORF-containing RNAs. *Nucleic Acids Res* 25:4619-4625.

Olivera-Botello, G., L. Coudeville, K. Fanouillere, B. Guy, L. Chambonneau, F. Noriega, N. Jackson, and C.-T.V.T. Group. 2016. Tetravalent Dengue Vaccine Reduces Symptomatic and Asymptomatic Dengue Virus Infections in Healthy Children and Adolescents Aged 2-16 Years in Asia and Latin America. *J Infect Dis* 214:994-1000.

Oshiumi, H., M. Miyashita, M. Matsumoto, and T. Seya. 2013. A distinct role of Riplet-mediated K63-Linked polyubiquitination of the RIG-I repressor domain in human antiviral innate immune responses. *PLoS Pathog* 9:e1003533.

Pacheco, O., M. Beltran, C.A. Nelson, D. Valencia, N. Tolosa, S.L. Farr, A.V. Padilla, V.T. Tong, E.L. Cuevas, A. Espinosa-Bode, L. Pardo, A. Rico, J. Reefhuis, M. Gonzalez, M. Mercado, P. Chaparro, M. Martinez Duran, C.Y. Rao, M.M. Munoz,

A.M. Powers, C. Cuellar, R. Helfand, C. Huguett, D.J. Jamieson, M.A. Honein, and M.L. Ospina Martinez. 2016. Zika Virus Disease in Colombia - Preliminary Report. *N Engl J Med*

Paisley, J.E., A.F. Hinckley, D.R. O'Leary, W.C. Kramer, R.S. Lanciotti, G.L. Campbell, and E.B. Hayes. 2006. West Nile virus infection among pregnant women in a northern Colorado community, 2003 to 2004. *Pediatrics* 117:814-820.

Panayiotou, C., R. Lindqvist, C. Kurhade, K. Vonderstein, J. Pasto, K. Edlund, A.S. Upadhyay, and A.K. Overby. 2018. Viperin Restricts Zika Virus and Tick-Borne Encephalitis Virus Replication by Targeting NS3 for Proteasomal Degradation. *J Virol* 92:

Pantoja, P., E.X. Perez-Guzman, I.V. Rodriguez, L.J. White, O. Gonzalez, C. Serrano, L. Giavedoni, V. Hodara, L. Cruz, T. Arana, M.I. Martinez, M.A. Hassert, J.D. Brien, A.K. Pinto, A. de Silva, and C.A. Sariol. 2017. Zika virus pathogenesis in rhesus macaques is unaffected by pre-existing immunity to dengue virus. *Nat Commun* 8:15674.

Parisien, J.P., J.J. Lenoir, R. Mandhana, K.R. Rodriguez, K. Qian, A.M. Bruns, and C.M. Horvath. 2018. RNA sensor LGP2 inhibits TRAF ubiquitin ligase to negatively regulate innate immune signaling. *EMBO Rep*

Park, M.-S., Y.-Q. Deng, J.-X. Dai, G.-H. Ji, T. Jiang, H.-J. Wang, H.-o. Yang, W.-L. Tan, R. Liu, M. Yu, B.-X. Ge, Q.-Y. Zhu, E.D. Qin, Y.-J. Guo, and C.-F. Qin. 2011. A Broadly Flavivirus Cross-Neutralizing Monoclonal Antibody that Recognizes a Novel Epitope within the Fusion Loop of E Protein. *PLoS ONE* 6:e16059.

Pattabhi, S., C.R. Wilkins, R. Dong, M.L. Knoll, J. Posakony, S. Kaiser, C.E. Mire, M.L. Wang, R.C. Ireton, T.W. Geisbert, K.M. Bedard, S.P. Iadonato, Y.M. Loo, and M. Gale, Jr. 2015. Targeting Innate Immunity for Antiviral Therapy through Small Molecule Agonists of the RLR Pathway. *J Virol* 90:2372-2387.

Paul, L.M., E.R. Carlin, M.M. Jenkins, A.L. Tan, C.M. Barcellona, C.O. Nicholson, S.F. Michael, and S. Isern. 2016. Dengue virus antibodies enhance Zika virus infection. *Clin Transl Immunology* 5:e117.

Petersen, L.R., D.J. Jamieson, and M.A. Honein. 2016a. Zika Virus. *N Engl J Med* 375:294-295.

Petersen, L.R., D.J. Jamieson, A.M. Powers, and M.A. Honein. 2016b. Zika Virus. *N Engl J Med* 374:1552-1563.

Pettersson, J.H., V. Eldholm, S.J. Seligman, A. Lundkvist, A.K. Falconar, M.W. Gaunt, D. Musso, A. Nougairede, R. Charrel, E.A. Gould, and X. de Lamballerie. 2016. How Did Zika Virus Emerge in the Pacific Islands and Latin America? *MBio* 7:

Pichlmair, A., O. Schulz, C.P. Tan, T.I. Naslund, P. Liljestrom, F. Weber, and C. Reis e Sousa. 2006. RIG-I-mediated antiviral responses to single-stranded RNA bearing 5'-phosphates. *Science* 314:997-1001.

Pichlmair, A., O. Schulz, C.P. Tan, J. Rehwinkel, H. Kato, O. Takeuchi, S. Akira, M. Way, G. Schiavo, and C. Reis e Sousa. 2009. Activation of MDA5 requires higher-order RNA structures generated during virus infection. *J Virol* 83:10761-10769.

Pijlman, G.P., A. Funk, N. Kondratieva, J. Leung, S. Torres, L. van der Aa, W.J. Liu, A.C. Palmenberg, P.Y. Shi, R.A. Hall, and A.A. Khromykh. 2008. A highly structured, nuclease-resistant, noncoding RNA produced by flaviviruses is required for pathogenicity. *Cell Host Microbe* 4:579-591.

Pinto, A.K., H.J. Ramos, X. Wu, S. Aggarwal, B. Shrestha, M. Gorman, K.Y. Kim, M.S. Suthar, J.P. Atkinson, M. Gale, Jr., and M.S. Diamond. 2014. Deficient IFN signaling by myeloid cells leads to MAVS-dependent virus-induced sepsis. *PLoS Pathog* 10:e1004086.

Pippig, D.A., J.C. Hellmuth, S. Cui, A. Kirchhofer, K. Lammens, A. Lammens, A. Schmidt, S. Rothenfusser, and K.P. Hopfner. 2009. The regulatory domain of the RIG-I family ATPase LGP2 senses double-stranded RNA. *Nucleic Acids Res* 37:2014-2025.

Piret, J., J. Carbonneau, C. Rheaume, M. Baz, and G. Boivin. 2018. Predominant role of IPS-1 over TRIF adaptor proteins in early innate immune response against Zika virus in mice. *J Gen Virol* 99:209-218.

Platt, D.J., A.M. Smith, N. Arora, M.S. Diamond, C.B. Coyne, and J.J. Miner. 2018. Zika virus-related neurotropic flaviviruses infect human placental explants and cause fetal demise in mice. *Sci Transl Med* 10:

Pollpeter, D., A. Komuro, G.N. Barber, and C.M. Horvath. 2011. Impaired cellular responses to cytosolic DNA or infection with Listeria monocytogenes and vaccinia virus in the absence of the murine LGP2 protein. *PLoS One* 6:e18842.

Pridjian, G., P.A. Sirois, S. McRae, A.F. Hinckley, S.A. Rasmussen, P. Kissinger, P. Buekens, E.B. Hayes, D. O'Leary, S. Kuhn, K.F. Swan, X. Xiong, and D.M. Wesson. 2016. Prospective study of pregnancy and newborn outcomes in mothers with West nile illness during pregnancy. *Birth Defects Res A Clin Mol Teratol* 106:716-723.

Prins, K.C., W.B. Cardenas, and C.F. Basler. 2009. Ebola virus protein VP35 impairs the function of interferon regulatory factor-activating kinases IKKepsilon and TBK-1. *J Virol* 83:3069-3077.

Priyamvada, L., A. Cho, N. Onlamoon, N.Y. Zheng, M. Huang, Y. Kovalenkov, K. Chokephaibulkit, N. Angkasekwinai, K. Pattanapanyasat, R. Ahmed, P.C. Wilson, and J. Wrammert. 2016. B Cell Responses during Secondary Dengue Virus Infection Are Dominated by Highly Cross-Reactive, Memory-Derived Plasmablasts. *J Virol* 90:5574-5585.

Pulendran, B. 2015. The varieties of immunological experience: of pathogens, stress, and dendritic cells. *Annu Rev Immunol* 33:563-606.

Querec, T., S. Bennouna, S. Alkan, Y. Laouar, K. Gorden, R. Flavell, S. Akira, R. Ahmed, and B. Pulendran. 2006. Yellow fever vaccine YF-17D activates multiple dendritic cell subsets via TLR2, 7, 8, and 9 to stimulate polyvalent immunity. *J Exp Med* 203:413-424.

Querec, T.D., R.S. Akondy, E.K. Lee, W. Cao, H.I. Nakaya, D. Teuwen, A. Pirani, K. Gernert, J. Deng, B. Marzolf, K. Kennedy, H. Wu, S. Bennouna, H. Oluoch, J. Miller, R.Z. Vencio, M. Mulligan, A. Aderem, R. Ahmed, and B. Pulendran. 2009. Systems biology approach predicts immunogenicity of the yellow fever vaccine in humans. *Nat Immunol* 10:116-125.

Rasmussen, S.A., D.J. Jamieson, M.A. Honein, and L.R. Petersen. 2016. Zika Virus and Birth Defects--Reviewing the Evidence for Causality. *N Engl J Med* 374:1981-1987.

Reagan-Steiner, S., R. Simeone, E. Simon, J. Bhatnagar, T. Oduyebo, R. Free, A.M. Denison, D.B. Rabeneck, S. Ellington, E. Petersen, J. Gary, G. Hale, M.K. Keating, R.B. Martines, A. Muehlenbachs, J. Ritter, E. Lee, A. Davidson, E. Conners, S. Scotland, K. Sandhu, A. Bingham, E. Kassens, L. Smith, K. St George, N. Ahmad, M. Tanner, S. Beavers, B. Miers, K. VanMaldeghem, S. Khan, I. Rabe, C. Gould, D. Meaney-Delman, M.A. Honein, W.J. Shieh, D.J. Jamieson, M. Fischer, S.R. Zaki, U.S.Z.P.R. Collaboration, E. Zika Virus Response, and T. Surveillance Task Force Pathology. 2017. Evaluation of Placental and Fetal Tissue Specimens for Zika Virus Infection - 50 States and District of Columbia, January-December, 2016. *MMWR Morb Mortal Wkly Rep* 66:636-643.

Reefhuis, J., S.M. Gilboa, M.A. Johansson, D. Valencia, R.M. Simeone, S.L. Hills, K. Polen, D.J. Jamieson, L.R. Petersen, and M.A. Honein. 2016. Projecting Month of Birth for At-Risk Infants after Zika Virus Disease Outbreaks. *Emerging infectious diseases* 22:828-832.

Rice, G.I., G.M. Forte, M. Szynkiewicz, D.S. Chase, A. Aeby, M.S. Abdel-Hamid, S. Ackroyd, R. Allcock, K.M. Bailey, U. Balottin, C. Barnerias, G. Bernard, C. Bodemer, M.P. Botella, C. Cereda, K.E. Chandler, L. Dabydeen, R.C. Dale, C. De Laet, C.G. De Goede, M. Del Toro, L. Effat, N.N. Enamorado, E. Fazzi, B. Gener, M. Haldre, J.P. Lin, J.H. Livingston, C.M. Lourenco, W. Marques, Jr., P. Oades, P. Peterson, M. Rasmussen, A. Roubertie, J.L. Schmidt, S.A. Shalev, R. Simon, R. Spiegel, K.J. Swoboda, S.A. Temtamy, G. Vassallo, C.N. Vilain, J. Vogt, V. Wermenbol, W.P. Whitehouse, D. Soler, I. Olivieri, S. Orcesi, M.S. Aglan, M.S. Zaki, G.M. Abdel-Salam, A. Vanderver, K. Kisand, F. Rozenberg, P. Lebon, and Y.J. Crow. 2013. Assessment of interferon-related biomarkers in Aicardi-Goutieres syndrome associated with mutations in TREX1, RNASEH2A, RNASEH2B, RNASEH2C, SAMHD1, and ADAR: a case-control study. *Lancet Neurol* 12:1159-1169.

Robertson, S.J., K.J. Lubick, B.A. Freedman, A.B. Carmody, and S.M. Best. 2014. Tick-borne flaviviruses antagonize both IRF-1 and type I IFN signaling to inhibit dendritic cell function. *J Immunol* 192:2744-2755.

Rosenberg, A.Z., W. Yu, D.A. Hill, C.A. Reyes, and D.A. Schwartz. 2017. Placental Pathology of Zika Virus: Viral Infection of the Placenta Induces Villous Stromal Macrophage (Hofbauer Cell) Proliferation and Hyperplasia. *Arch Pathol Lab Med* 141:43-48.

Rossi, S.L., R.B. Tesh, S.R. Azar, A.E. Muruato, K.A. Hanley, A.J. Auguste, R.M. Langsjoen, S. Paessler, N. Vasilakis, and S.C. Weaver. 2016. Characterization of a Novel Murine Model to Study Zika Virus. *Am J Trop Med Hyg* 94:1362-1369.

Rothenfusser, S., N. Goutagny, G. DiPerna, M. Gong, B.G. Monks, A. Schoenemeyer, M. Yamamoto, S. Akira, and K.A. Fitzgerald. 2005. The RNA helicase Lgp2 inhibits TLR-independent sensing of viral replication by retinoic acid-inducible gene-I. *J Immunol* 175:5260-5268.

Saito, T., R. Hirai, Y.M. Loo, D. Owen, C.L. Johnson, S.C. Sinha, S. Akira, T. Fujita, and M. Gale, Jr. 2007. Regulation of innate antiviral defenses through a shared repressor domain in RIG-I and LGP2. *Proc Natl Acad Sci U S A* 104:582-587.

Saito, T., D.M. Owen, F. Jiang, J. Marcotrigiano, and M. Gale, Jr. 2008. Innate immunity induced by composition-dependent RIG-I recognition of hepatitis C virus RNA. *Nature* 454:523-527.

Samanta, M., D. Iwakiri, T. Kanda, T. Imaizumi, and K. Takada. 2006. EB virus-encoded RNAs are recognized by RIG-I and activate signaling to induce type I IFN. *EMBO J* 25:4207-4214.

Samuel, M.A., and M.S. Diamond. 2006. Pathogenesis of West Nile Virus infection: a balance between virulence, innate and adaptive immunity, and viral evasion. *J Virol* 80:9349-9360.

Sanchez-Aparicio, M.T., L.J. Feinman, A. Garcia-Sastre, and M.L. Shaw. 2018. Paramyxovirus V Proteins Interact with the RIG-I/TRIM25 Regulatory Complex and Inhibit RIG-I Signaling. *J Virol* 92:

Sangkawibha, N., S. Rojanasuphot, S. Ahandrik, S. Viriyapongse, S. Jatanasen, V. Salitul, B. Phanthumachinda, and S.B. Halstead. 1984. Risk factors in dengue shock syndrome: a prospective epidemiologic study in Rayong, Thailand. I. The 1980 outbreak. *Am J Epidemiol* 120:653-669.

Sarno, M., G.A. Sacramento, R. Khouri, M.S. do Rosario, F. Costa, G. Archanjo, L.A. Santos, N. Nery, Jr., N. Vasilakis, A.I. Ko, and A.R. de Almeida. 2016. Zika Virus Infection and Stillbirths: A Case of Hydrops Fetalis, Hydranencephaly and Fetal Demise. *PLoS Negl Trop Dis* 10:e0004517.

Satoh, T., H. Kato, Y. Kumagai, M. Yoneyama, S. Sato, K. Matsushita, T. Tsujimura, T. Fujita, S. Akira, and O. Takeuchi. 2010. LGP2 is a positive regulator of RIG-I- and MDA5-mediated antiviral responses. *Proc Natl Acad Sci U S A* 107:1512-1517.

Savidis, G., J.M. Perreira, J.M. Portmann, P. Meraner, Z. Guo, S. Green, and A.L. Brass. 2016. The IFITMs Inhibit Zika Virus Replication. *Cell Rep* 15:2323-2330.

Schafer, S.L., R. Lin, P.A. Moore, J. Hiscott, and P.M. Pitha. 1998. Regulation of type I interferon gene expression by interferon regulatory factor-3. *J Biol Chem* 273:2714-2720.

Schliefsteiner, C., M. Peinhaupt, S. Kopp, J. Logl, I. Lang-Olip, U. Hiden, A. Heinemann, G. Desoye, and C. Wadsack. 2017. Human Placental Hofbauer Cells Maintain an Anti-inflammatory M2 Phenotype despite the Presence of Gestational Diabetes Mellitus. *Front Immunol* 8:888.

Schmid, M.A., and E. Harris. 2014. Monocyte recruitment to the dermis and differentiation to dendritic cells increases the targets for dengue virus replication. *PLoS Pathog* 10:e1004541.

Schnell, G., Y.M. Loo, J. Marcotrigiano, and M. Gale, Jr. 2012. Uridine composition of the poly-U/UC tract of HCV RNA defines non-self recognition by RIG-I. *PLoS Pathog* 8:e1002839.

Schoggins, J.W., and C.M. Rice. 2011. Interferon-stimulated genes and their antiviral effector functions. *Curr Opin Virol* 1:519-525.

Schoggins, J.W., S.J. Wilson, M. Panis, M.Y. Murphy, C.T. Jones, P. Bieniasz, and C.M. Rice. 2011. A diverse range of gene products are effectors of the type I interferon antiviral response. *Nature* 472:481-485.

Schuessler, A., A. Funk, H.M. Lazear, D.A. Cooper, S. Torres, S. Daffis, B.K. Jha, Y. Kumagai, O. Takeuchi, P. Hertzog, R. Silverman, S. Akira, D.J. Barton, M.S. Diamond, and A.A. Khromykh. 2012. West Nile virus noncoding subgenomic RNA contributes to viral evasion of the type I interferon-mediated antiviral response. *J Virol* 86:5708-5718.

Schulz, O., A. Pichlmair, J. Rehwinkel, N.C. Rogers, D. Scheuner, H. Kato, O. Takeuchi, S. Akira, R.J. Kaufman, and C. Reis e Sousa. 2010. Protein kinase R contributes to immunity against specific viruses by regulating interferon mRNA integrity. *Cell Host Microbe* 7:354-361.

Schwartz, D.A. 2017. Viral infection, proliferation, and hyperplasia of Hofbauer cells and absence of inflammation characterize the placental pathology of fetuses with congenital Zika virus infection. *Arch Gynecol Obstet* 295:1361-1368.

Shan, C., X. Xie, A.E. Muruato, S.L. Rossi, C.M. Roundy, S.R. Azar, Y. Yang, R.B. Tesh, N. Bourne, A.D. Barrett, N. Vasilakis, S.C. Weaver, and P.Y. Shi. 2016. An Infectious cDNA Clone of Zika Virus to Study Viral Virulence, Mosquito Transmission, and Antiviral Inhibitors. *Cell Host Microbe*

Shapiro-Mendoza, C.K., M.E. Rice, R.R. Galang, A.C. Fulton, K. VanMaldeghem, M.V. Prado, E. Ellis, M.S. Anesi, R.M. Simeone, E.E. Petersen, S.R. Ellington, A.M. Jones, T. Williams, S. Reagan-Steiner, J. Perez-Padilla, C.C. Deseda, A. Beron, A.J. Tufa, A. Rosinger, N.M. Roth, C. Green, S. Martin, C.D. Lopez, L. deWilde, M. Goodwin, H.P. Pagano, C.T. Mai, C. Gould, S. Zaki, L.N. Ferrer, M.S. Davis, E. Lathrop, K. Polen, J.D. Cragan, M. Reynolds, K.B. Newsome, M.M. Huertas, J. Bhatangar, A.M. Quinones, J.F. Nahabedian, L. Adams, T.M. Sharp, W.T.

Hancock, S.A. Rasmussen, C.A. Moore, D.J. Jamieson, J.L. Munoz-Jordan, H. Garstang, A. Kambui, C. Masao, M.A. Honein, D. Meaney-Delman, P. Zika, and G. Infant Registries Working. 2017. Pregnancy Outcomes After Maternal Zika Virus Infection During Pregnancy - U.S. Territories, January 1, 2016-April 25, 2017. *MMWR Morb Mortal Wkly Rep* 66:615-621.

Sharp, T.M., J. Munoz-Jordan, J. Perez-Padilla, M.I. Bello-Pagan, A. Rivera, D.M. Pastula, J.L. Salinas, J.H. Martinez Mendez, M. Mendez, A.M. Powers, S. Waterman, and B. Rivera-Garcia. 2016. Zika Virus Infection Associated With Severe Thrombocytopenia. *Clin Infect Dis*

Sheridan, M.A., D. Yunusov, V. Balaraman, A.P. Alexenko, S. Yabe, S. Verjovski-Almeida, D.J. Schust, A.W. Franz, Y. Sadovsky, T. Ezashi, and R.M. Roberts. 2017. Vulnerability of primitive human placental trophoblast to Zika virus. *Proc Natl Acad Sci U S A* 114:E1587-E1596.

Si-Tahar, M., F. Blanc, L. Furio, D. Chopy, V. Balloy, M. Lafon, M. Chignard, L. Fiette, F. Langa, P. Charneau, and J. Pothlichet. 2014. Protective role of LGP2 in influenza virus pathogenesis. *J Infect Dis* 210:214-223.

Simister, N.E., and C.M. Story. 1997. Human placental Fc receptors and the transmission of antibodies from mother to fetus. *J Reprod Immunol* 37:1-23.

Simister, N.E., C.M. Story, H.L. Chen, and J.S. Hunt. 1996a. An IgG-transporting Fc receptor expressed in the syncytiotrophoblast of human placenta. *Eur J Immunol* 26:1527-1531.

Simister, N.E., C.M. Story, H.L. Chen, and J.S. Hunt. 1996b. An IgG-transporting Fc receptor expressed in the syncytiotrophoblast of human placenta. *Eur J Immunol* 26:1527-1531.

Sirohi, D., Z. Chen, L. Sun, T. Klose, T.C. Pierson, M.G. Rossmann, and R.J. Kuhn. 2016. The 3.8 A resolution cryo-EM structure of Zika virus. *Science* 352:467-470.

Sirois, P.A., G. Pridjian, S. McRae, A.F. Hinckley, S.A. Rasmussen, P. Kissinger, P. Buekens, E.B. Hayes, D.R. O'Leary, K.F. Swan, X. Xiong, and D.M. Wesson. 2014. Developmental outcomes in young children born to mothers with West Nile illness during pregnancy. *Birth Defects Res A Clin Mol Teratol* 100:792-796.

Smith, K.G., and M.R. Clatworthy. 2010. FcgammaRIIB in autoimmunity and infection: evolutionary and therapeutic implications. *Nat Rev Immunol* 10:328-343.

Smith, S.A., Y. Zhou, N.P. Olivarez, A.H. Broadwater, A.M. de Silva, and J.E. Crowe, Jr. 2012. Persistence of circulating memory B cell clones with potential for dengue virus disease enhancement for decades following infection. *J Virol* 86:2665-2675.

Stettler, K., M. Beltramello, D.A. Espinosa, V. Graham, A. Cassotta, S. Bianchi, F. Vanzetta, A. Minola, S. Jaconi, F. Mele, M. Foglierini, M. Pedotti, L. Simonelli, S. Dowall, B. Atkinson, E. Percivalle, C.P. Simmons, L. Varani, J. Blum, F. Baldanti, E. Cameroni, R. Hewson, E. Harris, A. Lanzavecchia, F. Sallusto, and D. Corti. 2016. Specificity, cross-reactivity, and function of antibodies elicited by Zika virus infection. *Science* 353:823-826.

Story, C.M., J.E. Mikulska, and N.E. Simister. 1994. A major histocompatibility complex class I-like Fc receptor cloned from human placenta: possible role in transfer of immunoglobulin G from mother to fetus. *J Exp Med* 180:2377-2381.

Sultana, H., H.G. Foellmer, G. Neelakanta, T. Oliphant, M. Engle, M. Ledizet, M.N. Krishnan, N. Bonafe, K.G. Anthony, W.A. Marasco, P. Kaplan, R.R. Montgomery, M.S. Diamond, R.A. Koski, and E. Fikrig. 2009. Fusion loop peptide of the West Nile virus envelope protein is essential for pathogenesis and is recognized by a therapeutic cross-reactive human monoclonal antibody. *J Immunol* 183:650-660.

Sun, X., S. Hua, H.R. Chen, Z. Ouyang, K. Einkauf, S. Tse, K. Ard, A. Ciaranello, S. Yawetz, P. Sax, E.S. Rosenberg, M. Lichterfeld, and X.G. Yu. 2017.

Transcriptional Changes during Naturally Acquired Zika Virus Infection Render Dendritic Cells Highly Conducive to Viral Replication. *Cell Rep* 21:3471-3482.

Sun, Y., C. Jin, F. Zhan, X. Wang, M. Liang, Q. Zhang, S. Ding, X. Guan, X. Huo, C. Li, J. Qu, Q. Wang, S. Zhang, Y. Zhang, S. Wang, A. Xu, Z. Bi, and D. Li. 2012. Host cytokine storm is associated with disease severity of severe fever with thrombocytopenia syndrome. *J Infect Dis* 206:1085-1094.

Suthar, M.S., M.M. Brassil, G. Blahnik, and M. Gale, Jr. 2012a. Infectious clones of novel lineage 1 and lineage 2 West Nile virus strains WNV-TX02 and WNV-Madagascar. *J Virol* 86:7704-7709.

Suthar, M.S., M.M. Brassil, G. Blahnik, A. McMillan, H.J. Ramos, S.C. Proll, S.E. Belisle, M.G. Katze, and M. Gale, Jr. 2013a. A systems biology approach reveals that tissue tropism to West Nile virus is regulated by antiviral genes and innate immune cellular processes. *PLoS Pathog* 9:e1003168.

Suthar, M.S., M.S. Diamond, and M. Gale, Jr. 2013b. West Nile virus infection and immunity. *Nat Rev Microbiol* 11:115-128.

Suthar, M.S., D.Y. Ma, S. Thomas, J.M. Lund, N. Zhang, S. Daffis, A.Y. Rudensky, M.J. Bevan, E.A. Clark, M.K. Kaja, M.S. Diamond, and M. Gale, Jr. 2010. IPS-1 is essential for the control of West Nile virus infection and immunity. *PLoS Pathog* 6:e1000757.

Suthar, M.S., H.J. Ramos, M.M. Brassil, J. Netland, C.P. Chappell, G. Blahnik, A. McMillan, M.S. Diamond, E.A. Clark, M.J. Bevan, and M. Gale, Jr. 2012b. The RIG-I-like receptor LGP2 controls CD8(+) T cell survival and fitness. *Immunity* 37:235-248.

Swanstrom, J.A., J.A. Plante, K.S. Plante, E.F. Young, E. McGowan, E.N. Gallichotte, D.G. Widman, M.T. Heise, A.M. de Silva, and R.S. Baric. 2016. Dengue Virus Envelope Dimer Epitope Monoclonal Antibodies Isolated from Dengue Patients Are Protective against Zika Virus. *MBio* 7:

Tabata, T., M. Petitt, H. Puerta-Guardo, D. Michlmayr, C. Wang, J. Fang-Hoover, E. Harris, and L. Pereira. 2016. Zika Virus Targets Different Primary Human Placental Cells, Suggesting Two Routes for Vertical Transmission. *Cell Host Microbe* 20:155-166.

Takahasi, K., H. Kumeta, N. Tsuduki, R. Narita, T. Shigemoto, R. Hirai, M. Yoneyama, M. Horiuchi, K. Ogura, T. Fujita, and F. Inagaki. 2009. Solution structures of cytosolic RNA sensor MDA5 and LGP2 C-terminal domains: identification of the RNA recognition loop in RIG-I-like receptors. *J Biol Chem* 284:17465-17474.

Takahasi, K., M. Yoneyama, T. Nishihori, R. Hirai, H. Kumeta, R. Narita, M. Gale, Jr., F. Inagaki, and T. Fujita. 2008. Nonself RNA-sensing mechanism of RIG-I helicase and activation of antiviral immune responses. *Mol Cell* 29:428-440.

Tang, H., C. Hammack, S.C. Ogden, Z. Wen, X. Qian, Y. Li, B. Yao, J. Shin, F. Zhang, E.M. Lee, K.M. Christian, R.A. Didier, P. Jin, H. Song, and G.L. Ming. 2016. Zika Virus Infects Human Cortical Neural Progenitors and Attenuates Their Growth. *Cell Stem Cell* 18:587-590.

Tang, Z., S. Tadesse, E. Norwitz, G. Mor, V.M. Abrahams, and S. Guller. 2011. Isolation of hofbauer cells from human term placentas with high yield and purity. *Am J Reprod Immunol* 66:336-348.

Tappe, D., J.V. Perez-Giron, L. Zammarchi, J. Rissland, D.F. Ferreira, T. Jaenisch, S. Gomez-Medina, S. Gunther, A. Bartoloni, C. Munoz-Fontela, and J. Schmidt-Chanasit. 2016. Cytokine kinetics of Zika virus-infected patients from acute to reconvalescent phase. *Med Microbiol Immunol* 205:269-273.

Tappe, D., J. Rissland, M. Gabriel, P. Emmerich, S. Gunther, G. Held, S. Smola, and J. Schmidt-Chanasit. 2014. First case of laboratory-confirmed Zika virus infection imported into Europe, November 2013. *Euro Surveill* 19:

Taylor, A., S.S. Foo, R. Bruzzone, L.V. Dinh, N.J. King, and S. Mahalingam. 2015. Fc receptors in antibody-dependent enhancement of viral infections. *Immunol Rev* 268:340-364.

Thio, C.L. 2008. Host genetic factors and antiviral immune responses to hepatitis C virus. *Clin Liver Dis* 12:713-726, xi.

Travanty, E., B. Zhou, H. Zhang, Y.P. Di, J.F. Alcorn, D.E. Wentworth, R. Mason, and J. Wang. 2015. Differential Susceptibilities of Human Lung Primary Cells to H1N1 Influenza Viruses. *J Virol* 89:11935-11944.

Tsai, T.T., Y.J. Chuang, Y.S. Lin, C.P. Chang, S.W. Wan, S.H. Lin, C.L. Chen, and C.F. Lin. 2014. Antibody-dependent enhancement infection facilitates dengue virus-regulated signaling of IL-10 production in monocytes. *PLoS Negl Trop Dis* 8:e3320.

Van der Hoek, K.H., N.S. Eyre, B. Shue, O. Khantisitthiporn, K. Glab-Ampi, J.M. Carr, M.J. Gartner, L.A. Jolly, P.Q. Thomas, F. Adikusuma, T. Jankovic-Karasoulos, C.T. Roberts, K.J. Helbig, and M.R. Beard. 2017. Viperin is an important host restriction factor in control of Zika virus infection. *Sci Rep* 7:4475.

van der Linden, V., A. Pessoa, W. Dobyns, A.J. Barkovich, H.V. Junior, E.L. Filho, E.M. Ribeiro, M.C. Leal, P.P. Coimbra, M.F. Aragao, I. Vercosa, C. Ventura, R.C. Ramos, D.D. Cruz, M.T. Cordeiro, V.M. Mota, M. Dott, C. Hillard, and C.A. Moore. 2016. Description of 13 Infants Born During October 2015-January 2016 With Congenital Zika Virus Infection Without Microcephaly at Birth - Brazil. *MMWR Morb Mortal Wkly Rep* 65:1343-1348.

van der Veen, A.G., P.V. Maillard, J.M. Schmidt, S.A. Lee, S. Deddouche-Grass, A. Borg, S. Kjaer, A.P. Snijders, and E.S.C. Reis. 2018. The RIG-I-like receptor LGP2 inhibits Dicer-dependent processing of long double-stranded RNA and blocks RNA interference in mammalian cells. *EMBO J* 37:

Vanchiere, J.A., J.C. Ruiz, A.G. Brady, T.J. Kuehl, L.E. Williams, W.B. Baze, G.K. Wilkerson, P.N. Nehete, G.B. McClure, D.L. Rogers, S.L. Rossi, S.R. Azar, C.M. Roundy, S.C. Weaver, N. Vasilakis, J.H. Simmons, and C.R. Abee. 2018. Experimental Zika Virus Infection of Neotropical Primates. *Am J Trop Med Hyg* 98:173-177.

Vanden Berghe, T., P. Hulpiau, L. Martens, R.E. Vandenbroucke, E. Van Wonterghem, S.W. Perry, I. Bruggeman, T. Divert, S.M. Choi, M. Vuylsteke, V.I. Shestopalov, C. Libert, and P. Vandenabeele. 2015. Passenger Mutations Confound Interpretation of All Genetically Modified Congenic Mice. *Immunity* 43:200-209.

Vaughn, D.W., S. Green, S. Kalayanarooj, B.L. Innis, S. Nimmannitya, S. Suntayakorn, T.P. Endy, B. Raengsakulrach, A.L. Rothman, F.A. Ennis, and A. Nisalak. 2000. Dengue viremia titer, antibody response pattern, and virus serotype correlate with disease severity. *The Journal of infectious diseases* 181:2-9.

Venkataraman, T., M. Valdes, R. Elsby, S. Kakuta, G. Caceres, S. Saijo, Y. Iwakura, and G.N. Barber. 2007. Loss of DExD/H box RNA helicase LGP2 manifests disparate antiviral responses. *J Immunol* 178:6444-6455.

Ventura, C.V., M. Maia, V. Bravo-Filho, A.L. Gois, and R. Belfort, Jr. 2016. Zika virus in Brazil and macular atrophy in a child with microcephaly. *Lancet* 387:228.

Vielle, N.J., B. Zumkehr, O. Garcia-Nicolas, F. Blank, M. Stojanov, D. Musso, D. Baud, A. Summerfield, and M.P. Alves. 2018. Silent infection of human dendritic cells by African and Asian strains of Zika virus. *Sci Rep* 8:5440.

Visvanathan, K.V., and S. Goodbourn. 1989. Double-stranded RNA activates binding of NF-kappa B to an inducible element in the human beta-interferon promoter. *EMBO J* 8:1129-1138.

Vogt, M.R., K.A. Dowd, M. Engle, R.B. Tesh, S. Johnson, T.C. Pierson, and M.S. Diamond. 2011. Poorly Neutralizing Cross-Reactive Antibodies against the Fusion Loop of West Nile Virus Envelope Protein Protect In Vivo via Fc Receptor and Complement-Dependent Effector Mechanisms. *Journal of Virology* 85:11567-11580.

Wahala, W.M., and A.M. Silva. 2011. The human antibody response to dengue virus infection. *Viruses* 3:2374-2395.

Wang, F., X. Gao, J.W. Barrett, Q. Shao, E. Bartee, M.R. Mohamed, M. Rahman, S. Werden, T. Irvine, J. Cao, G.A. Dekaban, and G. McFadden. 2008. RIG-I mediates the co-induction of tumor necrosis factor and type I interferon elicited by myxoma virus in primary human macrophages. *PLoS Pathog* 4:e1000099.

Wang, L., S.G. Valderramos, A. Wu, S. Ouyang, C. Li, P. Brasil, M. Bonaldo, T. Coates, K. Nielsen-Saines, T. Jiang, R. Aliyari, and G. Cheng. 2016. From Mosquitos to Humans: Genetic Evolution of Zika Virus. *Cell Host Microbe* 19:561-565.

Wang, S., J.P. Sundaram, and T.B. Stockwell. 2012. VIGOR extended to annotate genomes for additional 12 different viruses. *Nucleic Acids Res* 40:W186-192.

Wang, W., G. Li, W. De, Z. Luo, P. Pan, M. Tian, Y. Wang, F. Xiao, A. Li, K. Wu, X. Liu, L. Rao, F. Liu, Y. Liu, and J. Wu. 2018. Zika virus infection induces host inflammatory responses by facilitating NLRP3 inflammasome assembly and interleukin-1beta secretion. *Nat Commun* 9:106.

Weaver, S.C., F. Costa, M.A. Garcia-Blanco, A.I. Ko, G.S. Ribeiro, G. Saade, P.Y. Shi, and N. Vasilakis. 2016. Zika virus: History, emergence, biology, and prospects for control. *Antiviral Res* 130:69-80.

Weisblum, Y., E. Oiknine-Djian, O.M. Vorontsov, R. Haimov-Kochman, Z. Zakay-Rones, K. Meir, D. Shveiky, S. Elgavish, Y. Nevo, M. Roseman, M. Bronstein, D. Stockheim, I. From, I. Eisenberg, A.A. Lewkowicz, S. Yagel, A. Panet, and D.G. Wolf. 2017. Zika Virus Infects Early- and Midgestation Human Maternal Decidual Tissues, Inducing Distinct Innate Tissue Responses in the Maternal-Fetal Interface. *J Virol* 91:

Wells, M.F., M.R. Salick, O. Wiskow, D.J. Ho, K.A. Worringer, R.J. Ihry, S. Kommineni, B. Bilican, J.R. Klim, E.J. Hill, L.T. Kane, C. Ye, A. Kaykas, and K. Eggan. 2016. Genetic Ablation of AXL Does Not Protect Human Neural Progenitor Cells and Cerebral Organoids from Zika Virus Infection. *Cell Stem Cell* 19:703-708.

Welsch, S., S. Miller, I. Romero-Brey, A. Merz, C.K. Bleck, P. Walther, S.D. Fuller, C. Antony, J. Krijnse-Locker, and R. Bartenschlager. 2009. Composition and three-dimensional architecture of the dengue virus replication and assembly sites. *Cell Host Microbe* 5:365-375.

Widau, R.C., A.D. Parekh, M.C. Ranck, D.W. Golden, K.A. Kumar, R.F. Sood, S.P. Pitroda, Z. Liao, X. Huang, T.E. Darga, D. Xu, L. Huang, J. Andrade, B. Roizman, R.R. Weichselbaum, and N.N. Khodarev. 2014. RIG-I-like receptor LGP2 protects tumor cells from ionizing radiation. *Proc Natl Acad Sci U S A* 111:E484-491.

Wies, E., M.K. Wang, N.P. Maharaj, K. Chen, S. Zhou, R.W. Finberg, and M.U. Gack. 2013. Dephosphorylation of the RNA sensors RIG-I and MDA5 by the phosphatase PP1 is essential for innate immune signaling. *Immunity* 38:437-449.

Wikan, N., Y. Suputtamongkol, S. Yoksan, D.R. Smith, and P. Auewarakul. 2016. Immunological evidence of Zika virus transmission in Thailand. *Asian Pac J Trop Med* 9:141-144.

Wrammert, J., D. Koutsonanos, G.M. Li, S. Edupuganti, J. Sui, M. Morrissey, M. McCausland, I. Skountzou, M. Hornig, W.I. Lipkin, A. Mehta, B. Razavi, C. Del Rio, N.Y. Zheng, J.H. Lee, M. Huang, Z. Ali, K. Kaur, S. Andrews, R.R. Amara, Y. Wang, S.R. Das, C.D. O'Donnell, J.W. Yewdell, K. Subbarao, W.A. Marasco, M.J. Mulligan, R. Compans, R. Ahmed, and P.C. Wilson. 2011. Broadly cross-reactive antibodies dominate the human B cell response against 2009 pandemic H1N1 influenza virus infection. *J Exp Med* 208:181-193.

Wu, K.Y., G.L. Zuo, X.F. Li, Q. Ye, Y.Q. Deng, X.Y. Huang, W.C. Cao, C.F. Qin, and Z.G. Luo. 2016. Vertical transmission of Zika virus targeting the radial glial cells affects cortex development of offspring mice. *Cell Res* 26:645-654.

Wu, Y., Q. Liu, J. Zhou, W. Xie, C. Chen, Z. Wang, H. Yang, and J. Cui. 2017. Zika virus evades interferon-mediated antiviral response through the co-operation of multiple nonstructural proteins in vitro. *Cell Discov* 3:17006.

Xu, M., V. Hadinoto, R. Appanna, K. Joensson, Y.X. Toh, T. Balakrishnan, S.H. Ong, L. Warter, Y.S. Leo, C.I. Wang, and K. Fink. 2012. Plasmablasts generated during repeated dengue infection are virus glycoprotein-specific and bind to multiple virus serotypes. *J Immunol* 189:5877-5885.

Ye, Q., Z.Y. Liu, J.F. Han, T. Jiang, X.F. Li, and C.F. Qin. 2016. Genomic characterization and phylogenetic analysis of Zika virus circulating in the Americas. *Infect Genet Evol* 43:43-49.

Yockey, L.J., K.A. Jurado, N. Arora, A. Millet, T. Rakib, K.M. Milano, A.K. Hastings, E. Fikrig, Y. Kong, T.L. Horvath, S. Weatherbee, H.J. Kliman, C.B. Coyne, and A. Iwasaki. 2018. Type I interferons instigate fetal demise after Zika virus infection. *Sci Immunol* 3:

Yockey, L.J., L. Varela, T. Rakib, W. Khoury-Hanold, S.L. Fink, B. Stutz, K. Szigeti-Buck, A. Van den Pol, B.D. Lindenbach, T.L. Horvath, and A. Iwasaki. 2016. Vaginal Exposure to Zika Virus during Pregnancy Leads to Fetal Brain Infection. *Cell* 166:1247-1256 e1244.

Yoneyama, M., M. Kikuchi, K. Matsumoto, T. Imaizumi, M. Miyagishi, K. Taira, E. Foy, Y.M. Loo, M. Gale, Jr., S. Akira, S. Yonehara, A. Kato, and T. Fujita. 2005. Shared and unique functions of the DExD/H-box helicases RIG-I, MDA5, and LGP2 in antiviral innate immunity. *J Immunol* 175:2851-2858.

Yoneyama, M., M. Kikuchi, T. Natsukawa, N. Shinobu, T. Imaizumi, M. Miyagishi, K. Taira, S. Akira, and T. Fujita. 2004. The RNA helicase RIG-I has an essential function in double-stranded RNA-induced innate antiviral responses. *Nat Immunol* 5:730-737.

Yuan, L., X.Y. Huang, Z.Y. Liu, F. Zhang, X.L. Zhu, J.Y. Yu, X. Ji, Y.P. Xu, G. Li, C. Li, H.J. Wang, Y.Q. Deng, M. Wu, M.L. Cheng, Q. Ye, D.Y. Xie, X.F. Li, X. Wang, W. Shi, B. Hu, P.Y. Shi, Z. Xu, and C.F. Qin. 2017. A single mutation in the prM protein of Zika virus contributes to fetal microcephaly. *Science* 358:933-936.

Zanluca, C., V.C. Melo, A.L. Mosimann, G.I. Santos, C.N. Santos, and K. Luz. 2015. First report of autochthonous transmission of Zika virus in Brazil. *Mem Inst Oswaldo Cruz* 110:569-572.

Zhao, T., L. Yang, Q. Sun, M. Arguello, D.W. Ballard, J. Hiscott, and R. Lin. 2007. The NEMO adaptor bridges the nuclear factor-kappaB and interferon regulatory factor signaling pathways. *Nat Immunol* 8:592-600.

Zhu, Z., J.F. Chan, K.M. Tee, G.K. Choi, S.K. Lau, P.C. Woo, H. Tse, and K.Y. Yuen. 2016. Comparative genomic analysis of pre-epidemic and epidemic Zika virus strains for virological factors potentially associated with the rapidly expanding epidemic. *Emerg Microbes Infect* 5:e22.